A COMPUTATIONAL MODELLING STRATEGY FOR HISTORIC MASONRY STRUCTURES

Simin Karimian

Submitted in accordance with the requirements for the degree of

Doctor of Philosophy

The University of Leeds

School of Civil Engineering

June 2015

The candidate confirms that the work submitted is her own and that appropriate credit has been given where reference has been made to the work of others.

This copy has been supplied on the understanding that it is copyright material and that no quotation from the thesis may be published without proper acknowledgement.

The right of Simin Karimian to be identified as Author of this work has been asserted by her in accordance with the Copyright, Designs and Patents Act 1988.

Acknowledgment

First and foremost, I would like to acknowledge the assistance given to me by my academic supervisors, Professor Stephen Garrity, Dr. Dongmin Yang, and Professor Vassili Toropov, without whom this work would not have been possible and gratefully thank them for their kindness, everyday motivation, support and excellent technical guidance.

I would also like to express my gratitude to all other staff and research students from the School of Civil Engineering at the University of Leeds, in particular Dr. Lee Etchels and Dr. Lim Chin Wei. Thanks are also due to Dr. Arul Bitro from the University of Cambridge. I thank them for their helpful insight and advice, stimulating discussions and assistance on different aspects of my research work.

Last but not least, my special and sincere thanks go to my dear family members, my father Professor Hassan Karimian, my mother Mrs Frouhandeh Sanai, my brother Dr Shokrollah Karimian and my sister Dr Noushin Karimian, for their endless and unconditional support, sacrifices, encouragements and patience throughout the past few years of my studies.

Dedicated to my parents, grandparents and all of

my family members…

Abstract

The inherent complexities of masonry structures make prediction of their life expectancy very challenging. Moreover, the combined actions of time-dependent defects in structures under sustained stress greatly influence the stability and safety of these structures. Consequently, it is very difficult to identify and simulate such defects in a realistic manner without the knowledge of, and access to, the mechanical properties of the constituent materials, the construction details and the long-term effects of weathering. As a result, it is difficult to make any accurate predictions of the long-term deformation, stability and safety of the historic masonry.

This thesis describes a computational modelling strategy for the structural analysis of historic masonry structures subjected to static loading. The modelling strategy includes loss of section effects (caused by freeze-thaw action, salt crystallisation damage and exfoliation); creep and creep-induced cracking. The proposed strategy also includes the effects of reconstruction and repair. This approach should help those responsible for the operation and management of historic masonry structures to make better informed decisions about safety, stability and maintenance in the future.

The computational strategy employs the finite element method, using an elastic-plastic constitutive law for masonry, to develop a computational tool using Abaqus software. The tool was used to predict the structural response of a tall solid brickwork pier of a multi-span Victorian former railway viaduct in Whitby, Northern England. The pier is known to have suffered from a loss of section caused by frost damage and parts of it have been repaired with replacement brickwork. The pier also has clear visible signs of vertical cracking in the regions above its foundation. As there are no signs of settlement, it has been assumed that these cracks have been induced by long-term creep effects. In spite of the inherent variability of masonry and the uncertainties in the material parameters and mechanical behaviour, quite good correlation was obtained between the crack patterns in the pier predicted using the computational tool and those observed in the real viaduct, thus, validating the strategy. The findings of this research allow for simple, flexible and reliable structural analysis of present state and predictions of future conditions of historic masonry structures.

Table of Contents

List of Figures

List of Tables

Abbreviations and Acronyms

ACT	Accelerated Creep Tests
AE	Acoustic Emission
B.C.	Before Christ
BC	Boundary Conditions
CAD	Computer-Aided Design
CETOL	Accuracy Tolerance
CT	Compressive Tests
DDA	Discontinuous Deformation Analysis
DEM	Discrete Element Method
FDEM	Finite/Discrete Element Method
FE	Finite Element
FEM	Finite Element Method
FRP	Fibre-Reinforced Polymer
ICOMOS	International Council on Monuments and Sites
LSF	Least Squares Fitting
MAXPE	Maximum Principal Strain
MAXPS	Maximum Principal Stress
MCT	Monotonic Compressive Tests
NDT	Non-Destructive Techniques
OPC	Ordinary Portland Cement
QUADE	Quadratic Nominal Strain
QUADS	Quadratic Nominal Stress
RC	Reinforced Concrete

RCCM	Remote controlled crack monitoring
REV	Representative Equivalent Volume
RHC	Rapid Hardening Cement
RPL	Railway Paths Limited
SHM	Structural Health Monitoring
SMOOHS	Smart Monitoring of Historic Structures
UDEC	Universal Distinct Element Code
UMAT	Users Constitutive Model
XFEM	Extended Finite Element Method
LVDT	Linear Variable Differential Transformer

Symbols

E	Elastic Young's Modulus (N/mm^2)
v	Poisson's Ratio
$C3D8R$	Continuum, 3-D, 8-node, Reduced Integration Element
α_1	Coefficient of Thermal Expansion (K^{-1}) of material 1 (typically the existing substrate)
α_2	Coefficient of thermal expansion (K^{-1}) of material 2 (typically the repair material)
n	E_1/E_2 where E_1 and E_2 are the Elastic modulus values for materials 1 and 2, respectively
m	t_1/t_2, the ratio of thickness of the bimetallic strip
T_1	Initial temperature (K)
T_2	Final temperature (K)

Chapter 1 : Introduction

1.1 Overview

There are many masonry structures throughout the World that are considered to be of historical, architectural and cultural importance. Some of these are still in use today (Tilly, 2002; Fielden, 2003) whereas others remain as ruins (Ashurst, 2007). In addition to their cultural value, historic masonry structures can also be of considerable economic value as they play an important role as part of a nation's transport infrastructure, in the case of masonry bridges, or as a tourist attraction and educational resource.

Inevitably, historically important masonry structures will deteriorate with time for a number of reasons. Many of these are as a result of changes to or variations in the natural environmental conditions but some are as a result of human intervention. The people who have the responsibility for managing and operating these structures are faced with the challenge of restoring, preserving, conserving and maintaining them whilst, at the same time, meeting acceptable levels of performance and safety. Article II of the League of Nations' Athens Charter of 1931 emphasises the challenge facing the owners or managers of historical structures by stating: *"The conservation and restoration of monuments must have recourse to all the sciences and techniques which can contribute to the study and safeguarding of the architectural heritage"* (ICOMOS, 1931). Changes in the environmental conditions resulting from the effects of climate change are likely to increase further the level of challenge.

Careful decisions also need to be taken to meet the statutory requirements for conservation and restoration works that now exist in many countries (Garrity, 2015). These are based on the articles of the United Nations Educational, Scientific and Cultural Organisation's convention concerning the protection of the World's cultural and natural heritage (UNESCO, 1972). This informed the Council of Europe's 1985 Granada convention for the protection of the architectural heritage of Europe (Council of Europe 1985). In the UK, legislation subsequently led to the formation of executive agencies such as Cadw (Wales), English Heritage and Historic Scotland which have responsibility for advising the UK government on all aspects of the historic environment. Underpinning much of the guidance are management guides and charters produced by a number of independent organisations such as the International Council on Monuments and Sites (ICOMOS, 2011; ICOMOS, 2003).

The challenge with the management of historic masonry buildings when compared with their more modern counterparts is the need to retain as much of the original construction as possible and, wherever possible, to avoid the need for any repair or strengthening measures. Indeed, one of the main principles of conservation is that of minimum or, better still, zero intervention (Fielden, 2003). As a result, it is necessary for engineers and other conservation practitioners to be able to predict various aspects of the behaviour of historic masonry structures including the magnitude of the stresses in the existing masonry, the factors of safety of different parts of the building against collapse, the reliability of the structures under a range of environmental conditions and the effectiveness and impact of any possible future repair or strengthening measures.

The inherent complexity of historic masonry buildings with the interaction between arches, domes, vaults, ribs, walls as well as other elements of construction and the supporting ground means that simple mathematical methods cannot be used to provide the aforementioned information with sufficient levels of confidence. Instead it is necessary to make use of computational models in conjunction with practical engineering and conservation expertise and information from any records of previous maintenance and repair works in order to make informed decisions relating to the future safety, management and operation of historic masonry buildings. Such models must be capable of accommodating the various physical features of the masonry building, the mechanical characteristics of the masonry and the supporting ground and any changes that might occur (or have occurred) during the life of the structure. These latter effects may be changes in the environmental conditions or changes in the condition of the structure itself.

As indicated in the literature review reported in Chapter 2 of this thesis, historic masonry and masonry structures experience a great deal of change because of the long-term effects of weathering, erosion and a change in the support conditions caused by settlement effects or the partial collapse of adjacent parts of the structure. Over a prolonged period of time (typically several centuries), historical structures are also subjected to climate change effects.

In order to predict the future condition of historic masonry structures and to provide more reliable guidance on the future safety and reliability of these monuments, structural analysis including an evaluation of the effects of deterioration is of utmost

importance. In fact, those who are involved in conservation and restoration of historic structures and monuments utilise the results from structural analysis to:

(a)   Gain an improved understanding of the structural behaviour of historic structures and monuments,

(b)   Characterise their present condition and residual factors of safety against full or partial collapse,

(c)   Evaluate the effects of foundation settlement, extreme wind loading; seismic activity, etc. on the existing construction,

(d)   Investigate and evaluate alternative remedial measures to inform future management decisions.

To this end, the research described in this thesis concerns the development of a reliable computational tool to analyse the structural damages, to examine the effects of reconstruction and repair on historic masonry structures, and to offer (alongside the experience and knowledge of the maintenance and repair experts) safety guidelines for maintenance of these structures. Indeed, this tool provides an improved approach for a more accurate structural analysis, to avoid erroneous or defective conclusions leading to either over-strengthening of the structure, or to make unnecessary or insufficient intervention, and hence generate inadmissible risks on culturally and historically important heritage structures.

It should be noted that most of the previous works on historic masonry structures concentrate on the *material analysis* of climate change effects, while there still remain many unexplored areas relating to the *structural analysis* aspect of these structures. Additionally, previous research has focused on modelling individual defects in historic structures. To the best of author's knowledge, no significant research has been carried out to simulate the combination of these defects. Certainly, the principal original feature of the work described in this thesis is the structural analysis of historic masonry including time-dependent defects.

1.2   Aim and objectives

The main aim of the research presented in this thesis is to develop a reliable and flexible computational modelling strategy which can be used to structurally analyse historic masonry structures subjected to time-dependent damage such as loss of section

thickness (caused by frost damage, erosion, salt crystallisation effects, exfoliation, etc.), creep and creep-induced cracking. The strategy also includes the modelling of modern repair materials used in conjunction with the original masonry.

The principal objectives of the research are:

Objective 1: To gain an up-to-date understanding of historic masonry materials and the principal defects that commonly occur in historic masonry structures,

Objective 2: To gain knowledge and an understanding of the computational modelling techniques that have been developed for historic masonry structures particularly those modelling time-dependent damage. This is to identify an appropriate computational modelling approach for historical masonry,

Objective 3: To develop a computational modelling tool that can be used to model time-dependent defects in historical masonry,

Objective 4: To validate the computational tool.

1.3 Research methodology

In order to achieve the aims and objectives, the following research methodology has been used:

- To achieve objective 1, a review of the published literature on masonry units and their mechanical properties, with a particular focus on historic masonry structures, their defects (natural and human interventions), maintenance and repair is first carried out.

- To achieve objective 2, a review of the literature on the computational modelling of masonry, in particular historic masonry is carried out. The different computational modelling strategies are critically evaluated with a view to identifying an appropriate modelling strategy for historic masonry.

- Using the results from the literature reviews, a computational modelling tool is developed to capture the behaviour of masonry including the time-dependent damage resulting from the effects of weathering and creep. This part-satisfies objective 3. The model is developed to capture the following features:

  a. A reduction in the stiffness of the masonry with time,

b. The effect of temperature variation with time,

c. The presence of more than one material property in the model,

d. The softening zone and the controlled degradation of masonry to a low stiffness material (to simulate the mechanical effects of the gradual loss of masonry because of different types of deterioration with time),

e. Exfoliation (surface peeling) of the external (exposed) faces of the block; indicating the gradual loss of thickness, due to wind erosion, chemical reactions, etc., over a long-term period of time,

f. Repair of a damaged zone in the masonry,

g. Long-term creep behaviour,

h. Creep-induced cracking.

- Parametric studies are then carried out for the creep simulations as part of the model development process (to part-satisfy objective 3).

- To part-satisfy objective 4, the computational tool is initially validated through the comparison of simple simulations (using a reinforced concrete column, steel and a bimetallic strip) with hand calculated results. This is to demonstrate that the model can accommodate temperature change, changes in the modulus of elasticity, differential thermal expansion effects and composite action under applied load. A simple block of masonry is then used to validate repairs, creep and creep-induced cracking using the results from laboratory-based creep tests carried out on 5 different types of masonry.

- Objective 4 (validation) is completed by using the model to simulate the loading history of one of the piers of an existing 130 years old multi-span clay brick railway viaduct. The model predicts the behaviour of the repaired sections of the pier and also identifies the formation of vertical creep-induced cracks close the lower portion of the pier (i.e. the section just above foundation level). Comparisons are made between the predicted cracking and the crack pattern identified from a visual inspection of the viaduct pier. This further reinforces the initial validation of the model carried out using a small representative block of masonry.

1.4   Scope and limitations of the research

As discussed in the previous section, the research described in this thesis seeks to develop a reliable and customisable computational tool that can be used for the structural analysis of historic masonry structures including time-dependent effects. It is assumed that the proposed computational tool described herein would also be applicable to any type of historic masonry structure, as long as the criteria for the given set of defects are satisfied. It is hoped that this tool can contribute to the research, construction and conservation of historic monuments. It should be noted that a relatively simple constitutive law has been used in the research. It is anticipated that a similar strategy could be used for many other masonry materials provided that the constitutive laws reflect the behaviour of the masonry. It has been assumed in this research that the masonry consists of rigid masonry units such as fired clay bricks, concrete blocks or stones laid in a hardened lime or cementitious mortar. The research is not aimed at masonry comprised of softer masonry units such as adobe or tuff.

This research does not aim to recreate the chemical processes of defects in historic masonry. Instead, the modelling strategy allows the end-user to apply different rates of surface deterioration (in particular the loss of section thickness) based on maintenance records, historical records or local knowledge. Thus, the aim of the strategy is to allow for the effects of defects in the analysis rather than attempting to model how such defects have occurred. In addition, the strategy includes the modelling of new additional repair materials that are assumed to be fully bonded to the existing substrate. The use of internal or externally bonded reinforcement is considered to be outside the scope of the research.

Seismic effects are not included in the research; even though seismic activity (not a time-dependent effect) is one of the main causes of the destruction of historic masonry structures, and as severe seismic activity does not occur in the UK. Furthermore, the research does not include any dynamic load effects or the effects of fatigue. Hence the research is limited to static load conditions only.

Simplicity is the underlying fundamental approach used when developing the proposed computational tool; as such, simple masonry blocks are used when modelling the defects that commonly occur in historic masonry. It is not the intention to model a specific type of masonry. Instead, the author proposes to create a generic computational strategy that can be applied to any form of masonry, although the primary focus of this

thesis is historic masonry. As indicated earlier, it is assumed that the masonry units are rigid.

The author is aware of a number of challenges that exist when attempting to model historic masonry. These are outlined below:

- Limited research exists on the *structural* analysis of *combined* damage and applied repairs in historic masonry structures, as opposed to research on *material* behaviour.

- The difficulty of defining accurate constitutive laws for masonry, lack of adequate knowledge on the geometrical and material details of historic masonry and the fact that very little or no reliable information exists on the historical background of many of these structures in the literature, causes substantial difficulties (in terms of accuracy, reliability of data, etc.) when attempting to develop a reliable computational tool.

- Due to the difficulties in recreating (duplicating) identical historic masonry samples with exact material properties as those collected from the site, secondary data will have to be used.

- When modelling creep in historic masonry, there will be significant limitations in obtaining the material parameters for the computational model. This is due to the high cost of such tests and limitations in the availability of ancient masonry specimens, as well as test time durations ($\approx$ 500-1000 days); which means that there are very few useful experimental results from long-term creep tests.

- Creep-induced defects mainly occur in the mortar and since a higher percentage of mortar exists in historic brick masonry compared with stone masonry, the majority of the available creep experiment results are for brick masonry. As a result, the principal research focus of the author has been on the creep-induced cracking of brick masonry.

1.6 Thesis outline

This thesis consists of six chapters, the outlines of which are briefly presented below. Following this introductory chapter, **Chapter Two** presents a review of the literature and briefly provides a background overview of historic masonry, its mechanical behaviour and the factors that influence its mechanical response. It also describes

individual and combinations of defects that are commonly found in historic masonry. The possible causes of creep and crack formation and failure modes, as well as various types and effects of intervention and repair are also identified.

A review of the literature on the computational modelling of historic masonry is presented in **Chapter Three**. The principal aim of this review is to identify then compare and critically review the existing strategies and techniques used in the modelling of historic masonry including forms of deterioration such as exfoliation, frost damage, creep, and creep-induced cracking. The discussions in Chapters two and three, lead to development of a tool, based on an appropriate constitutive law for masonry structures.

Chapter Four concentrates on the development of computational modelling tool, by illustrating the *basic* features of the tool through various models of: reduction in elastic modulus with time, presence of more than one material in a structure and change in temperature with time. These features are validated using various models and hand calculations.

The validated basic features are then used to develop and validate the main features, illustrating the three main defects of historic masonry; i.e. localised damage to represent the exfoliation of stone (or frost damage in brick masonry), creep deformation occurring in different types of masonry and creep-induced cracking. Parametric studies and mesh sensitivity analysis are also carried out to understand the effect of each parameter and mesh size on the results.

The main aim of **Chapter Five** is to further validate the proposed computational tool. This is done by applying combination of these features to specific models, representing experimental tests from the literature. Furthermore, the tool's ability to reproduce and predict the long-term behaviour of masonry subjected to combination of defects is validated by applying it to a real-life masonry structure. The existing repair on this structure will also be simulated to examine the effect of a simple patch-type (brick replacement) repair on the long-term behaviour of the structure.

Finally in **Chapter Six**, the objectives of the research are reviewed, conclusions are drawn from the research carried out, and possible future work is proposed.

An overall outline of the thesis is illustrated in Figure 1.1.
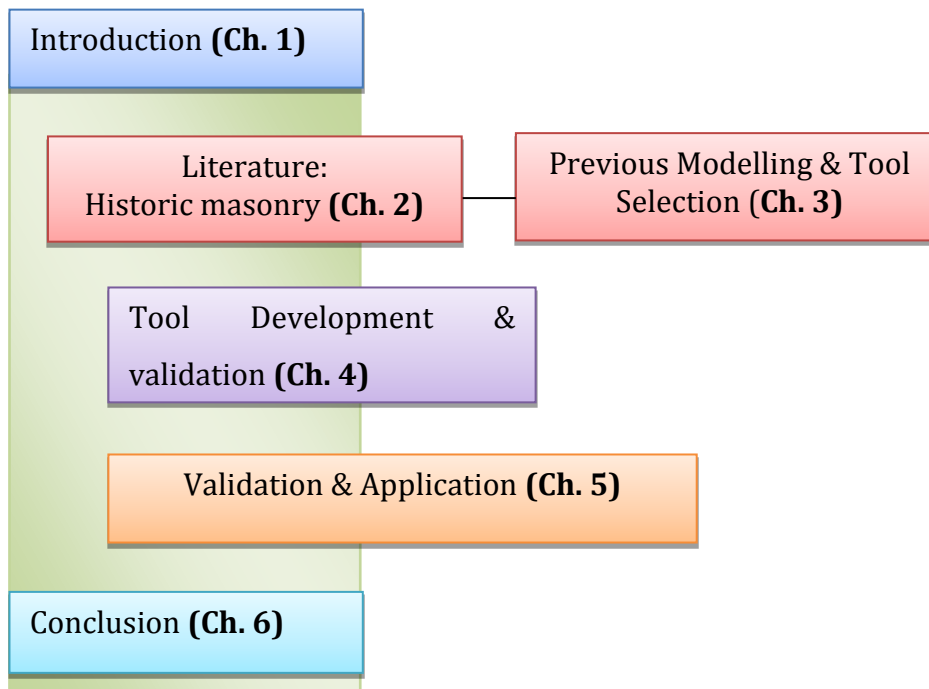
Figure 1.1: The outline structure of the thesis.

Chapter 2 : Literature Review (Part A) - Historic Masonry, Interventions and Repair

2.1 Introduction

A review of the literature on the mechanical properties of historical masonry, the factors influencing these properties and the failure of such masonry is presented in this chapter. This is to establish the principal aspects of historical masonry behaviour that will underpin the selection and development of the computational tool adopted in the research.

The review then identifies the range of defects that can occur in historical masonry that can contribute to failure over time, with the aim of determining those with the highest influence on failure. This is followed by an assessment of the effects of human intervention scenarios such as repair. A summary of the review is provided at the end of the chapter.

2.2 Historic masonry: mechanical properties, defects and failure

One of the early methods that humans used to build structures was to lay individual units such as bricks or stones on top of each other, with or without bonding materials (e.g. mortar) to form walls and other fairly massive constructions, giving birth to the material we now call 'masonry'. As a result, masonry probably dates from the earliest civilisations, around ten thousand years ago, when it first seemed to emerge as a form of construction.

Masonry can be divided into two types, namely *historic* and *modern* masonry. Historic masonry can be defined as unreinforced masonry structures which are the reminders of the early days of the use of masonry in construction (*c.* 600 B.C.) until the introduction of reinforced masonry (*c.*1800 B.C.) (Hendry, 1990). This definition has indeed been the basis for the official classification of structures by conservation and maintenance institutions such as the International Council on Monuments and Sites (ICOMOS).

Masonry has been a structural success due to the relative abundance and availability of raw materials such as clay or stone and thanks also to its flexibility, cost effectiveness, durability and attractive external appearance. In addition, as a walling material in buildings it has, for many years, fulfilled several functions providing form, partition, shelter against weather, fire protection, acoustic insulation and thermal insulation

(Hendry, 1990). Although masonry generally consists of masonry units and some form of binder, many different forms of masonry construction and materials have been developed throughout the World. These reflect differences in local, regional and national culture, wealth and material availability; local knowledge of masonry and the associated skills and tools used in construction and architectural requirements (Roca *et al*., 1998).

Despite being, with timber, the most popular construction material for several centuries, with widespread applications for historic buildings and the later constructions of the industrial revolution, by the early 20th century masonry was in decline as a structural material having been gradually overtaken by structural steel and reinforced concrete. Most modern applications of masonry now tend to be as a structural material for low rise domestic construction or as non-structural cladding or partition walling (Hendry and Khalaf 2001). Nevertheless, the World has been left with many fine examples of historic masonry construction that are of considerable value to Society. It is these that are the principal focus of the research described in this thesis.

2.2.1 Characteristics of masonry units

The term masonry describes a heterogeneous brittle material, consisting of units and joints (Lourenço, 2002). Typical units used in construction of masonry are fired clay, adobe, bricks, concrete blocks, irregular stones (naturally occurring size and shape such as marble, granite, limestone and travertine), tiles, glass blocks and ashlars. The standard types of binder used for mortars in masonry are lime or cement-based mortar, bitumen, clay and glue. The mixture of the mortar joint usually varies according to the volume or weight ratio of the mix constituents, i.e. the ratio of binders to aggregates (Sarhosis, 2011; Lourenço, 2002).

Traditionally, masonry has been constructed using rigid elements (such as blocks of stones or bricks), joined together in different ways; in some cases using mortar with low mechanical properties, and in other cases, without any mortars (Cecan, 2012).

In contrast to the traditional masonry, modern masonry construction mostly uses Portland Cement as the binder. To help with cohesiveness, workability and strength development of the OPC, specific quantities of hydrated lime and water are added to the mortar (Lourenço, 2002; Sarhosis, 2011).

Since a wide variety of materials (perhaps with different mixing ratios) are used in construction of masonry, its structural behaviour cannot be fully understood. Therefore, in order to grasp this understanding, the properties of each of the constituent materials as well as their interfaces should be studied. Consequently, this section describes the physical and behavioural properties of historic masonry units, their resistance and failure, and pros and cons of their use in construction.

2.2.1.1 Mortar characteristics

Mortar is a mixture of water, binder (cement and/or lime) and fine aggregate such as sand to bind masonry units together for load bearing purposes and to produce an even distribution of forces. The use of a good quality mortar can improve the mechanical properties of brickwork and other forms of masonry. A good mortar should have adequate and uniform bond strength as well as being able to prevent water leakage. In other words, it should (Cecan 2012; Avallone *et al.*, 2007; Hendry *et al.*, 1997; Robinson *et al*,. 1988):

- Form a cohesive structural unit, which also performs as a composite material,

- Provide adequately significant strength in bond development,

- Promote load transfer between the masonry units, to avoid excessive load stress,

- Demonstrate early strength development,

- Show high resistance to weathering induced defects; cracking, frost, chemical attacks and creep,

- Have a low water absorption; preserving bricks against the suction of water,

- Accommodate small movements,

- Illustrate good workability and ability of rapid expansion/contraction.

The mechanical properties of mortar can vary even within the same structure. This is due to the following factors (Sarhosis, 2011):

- The interaction of mortar with the surrounding units (Brocken and Pel*,* 1995),

- Orientation of the joints,

- Different locations of the joints; hence different deterioration rate (due to exposure to weathering, etc.)

- The quality of constitutive materials during the mortar-making process.

It is important to note that the strength of the bed joints is higher than that of the head joints, since the head joints are often not completely filled with mortar and have higher rate of mortar shrinkage (Dialer, 1990). The difference in their strength, can lead to:

- Non-uniform stress distribution in masonry subjected to in-plane loading (Mann and Muller, 1982),

- Distinct directional properties; stress acting on the joints, significantly influences the failure of masonry in the joints (Andreaus, 1996).

Mortars are generally classified into two main types of 'cement' and 'lime mortar'. Since mortars used in historic masonry structures were most commonly based on lime mortar, further attention will be given to lime mortar.

Lime mortars are known mainly for having low strength, and being softer than the other mortars; providing a higher degree of flexibility to large movements such as ground shifting or other conditions, without any sign of distress (Cecan, 2012; Hendry *et al*., 1997). These mortars are considered as a 'breathable paste', as they allow for moisture movement throughout the structure and evaporation on the surface. Presence of moisture over a long-time in historic mortars leads to defects such as creep (Cecan, 2012).

Lime mortars are mainly divided into two categories of non-hydraulic (air-hardening) and hydraulic mortars. Non-hydraulic lime mortars strengthen by the carbonation; process of bonding with the CO_2 from the surrounding air. On the other hand, hydraulic mortars require water for their bonding process (Verstrynge, 2010b). Modern mortars are mainly based on hydraulic limes (Cecan, 2012; Melbourne *et al*., 2006).

A summary of mechanical properties of different types of mortars is presented in Table 2.1. As it can be seen from this table, traditional lime mortars (i.e. the non-hydraulic types) have lower material properties than other two mortar types. It can also be seen that lime mortars are significantly weaker than most conventional cementations mortars.

Table 2.1: Mechanical properties of different types of mortars (Melbourne *et al*., 2006).

Mortar Type	Compressive Strength (MPa)	Traction Strength (MPa)	Elastic Modulus (MPa)
Non hydraulic lime mortar	0.5-3	0.3-7	1000-3000
Hydraulic lime mortar	1-6	1-1.5	3000-5000
Cementitious mortar	10-20	2-4	6000-9000

2.2.1.2 Fired clay brick characteristics

Fired clay bricks are one of the oldest forms of masonry unit used in historic masonry construction. Since clay is an inherently variable material, the mechanical properties of fired clay bricks such as the elastic modulus and compressive strength can vary widely - even when sampled from the same batch (Bingel 1993). Variations in the material properties of bricks used in a structure and the factors outlined below affect their material properties (Sarhosis, 2011):

- Different geographical locations of bricks; thus variance in exposure to temperature and climate change,

- Ageing of bricks,

- Different moisture expansions of brick, and hence different brick shape; depending on location of the brick in structure,

- Natural variations in the material properties of the constitutive raw materials of the brick, such as stone inclusions that may be found in raw materials,

- Moisture movement; due to change in temperature and relative humidity of the environment, permanent moisture expansion of bricks, as well as drying shrinkage of the mortar (Bingel, 1993).

2.2.1.3 Stone characteristics

Many different types of building stone have been used for the construction of historical masonry buildings. Stone can have important physical characteristics and advantages when compared with other types of masonry unit; including good compressive and shear strengths, hardness and workability, durability, porosity, aesthetics and

availability (SETRA, 1982). This had led to popularity and use of irregular stone construction in most of the remaining masonry monuments; some without any mortar contributing to the inhomogeneity of these structures. Figure 2.1 shows an example of inhomogeneity in irregular multi-leaf stone masonry walls.

(a)   (b)   (c)
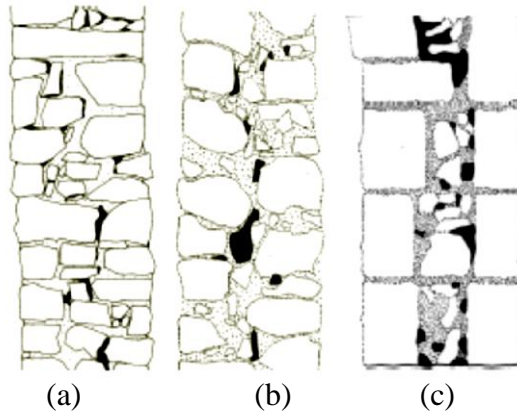
Figure 2.1: Different kinds of multi-leaf stone masonry sections: (a) two leaves with connections, (b) without connections, and (c) three-leaf stone masonry (Binda and Saisi, 2001).

Understanding the stone's chemical components, the nature of contaminant salts and other deposited materials on and within the stone, and also the cohesion between its crystals or grain structure will allow one to judge its deterioration rate. The most common defects of stone masonry are spalling, delamination and layering of the outer surface (Weaver and Matero, 1997). Due to the deterioration of these structures, there are considerable numbers of empty head joints in masonry, which increase the susceptibility to cracking and decrease the stiffness of the masonry. This is largely the case for smaller size stones, where significant stone rotations result in a decrease in the load-bearing capacity. In addition, factors such as stone format and the state of rotation, and increase in both size and strength of the head joints can cause discontinuous stress in masonry (Schlegel and Rautenstrauch, 2004).

The three most common stones used in historic masonry are granite, sandstone and limestone. Granite and sandstone have very high resistance to weathering and moisture penetration, while limestone is at high risk of erosion when exposed to pollution. Weathering and erosion weaken the stone and form localised strain; and in the cases where micro-cracks are present, they accelerate deterioration and eventual failure of the stone (Veterans Affaris Canada, 2010).

2.2.1.4 Unit-mortar bond characteristics

The unit-mortar bond is the most important and yet the weakest link in historic masonry. It has a significant effect on the mechanical behaviour of masonry, as it controls the non-linear response of the joints and has a major effect on the transfer and resistance of load, and the cracking of historic masonry (Sarhosis, 2011; Lourenço, 2002). The unit-mortar bond strength is influenced by several important factors (Sarhosis, 2011; Kjaer, 2010; Lawrence and Cao, 1987 ; Goodwin and West, 1982) such as:

- The mortar composition and water absorption,

- Texture, size, suction rate and behaviour of units,

- Size of the aggregate in mortar,

- Type of admixtures and binders used in mortar construction.

As mentioned above, the porous nature of historic masonry has significant influence on its structural performance, in particular where restoration is carried out. The high suction rate of the unit leads to absorption of water from mortar into units. This results in dehydration of the mortar, which in turn leads to low bond strength (Hendry, 2004; Throop and Klingner, 2002). Detailed information on the methods, approaches, and choice of appropriate mortar ingredients (to achieve high bond strength) can be found in (Sarhosis, 2011; Lourenço, 1996).

Two types of failures reported for the unit-joint bond are 'Mode I (tensile failure)' and 'Mode II (shear failure)' (Roca *et al*., 1998). These are described in the next section.

a) **Mode I (tensile failure)**

Tensile behaviour of the unit-mortar interface can be identified using various test set-ups, such as 'diametral compression (splitting test)', 'direct tension test', and 'flexural tests' (Roca *et al*. 1998). The fracture energy obtained from these tests represents "the amount of energy required to create a unitary area of a crack along the unit-mortar interface" (Roca *et al*., 1998). Further information on obtaining test results and adjusting them (by a correction factor), can be found in the literature (Roca *et al*., 1998; Hendry, 1990; Gazzola *et al*., 1985; Drysdale, 1979; Johnson *et al*., 1969).

a) Mode II (shear failure)

The shear response of masonry joints can be determined by using the following test set-ups to generate a uniform state of stress in such joints and to identify the shear behaviour of the interfaces (seen in Figure 2.2):

(a)   (b)
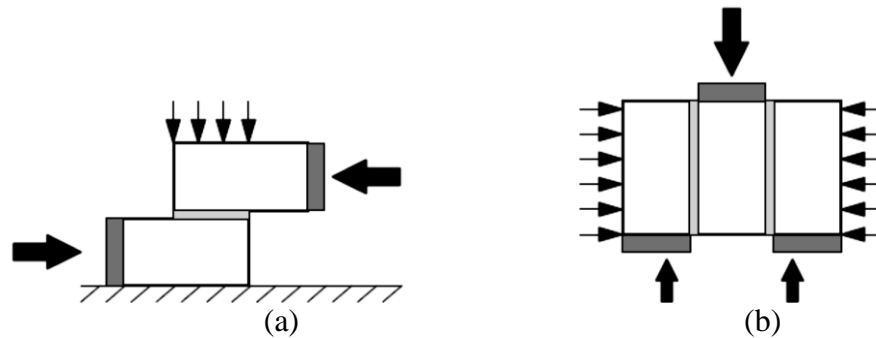
Figure 2.2: Test set-ups for shear strength (a) couplet test, and (b) triplet test (Roca *et al*., 1998).

For further information on these tests, the reader is referred to (Roca *et al*., 1998; Hofmann and Stockl, 1986; Hendry, 1978; Smith and Carter, 1971; Sinha and Hendry, 1966).

2.2.2 Mechanical properties and response of masonry

Masonry exhibits complex mechanical behaviour. The complexity is due to it being a heterogeneous material, constituting of a broad range of bonding patterns of variant units and mortars (Cecan, 2012; Sarhosis, 2011). Subsequently, different degradation levels of each of the components over time makes generalisation of historic masonry properties very difficult (Naguib and Suter, 1991; Hendry, 1990). One of the reasons for this difficulty is that such buildings are constructed using local materials and techniques with various levels of workmanship involved; some of which are unknown to current masons and engineers (Lemos, 1998a).

Historic masonry has a non-linear stress-strain relationship, which is characterised by the strength of the units and the joints (Schlegel and Rautenstrauch, 2004), and is highly dependent on the constitutive materials of the masonry (Crisafulli, 1997).

The main mechanical characteristic of masonry is the high rigidity of its units, and hence its high compressive strength. However, its behaviour is dominated by the low tensile strength of the mortar joints and weak frictional properties of the unit-mortar

interface; particularly in historic masonry (Cecan, 2012; Sarhosis, 2011; Fouchal, 2009). Consequently, historic masonry has often been seen to fail mainly due to formation of cracks in the joints, details of which are discussed in Section 2.4.1.2.

The following factors are known to have the highest influence on strength and mechanical properties of masonry structures (Sarhosis, 2011; Van Der Pluijm, 1999; Hendry, 1998; Crisafulli, 1997; Rots 1997):

- Unit and mortar characteristics,

- Unit-mortar bond characteristics,

- The unit dimensions and the way the units are laid upon,

- Workmanship,

- Curing process,

- Moisture content and water absorption of units and mortar.

2.2.2.1 Masonry in compression

Masonry structures have long been designed to resist compressive stress. Masonry under compression has almost a linear stress-strain relationship (Crisafulli, 1997). The constituent elements of masonry have great influence on the quality of masonry, as it is believed that the difference in elastic properties of unit and mortar is the main factor affecting the compressive strength and failure of masonry structures (Cecan, 2012; Lourenço, 1996; 2002). In the case of historic masonry, inclusion of different raw materials in masonry units causes major variation on compressive strength of masonry. For instance, presence of stone parts in raw materials of clay brick masonry can increase the compressive strength of the masonry structure (Sarhosis, 2011).

It is known that that under uniaxial compression conditions, the masonry units and mortar joints are in states of biaxial tension and triaxial compression, respectively. The 'stacked bond test' is generally used to identify the uniaxial compressive strength of masonry (Cecan, 2012; Lourenço, 1996; Melbourne *et al*., 2006).

Compression tests, such as the 'direct compression test', help researchers to identify the compressive strength of masonry units. Samples of methods for compression tests on mortar specimen are presented by Binda (1998a). Table 2.2 summarises the compressive strength range for constitutive materials of masonry (Crisafulli, 1997).

Table 2.2: Summary of compressive strength of masonry materials (Crisafulli, 1997).

Material	Compressive strength (MPa)
Clay masonry	8-50
Concrete masonry unit	10-40
Mortar	5-20

Factors affecting the compressive strength of masonry can be listed as (Giordano *et al*. 2002; Hendry, 1990):

- Unit characteristics: strength of unit, type of unit, absorption rate of unit, and direction of unit,

- Mortar characteristics: mortar strength, relative deformation and thickness,

- The bond between the masonry units,

- Direction of stress on masonry.

Various factors influence the compressive strength of mortar, which in turn affect the compressive strength of masonry. These factors include: (a) the curing process, (b) the lime content, (c) the characteristics of the aggregates, (d) the water-cement ratio, (e) the age of the materials, and (f) the cement (or binder) content (Brooks and Amjad, 1988; Crisafulli, 1997).

Compression tests on masonry and its associated standard materials have also shown that (Hendry, 1990):

- Masonry under uniform compression load may fail due to: (a) development of tension cracks parallel to the axis of loading or (b) shear failure along certain lines of weakness, such as mortar,

- The strength of masonry is smaller than the nominal strength of the unit in a compression test.

Figure 2.3 illustrates the typical appearance and growth of crack in masonry under uniaxial compression.
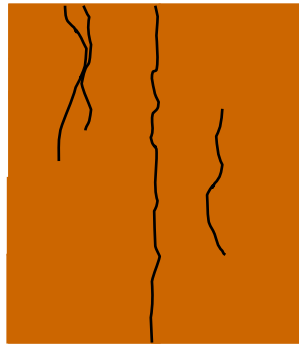
Figure 2.3: Crack propagation of masonry under uniaxial compression (Crisafulli, 1997).

2.2.2.2 Masonry in tension

Numerous experimental studies have shown that despite having high compressive strength, masonry has quite low and variable tensile bearing capacity across its bed joints (Mckenzie, 2001; Sarhosis, 2011); a behaviour that is mainly affected by the strength of the mortar and the development of the 'mortar-unit bond' (Lourenço, 1996; Mckenzie, 2001; Sarhosis, 2011). The 'mode' of tensile behaviour can be determined through the relationship between the tensile strength of bond and unit (Lourenço, 1996).

The tensile strength of masonry can be taken as the lowest value of the unit and unit-mortar bond's tensile strength (Cecan, 2012; Lourenço, 1996). It has been suggested that where tensile stress is applied in a parallel direction to the bed joints, the tensile strength of masonry is approximately half of that of the unit; provided that masonry's tensile stress exceeds the tensile strength of the unit (Hendry, 1990).

Masonry in tension has a linear stress-strain relationship. However, once the stress has reached its maximum level, brittle failure takes place (Crisafulli, 1997). There are many factors that have a major influence on the tensile strength of masonry, some of which are outlined below (Sarhosis, 2011; Lawrence *et al.*, 2005):

- Workmanship,

- The composition of mortar,

- Type of constituent masonry units,

- Admixtures that might be present in the mortar and unit.

Tensions could be provoked by internal and/or external forces such as wind load, accidental damage, eccentric gravity load, foundation movement, and thermal/moisture movements (Mckenzie, 2001). It is interesting to note that an increase in the height of masonry unit decreases the unit strength. Therefore, the taller the structure, the larger the deformation in the mortar, as more units have to resist the tensile force (Hendry *et al.*, 1997). The literature also indicates that the restrained deformation of mortar in the bed joints of masonry results in secondary tensile stress, which in turn leads to splitting of the masonry (Hendry *et al.*, 1997).

There are five different failure modes in masonry whose occurrence depends on the direction and magnitude of the normal and shear stress in the structure; shown in Figure 2.4 (Sarhosis, 2011; Chaimoon and Attard, 2007; Lourenço and Rots, 1997; Lourenço, 1996; Lourenço, 1994). The failure modes of masonry are:

a) Unit diagonal tension crack,

b) Unit direct tensile crack,

c) Masonry crushing ,

d) Joint slip ,

e) Joint tensile cracking.

From the reported experimental tests, the following points on the failure of masonry can be noted (Roca *et al.*, 1998):

- The micro-crack of the units and micro-slip of the joints generally occur when tensile strength of masonry is reduced by the applied lateral compressive stress.

- When masonry is exposed to tension-compression loading, failure typically occurs in both the units and joints, or in the form of sliding and cracking of the joints; leading to failure of masonry.

If tension is applied to a masonry structure, in the direction parallel to the bed joints, two types of failure can occur, namely 'vertical crack through head and bed joints' and 'stepped crack through head and bed joints'; as depicted in Figure 2.5.

Tensile strength of masonry under tension can be examined using two types of tests: 'Direct tensile strength' and 'Flexural tensile strength' (Sarhosis, 2011; Hendry 2001; Hendry *et al.* 1997; Jukes and Riddington, 1997; Naguib and Suter, 1991; Schubert,

1994). High initial suction rates of units can improve the flexural bond strength of masonry (James 1973; Sarhosis 2011).

(a) Cracking of unit in diagonal tension   (b) Cracking of unit in direct tension   (c) Masonry crushing

(d) Joint slip   (e) Joint tension racking
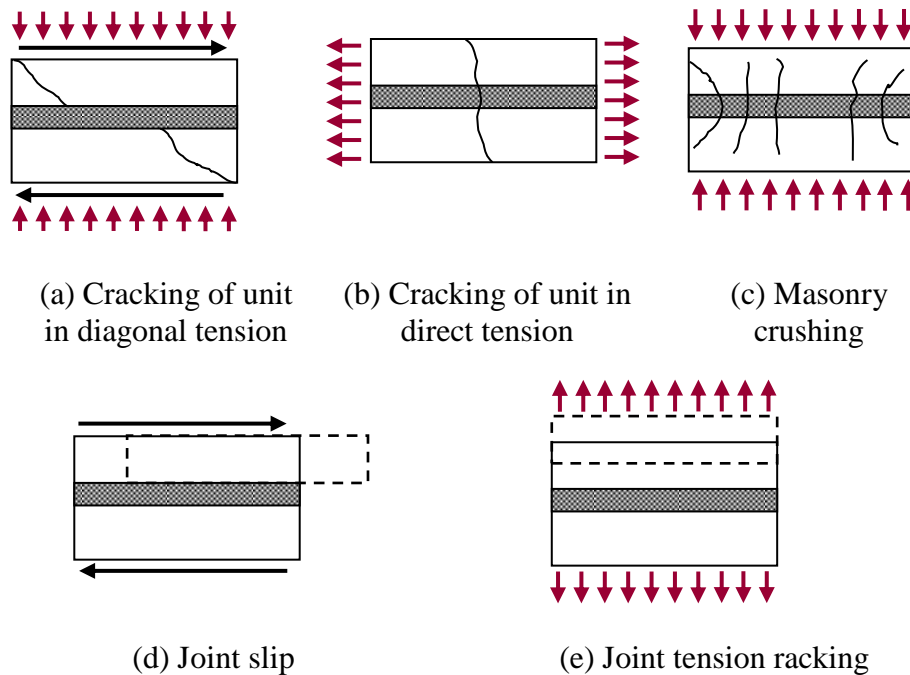
Figure 2.4: Different failure modes in masonry (Lourenço, 1996a).

(a)   (b)
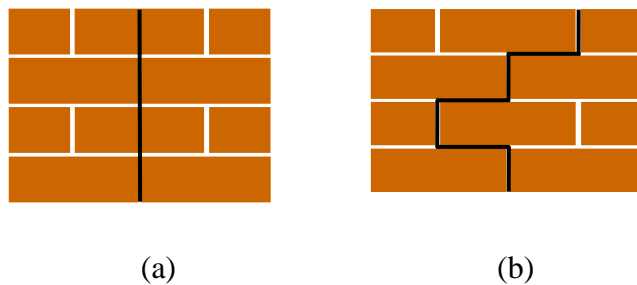
Figure 2.5: Typical failure diagrams for masonry under tension in the direction parallel to the bed joints: (a) vertical crack through head joints and units; (b) stepped crack through head and bed joints (Cecan 2012; Lourenço 1996).

2.2.2.3 Masonry in shear and biaxial stress

a) <u>Masonry in shear</u>

The shear failure is defined as the gradual damage of the cohesion in Coulomb friction models, subjected to normal compressive stress (Cecan, 2012; Lourenço, 1996). The shear strength of masonry is highly dependent on the strength and resistance of the unit-

interface bond, as well as the existing pre-compressions in masonry. The shear strength of the masonry joints depends on cohesion, friction angle and masonry assembly (Hendry, 1990; Mckenzie, 2001; Sarhosis, 2011). There are two shear failure modes for masonry: (a) vertical crack in the mortar and (b) failure at the top or bottom of the unit-mortar interface; shown in Figure 2.6 (Schlegel and Rautenstrauch, 2004).

(a)   (b)
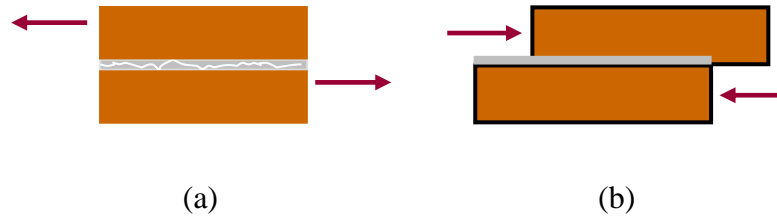
Figure 2.6: (a) Shear failure in the mortar, and (b) shear failure at the unit/mortar interface (Schlegel and Rautenstrauch, 2004).

More importantly, it is quite difficult to predict shear crack propagation. This is mainly due to the following reasons (Kim *et al.,* 2014):

- Crack propagation being dependent on the geometry of mortar joints,
- The complex stress state at the unit-joint interface,
- Significant difference in tensile strength between the mortar and unit.

Three different types of tests are often used to understand the behaviour of masonry under compression and shear, namely 'Direct shear test', 'Triplet test', and 'Van der Pluijim test'; depicted in Figure 2.7 (Jukes and Riddington, 1997).

(a)   (b)   (c)
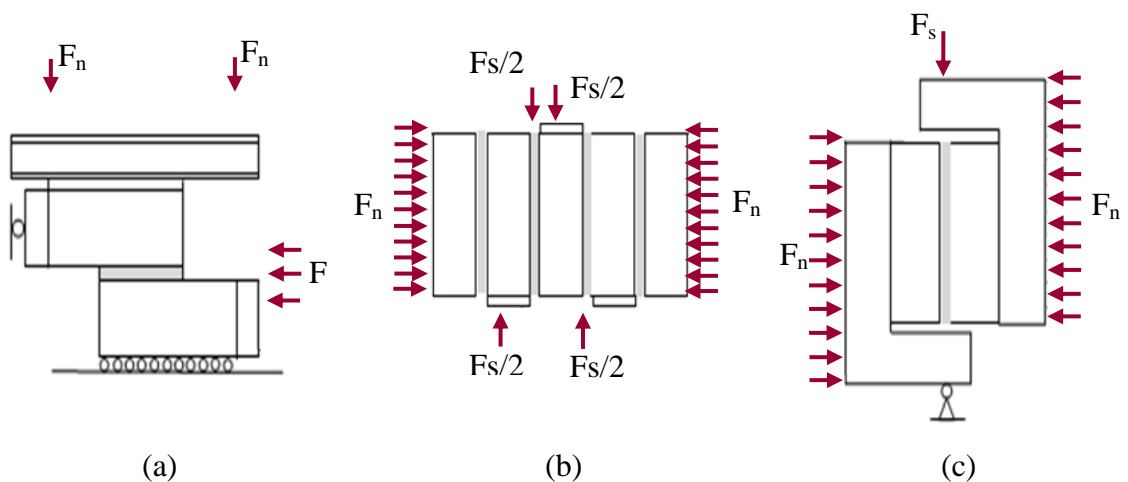
Figure 2.7: Types of shear test (a) Direct shear test; (b) Triplet test; (c) Van der Pluijim test (Jukes and Riddington, 1997).

b) <u>Biaxial behaviour of masonry</u>

Due to anisotropic behaviour of masonry, the influence of the biaxial stress state cannot be described only based on principal stress. So, a biaxial strength envelope is used. This envelope can be described in terms of either of the following (Roca *et al*., 1998):

- The principal stress; the rotation angle θ between the material axes and the principal stress,
- The full stress vector; in a fixed set of material axes.

'Uniaxial loading compression test', and 'true biaxial loading test' can be used to measure biaxial strength of masonry (Roca *et al*., 1998). Review of the literature on the above tests suggests (Roca *et al*., 1998):

- Masonry under biaxial compression load, in a plane parallel to masonry's free surface, generally splits at the mid-thickness (regardless of the orientation of the principal stress),
- Existing friction in the unit, mortar and the joints, increases the compressive strength of masonry under biaxial compression,
- Existence of various shapes, geometry and materials in masonry affects its failure modes and strength envelope.

2.2.2.4 Stress-strain behaviour of masonry

Masonry has an anisotropic stress-strain behaviour, which is characterised by the matrix strength of units and joints (Schlegel and Rautenstrauch, 2004). The stress-strain behaviour of masonry is non-linear and highly influenced by properties of its constituent materials (Brooks and Amjad, 1988). Considerable research has been carried out on the effects of different types of mortars on the stress-strain behaviour of masonry. It is understood that the stress-strain relationship for low strength mortar (historic masonry) is non-linear up to failure, whereas that of high strength mortar is linear up to failure (Brooks and Amjad, 1988). Such behaviour is evident from Figure 2.8, where typical stress-strain and stress-displacement relations are evident (Lourenço, 2014). This Figure can be used to determine and calculate mechanical properties of masonry:

- Compressive strength (σ_{max}); maximum value of the stress-strain curve

- Maximum Strain at peak strength (ε_u)

- Elastic modulus (E); the slope of the stress-strain between 30% and 80% of the maximum stress in Figure 2.8(a)

- The compressive fracture energy (Gc); the marked area in Figure 2.8(b) which will be explained further in details in Section 3.3.2.
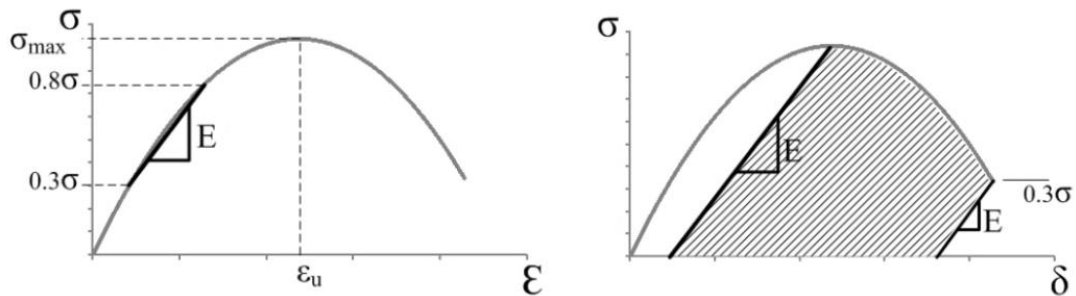
Figure 2.8: Typical relations for masonry of (a) stress-strain, and (b) stress-displacement (Lourenço, 2014).

2.2.2.5 Strain softening behaviour of masonry

Strain softening is an important and common feature of quasi-brittle materials such as masonry, and can be described as the "gradual decrease of mechanical resistance under a continuous increase of deformation forced upon a material specimen or structure" (Lourenço, 1996c).

Softening of masonry leads to induction of micro-cracks, which propagate when subjected to increase in load. Contributions of other defects such as shrinkage and creep (as will be explained in Section 2.4.1.2) and variety in strength and stiffness of constituting material parameters, increases the propagation rate of the micro-cracks. At the peak load, the micro-cracks start joining, and the accumulated effect leads into formation of macro-cracks. Increase in the load is directly proportional to propagation of macro-cracks and, therefore, localisation of crack and softening of the zone (Roca *et al.*, 1998; Lourenço 1996).

In addition to the explained complexity and variety of mechanical properties of historic masonry, other factors such as 'natural' and 'human' interventions, also have significant effect on their behaviour (Ashurst, 2012). These factors and their effects are explained in following sections.

2.3 Natural interventions

Throughout the history, nature has brought in its most destructive disasters upon cultural properties, in particular historic masonry. These natural disasters and causes generally fall into the following categories (Ashurst, 2012; Feilden, 1982):

- Ground movement: earthquakes, landslides,

- Wind erosion: hurricanes,

- Rain and water action: flood,

- Fire caused by lighting,

- Volcanic eruptions,

- Thermal stresses and frost,

- Rodent activity,

- Vegetation and root damage.

In the case of historic masonry, occurrences of one or more of the above causes combined with the effects of accumulated damage and strength reduction in structures increases the chance of failure in such structures (Feilden, 1982).

Historic masonry structures are extremely vulnerable to earthquakes and, therefore, are at great risk of sudden collapse when subjected to a seismic event. However, as seismic destructions do not fit in the main scope of this thesis, they will not be discussed here. Instead, one of the long-term agents of nature, 'the climate change', which greatly affects the cultural property of historic masonry structures, is discussed in the following section.

Climate change is thought to have direct and indirect effects on the natural and built environments (Sabbioni *et al*., 2006). The variety in climate means that structures at different locations of the world are affected differently by the climate change (Feilden, 1982). Significant research has gone into study of the climate change and its effects on historic structures; 'NOAH's Ark Project' (Weitzman, 1998) and 'Parnassus project' (Parnassus, 2013) are examples. The reported results suggest that parameters such as temperature, moisture (in the forms of rain, ice, snow and vapour clouds), soil conditions, radiation (in particular short-wave radiation), wind and pollution-derived parameters, play the most significant role in long-term erosion of historic structures

(Schloeglmann, 2008; Brimblecombe *et al.*, 2006; Feilden, 1982). Regardless of the source of erosion, deterioration in masonry structures can be divided into two main categories of 'short-term' and 'long-term', which are described in the following sections.

2.3.1 Short-term effects

The short-term effects are referred to those effects that occur in few seconds to few days. Examples of the most effective short-term defects include flooding, sea level rise and wind, which are explained below.

a) Flooding

Research has suggested that climate change may result in damper, more humid winters and drier, waterless summers in some parts of the World, leading to an increased risk of flooding. Moreover, local flooding is becoming more frequent, in urban areas and developing cities, due to the short strong rainstorms (Fudge, 2009). Alongside its economical and health-related effects, flooding has devastating effects on the natural and built environments. These effects can be summarised as follows (Binda, 2010):

- The structure being washed away; as a result of impact of water under high stream velocity,
- Inundation of the structure (no instant structural damage); however gradual penetration of moisture into the masonry, deteriorates the compositing materials (generally stone or concrete masonry),
- Complete scour of foundation or the earth under the foundation; due to high velocity of flood and hence collapse of the entire structure,
- Considerable structural damage can be caused via floating of debris.

Historic structures are particularly vulnerable to the effects of flooding. The cumulative effect of frequent rainfall events increases the height of the water table and can create the blockage of drainage systems (e.g. due to presence of garbage and other flood debris) (Salami and Adedeji., 2011) leading to further flooding.

Although the use of low permeable materials (e.g. sandstone) at places, where flooding is frequent, can be tolerated in terms of possible induced damages, but problems can escalate in the presence of surface treatment. It is important to note that if high

permeable materials such as brick are used at the presence of salt, a higher decay is expected (Binda, 2010). These defects can be reduced or even prevented by strengthening the structure, its foundation and the surrounding area, e.g. by planting trees near the structure to absorb the water of soil and foundation.

b) Sea level rise

It has been revealed that sea level rise depends significantly on the climate change and global warming. It has also been known that increase in temperature and thermal expansion of water, melting of ice caps, ice sheets and glaciers are all directly proportional to sea level rise. Any significant rise in the sea level mainly influences coastal structures, as their foundation is immersed in water. High exposure of these structures to capillary rise of salty water brings distresses of chemical and physical attack to structure. These stresses induce *cracking* and *spalling* of the rendering mortar, and deteriorating effects of *efflorescence* and *subflorescence,* in brick and stone masonry; these defects are explained in Section 2.4.2.2. Type and degree of these defects highly depend on the composition of masonry (particularly the mortar), its salt contamination and degree of porosity, and climatic effects such as relative humidity, temperature and wind levels and directions (Collepardi, 1994).

c) Wind

Different atmospheric pressures in the weather system induce wind, which can have variant speed at different heights, causing turbulence. So, the resulting effects on masonry, could depend on many parameters such as their geographical location (Feilden,1982). The wind that can carry and drive rain on façade of buildings, known as *driving rain* (explained in Section 2.4.2).

2.3.2 Long-term effects

Long-term effects are referred to the effects that take decades or centuries to appear in historic masonry monuments. Water in all forms (E.g. moisture, vapour, etc.), is considered as the most destructive long-term agent, particularly in combination with other effects (Feilden, 1982). A review of some of these long-term effects is provided below.

a) Driving rain

As mentioned before, frequent occurrence of driving rain (also known as wind-driven rain), affects cladding of historic structures. Depending on the severity and regularity of wind driven rain, and mechanical properties of the constitutive materials, the level at which masonry structures get affected varies.

Previous research and observations have revealed that most deterioration mechanisms are triggered by rainwater. This is evident as most damaged parts of monuments and historic structures are those exposed to the rainwater (Kvande and Lisø, 2009).

Structures with low porous materials can be damaged in the form of mould growth (structural damage), and damage to structure façade (non-structural damage) (Kvande and Lisø, 2009). However, materials with high porosity are at higher risks, as they retain the water from driving rain, and allow movements of salt solutions and chemicals through masonry pores. With time, the existing moisture in historic structures increases humidity of structure, leads to mould growth at the interior surfaces of structure, induces creep and creep-induced cracks in the masonry, etc., and in some cases eventual failure of the structure (Abuku *et al*., 2009; Kvande and Lisø, 2009). Further damages from the driving rain, can be prevented by applying suitable wind and rain barriers near the affected areas.

b) Variation of solar radiation

Change in the climate has major effects on variation of solar radiation, which in turn affects historic masonry structurally and/or non-structurally. Such variations in solar radiation cause spalling of the cladding, and cracking of the masonry. Some of the structural changes that are imposed by solar variations include: internal air volume of the structure, internal temperature of the structure (through windows and openings), and temperature of the constitutive material. The above effects are, in turn, influenced by (Feilden, 1982):

- The absorption level of surface of the constitutive materials,

- Surface colour of the constitutive materials,

- The angle of incidence of the radiation.

Similar to driving rain and wind, solar gain of structures varies with their location. For example, during September and March, solar gain in Scotland can be greater than places like Sahara. In such cases, solar radiation has higher destructive effects on structures compared with frost (Feilden, 1982).

c) Moisture

As pointed out earlier, moisture (being a form of water) has, by far, the most destructive effects on historic masonry by penetrating through its materials (Ashurst, 2012). Research has shown that structures constructed from adobe masonry, when exposed to moisture have lasted for almost a decade (e.g.in Nigeria), whereas similar structures have lasted for a millennium in desert (e.g. North Peru) (Feilden, 1982).

Moisture penetration highly affects the height of capillary rise in masonry structures. This height is mainly dependent on the following factors (Bingel, 1993):

- The pore size of masonry: the smaller the pore size, the higher the capillary rise,
- Moisture evaporation from the external surface: increase in evaporation rate reduces the capillary rise,
- Structure's age: the capillary rise increases with time. For instance, historic masonry structures generally have capillary rise of 4-5 metres.

Geometry of masonry structures has been known to have an effect on moisture movement strain (Brooks *et al*., 1997). Moisture penetration in historic masonry has consequential defects such as *crack*, *freeze-thaw*, *mould growth* and *shrinkage/expansion*; each of which is explained below.

Cracking

As mentioned before, macroscopic fracture in brittle materials such as historic masonry under uniaxial compression is caused by formation, growth and progression of the internal micro-cracks prior to loading. Cracks can occur in the masonry unit, mortar, and at the interface of masonry walls, and can continue through bricks in continuous paths. These cracks have major influence on resistance of historic masonry structures towards load (Tomor and Verstrynge, 2013;Cecan, 2012).

Pattern and number of cracks in masonry structures indicate the main driving factor of occurrence of cracks. Typically, several parallel cracks appear when compressive principal stress is the driving factor of crack formation. A single crack usually implies

tension as the predominant cause of cracking. In masonry subjected to tension, the largest flaw perpendicular to the principal tension initiates cracking (Kim *et al*., 2014).

As mentioned in Section 2.2.1, when normal stress is applied, masonry usually fails either in the mortar joints or at the brick-mortar interface. This failure is sometimes accompanied by frictional sliding parallel to head or bed joints (Garrity *et al*., 2010; Abdou *et al*., 2006). This behaviour is more evident in historic masonry, where the stiffness of the unit is significantly higher than that of mortar. Application of load to such masonry, causes triaxial compressive stress in mortar, which in turn increases local tensile stress in its adjacent units (Tomor and Verstrynge, 2013). Cracks can occur in various forms, including: horizontal, vertical, stepped, cogged, or a combination of these. Form of the crack usually indicates its cause. A summary of typical crack formation in the masonry assembly (both the stone and joint failure) can be seen in Figure 2.9.
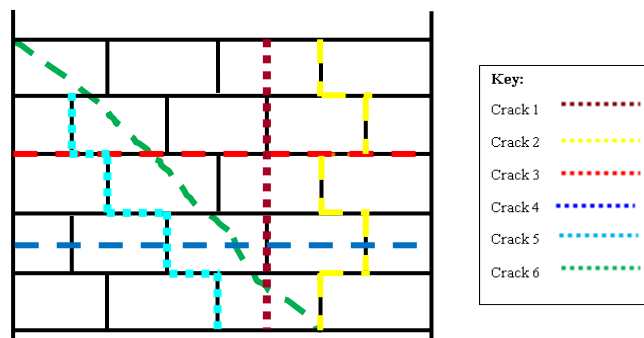
Figure 2.9: Typical cracks in masonry: 1, 4, 6 represent unit failure, and 2, 3, 5 denote joint failure.

Cracking in historic masonry can be induced due to factors such as (Sarhosis, 2011; Hendry, 1998; 1990):

- Movement/settlement of foundation,

- Moisture movements in materials,

- Expansion/contraction due to moisture variation,

- Cyclic change in temperature, freeze-thaw action,

- Chemical reactions in materials- such as chemical attack,

- Strains resulting from applied loads,

- Creep,

- Restarting natural movement of the structure.

Cracks in masonry can also be classified into 'active' and 'inactive' cracks. Depending on the initiation source of the crack, they may 'open' or 'close'. For example, cracks associated with cyclic change in temperature may open and close with different seasons. Occurrence and severity of cracks depend on repetitiveness of cyclic changes in temperature, the range of temperature change experienced by the building elements, rate of moisture penetration, and the coefficient of expansion of material (Rahman and Suter, 1993).

Cracks can appear in some structures without causing failure. However, continuous occurrence of opening/closing of these cracks can lead into propagation and increase in crack size. These cracks grow significantly with increase in the applied load (Tomor and Verstrynge, 2013). Cracks may also open and close with temperature over time, depending upon the types of applied stress. Combinations of different stresses on a structure can cause failure of structure (Garrity, 1995). Rapid and continuous increase of load leads to propagation of the micro-cracks and formation of macro-cracks, which can lead to eventual failure of the masonry structure (Cecan, 2012). The rate of crack growth (in width and length), is a clear indication of structure's state. For instance a fast rate of crack growth (much faster than effect of temperature variation), indicates a high risk of collapse, and, thus immediate action is required to prevent failure of a structure (Kim *et al*., 2014). If crack in masonry is not cured appropriately and on-time, it can put structure at risk in the long-term, potentially affecting public comfort and safety (Naguib and Suter, 1991).

Moisture-induced cracking can lead to structural damage. This, however, can be prevented by ensuring adequate waterproofing of the rubble foundation, as it prevents moisture penetration into parts of the structure. Generally, such structural damages can be reduced and perhaps prevented by minimising the amount of water penetrating, and separation of brickwork from possible sources of salts; by the use of appropriate materials, and careful design and construction (Vlasov, 2009).

In the case of historic masonry, where details of masonry used for construction are unknown, the existing cracks can be evaluated, through identification of the following items (Heritage, 2005; Clifton, 1986):

- Cleanness of the crack: dirty crack represents inactive crack, whereas clean crack is a sign of recent movement,

- The width of large cracks: the width depending on age of the building has different interpretations as to whether it is a rapid (in new structures) or slow settlement (in old structures). Cracks with a width of 0.2mm or more are classified as significant and, therefore, extra care should be taken while maintaining these cracks, as further propagation of such cracks can lead to failure of the masonry (Sarhosis, 2011).

Freeze-thaw

Constant change in climate and cyclic change in temperature and humidity, cause frequent expansion and contraction of moisture in historic masonry materials, particularly in the joints. This leads to formation of micro- and macro-cracks, resulting in loss of strength in masonry unit. Once cracks have formed (for instance on the exterior surface), factors such as leakage of air, and continuous penetration of moisture can lead to occurrence of freeze-thaw (Naguib and Suter, 1991). Cyclic appearance of freeze-thaw and propagation of cracks in a historic masonry structure and its foundation, results in reduction of its strength, making it more vulnerable to structural defects such as frost, salt crystallisation and further cracks (Vlasov, 2009).

Continuous accumulation of moisture in historic masonry structures, especially in areas under severe natural-climatic conditions, usually results in regular freeze-thaw process. Ineffective waterproofing or missing rubble foundation results in further moisture penetration into the structure; leading to deformation defects such as moisture movements during warm periods, and moisture freeze during cold periods of the year (Kralj *et al.*, 1991).

When constructing new masonry structures, freeze-thaw defects can be reduced by choosing appropriate masonry materials with low moisture absorption capacity. In the case of existing structures, the area exposed to the rain and the outside weather can be reduced. Special machines can also be installed to balance the temperature difference in the structure (Rahman and Suter, 1993).

Frost Action

Frost results from sudden change in temperature can cause structural damage (Kralj *et al.*, 1991). For instance, a sudden increase in temperature leads to low permeability of

the masonry matrix and formation of sealed container[1]. In historic masonry, this results into formation of high pressure on the ice inside the pores, induction of tensile stress in masonry matrix. Therefore, cracks form in masonry, causing consequential material damage (Kralj *et al*., 1991). Frequent occurrence of such cracks understandably leads to damage in the structure (Kralj *et al*., 1991). It is perhaps worth mentioning that frost action can be reduced or prevented by providing a rendered finish to the masonry (Bowler and Fisher, 1989).

Biological Growth

Biological growth on historic masonry is inevitable; some cause damage to the structure and some don't. However, biological growths such as mould and algae are problematic[2] (Eklund, 2013; Fudge, 2009). As mentioned before, the moisture content of an exterior surface of masonry is highly variable, depending on factors such as moisture absorption capacity of the surface material, severity of exposure to rain, and the possibility of condensation occurring within the external surface (Rahman and Suter, 1993). A summary of different types and effects of biological growth on historic masonry structures, are given in Appendix A (Eklund, 2013).

Shrinkage/Expansion

Depending on the type of masonry used, presence and movement of moisture causes shrinkage or expansion. Moisture expansion accounts for volume instability in masonry materials. Sever climatic conditions are the destruction source of approximately 76% of historic masonry cases (Kvande and Lisø, 2009). Masonry expands or contracts as the moisture contents vary at all stages of their existence (Hendry, 1990). As a result of continuous expansion and contraction of masonry materials, moisture movement induces strain in masonry[3] (Bremner, 2002).

Bremner describes shrinkage as "the time-dependent strain generated due to moisture loss at a constant temperature without a load". So, shrinkage is result of (Bremner, 2002):

---

[1] Sealed container: where the masonry matrix has a very low permeability (the larger masonry pores are filled with ice), hindering passage of water out of masonry.

[2] They are effects of moisture being adsorbed on outer surfaces and absorbed in inner surfaces of masonry structures.

[3] The total strain is dependent on the difference between the moisture expansion and shrinkage of the masonry.

- Thermal shrinkage: change in temperature,
- Carbonation shrinkage: reaction between CO_2 in the air and hydrated cement paste,
- Loss of damp and moisture, through:
  - Cement paste hydration
  - Loss of damp and moisture by evaporation
- Drying shrinkage: takes place in hardened mortar.

Reduction in moisture content of masonry, increases surface tensile forces. This compresses the material, reducing the overall volume of masonry. In the case of clay bricks, when masonry has dried out completely, despite the theoretical expectation (which predicts a return to the original size) further shrinkage takes place and is known to be irreversible; due to the carbonation effects (Bingel, 1993). Shrinkage of mortar in historic masonry reduces the unit and mortar bond strength. Defects caused by shrinkage influence concrete masonry, more than brick masonry (Kvande and Lisø, 2009).

There are a number of factors that highly influence the shrinkage rate of historic masonry; these are: moisture content, relative humidity, type of aggregate, mortar joint, volume-surface ratio, initial suction rate of brick, exposure time and, curing method (Bingel, 1993).

Research suggests that moisture induced defects in historic masonry structures can be prevented by applying a good drainage system and employing the two-stage tightening principle. Presence of natural ventilation in historic masonry also helps reducing the existing moisture content, and preventing further ingression of moisture in the structure. In the cases where natural ventilation does not exist, the change in climate, affects the internal temperature, moisture content and vapour pressure of the structure (Veterans Affaris Canada, 2010).

d) Thermal movement

Heat in a structure causes expansion and contraction of its materials; known as thermal movement[4] (Feilden, 1982). Usually all building materials show thermal movement, which depends on material's coefficient of expansion, and range of temperature experienced by the building (Bingel, 1993). The defects caused by thermal movements

---

[4] E.g. the expansion coefficients of clay brickwork it is 4-8 per $Cx10^{-6}$.

have a larger influence on concrete masonry compared to brick masonry (Kvande and Lisø, 2009). The expansion coefficient of each masonry type varies; thus, any variations formed in the temperature of brick or blockwork results in a tendency for differential movement between the unit and mortar (Bingel, 1993). Accumulation of small thermal movements in historic masonry, leads to other defects such as creep (Bingel, 1993; Feilden, 1982).

Factors influencing the thermal movement of masonry structures include (Feilden, 1982):

- Thermal expansion coefficient of the material,
- Material thickness,
- Material conductivity,
- Thermal capacity of the structure,
- Rate of moisture evaporation in porous masonry (varies according to exposure of structure to wind).

Thermal movement in historic masonry can cause internal stress in building materials, the level of which is dependent upon the following factors (Bingel, 1993; Feilden, 1982):

- Change in moisture content via evaporation,
- Elasticity of the materials,
- Creep capacity of materials towards the applied load,
- Magnitude of absolute change in dimension of the material,
- Degree of restraint as element connections, towards movement of materials.

The effects of temperature on stone masonry structures are often neglected, as they are considered to be minor, with respect to settlements, earthquakes or self-weight. However, these temperatures (though being low), can have negative effects such as formation of excess strain and stress (Iigo and Vicente-Tavera, 2002). Stone masonry has low tensile strength, and even small tractions can cause unexpected cracks. This is likely to happen when materials within a structure have large thermal differences, and are exposed to different thermal behaviours; causing strain and cracks in the joints, and spalling of masonry surfaces (Blasi, 2008).

This can lead to hazardous failure of parts of the structure such as buckling of entire panels of masonry veneers and claddings (Rahman and Suter, 1993). Figure 2.10 also

depicts spalling of the surface on roof of the church of Santa Maria Della Steccta in Parma.

The literature indicates that the stone surfaces used in historic masonry structures have much higher temperatures than the atmosphere. For instance, the readings taken on surfaces of Persepolis in Iran indicate rise in temperature of 2º to 34ºC in 6 hours with a maximum rise of 16ºC in half an hour. This leads to higher deterioration rate of the structure; as in case of the Persepolis the sharp outlines of the limestone reliefs are lost only within few decades (in comparison to the time where the structure was preserved by soil for approximately 2500 years) (Feilden, 1982).
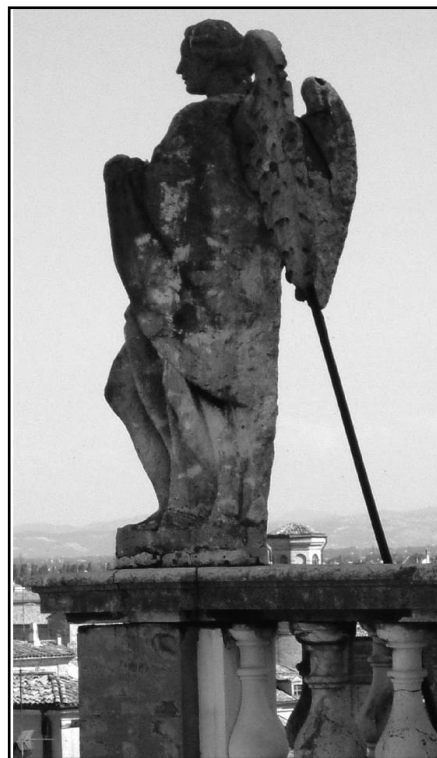
Figure 2.10: Roof statue of the church of Santa Maria Della Steccta, Parma. Note the induced gap between the supporting pillar and the statue base, as well as the supporting iron bar (Rahman and Suter, 1993).

e) Settlement, subsidence and heave

Historic masonry with openings are more vulnerable to settlement; cracks that occur at early stages, open and stretch out to a greater extend and show larger displacements (De Vent, 2009). The variations in the crack width along the crack length indicate the point, and not the direction of rotation. Therefore, a crack that is widest at the bottom can be associated to settlement below this point, or heave at one or both sides. On the contrary,

a crack that is widest at the top can be related to settlement at one or both sides, or from heave below this crack point (De Vent, 2009).

Subsidence and heave cause structural damage, in the forms of internal and/or external cracking. These effects can be more severe in the case of clay soils, due to its high reactivity to dry and wet periods; long dry periods have the greatest risk.

f) Salt-damp effects

In the long-term, penetration of moisture and upward movement of damp eases the deposition of salt in pores of masonry - the rate of which increases with change in temperature and humidity. Presence of hygroscopic salt available close to the wall surfaces can result in direct moisture absorption from the atmosphere. This induces high stress level into masonry, which disintegrates masonry's microstructure. Thus, excess pores are induced in the structure, which in turn increases the rate of crystal growth. Changes in humidity and temperature can result in the salts going through cycles of solution and crystallisation; causing the dampness to persist and fretting of the masonry to continue (Leif, 1982).

Further crystallisation of salts, can lead to deterioration of masonry. Distinctive defects of this phenomenon are 'exfoliation of stone', 'render of plaster' and 'erosion of the exposed masonry' (Bremner, 2002). Figure 2.11 shows a picture of a severe salt-damp attack on sandstone walls in the basement of a building erected in 1835.

Figure 2.11: A severe salt-damp attack on sandstone walls in the basement of a building (Bremner, 2002).

Other defects of salt-damp combination include '*Sulphate attack*', '*Efflorescence*' and '*Crypto-florescence/Sub-florescence*', which are briefly described below.

Sulphate attack

As mentioned in previous sections, the unit-mortar bond is the most significant interfacial zone with a region of high porosity, where sulphates and other chemicals enter masonry, and hence the term sulphate attack (Bremner, 2002). Sulphate attack explains failure of mortar, particularly the low-strength mortar in historic masonry, which is deficient in cement, or has been subjected to frost action during its early life (Bowler and Fisher, 1989). The sulphate attack causes a loss of strength and adhesion[5]. Literature also reveals that the pore structure variation in masonry due to the pressure induced by crystal growth in masonry (Bremner, 2002).

Efflorescence

When moisture, contaminated with dissolved salts, penetrates through pores of mortar or units, and/or between mortar and units interface, moisture can move through the masonry and reach its surface. Efflorescence takes place with formation of soluble salts (usually carbonates or sulphates) on the surface of masonry[6]; generally bricks or stones with low water absorption (Brick Industry Association, 2006). Adverse efflorescence is usually not harmful to brick masonry. However, under certain conditions, there is a possibility that the crystals of efflorescence are formed within the bodies of bricks. So, the growth of crystals and the resulting pressure can cause distress and cracking in masonry (Brick Industry Association, 2006).

Efflorescence generally occurs in relatively calm and dry air, and causes excessive wetting of mortar joints (Brocken and Nijland, 2004). It occurs when the following conditions are satisfied simultaneously (Brick Industry Association, 2006):

- Soluble salts must be present within or in contact with masonry units; they can be present in brick, mortar ingredients, backing materials, adjacent soil, and so on,

---

[5] As ettringite formation is the consequence of chemical decomposition of the primary products of cement hydration, calcium silicate hydrate and calcium hydroxide.

[6] Due to evaporation of moisture from masonry

- There must be a source of water in contact with the salts for a period of time sufficient to dissolve the salts,
- The masonry must be a porous structure that allows the migration of salt solutions to the surface or other locations where evaporation of water can take place.

In Europe, efflorescence has been observed on masonry structures for decades and has proved to be very persistent and difficult to remove in many cases (Brocken and Nijland, 2004). In the case of historic masonry, depending on 'type of the substrate material', 'type of the salt' and its 'age of appearance', efflorescence can be divided into the following four categories (Collepardi, 1994):

1. Late efflorescence of gypsum on clay brick masonry,
2. Early efflorescence of sulphates on clay brick masonry,
3. Efflorescence/wash out of lime on masonry.
4. Efflorescence of sulphates of lime on (coloured) concrete.

The most effective means of preventing and reducing efflorescence is to control and minimise the amount of moisture and salts that penetrate into brickwork. It is, however, almost impossible and impractical to prevent all soluble salts from penetrating into masonry materials, or to preclude moisture from coming in contact with masonry exposed to weather. Nonetheless, it is a realistic approach to reduce each contributing factor, in order to prevent their occurrence and, therefore, to reduce the severity of efflorescence. Controlling moisture as well as separating masonry units from sources of salts, is primarily achieved through careful design and construction (Brick Industry Association, 2006).

Usually efflorescent stain disappears after a heavy and prolonged rain. This is due to the high water solubility of the salts that are present in the efflorescence. If these salts originate from sea water, the efflorescence can appear again sometime after the rain. If the efflorescence disappears certainly after one or more rainy occasions, then it indicates that the salts were generated from masonry unit when exposed to rain (Collepardi, 1994).

Crypto-florescence/Sub-florescence

In fired-clay masonry, there exists a phenomenon called crypto-florescence, which is also known as crypto-efflorescence[7] or sub-florescence (De Vent, 2009). Crypto-florescence is described as "a harmful mechanism whereby various soluble salts, crystallise in pores below the surface of the brick" (De Vent, 2009; Forth and Brooks, 2000).

In masonry structures, normally when brick dries out, the existing salts are pushed to the surface of the brick. However, a situation could arise where the water evaporates before the salts gets to the surface. This is when the salts turn into crystals by getting deposited into the brick pores, forming a dried zone in masonry. These salts cause expansion, and so, an internal pore pressure below surface of the brick, at the interface of mortar bed joint and brick. The now-crystallised-salts spall the brick and in some cases result in removal of the whole brick surface; hence the term crypto-efflorescence (Bremner, 2002; Forth and Brooks, 2000; Harrison and De Vekey, 1998; Hardesty, 1944; Butterworth, 1933; Chin and Petry, 1993). Typical examples of efflorescence and crypto-florescence can be seen in Figure 2.12.

Figure 2.12: An example of efflorescence and crypto-florescence (Harrison, 1998).

The dried zone beneath the masonry surface, where crypto-florescence occurs is mainly affected by:

- The rate of flow of salt solution through the brick pores,
- And the water evaporation rate.

---

[7] The term refers to a hybrid of the words 'crypto' and 'florescence' that mean to lock-in and to bloom, respectively.

In other words, the dried zone is only created if and when rate of solution drain is lower than the rate of water evaporation[8] (Bremner, 2002; Forth and Brooks, 2000; Harrison and De Vekey, 1998;Hardesty, 1944;Butterworth, 1933; Chin and Petry, 1993).

There are several factors that influence the resistance of masonry towards crypto-florescence. These factors include the 'brick type' (which is a determinant of its construction material and directly relates to the water absorption and pore size), 'storage and curing conditions of masonry' and 'its volume/surface action' (Binda, 2010).

The main difference between efflorescence and crypto-efflorescence is that, the former occurs in the presence of plentiful water supply, whereas the latter happens when the water supply is limited (Hong *et al*., 2003; Harrison and De Vekey, 1998).

g) Exfoliation of stones

Exfoliation of stone can be described as "peeling, swelling or scaling of stone or mineral surfaces in thin layers". It is a result of weathering (both chemical and physical), extreme temperatures, and moisture, and leads to gradual deterioration and erosion of stone (Veterans Affaris Canada, 2010). When sandstone is in contact with other stones such as marble or limestone, and where sandstone is exposed to acid rain, the rate of deterioration increases. This rate can increase even further in the presence of cracks in sandstone (Veterans Affaris Canada, 2010).

Contour scaling is a type of exfoliation of historic masonry structures, which can happen due to continuous contact of stone with airborne pollutants. As a result of contour scaling, brittle crust appears on outer surface of the stone. With constant change in climate, moisture is trapped underneath this crust. In extreme cold weather conditions, this moisture freezes, expands and causes spalling of the outer layer of the stone. With cyclic change in the climate, appearance of counter scaling repeats, which means on every occurrence, new layers of stone spall. Stain can also appear on stones, as a result of deposition of clay or natural minerals on their surface (Veterans Affaris Canada, 2010).

---

[8] It is also interesting to note that Sodium Sulphate (Na_2SO_4), Potassium Sulphate (K_2SO_4), Calcium Sulphate ($CaSO_4$) and Magnesium Sulphate ($MgSO_4$) are all observed to be the likely salts causing these dried zones.

h) Creep

Despite numerous research carried out on historic masonry structures, several questions still remain on the long-term behaviour of such structures; particularly on damage accumulation and alteration of mechanical properties of ancient masonry under persistent heavy vertical loading for centuries (Verstrynge *et al*., 2008; Binda, 2001). A solid understanding of this behaviour is essential, as the creep behaviour and creep-fatigue interactions have proved to have significant influence on the behaviour of historical masonry structures (Anzani, 2000; Anzani *et al*., 1993).

Creep can be defined as "the gradual increase of strain in masonry with time under constant load" (Bremner, 2002). Creep occurs over a long period of time, and is not necessarily related to sudden change in the loading conditions of the structure (Tomor and Verstrynge, 2013).

Creep is mainly induced in historic masonry and in particular historic brickwork, as a result of penetration of the adsorbed water in mortar (Bingel, 1993). Cracks are normally observed in mortar[9], mostly in form of a series of vertical cracks through the vertical mortar joints and sometimes in masonry units (generally bricks) (Tomor and Verstrynge, 2013). According to Brooks "reduction of the mortar strength increases the creep stain and the same correlation exists for the stiffness of the bricks" (Verstrynge, 2010b).

Creep is often observed in structures with similar geometrical properties (slender or heavily loaded elements); mostly columns, pillars, churches, bell or medieval city towers. This is due to application of high persistent loading, the self-weight of the tower and consequently, the presence of high stress levels at the structure base (Grazzini, 2006). Moreover, in such structures, where multiple leaf masonry is present, non-homogenous cross-section causes non-uniform stress distribution (Pina-Henriques and Lourenço, 2003; Anzani, 2000; Papa and Taliercio, 2000).

Examples of sudden failure of historic masonry structures, subjected to creep, can be given as (Verstrynge, 2008; Anzani, 2000).

- 'Maagdentoren tower' at Zichem, Belgium, 2006 (Figure 2.13),
- 'Civic tower of Pavia', Italy, 1989,

---

[9] As there is high percentage of mortar present in brick masonry.

- 'Church of Keksken', Belgium, 1990,

- 'St. Magdalena bell-tower' in Goch, Germany, 1993,

- Partial collapse of the 'Noto Cathedral', Italy, 1996,

- Severe damage of the bell-tower of 'Monza Cathedral', Italy.

It can, therefore, be suggested that such collapses concern structures under high sustained compressive loading.

Masonry creep effects depend upon a number of factors, including stress level, material strength, and also temperature and humidity conditions. A combination of these factors, with the fatigue effects resulting from cyclic actions[10] and traffic-induced vibrations are known to result in synergetic structural damages (Lourenço and Pina-Henriques, 2008; Henriques, 2005; Anzani, 2000; Papa and Taliercio, 2000). The rate of moisture seepage varies according to the volume-surface ratio and strength of brickwork (high rigidity allows a lower rate of lateral spread of mortar) (Bingel, 1993).

(a)   (b)
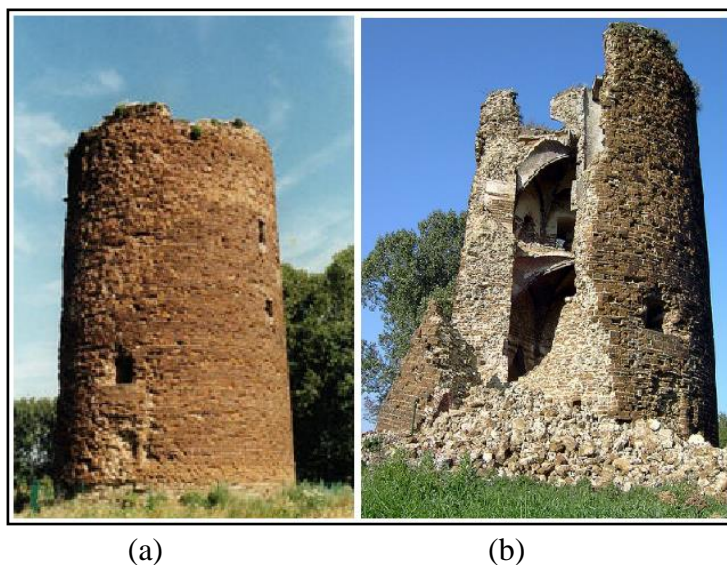
Figure 2.13: Magden Toren at Zichem, Belgium, (a) before collapse, and (b) after collapse (Flickr, 2013).

The exact effect of carbonation on creep damage rates does not seem to be well-understood. While Verstrynge claims that the carbonation process increases the strength of masonry, hence decreasing creep damage accumulation (Verstrynge, 2010b). Baˇzant and Feretti, state that carbonation process is one of the main causes of creep (Ferretti, 2006). Nevertheless, it seems that the stress redistributions (induced by carbonation),

---

[10] Examples of cyclic actions, are wind and temperature variations, carbonation shrinkage, thermal movement, drying shrinkage, and moisture expansion (Papa and Taliercio, 2000).

that initiate or develop the existing stress concentrations, which in turn trigger and propagate the creep effects (Verstrynge, 2010b).

In addition, the age of structure before the loads are applied, considerably affects the creep in masonry; increasing the loading age, decreases the creep rate (Brooks *et al*., 1997).

Experimental research results indicate that the creep behaviour in masonry under high persistent loading can be shown as a typical three-phase curve. As depicted in Figure 2.14, this curve indicates the increase in strain (ε_v) over time in masonry. The three phases are (Verstrynge, 2010b ; Lourenço and Pina-Henriques, 2008; Verstrynge *et al*., 2008; Garavaglia, 2006; Pina-Henriques and Lourenço, 2003):

- The *primary* creep phase (visco-elastic phase), which signifies the period of time[11], where reversible strain and deformation are developed with gradual decrease on strain rate in time (eventually evolving to zero).

- The *secondary* phase (visco-plastic phase), where the creep remains approximately constant. Strain development is dependent on the stress level and continuous deformation over a large period of time occurs with progressive damage accumulation.

- The tertiary creep phase (highly unstable behaviour): the accumulated damage during the secondary phase can develop to an unstable situation- creep/viscosity limit (Tomor and Verstrynge, 2013). This is when creep rate increases rapidly towards failure.

The secondary creep phase usually initiates when reasonably high stress levels are applied to the structure. At this stage, thin micro-cracks diffuse and propagate to form macro-cracks, leading to unstable crack development (Tomor and Verstrynge, 2013). This is when the tertiary phase initiates, resulting in creep failure in the structure. This phase is triggered by loss of material cohesion and hence damage accumulation in the material (in form of internal cavities), as it increases the strain of the tertiary creep. As these cavities grow, the stress accumulates in the damaged sections (Ashby and Jones, 2005; Verstrynge, 2009; Verstrynge *et al*., 2008; Binda and Anzani, 1993). The concept of creep can be summarised in Figure 2.15.

---

[11] In historic masonry, generally first couple of years during and after construction.
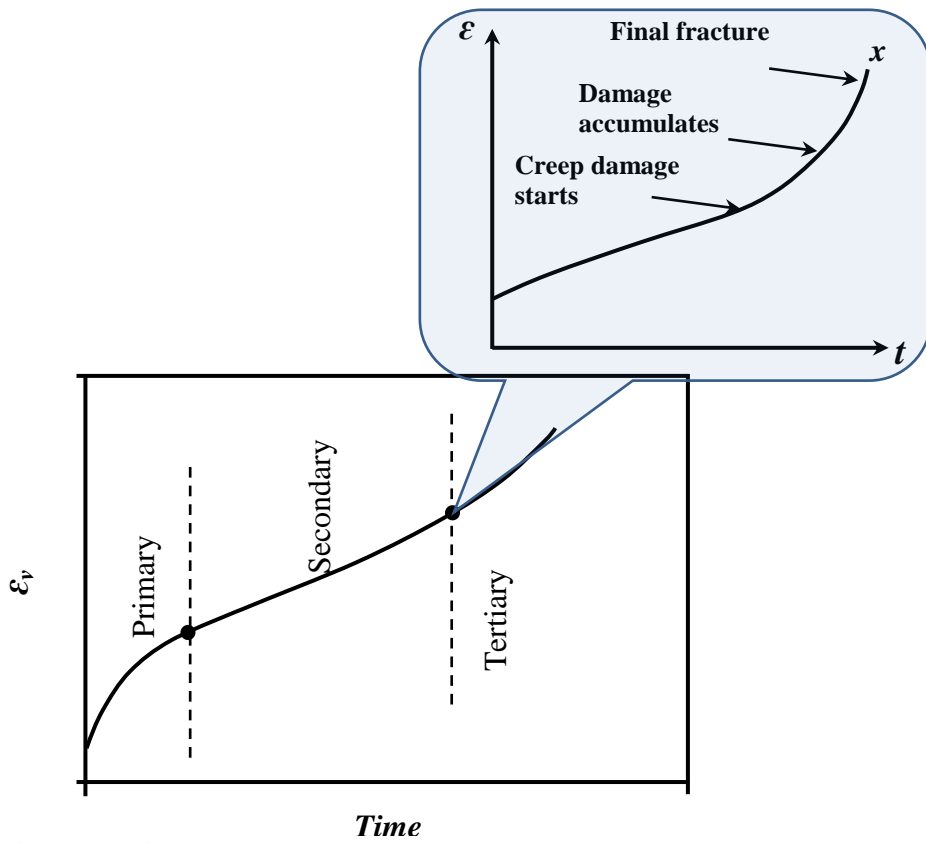
Time

Figure 2.14: Vertical **c**reep strain varying with time under constant uniaxial compression stress (Anzani, 2009).
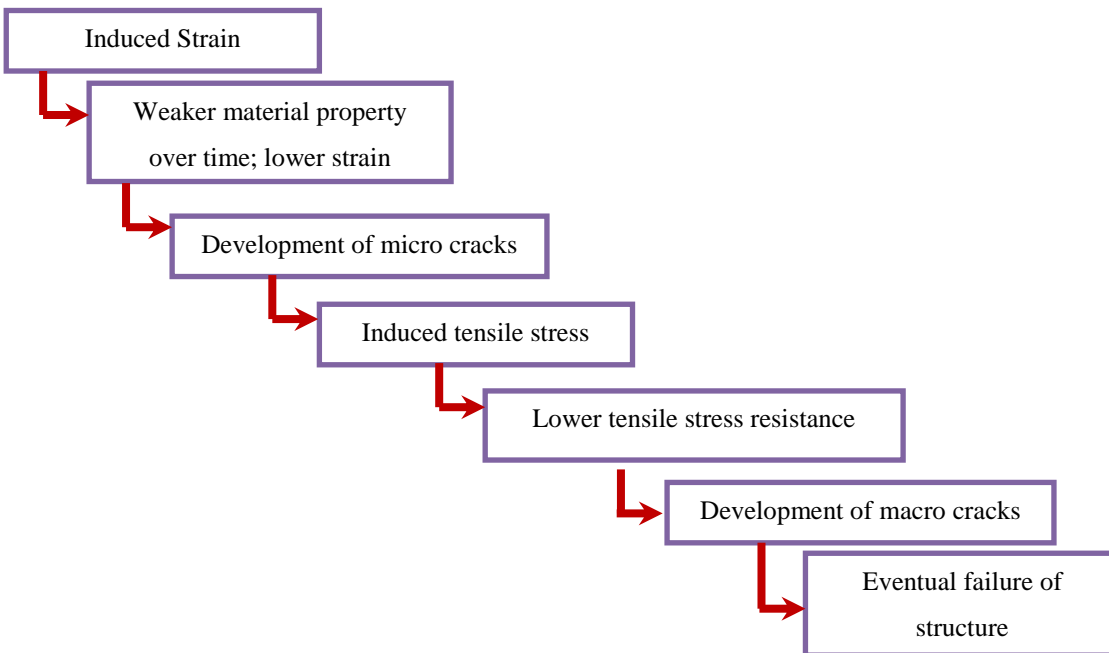
Figure 2.15: Concept of creep-induced failure in masonry

Two types of test have been carried out to measure creep in historic masonry over short and long periods of time. However, in this thesis, more attention will be paid to the tests carried out on obtaining information on long-term behaviour of historic masonry.

Masonry's time-dependent behaviour has been identified in several tests[12] including short-term or 'accelerated creep tests' (ACT), 'monotonic compressive tests' (MCT), and 'long-term creep tests'; these tests are briefly described below (Verstrynge, 2009; Binda, 2008a; 2008b; 1993; 1992; Porto *et al.*, 2004; Gentile *et al.*, 2002; Anzani, 2000; Binda *et al.*, 1991):

- Accelerated creep tests[13]: these tests are carried out to replace long term creep tests. ACT are carried out at constant load steps, where the applied stress is kept constant for a specific period of time (usually several months), and is then increased with a specific load increment; repeating the procedure until failure is achieved. This is to obtain a throughout description of the viscous behaviour of the constituting material. Results obtained from these tests are generally used to study the influence of the various loading velocities on the material resistance, and to capture both transient phenomena and the viscous creep phase of masonry structure.

- Compressive tests (CT): monotonic loading is applied in these tests (often treated as preliminary tests), where the obtained results are used to have an indication of the compressive strength of the material, and the peak stress and peak strain values.

- Long-term creep tests: a constant load is applied to produce a reasonably realistic set of creep results. Due to difficulties associated with these tests, they are often replaced by creep tests; explained earlier. There have also been statements that, due to high scatter in mechanical properties of historic masonry, these tests are inadequate for predicting the creep behaviour.

The above tests are mainly carried out to obtain the creep effects on strain level, under constant load. Other tests are also done to obtain the creep effects on structures (subjected to constant stress) with time (Kim *et al.*, 2012; Fan *et al.*, 2009; Taha and Shrive, 2006; Sayed-Ahmed *et al.*, 1998; Shrive, 1997; Shrive and England, 1981). The experimental tests have revealed that applying constant load steps, tests are easier to carry out[14]. It is also easier to detect a clear creep behaviour, and hence are a more

---

[12] Research also indicates that non-destructive techniques (NDT), such as Acoustic Emission (AE) and deformation monitoring techniques have also been used to detect damage accumulation, and monitoring the crack width of deformed sections in historic masonry structures (Verstrynge, 2010b).

[13] Also called step-by-step tests, short term or pseudo creep tests.

[14] As these tests need to be under constant loads and thermo-hygrometric conditions.

suitable and popular testing approach to use for creep tests (Verstrynge, 2010b; Binda *et al*., 2001; Anzani, 2000).

These tests can be accelerated by keeping the initial stress of the specimen close to the ultimate strength of the materials (Anzani, 2000). Application of the test load in steps can be seen in the stress (σ) versus strain (ε) curves shown in Figure 2.16 (Verstrynge, 2010b), where paths 1 and 2, represent short-term and long-term creep, respectively. The influence of different constant applied stress levels on the magnitude of the creep deformation (ε) in masonry is shown in Figure 2.17 (Verstrynge, 2010b).
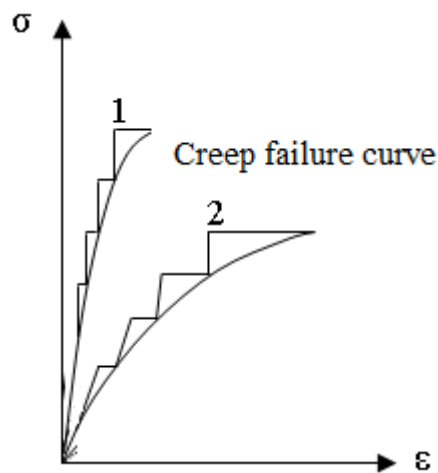
Figure 2.16: Principal of stepwise performed creep tests (Verstrynge, 2010b).
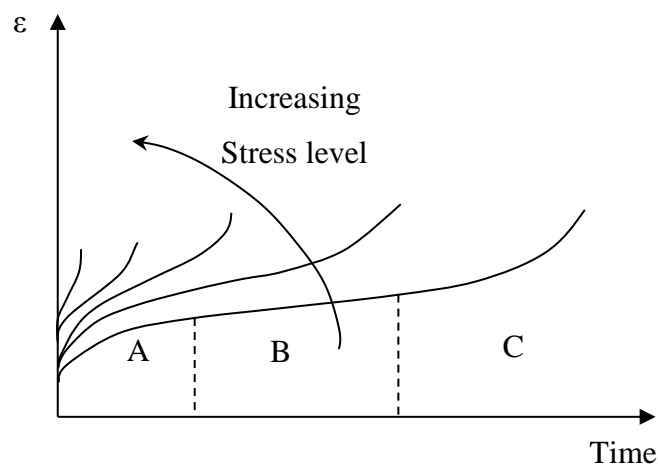
Figure 2.17: Influence of the increase in stress level on creep strain (ε) (Verstrynge, 2010b).

Verstrynge indicates that for such tests, based on the compressive strength of masonry, the stress limit for creep damage initiation for low- and high strength masonries ranges from 40-50% to 60-70% a respectively (Tomor and Verstrynge, 2013; Verstrynge,

48

2011). Also Verstrynge states that results obtained for masonry composed of air-hardening lime mortar and Diestian ferruginous sandstone, have the following stress levels[15], stated in Table 2.3 (Verstrynge, 2010b).

Creep-induced strains can have significant effect on historic structures subjected to long-term loading; in particular in cases where differential movements occur between constituent materials [16] (Hendry, 1990). During the creep formation process, due to compressive stress applied to structure, propagation of vertical crack leads to considerable increase in lateral deformation in time (Binda *et al*., 2001). Significant values of horizontal strain are also induced in the constituent materials, leading to dilation of masonry; an apparent increase in volume of masonry (Garavaglia, 2006; Binda *et al*., 2001). A sample of crack pattern in a pillar, due to creep, is shown in Figure 2.18.

Table 2.3: The relative stress levels at which various masonry's creep damage accumulation is initiated (Verstrynge, 2010b).

Masonry	Relative stress level (%)
Diestian ferruginous sandstone	40
Masonry with low-strength bricks and air-hardening lime mortar	45
Masonry with low-strength bricks mixed with hydraulic lime mortar, or hybrid lime-cement mortar Low-strength cement mortar	60-70
Concrete	80

---

[15] This table can be used to define the creep limit of these materials.
[16] Multi-leaf walls (clay brickwork and concrete block work) are examples where differential movement is likely to occur.
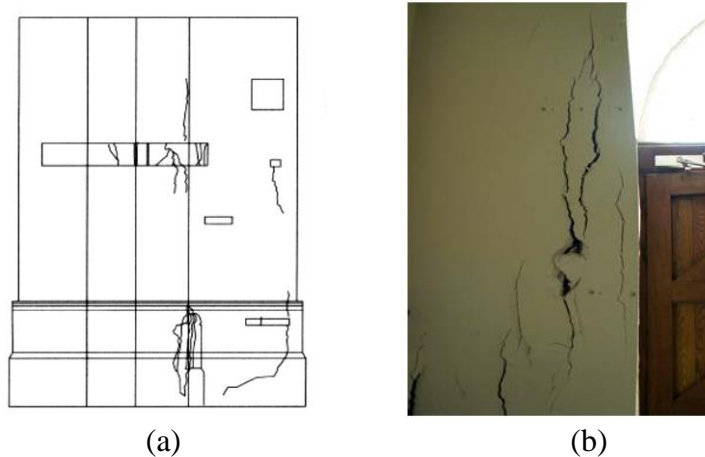
Figure 2.18: Creep-induced crack pattern of (a) a pillar in Annunziata church (Binda *et al*., 2001), and (b) the base of a bell tower; Saint- Willibrordus church in Belgium (Tomor and Verstrynge, 2013).

Mechanical, physical or chemical experimental works have also been carried out on several masonry blocks (from ruins of the collapsed structures) to study the time-dependent mechanical damages of historic masonry (Lourenço and Pina-Henriques, 2008). In addition to the above mentioned creep tests, 1-step tests have also been carried out in the literature. During such tests, to avoid other factors influencing the deformation of specimens, they were tested and stored in constant environmental conditions (Verstrynge, 2010b). Failure to keep these conditions constant has proved to affect the results. For example in the tests carried out by Verstrynge, it is noted that variation in humidity has caused non-negligible creep deformation on specimen, as humidity is main source of moisture transport (Verstrynge, 2010b).

It is interesting to note that amongst the damaged historic buildings under creep test, most structures had been made from stone masonry with multiple leaf walls, the inner leaf of which is constructed of brick masonry (Anzani, 2005a). However, since creep defects mainly occur in mortar and since there exists a higher percentage of mortar in brick masonry, compared to stone masonry. The majority of creep tests concentrate on historic brick masonry, rather than stone masonry. Thus, the creep experimental results used in Chapter 4, are mostly concentrating on historic brick masonry.

Some work has also been done on numerical modelling of the long-term behaviour of historic masonry structures. As will be seen from the literature review in Chapter 3, this is a very difficult and complex matter due to heterogonous property of masonry (Verstrynge, 2008). For further information on the time-dependent behaviour of ancient masonry, related experimental and numerical modelling information in the literature, the

reader can be referred to (Verstrynge, 2010b; 2008; Pina-Henriques, 2005; Anzani, 2003; 2000; Binda, 2008a; 2000; 1997; 1992; Mirabella *et al*., 1997; Anzani *et al*., 1993; Anand and Gandhi, 1983; Shrive and England, 1981; and Lenczner, 1969; 1965). The combined effects of humidity, creep deformation and age at loading has been modelled by Choi and Van Zijl (Choi, 2007; Van Zijl *et al,*. 2000). This is followed by modelling the effects of carbonation on this model by Ferretti (2006). However, advanced modelling of deterioration in masonry structures, creep and creep-induced cracking has not been yet modelled; hence the need for such modelling to be carried out in this thesis.

2.4 Human intervention

As mentioned in previous sections, natural interventions have a significant influence on durability of historic masonry structures. In addition to these, are the actions of humans, the damages of which are considered to be the greatest type of damage to historic masonry, and are high on the list of defects which lead to failure (Ashurst, 2012; Feilden, 1982). The causes of such damages can be listed as (Ashurst, 2012; Feilden, 1982):

- War and vandalism,
- Fire: significant increase in arson incidents,
- Stealing from the ruins,
- Mistreatment of structural elements,
- Neglect of people responsible for maintenance of structures,
- Inadequate design and maintenance.

The defects caused by human intervention can be reduced by advanced planning and continuous international cooperation. Some of the above damage causes as well as repair concepts and approaches in historic masonry structures are briefly explained in the following section.

2.4.1 Lack of maintenance

Conservation institutions, such as ICOMOS, register some historic monuments as cultural properties. Assessing the stability of these structures is one of the priorities of conservation institutions. The outcomes of such assessments have a major effect on the required level of action (ranging from monitoring to strengthening actions) and funding

allocation to preserve these structures. Since the funding for historic masonry is limited, their repair may require private donors. Consequently, the conservation industry faces the 'quick and easy' solutions for such maintenances (Verstrynge, 2010b; Gigla and Schlesinger, 2008). Structural analysis is, therefore, hugely favoured to help such organisations and industries (a) diagnose the defects, (b) carry out reliability assessment and (c) design interventions; based on which an efficient conservation is granted to monuments (Roca, 2010).

Towards this, other institutions (E.g. Structural Health Monitoring (SHM)), have been monitoring changes in structural behaviour of historic monuments, detecting damage at early stages and avoiding its further development; further information can be found in (Verstrynge, 2010b). Projects, such as Smart Monitoring of Historic Structures (SMooHS), has undertaken significant tests and modelling of historic masonry structures, to monitor and understand their behaviour, assess the existing damages, and also to apply the most appropriate repair. The numerical and experimental results are published in (Smoohs 2011). Other methods of projects have also been done to assess structures by using damage detective methods such as vibration monitoring. Examples of this method and its application on historic sites can be found in (Ramos, 2007).

Due to the limited or unavailable funds, in some case no or very little maintenance can be applied to structures, meaning that the defects cannot be prevented from occurrence and propagation. As change in climate worsens conditions of historic masonry structures, the structures that are not well maintained would face continuous destruction and eventual failure of parts or the entire structure. However, according to (ICOMOS, 1931), it is essential that such conservations are carried out on a permanent basis.

2.4.2 Repair

Conservation can be described as a process that leads to the prolongation of the life of cultural property (Feilden, 1982). The main philosophy of the conservation engineering[17] is minimum intervention to the structure, which means that while deciding the appropriate approach for conservation of monuments, the original material should be respected and priority should be given to the approach, which involves the least alteration, modification or removal of the original material (Gigla and Schlesinger, 2008). While carrying out such conservation, no attempt for new modification,

---

[17] Established in Europe in 1980s.

construction, demolition or moving of all or parts of the monument should be made; except where the safeguarding of the monuments demands, as stated in Article 6 and 7 in (ICOMOS, 1931).

The conservation and repair of historic monuments, has significant, yet countless challenge that have been the focus of research for the past decade. One of the greatest challengers is selecting the most suitable repair strategy with the policy of focusing on the agents of deterioration, such conversation, demands sound judgment and wise management of resources (Feilden, 1982). Understanding and following these policies calls for skilled and qualified analysts, who are able to combine engineering reasoning and advanced knowledge in the area. A humble and time-consuming approach should be adapted, and the following principals considered (Lourenço, 2002):

- Safety of the construction,
- Removability; reversibility seems to be an out-dated concept,
- Durability and compatibility of the repair material,
- Unobtrusiveness; respect of the original conception by means of minimum invasion and repair and,
- Balance between available financial resources and maintenance cost.

Some of the most common approaches undertaken to repair historic masonry are (Weeks and Grimmer, 1995):

- Replacing the deteriorated or missing parts, such as joints;
- Preventing water penetration,
- Repairing materials due to creep,
- Repairing and testing of the cracked sections,
- Grouting injection: to reduce the stress concentration and increase masonry's coherence and strength[18],
- Patching,
- Reinforcing (using recognized preservation methods),
- Confinement; applicable to columns where the lateral forces of the confinement increase the load bearing capacity of the column.

---

[18] Precautions need to be taken to balance out the injected water effect, to avoid instability of the structure.

Out of the above, rehabilitation of the joints is of significant importance, due to properties and effect of mortar on mechanical behaviour of masonry; as explained before. The effectiveness and durability of the repair intervention should be assured (Lourenço and Pina-Henriques, 2006). The importance of appropriate and frequent repair and strengthening work on historic structures has also been highlighted in the research.

The Venice Charter, states that 'Replacements of missing parts must integrate harmoniously with the whole, but at the same time must be distinguishable from the original so that restoration does not falsify the artistic or historic evidence'(Verstrynge, 2010b).

Research has been carried out across the world to develop and suggest appropriate maintenance mechanisms and techniques for historic masonry structures. Karimian has suggested various restoration and protection approaches on stone masonry structures in Kafer-Keli (Karimian *et al*., 2013). Similarly, Binda has carried out several repair works on historic masonry (Binda *et al*., 2001a; Binda, 1999) and has outlined a methodology for investigating a non-destructive technique (NDT) that has minimum intervention in the structure (Binda, 2009). Valluzzi also presents several works on repair (experiencing creep), describing the problem and suggesting intervention strategies (Valluzzi *et al*., 2005). Grazzini (2006) has also developed a methodology (mostly of an experimental nature), to pre-qualify the strengthening of historic mortars.

A clear example of inappropriate repair and intervention of a historic masonry tower can be given as Monza tower; for further details and examples of the above repairs can be found (Verstrynge, 2010b; Modena *et al*., 2002).

In some cases, however, the track of minimum intervention has been abandoned and adequate research has not been carried out on the structure (Gigla and Schlesinger, 2008). This could be due to any of the following reasons:

- Poor management and limited funds,

- The monument becoming a popular tourist attraction; due to high demand from the local economy on fast construction progress of the monument (the reader is referred to (Gigla and Schlesinger, 2008).

As in most cases, there are uncertainties on true cause of deterioration, identifying a suitable and durable repair is extremely challenging and often inappropriate form of

repair is applied. It is also important that appropriate information is provided after the repair, to guide and aid the future treatment.

Brief descriptions of the most common approaches for repair of historic masonry (outlined above) are given below.

a) <u>Replacement of the deteriorated or missing parts</u>

Considerable care should be taken when applying new materials to historic monument. The repairing materials should be compatible (physically, chemically) with the existing materials. i.e. the repair should match the existing material, in terms of material property, texture, colour and design[19] (Lourenço and Pina-Henriques, 2006; Porto *et al*., 2004; and Weeks and Grimmer, 1995).

As mentioned, historic masonry generally fails due to deterioration of the mortar, which appears in forms of cracks in mortar joints, or disintegration of the mortar. One or more of the following can be done to repair the mortar (Verstrynge, 2010b; Weeks and Grimmer, 1995):

- Removal of the deteriorated mortar; care should be taken by hand-ranging the joints to avoid further damage of masonry,
- Duplication of the old mortar; the new mortar should have the same colour, strength, compatibility, composition and moisture transport as the original one,
- Supplementary injection anchors (illustrated in Figure 2.19), can be used to act as a pre-stressed tendon or un-tensioned steel reinforcement (to compensate for the lack of tension resistance in the joints),
- Stainless Steel (Gigla and Schlesinger, 2008).

Based on the information gathered from literature on properties of mortars used in the historical masonry structures, the following mortars can be used for repair of the appropriate area (Sc Alf and Waldum, 2009):

- Air lime- based mortar on most building facades,

- Mortar based on both air lime and hydraulic binders (either of hydraulic lime or cement): used in extension sills, ornaments, retaining walls, etc. exposed to strong climate change.

It is important to note that for each monument, appropriate sand and mortar composition should be designed (Sc Alf and Waldum, 2009).

---

[19] Although, this should be done in a way that the new material can be distinguished.

Climate change defects such as moisture cycles and temperature loosen the new mortar from the unit. The repaired mortars, therefore, should have a restricted durability and should be continuously maintained to prevent further weathering of the stone and mortar, as well as to help with transfer of load in masonry structure (Verstrynge, 2010b).
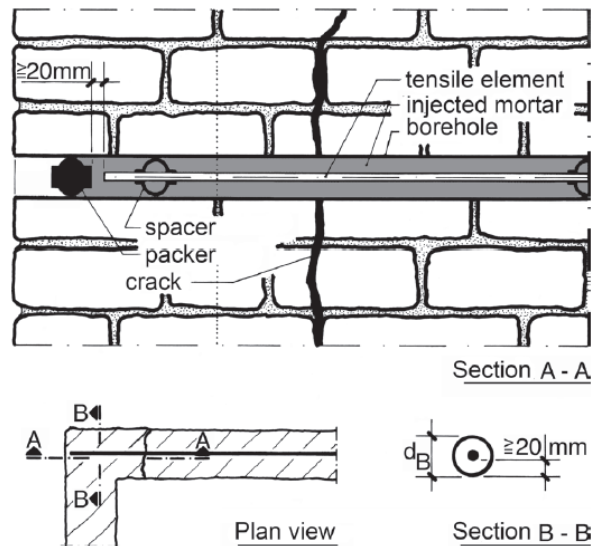
Figure 2.19: Supplementary injection anchor to be used in the joints (Weeks and Grimmer, 1995).

b) **Repairing due to creep damage**

As it has been concluded, many of historic structures suffer horizontal dilation, as a result of creep damage. Recently, the conservation industry has considered use of bed joint for repair of such structures. This phenomenon can also be delayed or stopped by joint reinforcement or confinement of pillar and columns with Fibre-reinforced plastic/polymers (FRP)[20] or stainless steel (Binda *et al*., 2001). This method is generally applied on stone masonry walls, constructed of regular unit arrangement with aligned horizontal bed joints (Lourenço and Pina-Henriques, 2006).

Moreover, after repair, creep in the original material will continue and may appear in the new material. The use of a computational tool, even after application of repair helps realising the effect of creep and time-dependent damages on repaired material, and enables development of a more retrofitting strategy to prevent further damage of historic masonry structure (Kim *et al*., 2014).

---

[20] Fibre-reinforced plastic/polymers are composite material made of polymer matrix reinforced with fibres.

It is important to note that upon maintenance and repair of historic masonry structures, previously repaired parts of the structure (such as plaster, cladding and rendering) should be checked for proper assessment of the repaired area. Otherwise, the existing cracks may remain unnoticed (Binda *et al*., 2001).

c) <u>Repair and test of the cracked sections</u>

Presence of cracks in historic stones used in masonry structures can be evaluated by testing the composite stones and/or mortar elements. Testing the bond characteristic for each structure is time-consuming, as usually mortars with different material properties are used in a structure (Twelmeier *et al*., 2008); an example of identifying the cracks present in a structure is given in (Binda, 2009). Rendering is a typical repair technique applied to the exterior surfaces of historic stone and bricks. The rendering procedure involves lime wash coating of repointing the natural stone masonry, and repair work on the exterior surface (Sc Alf and Waldum, 2009). In situations where masonry repairs have not been sufficient to prevent water prevention, water-repellent coatings can be applied (Weeks and Grimmer, 1995). Moreover, structures with 'active' cracks, should be sealed with flexible sealant. In particular, for cyclic cracks, appropriate sealants should be used and application of new mortar should be avoided – otherwise, further cracking will be induced (Web, 2000). The length and width of the cracks should be monitored; further propagation of crack's length signifies degradation of material, and increase in its width indicates impending failure of element or structure. In addition, appearance of new cracks, especially after an intervention, is an indicator of overload in that section; this calls for more intervention to prevent further cracking and perhaps failure of the structure (Kim *et al*., 2014).

2.4.3 Inappropriate repair

Research findings of RILEM TC[21] have revealed that the main causes of inappropriate repair was due to lack of knowledge of the constitutive materials, as well as inadequate workmanship skills. Moreover, the use of modern treatments and materials such as binders, are known to be the most common causes of damage.

One of the most important rules of repairing historic masonry structures is to avoid disturbance to appearance and function of the structure. If part of the monument is to be

---

[21] An institution carrying out repair on historic mortar.

replaced, appropriate physical and mechanical materials should be applied accordingly to model of the structure, to avoid further damage to the structure (Gigla and Schlesinger, 2008). This can be done by thorough understanding of the damage causes, before taking any actions on repair of the structure (Cullinane, 2012).

Applying various maintenances at different points in structure's life to has some effects on load resistance, material coherence or stress-strain distribution in the structure. In the cases where inappropriate maintenance is applied, the change in stress-strain distribution can endanger the stability of the structure, leading to further defects of the required part and in some cases failure of the structure (Porto *et al*., 2004).

A structure generally suffers further damage and deterioration where appropriate repair has not been carried out. A very common form of repair that affects the structure is patching the damaged section, without removal of the deteriorated part (Weeks and Grimmer, 1995). This repair generally applies permanent damage to masonry, as by sealing the surface, prevents moisture from vaporing out of masonry. Another example can be named as application of waterproof coating (such as stucco) on exterior surface of masonry structure. It is noted that inappropriate repair leads to further damage of historic masonry structures (Groot *et al*., 2004).

An important factor, when repairing historic mortar, is for the new mortar mix not have a higher stiffness than the existing historic material. This is because, in the case of damage to the new mortar, masonry deterioration and formation of cracks will continue until failure of masonry is reached (Cullinane, 2012). An example of formation of crack after repair is evident in Figure 2.20, after applying new mortar on the outer facade of the Liverpool Anglican Cathedral.

Another example of repair, where material coherence decreases is the restoration of the outer leaf of multi-leaf historic walls. Replacement of the outer leaf with new masonry causes disturbance in connection between the wall leaves. This means that the inner and outer leaves carry load separately, leading to failure of the wall with lower load bearing capacity.

Figure 2.20: Inappropriate repair on the outer surface of the Liverpool Anglican Cathedral has caused further crack and damage.

The example mentioned and the cases where the roof of historic structures are replaced, represent cases of disruption in stress-strain distributions (Verstrynge, 2010b). The appropriate choice of mortar for repair of historic masonry structure, therefore, needs to be made by an experienced engineer and mason. Material qualification tests should also be carried out on the structure to help with identification of the appropriate repair (Twelmeier et al., 2008). Towards this, the use of a computational tool where the repair can be simulated before its application to the structure would be a great incentive for predicting the durability and effectiveness of repair before its application on the structure. Should the repair be found inadequate, its material properties can be adjusted to obtain the most suitable and compatible repair for the structure avoiding the above problems. This helps to reduce and if possible prevent the costly and time consuming tests usually carried out on structures (Twelmeier *et al.*, 2008).

In the repair and maintenance of historic monuments, one or more different materials are used. Therefore, the same can be done in modelling such structures, to better understand the effect of such repair on behaviour of masonry structures; this is illustrated in Chapter 4.

2.6 Summary

This chapter has provided a review of the previous research on historic masonry structures and their mechanical properties, and also the effects of natural and human interventions on behaviour of these structures.

A summary of the principal findings are given below:

- The mechanical properties of historic masonry structures vary (even within the same structure), as it is an anisotropic, heterogeneous composite material. Such properties and the response of masonry due to applied loading are dominated by the mechanical properties of the mortar and the masonry units, the unit/mortar bond characteristics and the quality of workmanship.

- Most historic masonry structures were constructed of lime mortar. Therefore, in the work described in this thesis, the properties of lime mortar have been used in the computational model. As lime mortars have a lower Young's modulus than bricks or stones, tension and compression are evoked in the unit and mortar, respectively. The unit-mortar bond has a significant influence on the non-linear response of the joints under load and has a major effect on the load resistance, load transfer and cracking of masonry. The compositions, joint direction, type, suction properties and size and grading of the constitutive aggregates also have a major influence on the mechanical properties of mortar.

- Masonry has very rigid units and so, is highly resistant to compression. The failure mechanism of masonry can be named as shear failure of joints, tensile failure of units and joints, and compressive failure of the composites. Masonry has the failure modes of crushing, tension in unit, joint slip cracking and joint tensile cracking. Occurrence of these failures is influenced by magnitude and direction of normal and shear stress applied to masonry. A summary of masonry failures is shown in Table 2.4.

- The type of mortar influences the modulus of elasticity and the Poisson's ratio, and the lateral strain of masonry.

- Historical masonry structures are affected by natural and human interventions. Climate change is one the main forms of natural intervention and affects historic masonry structures over both short- and long-term periods. A summary of these effects, relevant types of damage and appropriate repair mechanisms are summarised in Table 2.5. Long–term effects of climate change lead to gradual deterioration of masonry, which appear in the form of exfoliation of layers and reduction in structure size, creep and creep-induced crack in historic masonry structures.

- Applying constant stress on historic masonry structures, can cause damage accumulation and increase in development of deformation.

- Masonry is understood to fail mainly due to growth and propagation of the internal micro-cracks prior to loading, which can occur in the mortar, at the unit-mortar interface, in the masonry unit, or a combination of these.

- Creep and fatigue can be described as time-dependent deterioration processes, under constant stress (stress level below the maximum strength of the material). Towards meeting the objectives of this research, focus is mainly on the experimental results obtained from creep test behaviour over long-term duration.

- The effects of creep are mainly visible in the forms of de-bonding and vertical cracks, and indicate possible signs of collapse. Factors such as temperature also influence creep rate.

- Creep presence leads to further formation of internal cracks. Combinations of creep and internal cracks, as well as other climate change defects (such as fatigue, moisture movement and variation in temperature), can considerably increase formation of micro-cracks. With time, these cracks propagate to form macro-cracks, reduce the residual strength, and result into structural damage and failure. This confirms the need for a better understanding of the structure's behaviour and appreciation of modelling the combination of defects (including creep and macro-cracking); thus hence being one of the main goals of the proposed computational tool. Table 2.6 summarises the effects of creep on various masonry structural compounds (Lourenço and Pina-Henriques, 2008; Verstrynge *et al.*, 2008).

- Human interventions cause the greatest damage to historic masonry structures; with the main ones being vandalism, fire, lack of maintenance (e.g. due to neglect of structures) and inappropriate repair. These damages can be categorised and modelled in two main types of external defects (loss of section), and internal defect (creep and creep-induced crack).

- Adequate knowledge of masonry constituting materials, can guide the conservation industry to appropriate and effective repair. The repair methods can be modelled in the form of adding a new material to the existing structure, to give one a better understanding of effects of such repair on historic masonry

structures. For modelling, such repairs can be categorised into external, and internal repair.

The above points on defects and sudden collapse of masonry structures are indicative of the importance of the need to be able to predict the residual life of massive masonry structures, which are mainly subjected to heavy dead loads.

Masonry materials are sensitive to construction sequence and change in geometry due to creep of structure and its foundation, which becomes of significant importance in historic masonry structures. Also, as such structures are exposed to climate change effects, a combination of defects such as creep, deterioration, etc., makes prediction of their life expectancy very difficult. Attempts have been made in simulating individual defects, but to the best of author's knowledge, no computational modelling has been provided to take combination of these defects (exfoliation, creep, and creep-induced crack) into account. Therefore, in this work special attention is given to creep and creep-induced crack, in Chapters 3 and 4. In addition, gradual deterioration and exfoliation of masonry structures is modelled.

In the next chapter, more reviews of the literature will be given on the computational modelling of historic masonry structures, including modelling approaches, strategies, techniques, and software packages. A review of previous modelling of historic masonry structures and their defects will also be provided, enabling a considerate selection of the most appropriate resources and techniques.

Table 2.4: Failure modes for masonry (Lourenço, 1996).
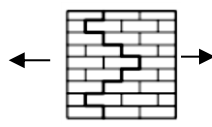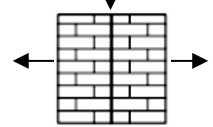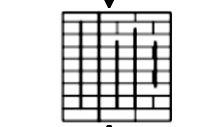
Uniaxial tension	Tension/ compression	Uniaxial compression

Table 2.5: A summary of defects of historic masonry structures and methods to overcome the damages.

Cause of damage	Damage type	Type of damage (Structural/ non-structural)	Methods to overcome the damage
Driving rain → Moisture	Mould growth	Structural damage	• Good drainage system • Application of separate wind and rain barriers)
Sea rise level → Moisture → Sulphate attack → Crystallisation of salts (salt-damp attack)	*Cracking* occurs due to chemical attack related to sulphate ions occur (with formation of ettringite and/or thaumasite).	Structural damage	• Adequate waterproofing of the rubble foundation to prevent moisture penetration into the foundation and sole sections of the walls
	Spalling of render mortar occurs due to chemical attack related to sulphate ions occur (with formation of ettringite & /or thaumasite).	Non-structural damage	
	Efflorescence occurs due to physical	Structural damage	• Minimise the amount of water that
	Attack related to crystallisation of salts within bricks and mortars causes efflorescence.	Structural damage	• Penetrate brick-work • Separating brickwork from sources of salts; accomplished through careful design, construction and material selection
	Crypto-florescence is concentration of soluble salts crystallising in the pores below the surface of the brick, creating internal pore pressure. As the brick dries out, the slats are drawn to the surface. If the water evaporates before the salts reach the surface, they are deposited in the pores of the brick as a crystallising salts result in spalling of the brick and, in extreme cases, lead to removal of the		

63

Cause of damage	Damage type	Type of damage (Structural/ non-structural)	Methods to overcome the damage
	whole surface.		
	Stone exfoliation: stones gradually deteriorate when exposed to the elements, resulting in erosion. Its surface and layers exfoliates and swells when exposed to moisture and freezing temperatures.	Structural damage	
Severe climate conditions → Moisture → Freeze-thaw	*Micro/macro cracks:* moisture penetration into the foundation material & brick masonry reduces their strength. Regular freeze-thaw gives rise to frost.	Structural damage	• Choose materials with a low moisture absorption capacity, • Reduce exposed areas to the rain
	Destruction with loss of strength in the brick masonry → appearance of micro- & macro-cracks.		• Reduce the possibility of condensation occurring within the wall.
Wetter winter & Short intense rainfalls → Flooding	*Washing away the structure-* due to the impact of the water under high stream velocity.	Structural damage	• Strengthen the foundation structurally & area surrounding it, • Strengthen the structure.
	Damage caused by inundation of structures- a structure may remain intact & stable on its foundation, while its material is gradually and severely damaged.	Non-structural damage	
	Undercutting of structure- the velocity of flood may erode the structure's foundation/the earth under the foundation, resulting in collapse of affected structures.	Structural damage	

Cause of damage	Damage type	Type of damage (Structural/ non-structural)	Methods to overcome the damage
	Damage caused by debris- massive floating objects like trees & materials from other collapsed house may have impact significant enough to cause damage to the standing structure.	Structural damage	
Shrinkage and thermal expansion/contraction	*Cracks*- depending on the coefficient of expansion & the range of temperature experienced by the building element, thermal movement occurs. This can cause distress such as spalling, cracking, & hazardous failures such as buckling out of entire panels of masonry veneers and claddings	Structural damage	• Installing machines which can balance the temperature differences.
Subsidence and heave	*Cracking*- Subsidence causes internal/external cracking → structural damage in case of clay soils (since reactive to dry and wet periods)- longer dry periods has greatest risk	Structural damage (particularly clay soil)	
Frost action	*Cracking*	Structural damage	• Provide rendering finish to resist the frost action.
Variation of solar radiation → Thermal movement	*Spalling*	Non-structural damage	
	Cracking	Structural damage	
	Buckling out of entire panels of masonry		

Table 2.6: Effects of creep on various masonry components (Lourenço and Pina-Henriques, 2008; Verstrynge *et al*., 2008).

Masonry Component	Effect of Creep
Weak mortar	• Large deformations; fails at short duration of time
Strong mortar	• Smaller deformations; fails at longer period of time • Creep rate initiates with a high rate and decreases with time
Cementitious materials	• Creep rate initiates with a high rate and decreases with time • Crack growth and inter-particle bond breakage due to moisture seepage • Sustained load; forced moisture redistribution, hence de-bonding and re-bonding of micro-structure

Chapter 3 : Literature Review (Part B) - Computational Modelling of Historic Masonry Structures

3.1 Introduction

This chapter builds on the principal findings of Chapter 2 by reviewing the research that has been carried out to develop computational models for historic masonry with a particular emphasis on the analysis of the effects of deterioration resulting in a loss of section (such as frost damage and exfoliation) and the long-term effects of creep including creep-induced cracking. A summary of how the effects of solar radiation, moisture change, thermal movement, etc., have been modelled is also briefly presented. The review also includes the modelling of repair measures together with a comparison of different modelling strategies and constitutive laws with a view to identify the most suitable computational tool.

The main structural defects that will be covered in this chapter are exfoliation (to represent loss of section), creep and creep-induced cracking in historic masonry.

Considering the characteristics and mechanical behaviour of historic masonry described in Section 2.3, the tool should be simple and accurate. The following criteria are used to select the most appropriate model to best simulate the behaviour of historic masonry:

- The capability of describing the geometry of real structures in terms of their overall form, mass, support measures and any external forces or stresses,
- The use of a constitutive law that is most suited to the type of masonry used in the original construction, to best describe the mechanical behaviour of the historic masonry,
- The option of providing the user with the capability of assigning more than one material property to randomly defined sets in a structure. This is to represent the existence of various materials used by masons over time (e.g. the different additional elements of construction added to a historic building over several decades or even centuries) as well as the modelling of repairs such as the re-pointing of mortar joints or grouting.
- The capability of taking into account the effect of any temperature variations including the gradual changes in annual temperature that can occur with climate change effects,

- The capability to capture any gradual change in the strength and stiffness of a structure or parts of a structure, representing the deterioration process,

- The ability to capture tensile failure of the masonry,

- The capability to simulate long-term damage caused by creep effects such as cracking,

- The ability to simulate the initiation of creep induced macro-cracks, and their subsequent propagation throughout the structure,

- The option to combine defects such as exfoliation (or similar losses of section) and creep-induced cracking,

- The ability to simulate post-cracking behaviour and failure of a structure (or part of it),

- The ability to predict the load-displacement and stress-strain relationships as a response to applied load for any part of the structure,

- To be capable of predicting a structure's behaviour with a satisfactory degree of accuracy and simplicity at an acceptable level of cost.

It is important to note that the computational tool which will be adopted in this chapter, does not aim to model the mechanical or chemical processes of the different defects that can occur in masonry but to model their outcome. It is also noteworthy that the knowledge of the required input properties in the model and the available experimental data, time requirements, the amount of financial resources and the experience of the modeller should also be considered when choosing an appropriate modelling strategy.

3.2 Modelling strategies and techniques

The following section attempts to critically review the literature to identify different types of material-based modelling, various modelling strategies, the available numerical modelling techniques and software packages. Figure 3.1 illustrates the modelling strategies that can be adopted in order to characterise the mechanical behaviour of masonry structures.
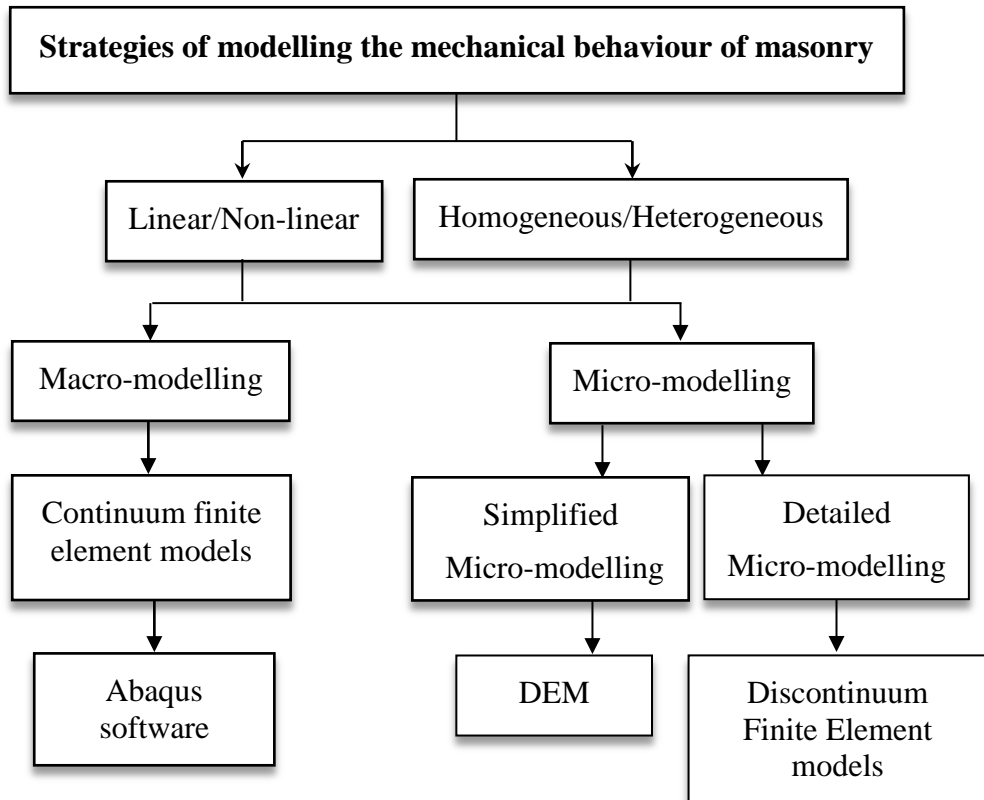
Figure 3.1: Modelling strategies of historic masonry structures.

3.2.1 Material-based modelling

Material behaviour can be considered as linear and non-linear. These are briefly explained below:

Linear elastic analysis

This is based on the theory of elasticity. It assumes that the material obeys Hooke's law. Since masonry under tension cracks at very low stress, this can be applied only to an analysis where the evolution of cracking is considered and a reduced stiffness is assumed for the fully cracked areas (Lourenço, 2002).

Where low tensile stresses exist in a masonry structure, the use of linear elastic material properties can help to accurately predict the behaviour of masonry structures under self-weight (Boothby *et al*., 2007).

As explained in Chapter 2, the stress-strain relationship for masonry is non-linear. A non-linear analysis is thought to be a suitable approach to simulate behaviour of masonry structures. However, Amjad (1990) suggests that since historic masonry has a brittle nature, non-linear analysis does not provide an accurate prediction of

unreinforced masonry under loading. He concludes that linear analysis provides more reliable results for modelling unreinforced masonry. Lourenco (2002) also stresses that linear elastic finite element models have been widely used for analysing historic structures. An example of linear analysis is described by Zucchini and Lourenço (2002), where a homogenous micro-model has been adopted.

Non-linear analysis

Non-linear analysis is known as one of the most powerful methods that can trace the response of complex structures (such as historic masonry) from the elastic range up to complete failure. It aims mainly to model pre and post-cracking behaviour. There are different types of nonlinearities (Boothby *et al.*, 2007; Lourenço, 2002), namely:

- Geometric: buckling of the structure due to instability
- Physical: non-linearity of the material
- Contact: addition/removal or change in support of contact between the bodies

Zucchini and Lourenço (2004) have used a non-linear approach to simulate a homogenous micro-model and to model the failure of a masonry cell under tensile loading applied parallel to the bed joint. A very similar approach was adopted in 2007 (Zucchini and Lourenço, 2007), to model historic masonry under compressive loading acting perpendicular to the bed joints. Other researchers have also proposed non-linear FE approaches for the analysis of the representative substructures (Genna *et al.* ,1998). This approach has also been adopted for modelling an entire structure in Pelà (2009).

Comparing the above categories, it is evident that both linear and non-linear analysis can provide reasonably adequate results depending on the modelling requirements. For the purpose of this research and, as the aim is to develop a simple computational tool, linear analysis seems to provide a reasonably well prediction of the general creep and behaviour of historic masonry (Lourenco, 2002; Zucchini and Lourenço, 2002). However, for simulating creep-induced cracking, a non-linear approach will be adopted; every effort will be made to choose the simplest constitutive law.

In addition to the above categories, there are two main techniques for modelling historic masonry structures. These techniques tend to be either 'homogenous' or 'heterogeneous' and are briefly explained below.

3.2.1.1 Homogeneous models

As mentioned previously, historic masonry is a heterogeneous material constituting two main components, each exhibiting very different material properties (Bull, 2001).

It is interesting to note, however, that masonry structures have been viewed as homogenous materials in most of the numerical analysis; shown in the form of average stress and strain, assuming an isotropic behaviour for mortar and brick (Roca *et al*., 1998). An appropriate constitutive law is commonly used in such technique to identify and describe behaviour of masonry (Cecan, 2012). In most cases, homogenous approaches are used in Finite element method (FEM)-based modelling packages, in the form of macro-modelling, to simulate the elastic-plastic behaviour of masonry. This enables one to model and analyse real masonry structures with an acceptable computational effort (Bull 2001). Examples of the use of homogenisation approach in modelling historic masonry structures can be given in (Al-Chaar and Mehrabi, 2008; Lourenco *et al*., 2007; Bull, 2001; Papa, 1996; Maier *et al*., 1991; Middleton *et al*., 1991; Pande *et al*., 1989), where the models are based on the definition of an equivalent continuum, and consist of periodic repetitions of micro-model of masonry unit and mortar. This micro-model is used as representative equivalent volume (REV), resembling a composite unit. Mechanical characteristics are defined for REV, to find an equivalent material property for composite materials with similar performance under application of load (Milani, 2007). These properties represent an average behaviour for the unit and mortar, so that the homogenised model has equivalent behaviour to the original composite unit. Figure 3.2 illustrates the schematic of homogenisation process in brickwork wall.

The use of this technique reduces memory and time requirements of computational effort and has a user friendly mesh generation, and is therefore, a very suitable approach for modelling large-scale masonry structures. This is, however, not adequate for detailed modelling and for capturing failure mechanisms (Lourenço, 1996).
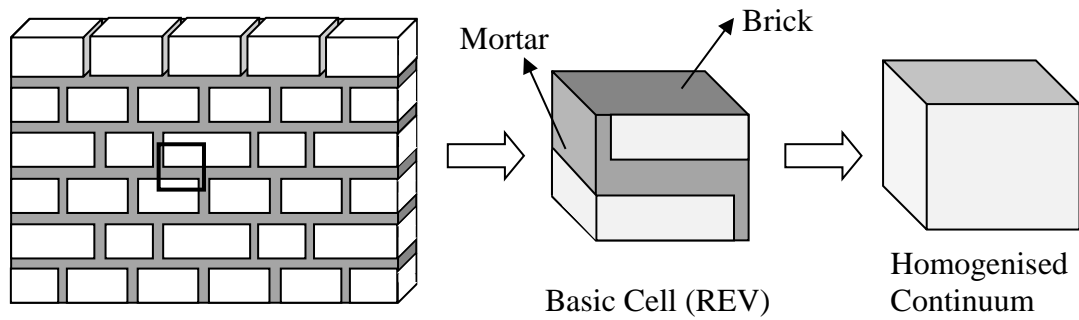
Figure 3.2: Schematic homogenisation procedure in brickwork wall (Maier *et al.*, 1991).

3.2.1.2 Heterogeneous models

Unlike homogenous modelling, in a heterogeneous model, all components of masonry structures (brick, mortar, etc.) can be modelled individually. The behaviour of each component can be replicated by application of appropriate constitutive law, that helps model the interactions between the two materials; unit and mortar (Usmani, 2010; Usmani, 2003; Bull, 2001).

The heterogeneous approach is used to model and analyse the stress distribution in a relatively small masonry specimens, and to provide the user with more accuracy in comparison with the homogenous approach (Bull, 2001). This approach also enables the modeller to reproduce the existing interactions between the two adjacent units. However, it has the drawback that an increase in structure size, results in a rapid increase in complexity of the numerical problems (Giordano *et al.*, 2002; Lourenço, 2002; and Bull, 2001). Example of using numerical modelling of historic masonry can be found in (Sarhosis, 2011; Lourenço *et al.*, 2006).

In heterogeneous modelling to represent failure of masonry units, the following two failure approaches have been introduced (Bull, 2001):

- Discrete approach: this approach uses reasonably sized continuum FEM that discretises brick and mortar joint and represents discontinuity of the materials, providing a reasonably accurate pattern of cracking.

- Smeared crack: represents uniform distribution of cracking, which has the drawback of inaccurate pattern in comparison with the discrete approach. In other words, this approach is founded on not being able to accurately define the

cracking pattern, but to create a consistent and uniform distribution of cracks inside the element.

Considering the above and the fact that the current study aims to model loss of section, creep and crack in the structure, the overall redistribution of stress and strain due to these defects and their combination is more evident using homogenous approach.

However, where the idea of repair is introduced with existence of more than one material, the heterogeneous approach will be adapted to model historic masonry.

3.2.2 Modelling strategies

Literature research reveals that currently macro-modelling is the most commonly studied approach in development of computational representation of masonry structures. Considerable research has also been carried out into individual modelling of masonry units or mortar. In other words, modelling of masonry structures can generally be categorised into two main classes of macro- and micro-modelling, (detailed and simplified micro-modelling) (Giordano *et al*., 2002; Lourenço, 2002). So, it is worth reviewing each category in nutshell, which can then be used to identify an appropriate modelling strategy.

3.2.2.1 Macro-modelling

In macro-modelling, masonry is treated as a homogenous anisotropic continuum, to indicate average stress and strain distribution in the structure; while it is assumed to have different elastic and inelastic properties along the material axes (Berto *et al*., 2002; Roca *et al*., 1998). This type of modelling does not differentiate between individual masonry units and mortar joints. Instead, it smears out the unit, mortar, and existing cracks (Sarhosis, 2011; Lourenço, 2002; Lourenço, 1996).

Complex geometries of historic structures often consist of parts (components) with enormous sizes (walls, vaults, arches, piers, etc.), for which two/three-dimensional models are usually employed. Use of macro-modelling assists the user to simplify the geometry and generate bigger mesh sizes, which in turn reduces the required memory size and storage, and simulation time of the structure. Moreover, due to simplification characteristic of this modelling strategy, the computational resources are reduced and analytical calculations can be carried out (Cecan, 2012; Giordano *et al*., 2002; Lourenço, 2002).

73

It is important to note that, this strategy should be used when the structure is composed of walls or parts with sufficiently large dimensions, so that the stress distribution across the structure is reasonably stable. However, it has the drawback of not being suitable for detailed studies and is unable to identify the weak areas and failure points of a structure. In such structures, locations of cracking and deformation also will not be evident (Cecan, 2012; Lourenço, 2002; 1996). Figure 3.3 represents a sample of macro-modelling.
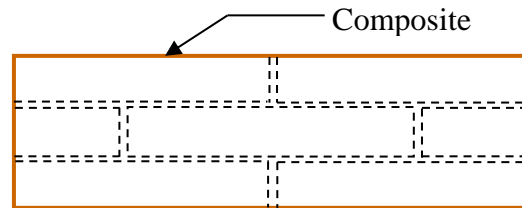
Figure 3.3: Macro-modelling; treating masonry as a composite material (Lourenço, 2002).

Examples of macro-modelling for historic masonry structures can be found in (Macchi, 2001; Lourenço, 1995). Lourenco (1995) has used this approach to present an orthotropic continuum model, which consists of a Hill-type yield criterion for compressive failure, and a Rankine-type yield criterion for tensile failure; making the following assumptions:

- Crack growth at micro-level, governs the failure mechanism of masonry structures loaded in compression and tension,
- Internal parameters related to fracture energy, can be used to model the internal damage which initiate each failure.

Localisation damage of a masonry wall has also been used macro-modelling (Massart *et al*., 2007). Andreaus states that even though using micro-modelling provides the user with a better understanding of failure mechanisms of the individual components and their interactions, only a macro-modelling of the entire structure can provide a realistic description of the overall behaviour of the structure (Andreaus, 1996). It is, therefore, highly dependent upon the user preferences, and the main goal and requirements of the research.

3.2.2.2 Micro-modelling

This approach is mostly used for small structures, and where modelling the interface between the components (unit and mortar), is the main concern of the model.

The micro-modelling approach (which is sub-divided into two classes of simplified and detailed approaches), is for modelling highly heterogeneous structures, such as historic masonry. This approach is used where there is a need for detailed presentation of masonry behaviour and a better understanding of its local behaviour (Cecan, 2012; Lourenço, 1996). It also enables the user to provide a specific geometry and characteristic of the model[22] , as well as its associated defects. Different constitutive models, geometrical and mechanical characteristics can be adopted for masonry components. A plane of weakness can also be used to model the interface between these components (Cecan, 2012).

It is known as a very useful approach for considering different failure mechanisms (Lourenço, 1995). It should be noted that, special care should be taken when modelling the masonry joints, as the crack propagation usually initiates from sliding of the joints. However, this approach has two main disadvantages (Giordano *et al*., 2002):

- The model requires large amount of initial data for modelling the materials and their interaction, and so, a high demand for computational resources,
- Extremely large numbers of elements are generated as the structure increases in size and complexity.

a) **Detailed micro-modelling**

As the name implies, detailed micro-modelling is probably the most accurate modelling approach available for simulating the real behaviour of masonry. This approach is used for presenting a detailed model of small specimens, and requires large computational effort and resources (Lourenco *et al*., 2007; Lourenço *et al*., 2006).

A suitable constitutive law is introduced in this approach, giving it the ability of illustrating a realistic behaviour of units, mortar and their interface (Sarhosis, 2011). In this method of modelling, both the units and mortar are treated as continuum elements. However, the mortar-joint interface is a discontinuum element, signifying a slip plane,

---

[22] Based on properties of each component and the unit-joint interface.

which has tendency to crack. The mechanical properties of unit and mortar (such as v, E, etc.) are also taken into account (Lourenço, 2002).

There have been many examples of using micro-modelling in the literature. For instance, in (Al-Chaar and Mehrabi, 2008) detailed micro-modelling approach has been used to analyse Mode-I fracture of brick masonry. Lourenço (1996) also presented a micro model, where a composite interface failure criterion was introduced. This included: (a) a tension cut-off for mode-I failure, (b) a Coulomb friction envelope for mode II failure, and (c) an elliptical cap mode for compressive failure.

The interface elements are also used for modelling potential cracks in the units. A detailed model of fracture in brick and mortar was presented by (Lourenço, 1996; 1995), using cohesive crack model. Figure 3.4 illustrates the concept of detailed micro-modelling for masonry.
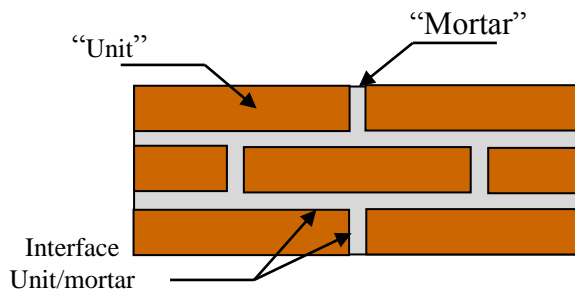
Figure 3.4: Detailed micro-modelling of masonry (Lourenço, 1996; 1995).

b) Simplified micro-modelling

In this approach, geometry of the masonry stays the same, through expansion of the units of masonry, as continuous elements. The joints (mortar and the unit-mortar interface) are lumped in together as an average interface, making it discontinuous elements. In other words, simplified micro-modelling allows modelling of masonry as a set of elastic blocks, which are bonded together by fracture lines (at the joints), as shown in Figure 3.5 (Cecan, 2012; Sarhosis, 2011; ; Lourenço, 2002; Lourenço, 1996)
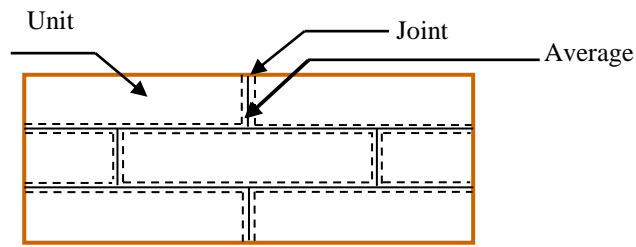
Figure 3.5: Illustration of micro-modelling of masonry (Lourenço, 1996).

Using this approach, cracking in the masonry units can also be simulated by assigning a vertical zero-thickness interface at the unit's centre line, as shown in Figure 3.6. In this method, initial location of the cracks can be specified, and crack propagation can be investigated. Also, since a reasonably simple approach is chosen, other defects such as creep (mentioned in Section 3.1), can be combined with crack.

The mortar's Poisson effect cannot be included in this type of modelling, therefore, accuracy is compromised; therefore, the behaviour of the unit-mortar interface can only be partially described. To compensate for this, it has been suggested that the unit should incorporate the compressive failure of masonry, as this involves the unit and mortar (Sarhosis, 2011).

It should also be noted that, increase in structure size, brings with it complexity to the numerical problem (Sarhosis, 2011). In addition, expanding the dimensions of the unit in this approach has an effect on the stiffness of the masonry units (in particular stone masonry), hence reducing the accuracy of the model (Sarhosis, 2011; Schlegel and Rautenstrauch, 2004). This accuracy can be obtained by adjusting the elastic properties of the 'interface joint' and 'expanded unit', so that correct simulation results can be obtained. Further information on this can be found in (Lourenço, 1996).
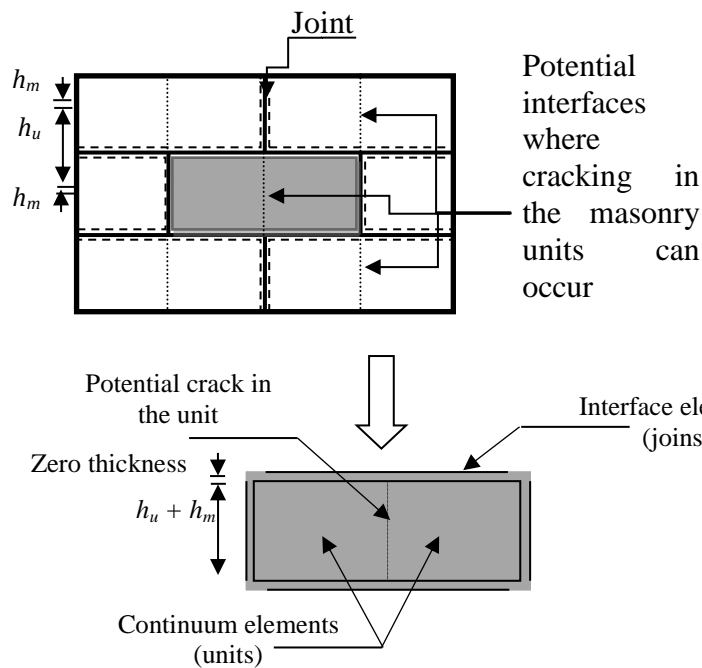
Figure 3.6: Simplified micro-modelling in masonry (Sarhosis, 2011).

Examples of where simplified micro-modelling has been used to model historic masonry, can be given as (Sarhosis, 2011; Zucchini and Lourenço. 2007; Lourenço and Rots, 1997; Lotfi and Shing, 1994; and Tzamtzis, 1994).

Having overlooked the above strategies, and since this thesis aims to model a simple masonry specimen, and not individual unit and mortars, micro modelling will not be adopted for this work.

For the purpose of this thesis, considering the existence of disordered networks of bricks, mortars and voids in historic masonry, and main concern of the modeller being stability and stress distribution of the entire structure, reduced time, and memory and mesh generation, macro-modelling is more practical and applicable. as well as different fields of applications of these strategies and techniques (their advantages and disadvantages), the author has decided that homogenous, and macro-modelling can give a simple, yet good understanding of small masonry structures, based on aims and objectives specified in this thesis. Although using this approach, the interaction between the components cannot be incorporated, but a realistic relation between average stress and strain is established.

Moreover, as combination of defect is one of priorities of this tool, macro-modelling can assist the user to achieve a realistic description of this defect and their effect on

overall behaviour of the structure. Due to its simplicity and accuracy, this strategy can be applied to bigger structures. It is also believed that in compensation for the lost accuracy, the overall applicability of the formulation, and computational efficiency and simplicity will be achieved. Heterogeneous material will be assumed, where repair is being applied to the structure. Accuracy can be improved by increase of memory, change mesh parameters, where there is less limitation on time.

3.2.3 Numerical modelling techniques

There has been an increase in modelling historic masonry structures. However, due to complex nature of masonry, difficulty in obtaining data, and hence suitable material parameters, and selecting the appropriate constitutive law, modelling these structures faces considerable difficulties.

The main methods available for modelling masonry structures using micro-modelling approach include 'Discrete Element Method (DEM)' and 'Finite Element Method (FEM)'. These methods are reviewed and compared, based on their efficiency and ability in representing a realistic simulation of masonry and in specific historic masonry structures. The suitable software for such modelling are reviewed and the most appropriate software fulfilling the main modelling aims of this thesis will be chosen.

In order to take the study of the structure further, numerical modelling of the structure can be carried out. The correct choice of masonry model is the key to a successful numerical analysis.

3.2.3.1 Discrete element method

The discrete element method (DEM) is an effective method to model the actual distribution of blocks and joints in a single structural element, as the behaviour of some materials (e.g. masonry and granular soils) cannot be simulated accurately by using continuum methods. Realistic results can therefore, be obtained by dividing the structure into several bodies, where contacts with various conditions and interaction properties are used in between these bodies (Jing and Stephansson, 2007; Giordano *et al.*, 2002). Finite displacements and rotations of the individual units or interface are allowed, and new contacts between the particles are identified and updated as the calculation proceeds. This approach gives reliable simulation of crack pattern and an estimation of the crack width (Sarhosis, 2011).

There are various branches for DEM, named as: 'Discrete-Finite Element Method[23], 'Distinct Element Method', 'Particle flow model' and 'Discontinuous Deformation Analysis (DDA)'. DEM has been implemented into a computer program called UDEC/3DEC software (Cecan, 2012). UDEC has the ability of handling compatible meshes and large displacements.

In terms of modelling historic masonry structures, DEM is a suitable method to model the actual distribution of blocks and joints in a single structural element. It is also used for simulating discontinuities and in specific where the main concern of the structure is to focus on mortar and unit-mortar interface. Further information on the background and examples of this approach, literature can be found in Giordano *et al.*, (2002). In addition, for a review of the application of this in simulating interface of historic masonry the reader can be referred to Sarhosis (2011).

The advantage of this technique are mainly its (Giordano *et al*. 2002):

- Suitability for parallel processing,
- Same algorithm for statics and dynamics,
- General and robust: non-linear materials and large displacements,
- Low storage,
- Simple to code

However, the software currently have their drawbacks mainly in dealing with complicated constitutive models of the internal elements of deformed blocks, thus research is still continuing on these topics.

This approach is also suitable where focus of the model is on behaviour of the contact between the bodies. It is however, not accurate for the study of stress states within the blocks. Further information, description and comparison of different approaches for modelling historical masonry structures, is presented in (Giordano *et al.*, 2002).

Since, a simple masonry specimen (consisting both unit and mortar) will be presented in this thesis and concentration will be on combination of different defects and their effects on stress state within the internal parts of the block (not the interface between the unit and masonry joints), DEM is not appropriate for use in this research.

---

[23] The blocks are represented using traditional continuum elements, linear or non-linear, whereas, interface elements, in this case the 'joint elements', are used to simulate the mortar joints; more information in (Jager & Vassilev, 2009; McKibbins, *et al.*, 2006).

3.2.3.2 Finite element method

Finite Element Method (FEM) is a continuum numerical modelling technique that can be explained as a process that analyses the structure by splitting it into small elements to describe the behaviour of each element. These elements are connected with each other using nodes, creating a grid called mesh; providing a better understanding of location of stress concentration. The loading history of structure is simulated and the state of stress and strain is updated step by step (Cecan, 2012). From engineering prospectus, FEM is known to be a very popular, due to being cost effective, flexible and practical (Liu and Quek, 2003).

The structures involved in civil engineering, especially historic masonry structures usually involve very complex geometry, materials (non-homogeneous and anisotropic), and connections. These structures have also experienced various actions and alterations with time, some that can be referred to as 'damage'[24]. FEM is known as a standard tool for modelling masonry structures. It helps the engineers present a realistic and accurate description of the mentioned complexities historic structures may have, as well as damages they might have or are facing (Bull, 2001; Pela *et al*., 2010).

Giordano highlights that in order to minimise the degree of inconvenience and for the sake of simplicity, essential assumptions from understanding the structure's behaviour, need to be made. Assumptions such as considering masonry as a homogenous material, can simplify the complexity of historic masonry structures (Giordano *et al*., 2002). The reader can be referred to (Johnson and Thompson, 1969), for further information on the literature of FEM theory and its mathematical concepts.

Numerical modelling of masonry structure, using computational software and FEM is very difficult task. This is due to the following reasons of (Anzani, 2009; Giordano *et al*., 2002):

   i.   Simplified static schemes of masonry cannot fully be carried out due to characteristics of masonry,

   ii. Difficulty in predicting the non-linear mechanical behaviour of masonry,

   iii. Uncertainty in calibration of numerical models due to lack of reliable experimental data.

---

[24] Some may be cyclic and repetitive (such as change in temperature), or may develop gradually (e.g. creep) and show their effects in long period.

Considerable research has been undertaken, using FEM for modelling masonry, some of which are arch bridges, some of examples and reviews of which can be found in (Cecan, 2012).

FE software selection

A good computational tool is one that is user driven, adoptable (to existing structures), customisable (in terms of material properties, loading and boundary conditions, etc.), dynamic and flexible. This is essential as in any structure; there exist various parts, conditions and material properties etc. that need to be modelled.

The software should be powerful to carry out solutions for sophisticated engineering problems. It should be cost effective, provide user friendly input and output formats and ease model construction. In doing so, three finite element packages of ANSYS, Abaqus and DIANA were reviewed on their capabilities for modelling continuum concrete and masonry structures, their units and interfaces, as well as discontinuity such as mortar joints.

For modelling historic masonry structures, the defining parameters for selecting the software, are ability of the software to simulate degradation of material properties with time, creep behaviour, crack initiation and propagation (in masonry units and interfaces). In addition, ability of the software in combining these defects in one model is of specific interest. Amongst this software, Abaqus is the most powerful engineering simulation modelling package with vast range of abilities. It is known for its abilities to solve linear, non-linear, explicit and multi-dynamic problems. It also uses the extended finite element method (XFEM) which allows for initiation and propagation of the crack, as well as combination of creep and crack. Based on these criteria, Abaqus was identified as the best software to fit the purposes of this study. It has also previously been used by many researchers to simulate the structural response of masonry, and is known to offer great flexibility towards modelling historic masonry structures (Huebner, 2009; Al-Chaar and Mehrabi, 2008; Chapelle and Bathe, 2003; Liu nd Quek, 2003; Hendriks M.A.N., 2002 ; and Bisagni, 2000).

The simulations are carried out in Abaqus/CAE, which is an interactive, graphical environment for Abaqus that allows for a quick and relatively easy input of information through graphical interfaces. The software also has a keyword edition, where codes are used for modelling and running the analysis. The software also has user-specified sub-

routines that allow for high flexibility in terms of specifying details of material and mechanical behaviour.

From the above information, it can be summarised that DEM is suitable for study of rigid body motions. It is also very good at illustrating discontinuities. On the other hand, FEM offers a good representation of the stress state of elements. However, majority of FEM-based software packages, do not simulate crack and only illustrate discontinuities with damage models; only software, such as Abaqus provide options for simulating damage in form of crack.

It can therefore, be stated that FEM and Abaqus are the most suitable technique and software to be used for modelling historic masonry structures.

3.3 Constitutive law and previous modelling of masonry structures

In this section, the existing constitutive laws as well as previous modelling of historic masonry structures will be briefly summarised and critically reviewed, with particular emphasis on identifying the most suitable constitutive law to be used in developing this computational tool.

3.3.1 Constitutive law

Constitutive law is a mathematical description of actual and essential material behaviour, mainly in terms of mechanical and strength features.

There have been recent FEM-based approaches in the literature to model masonry, recognising its inelastic and plastic behaviour, from initial stages of loading to failure of masonry structure, while taking into account the effect of damage accumulation.

From the material-based modelling perspective, different constitutive laws can be applied to models, depending on the linearity.

Simple modelling approaches have previously been used for simulating historic masonry structures, and satisfactory accuracy has been achieved with computer efficiency, for example (Chen, 2008; Casolo and Pena, 2007). As it has been mentioned before, and like these examples, the aim is to also adopt a simple constitutive law that provides a reasonably accurate prediction of historic masonry structures.

Limited constitutive models have been used in the linear range. However, there have been significant attempts in modelling masonry in the non-linear range. Genna has also carried out a comparison study amongst constitutive laws that can be adopted for numerical analysis of unreinforced masonry structures (Genna *et al*., 1998). The available constitutive laws can be divided in the following categories (Al-Chaar and Mehrabi, 2008; Bull, 2001; Genna *et al*., 1998):

- Standard plasticity,
- Continuum damage, possibly coupled with plasticity,
- Non-linear fracture mechanics models,
- The Galileo-Rankine elastic-plastic model,
- The no tension elastic-plastic model,
- The Drucker-Prager elastic-plastic constitutive law,
- A tension cracking constitutive model,
- Concrete-type material.

Table 3.1 presents a list of constitutive laws and their characteristics and abilities together with samples of their use in the literature.

Table 3.1: A list of constitutive laws, characteristics and abilities, & previous use in research.

Constitutive law	Characteristics and ability	Previous use in research/ references
Elastic-plastic	Model brittle behaviour; no tension, & limited compressive strength	(Caddemi, 1992; Maier and Nappi, 1990)
Drucker-Prager elastic-plastic	-Plastic compaction. Includes a compressive cap, and tension cut-off criterion, the coulomb friction criterion -Compressive cap models: plasticity & hardening of the cap, other yield surfaces are in plasticity. The ellipsoid model for orthotropic plasticity in a 3D configuration is used.	(Andreaus, 1996)
	2D continuum model based on Drucker-Prager failure criterion; Used as an interface model, and masonry units	(Manzouri *et al.,*1996)
	Combination of tension cut-off, tension softening and shear retention, and a Drucker-Prager plasticity model in compression. A 3D smeared crack model.	(Lourenço and Pina-Henriques, 2008; Rots, 1988)
Mohr- coulomb	Mohr-coulomb laws: historic masonry subjected to in-plane axial & shear loading Low compressive strength to avoid crushing failure Linear-elastic perfectly brittle behaviour is assumed in tension	(Sarhosis, 2011)
Mohr- coulomb	The coulomb friction criterion: Used for unit-mortar interface, DIANA A tension cut-off (to assure of a limited tensile strength of the brick-mortar interface) & a compression cap model (to model crushing of the joint)	(Lourenço, 1995)
Damage models	Various damage models, based on continuum models. Describing behaviour of masonry, in particular joints	(Gambarotta and Lagomarsino, 1997a; Gambarotta and Lagomarsino, 1997b; Maier, 1991)

Constitutive law	Characteristics and ability	Previous use in research/ references
	Orthotropic behaviour; different elastic and inelastic properties along the two material directions.	(Papa, 1996)
Creep	Rheological model; Kelvin and Maxwell chain, and viscoelastic Burger model with damage; (non-rotating smeared crack model; based on continuum damage mechanics).	(Verstrynge *et al*., 2008)
	Decrease in value of mechanical parameters with increasing strain; to represent tertiary creep.	(Binda *et al*., 1991)
Softening model	FEM based model; used for mortar joints, interface elements & masonry units Smeared crack elements; capable of simulating the initiation & propagation of interface fracture	(Lotfi and Shing, 1994; Lourenço, 1998; Lourénço, 1997)
Theory of plasticity	Plastic-fracturing; materials loaded in triaxial compressive shear comp; inelastic non-recoverable strains are observed.	(Chen and Han, 2007)
	Plastic models in framework of the homogenisation theories.	(Pietruszczak and Niu, 1992; Page, 1978)
Total strain cracking model	Smeared cracking approach; for material joint or brick, or material for masonry Softening behaviour is applied to describe the stress-strain relation	(Bull, 2001)
RCCM[25] model	Two internal variables, accounting for sliding with friction & damage Applied to small models; Used for mortar joints	(Fouchal *et al*., 2009)
Rankine-Hill model	An anisotropic composite yield surface: -Rankine yield criterion for the tensile & tensile-compressive regions -Hill criterion for the compressive region	(Lourenço, 1996)

---

[25] This model was developed by Raous, Cangemi, Cocu and Moerie, and is based on a surface based damage variable (Raous, 2009)

Constitutive law	Characteristics and ability	Previous use in research/ references
Concrete model	High compressive strength, & very low tensile strength; fails due to progressive internal crack growth.	(Giordano *et al.*, 2002)
	The smeared crack concrete model ;uses the yield surface criterion, to determine the elements affected by stress.	
Concrete model	The concrete damaged plasticity model; uses concepts of isotropic damaged elasticity, in combination with isotropic tensile & compressive plasticity.	
	The brittle cracking model; used where tensile cracking dominates the behaviour, & compressive behaviour is assumed linear elastic.	

3.3.2 Previous modelling of historic masonry structures

As mentioned in Section 2.6, loss of section with time, creep and creep-induced cracks are known to be the two most important defects in historic masonry structures, combination of which makes prediction of life expectancy of these structures very difficult. Therefore, modelling these defects is of significant importance, and so, it would be essential to critically review their previous modelling. It is also important to review previous attempts made on simulating repair of historic masonry structures. In doing so associated examples for each defect and repair are further elaborated in each of the following sections.

a) **Loss of section with time**

As mentioned in the previous chapter, over the past few years considerable numbers of researchers have contributed in the SMOOHS project, to use non-invasive methods to present the state-of-the-art of deterioration models and monitor effects of temperature, humidity, vibration, etc., to assess the risk of damage to historic structures (Smoohs, 2011). To do this, experimental and computational models have been used to implement and validate the case studies, to determine material and deterioration models. As it has been stated in the objectives of this research, simulation deterioration (reduction in size) is one of the main interests of this work. To do so, a review of previous simulations on this defect is covered here.

For example deterioration of concrete has been numerically modelled by (Bangert *et al*., 2003), where two models have been used to simulate the moisture and temperature related degradation process, and dissolution related degradation process.

Weathering and environmental actions on historic masonry have also been modelled, by using a microcell corrosion model based on thermodynamics and electro-chemistry. The model has been coupled with another model, which simulates the mechanical part of structure, using continuum plasticity, fracturing and cracking. The two models have been implemented in a commercial code called DUCOM3 (Maekawa and Ishida, 2002).

Effects of global changes on stones, leading to deterioration have also been modelled in the Noah's Ark project, and other researchers (Lengweiler, 2000; Lipfert, 1989a; 1989b; Weitzman, 1998). Physical, mathematical and statistical modelling has also been carried

out on stone deterioration (Bekker, 1999; Binda, 1999). The surface decay of masonry has also been modelled by stochastic analysis (Garavaglia *et al.*, 2002).

However, as it is evident, the majority of these models, concentrate on simulating the procedure of material erosion of structures, instead of their effects on structural aspects on historic masonry structures. Although in some papers, quite complex constitutive laws have been adopted. Moreover, it is important to use a simple computational tool to simulate structural effects of stone deterioration onthe overall stability of historic masonry.

b) Creep defects

The partial or total damage of historical monuments, has initiated many attempts on modelling and analysis of creep as a time-dependent defect in masonry structures. Additional perspective may be obtained from studying the multiple types of constitutive laws addressed in previous research carried out.

Two main and frequently used approaches for modelling creep behaviour in masonry can be named as *'rheological model'* and *'empirical formulae'*; a brief review and their use in the literature are given below:

Rheological models are commonly used in the literature, and can be referred to as a 1D, FEM-based model, proposed by Verstrynge (Verstrynge *et al.*, 2008). In this approach, a rheological model consists of a Kelvin model to simulate the primary creep, and Maxwell model representing secondary, steady-state creep. The Maxwell's model resembles the viscous behaviour. A Burgers damage parameter is also included, that allows for illustration of gradual loss of material cohesion and damage accumulation (decrease in strain resistance of material). The parameters used in the model for creep simulation, are only withdrawn from the experiments (including long and short-term creep tests) where the load is applied in steps. Further information on this model can also be found in (Verstrynge, 2010a). This model was also adopted by Binda, to simulate creep behaviour in adobe and clay brick masonry (Binda, 2008a).

The 1D rheological model, was then extended to a 3D version (Verstrynge, 2011), where an orthotropic, non-rotating smeared crack model (based on continuum damage mechanics), was used; shown in Figure 3.7. The orthotropic damage formulation, proposed by Papa and Taliercio (2005), describes the damage initiation in 3 orthotropic

directions. Once the damage has initiated, this formulation measures the damage accumulation in the 3 directions.
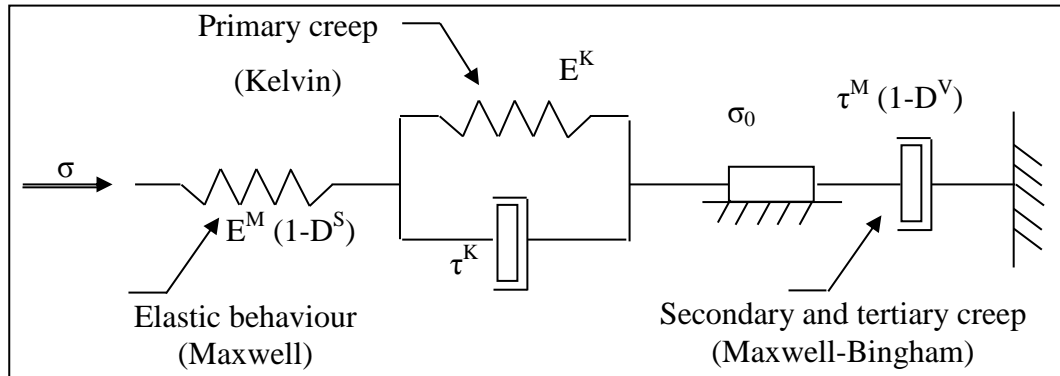
Figure 3.7: Schematic representation of the rheological model with damage variables (Verstrynge, 2011).

Van Zijl, developed the plasticity models proposed by Lourenco (1996); for both interface and continuum, into a creep model for concrete (Van Zijl *et al.*, 2001; Van Zijl *et al.*, 2000), where viscoelasticity and rate effects were used to model the combined behaviour of creep, shrinkage and cracking. However, as also stated by Verstrynge, 2010a, due to limited availability of data from experiments on masonry; this model has yet not been adopted to masonry structures.

While the above examples of creep simulations have focused on predicting the effect of creep on strain accumulation, Shrive and Taha and other researchers, have carried out experimental tests and numerical models to predict long-term creep behaviour and analyse its effect on stress distribution (Isfeld and Shrive, 2013; Kim *et al.*, 2012; Oan and Shrive, 2011; Fan, 2010; Fan *et al.*, 2009; Taha and Shrive, 2006; and Shrive and England, 1981). Probabilistic models have also been developed for assessment of historic brick subjected to creep defects (Garavaglia, 2006).

A significant drawback of the rheological model is its requirement for a large number of model parameters from the experimental tests. This is a very important disadvantage, as in the case of historic masonry (especially in case of rubble masonry), due to presence of various masonry types in one structure or even a specimen sample, it is very difficult to obtain all the model parameters. There is also huge uncertainty on the accuracy of these values, as well as unawareness of the outcome on their scatter.

Empirical formulae are also used very commonly in the literature. They are based on regression analysis of experimental data. The evolution of the creep coefficient as a function of time is described, by using either of 'power-law', 'logarithmic', 'hyperbolic', and 'exponential' expressions. In these expressions, under constant stress, the creep coefficient (t, t0) is defined as the ratio of the creep strain to the instantaneous elastic strain under constant stress (Verstrynge, 2010a). These models provide a simple and yet accurate approach in predicting the creep in historic masonry. In comparison to the rheological models, they also have the advantage that large number of model parameters is not required.

Three different types of empirical formulae exist for creep behaviour in Abaqus: 'power-law model', 'hyperbolic-sine law model' and 'user subroutine CREEP' (Simulia, 2013):

Power-law model is attractive for its simplicity in presenting creep behaviour in historic masonry, under relatively low stress. It is easy to work with, for its simplicity. It can be used in either of 'time-hardening' or 'strain-hardening' forms:

- Time-hardening form; the applied stress remains constant throughout the simulation. It is expressed as:

$$\dot{\bar{\varepsilon}}^{cr} = A\tilde{q}^n t^m \tag{3.1}$$

where:

$\dot{\bar{\varepsilon}}^{cr}$ is the uniaxial equivalent creep strain rate,

q is the uniaxial deviatoric stress,

t is the total time,

A, n and m are constants defined according to experimental data.

- Strain-hardening form, the stress varies during the analysis, which is calculated using Equation 3.2.

$$\dot{\bar{\varepsilon}}^{cr} = (A\tilde{q}^n[(m+1)\bar{\varepsilon}^{cr}]^m)^{(1/m+1)} \tag{3.2}$$

where $\dot{\bar{\varepsilon}}^{cr}$ is the equivalent creep strain rate.

Hyperbolic-sine law model, is applied where the model is exposed to high stress and the model is significantly stress-dependent (especially in areas such as crack tips). This model is available in the form of (3.3):

$$\dot{\bar{\varepsilon}}^{cr} = A(sinhB\tilde{q})^n exp\left(-\frac{\Delta H}{R(\theta - \theta^Z)}\right) \tag{3.3}$$

Where θ is the temperature, θ^Z is the user-defined value of absolute zero on the temperature scale used, ΔH is the activation energy, R is the universal gas constant, and A, B, and n are material constants.

User subroutine CREEP, allows wider range of capabilities for implementing viscoplastic models and also for addition of other solution-dependent state variables.

In addition, in cases where effect of cyclic loadings on creep and crack rate are to be considered, the users constitutive model (UMAT) can be used to write the desired constitutive model with appropriate cyclic loading.

However, as relatively low stresses levels are kept constant thorough the simulation, and to take into account for the creep trend and simplicity of the model, the power-law (time-hardening) model was selected. The hyperbolic-sine law model and the user subroutine CREEP were not considered, as they were quite complex and defeat the purpose of adopting a simple and efficient method in illustrating the creep behaviour.

c) Crack defect

Crack, is the other important defect, which has been the subject of many research works. Some of these studies have tried to assess the long-term effect of creep on crack initiation in brittle structures, such as historic masonry.

Generally, two main approaches are used in modelling crack in masonry structures, as outlined below (Giordano *et al*., 2002):

- Discrete crack models: the geometry is modified while the interior of the body is kept linearly elastic.

- Smeared crack models: introduce cracking as a process that is based entirely on constitutive law, while it keeps a fixed geometry. It is a finite element based approach that uses continuum damage mechanics to provide an approximate representation of damage occurring in the material.

For crack to form there must be enough stress to break the cohesive strength criterion defined in damage properties. Due to presence of very high tensile stress at the crack tip, this condition is usually met easily for tension being perpendicular to a sharp crack. In addition, the energy released by crack extension must be equal to or greater than the energy demanded for that extension. In other words, the stress intensity being equal to the fracture toughness plays a very important role in crack formation (Kim *et al*., 2014).

Although primarily exceeding the tensile strength was thought to cause complete loss of coherence in the direction of major principal stress, fixed-crack-models have been introduced and later updated, that consider other related phenomena including softening and stiffening of tensions, and shear capacity degradation. Yet more developments were introduced which meant that not only cracks in other directions could be formed, but the direction of the principle crack could also be changed. This allowed for multi-crack model generation and crack model rotation (De Borst, 1994). To these are added the damage and plasticity models with both isotropic and kinematic hardening (Giordano *et al*., 2002; Lotfi and Shing, 1991).

Tensile crack localisation has also been modelled previously, by means of a crack-tracking algorithm. In this model, continuum damage mechanics is used via FE to predict mechanical damage and long-term viscous effects. The crack-tracking technique has been used to identify areas where localised cracking takes place. The tensile cracks are forced to appear and develop along a row of finite elements, according to direction of the main tensile stress. Further information on this approach can be found in (Roca F. *et al*., 2013; Cervera *et al*., 2010).

Concrete models can also be used to model the main constitutive response for masonry. In such cases, software packages such as Abaqus, have built in concrete cracking models (Simulia, 2013; Cecan, 2012):

- The smeared crack concrete model; this approach does not track individual macro-cracks and is used where cracking is the most important defect of structure. The model consists of an isotopically hardening yield surface (active under compressive stress), and an independent crack detection surface that determines if a point fails by cracking.
- The concrete damaged plasticity model; this model uses concepts of isotropic damaged elasticity, combined with compressive plasticity and isotropic tensile

to represent the inelastic behaviour of concrete. This approach takes into account the degradation of the elastic and is therefore, suitable for using for cyclic types of loading.

- The brittle cracking model; this model is used where the behaviour is dominated by tensile cracking and compressive behaviour is assumed linear elastic. This model cannot track individual macro-cracks.

In general different theories such as 'Linear Elastic Fracture Mechanics' (LEFM), 'Cohesive zone model', 'Elastic Plastic Fracture Mechanics[26]' (EPFM), etc. have previously been used to describe the fracture process of materials. Moreover, Abaqus offers two different approaches to model crack (Simulia, 2013):

- The conventional finite element method: requires the user to conform the mesh to the cracked geometry, and the crack location needs to be identified

- The extended finite element method (XFEM): does not require the mesh to match the cracked geometry. The user does not have to indicate the crack location. The crack plane is solution dependent and the approach can also handle change in crack plane and predict the crack propagation direction.

For either of the above two approaches, 'damage model' can be used as the constitutive response to identify the limit criteria for damage to initiate and hence crack to form. However, as XFEM seems to be a more flexible option, a brief review of this approach is therefore, provided below:

Crack prediction in a structure can be achieved, using XFEM. It can be explained as a local partition of unity[27]; an extension of the conventional finite element method. The most important characteristics of this technique can be referred to as enrichment, where additional problem-specific functions are used to approximate displacements of nodes. XFEM makes it possible to model discontinuities and singularities independently of the mesh. Since it is not necessary to update the mesh to match the current geometry of the discontinuities, crack propagation can be simulated in a solution-dependent path. Examples of XFEM, and further information on its enrichment and formulations can be found in (Levén and Daniel, 2012).

---

[26] EPFEM is the extended version of LEFM to consider inelastic effects. Unlike its name, the theory is not based on elastic-plastic materials, but on a non-linear elastic material.

[27] The term 'local', refers to concept where the regions near the discontinuity, such as crack and holes are enriched.

The crack formation in XFEM technique takes place, through defining the damage in three steps of 'damage initiation', 'damage evolution' and 'damage stabilisation'; allowing for degradation and eventual failure of material. Amongst existing damages in Abaqus, the cohesive behaviour framework is used to model crack propagation, via LEFM principles (Simulia, 2013).

LEFM theory is adopted, as masonry is a brittle material and it has been assumed as an isotropic material. Using this theory, the local crack-tip stress field in the material, is characterized using a stress intensity factor (K). K is dependent on factors such as geometry of the structure, applied load, and, crack size and location of the pre-defined crack. It is used to predict the stress intensity near the crack front. Moreover, for materials such as masonry, where due to the brittle nature of the material, non-linearity is also evident, but over a short period of time, LEFM theory can also be applied; where it accurately establishes the criteria for failure[28].

Therefore, to model the crack propagation in masonry structures, the traction-separation damage model in Abaqus is used, where the initial response is assumed to have a linear elastic behaviour[29] prior to damage, followed by the initiation (based on the user-indicated damage initiation criterion) and evolution of damage (according to the user-defined damage evolution law).

Traction-separation damage approach can also be used to model the mortar or even the unit-mortar interface, as the features of this approach were primarily intended for modelling interfaces with fairly small thickness.

A typical failure mechanism, based on traction-separation response is shown in Figure 3.8. Note that it is very important for the damage evolution to be specified, as without this, no damage will occur as the damage initiation threshold is used for output purposes only.

---

[28] The term failure is referred to as complete loss of load carrying capacity in material.
[29] The elastic behaviour is written in form of an elastic constitutive matrix, relating the normal and shear stresses to the normal and shear separations across the model (Simulia, 2013).
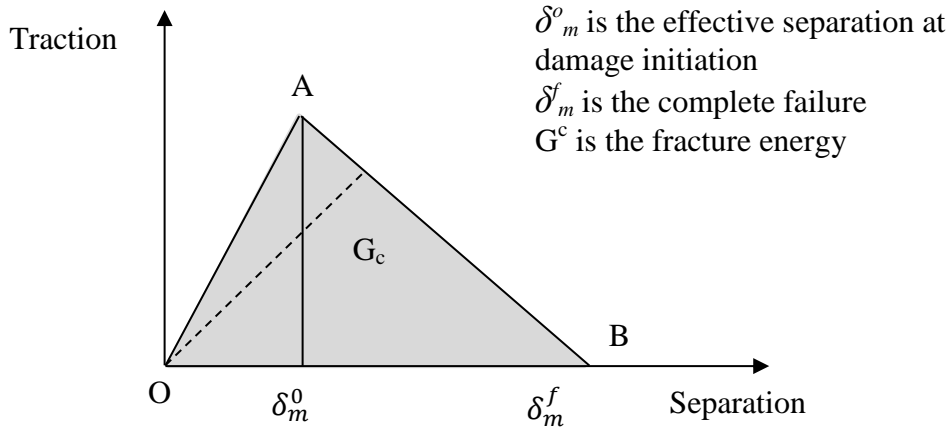
Figure 3.8: Failure mechanism, based on traction-separation response, showing linear initial response up to point A, and linear damage evolution up to point B (Simulia, 2013).

Damage initiation

The damage process initiates when either of the damage criterion is satisfied. In other words, the point is the beginning of degradation of the response of a material point, where the stresses and/or strains satisfy certain damage initiation criteria that you specify.

There are three stress-based and strain-based damage initiation criterions available in the traction-separation damage model: 'Maximum principal stress/strain', 'Maximum nominal stress/strain' and 'Quadratic nominal stress/strain'. As creep-induced cracks are the main interest of this thesis, Maximum principal strain (MAXPE) criterion is selected as the damage initiation threshold in the constitutive law of this tool.

Damage initiation occurs when the maximum principal stress or strain reaches a critical value of $f = 1$, of (3.4). MAXPE:

$$f = \frac{\langle \varepsilon_n \rangle}{\varepsilon_{max}^0} \tag{3.4}$$

Where,

ε_n is Maximum principal strain at damage initiation,

ε_{max}^0 is Maximum principal strain at each time increment.

The above damage initiation criterion has an output variable indicating whether the criterion is met, where a value of 1 or higher represents that the criterion has been satisfied.

Damage evolution

The damage process, assumes that the failure of elements is characterized by progressive degradation of the material stiffness. This tool allows use of multiple damage mechanisms, which can be used for various parts of a model, depending on the defect that the material is exposed to.

In general, there are two main components which help define damage evolution of material, in the traction-separation damage model (Simulia, 2013):

1. The first component is based on specifying the effective separation at *complete failure*, δ^f_m relative to either of:

   (a) The effective separation at damage initiation, δ^o_m, i.e. displacement; after damage initiation, the option is used to define damage as a function of the total or the plastic displacement.

   (b) The energy dissipated due to crack formation G^c (N/mm); also called the fracture energy, is absorbed during crack formation to form new crack surfaces which is equal to the area under the traction-separation curve.

   Both approaches require introduction of a characteristic length associated with a material point that is automatically computed by Abaqus based on element geometry.

2. The second component represents the overall damage in the material, taking into account the combined effects of all the active mechanisms in the material. is specifying the *nature of the evolution of the damage variable, D* [30], which is done by defining linear or exponential softening law, or specifying *D* directly[31]. Note that independent of the damage response (linear or exponential), Abaqus ensures that the area under the linear or the exponential damaged response is equal to the fracture energy. The damage parameter (D) evolves from 0 to 1 throughout the life time of material; where 0 represents no damage and 1 indicates total failure of material.

---

[30] between point A and B; between initiation of damage and final failure of material, in Figure 3.8.

[31] As a tabular function of the effective separation relative to δ^o_m.

Note that according to Figure 3.8, crack lines only appear in elements at point B, when the element has fully damaged. It is also important to mention that state of fracture energy and evolved damage in each element is updated at each increment. The formulation of the damage law ensures that mesh-sensitivity is minimized.

As the name suggests, linear and exponential damage softening indicate a linear and exponential evolution of the damage variable, with deformation for elastic-plastic materials, respectively.

Factors such as mix-mode, take into consideration contribution of fracture values from all directions for each element, indicating mode and direction of fracture. The dependence of fracture energy or displacement on the mix-mode can be specified directly via analytical forms[32], or in tabular form, each specifying different fracture criterions. Note that in use of analytical form, mix-mode is defined only in terms of energy, and when tabular form is used traction term is selected. Use of energy or traction terms leads to significant difference in the mode-mix ratios.

The above mix-mode forms are generally used for ductile and polymer materials, while mode-independent (which is the default selection) is mainly used for brittle materials; and hence is used in this tool. In cases where further data on masonry material is available, mode mix can be used to specify fracture energy to indicate energy as a function of the ratio of normal to shear deformation.

Moreover, mode-independent considers the highest value when calculating where the fracture has occurred.

Due to limited information on displacement values, fracture energy is used to specify the effective separation at complete failure of masonry material.

Moreover, as it has been mentioned in Section 2.2.2.4, the stress-strain relationship of masonry indicates a linear response up to failure. It is; therefore, fair to say that a linear damage evolution for the softening response of masonry is selected.

Damage stabilisation

As it has been mentioned before, fracture makes the structural response nonlinear. The material models with damage often have difficulty converging to a solution. The

---

[32] e.g. power-law, Benzeggagh-Kenane (BK).

viscous regularisation is therefore, used to help with the convergence of the Newton method[33].

To summarise the above examples, previous creep and crack models are outlined in Table 3.2, together with the masonry type that they are applied to and their previous use in research;

As it has already been explained, and as it can be seen from the table, the creep models are too complex to be used in this simple computational tool, and the damage models associated with these creep models (to model the creep-induced cracking), are based on continuum damage models and do not model individual or multiple macro-cracks. In addition, these creep-induced cracking are not presented explicitly. Since this tool, aims to demonstrate the main creep trend in a simple model, and to simulate the discontinuities explicitly, none of these models are adopted in this computational tool.

---

[33] The viscous legalisation coefficient, helps make the consistent tangent stiffness of softening material positive for sufficiently small time increments

Table 3.2: Previous modelling on creep and crack defects.

Application (Defect types)	Model	Masonry type Regular & rubble	Previous research/ references
Creep	A rheological model; based on theory of viscoelasticity, coupled with 2 anisotropic damage variables	ancient masonry	(Choi, 2007; Anzani *et al.* 2005b; Pina-Henriques and Lourenço, 2003; Papa, 2000; Anzani, 1995; and Anzani *et al.*, 1993)
	Static and viscous damage; FEM, DIANA, 1D Burger rheological model: -Kelvin and Maxwell chain -Viscoelastic Burger model with damage	Clay brick	(Verstrynge *et al.*, 2008)
		Adobe & clay brick masonry	(Binda, 2008a)
	Damage models; Exponential equation for damage development under constant stress	Historic Masonry	(Anzani *et al.* 2005b; Bodner and Chan, 1986)
Creep	3D rheological model in DIANA; same as the above model Orthotropic, non-rotating smeared crack model; based on continuum damage mechanics	Clay brick	(Verstrynge, 2011)
Crack	Fixed-crack models; exceeding the tensile strength initiates crack. Also includes softening & stiffening of tensions, & shear capacity degradation	Historic Masonry	(De Borst, 1994)
	Smeared crack, using FEM , in Abaqus	Historic masonry	(Theodossopoulos, 1995)
	Discontinuous deformation analysis; using the concept of	Framed masonry wall	(Al-Chaar and Mehrabi,

Application (Defect types)	Model	Masonry type Regular & rubble	Previous research/ references
Crack	artificial joints. Normal & shear cracking		2008)
	XFEM; extension of the conventional finite element method, based on the concept of partition of unity	Historic Masonry	
	Orthotropic, non-rotating smeared crack model; based on continuum damage mechanics	Historic Masonry	(Papa and Taliercio, 2005)
	Crack-tracking algorithm: FE continuum damage mechanics theory. Includes mechanical damage and long-term viscous effects	Historic Masonry	(Cervera *et al.*, 2010)
	Mode I fracture: Detailed micro-model: cohesive crack model	Historic Masonry (brick and mortar)	(Guinea *et al.*, 2000)
	Mortar: interface elements Units: smeared crack elements	Historic masonry panels	(Lotfi and Shing, 1991)

d) Repair

As it has been mentioned in Section 2.5.2, historic masonry structures subjected to weathering and other defects, often require maintenance and measures to restore their structural safety, serviceability and integrity.

Furthermore, the majority of the general assessment methods and simulations do not include previous strengthening applied on structure. In addition, prior to making a new repair, simulation of the structure can be used to obtain a better understanding of the structure's damage state (due to defect or previous poor restoration attempts), and to predict the impact of repair measures (Isfeld and Shrive, 2014). This is very important, as repair measures, could alter exiting mode of response and lead to new modes of failure in structure (Cecan, 2012). Such repairs play an important role in stability and stress distribution of unreinforced masonry structures. Study of these repairs and their effects, as well as other intervention methods through finite element modelling, can provide a better preview of change in stress-strain distributions in structures.

Over the past few years, attention has been drawn to repair and considerable repair has been applied to such structures (Garrity, 2008). However, only recently it has been known that simulation of repair is also an important task, and hence very few samples of such work are available in the literature. It is therefore, needed that in addition to review of the above previous modelling, a review should also be carried out on simulating repair on historic masonry structures.

Attempts have also been made, by Roca in the literature to examine the influence of the architectural alterations experience by Tarazona Cathedral in Spain (Roca, 2001). Isfeld and Shrive (2013) have also used DEM to model samples of repair (before completed the restoration process), on walls from Prince of Wales fort in northern Canada. Further attempts have been made by these researchers to present the in-situ conditions of the same damaged wall section before and after grout injection. A simple model was used, based on Finite element method (using Abaqus), where a linear elastic material property was adopted, to simulate these effects, and analyse stability of the wall (Isfeld and Shrive, 2014).

The above studies have identified the importance of carrying out such simulations, as well as efficiency and accuracy of simplified computational approach to present a better approximation of stability of the structure.

3.4 Discussion of development of new model based on appropriate constitutive law for historic masonry structures

Previous modelling and available constitutive laws on creep and crack were summarised in earlier sections. From the review of the literature, summarised in Table 3.2, it is now possible to lay the grounds for adopting the most suitable constitutive law, towards developing the computational tool, by comparing the two most commonly used laws.

It was identified that masonry is an anisotropic material. However, due to the existence of different masonry types in a structure and particularly their irregular layout in historic masonry, as well as lack of data on time-dependent material properties in all directions, an isotropic material is assumed for modelling historic masonry structures.

As researchers such as Roca and Lourenco suggest, it is not realistic to formulate a constitutive model that can incorporate all the interacting mechanisms of a specific material. Instead, constitutive laws should provide the simplest representation of reality, and yet best prediction from initial state to failure of the structure (Roca *et al*., 1998). Interestingly, Bull (2001) also shares the idea that it is impractical to put extra emphasis on the post-cracking behaviour, when dealing with such old structures. Instead, the model should account for material deterioration process, such as reduction in stiffness and loss of section over time. In addition, it should focus on basic creep features[34], and predict the crack initiation point, as well as its propagation path. The model should also allow for combination of these defects in large-scale structures. This enables the user to focus on more important aspects of modelling historic masonry structures, that is, to estimate the in-service life-times of structures.

Moreover, the use of complex constitutive law requires a considerable number of model parameters from experimental tests, which is very difficult to obtain, due to inherent complexity of masonry[35], and existence of a range of stress state that exist in such structures (Bull, 2001). To select the most suitable constitutive law, the rheological model was compared with a combination of empirical formula (creep power-law) and XFEM, as seen in Table 3.3.

---

[34] Such as developing strain accumulation, time-dependent inelastic deformations, and redistribution of stress in structure.

[35] In particular, historic masonry subjected to creep.

Table 3.3: Comparison of rheological model, with empirical formula and XFEM constitutive laws for analysis of historic masonry.

Criteria	Constitutive law	
	Empirical formulae & XFEM	Rheological model
Realistic representation of behaviour of historic masonry	✔	✘
Simplicity and ease of use	✔	✘
Limited number of parameters required	✔	✘
Ability to model strain accumulation; indicating creep	✔	✔
Ability to capture tensile failure in masonry	✔	✔
Ability to simulate explicit cracks (visible)	✔	✘
Ability to model macro crack	✔	✘
Ability to model multiple cracks	✔	✘
Ability to predict crack propagation path	✔	✘
Ability to apply existing crack to structure	✔	✘
Ability to model repair and strengthening techniques	✔	✘
Ability to model complex and 3D structures	✔	✔
Ability to model complex creep behaviours	✘	✔
Total	**12**	**4**
Note: ✔ :Advantage, ✘ : Disadvantage		

Evidently, the combination of empirical formulae and a bi-linear damage model XFEM is a better match for the criteria set out in the objectives defined for development of this computational tool and therefore, is adopted as the better choice for constitutive law.

Amongst the creep models in Abaqus, the power-law (time-hardening) model was selected, as relatively low stresses levels are kept constant thorough the simulation; assuming linear-elastic behaviour. The hyperbolic-sine law model and the user subroutine CREEP were not considered, as they were quite complex and defeat the purpose of adopting a simple and efficient method in illustrating the creep behaviour.

Also, as explained before, due to the inherent material properties of historic masonry and formation of discontinuities, it is inadequate to use a linear-elastic analysis without taking into account its non-linearities. In addition, with the influence of various parameters such as moisture and creep (in particular in tertiary creep phase, before failure), a 'softening zone' is formed[36], where the micro-cracks propagate to form macro-cracks. Since in the case of historic masonry structures, damage normally appears in the form of large individual cracks, macro-models will be used to illustrate the creep-induced crack in these structures. Perhaps this is why Binda suggests that micro-cracks are considered as superficial and not particularly worthy of modelling (Binda and Saisi, 2009; Binda, 1998b).

As such, the proposed computational tool is based on linear initial response, which is used alongside creep and the XFEM features in Abaqus; to present creep and creep-induced crack initiation and prediction. The adopted constitutive law uses the model's mechanical behaviour (creep and time-dependent feature), and combines it with the damage model to illustrate the induced damage; based on dis-continuum damage mechanics. The damage model, introduces an overall bi-linear behaviour in the structure, where maximum principal strain is used to indicate damage initiation and fracture energy and mode-independent forms are used to specify the effective separation at complete failure of masonry material. The damage evolution is also shown in form of linear softening response.

The computational tool, will simulate a simple and yet realistic behaviour of historic masonry structures, exposed to creep defect. However, it is important to state that the ability of the tool in simulating the long-term strain evolution in such structures is dependent on the accuracy of the input parameters.

3.5 Summary

This chapter presented a review of the literature on the available approaches, techniques and strategies that have been used to simulate the mechanical behaviour and failure of historic masonry under static load. A summary of the main findings, relevant to this thesis is given below:

---

[36] where many micro and macro cracks exist.

- There are many computational techniques available, use of which depends on the research objectives, existing information and desired level of accuracy.

- Due to brittle nature of unreinforced masonry, a bi-linear approach is adopted.

- The adopted strategy for simulating material behaviour of unreinforced masonry would be based on material assumption (homogenous or heterogeneous material), and dependent upon selecting one of the available modelling strategies (macro and micro-modelling).

- Homogenous modelling strategy assumes model as composites (equivalent-material approach) with reasonably large dimensions, subjected to uniform stress. In contrast, in heterogeneous modelling strategy, individual components (units and mortars) are considered, providing a better understanding of local behaviour of masonry structure.

- Macro-modelling can give a simple, yet good understanding of small- and large-scale masonry structures. Although less accurate (compared to micro-modelling), the overall formulation can be applied to the whole structure, and computational efficiency and cost-effectiveness can be achieved.

- In order to develop a simple and reasonably accurate computational tool, a macro-scale strategy is adopted. Similarly, homogeneity is assumed in the majority of the models, to simplify the properties of the constituting materials. Heterogeneous material is also adopted, where repair is applied to the structure.

- The main available numerical modelling techniques suitable for macro-modelling approach are:
  - DEM: is used for simulating behaviour and failure of discontinuities, such as mortar and unit-mortar interface.
  - FEM: uses small elements to provide better understanding of location of stress concentration, and presents a realistic and accurate description of overall response of historic masonry exposed to various defects, load conditions, etc.

- Since the overall effect of various forms of damage on the stress state of a simple masonry specimen (and not on the interface between the unit and masonry joints) has been considered, FEM is used; the technique that has also been previously used to simulate the structural response of historic masonry (both continuum and discontinuum modelling).

- Abaqus was identified as the most appropriate and powerful FEM-based software to have the ability of simulating defects in historic masonry structures, including degradation of material properties with time, creep behaviour, crack initiation and propagation.

- Considering the inherent complexity and variation of historic masonry materials, care should be taken when selecting an appropriate constitutive law and material properties. A review of the available constitutive laws, characteristics and abilities, as well as their previous use in the research has been provided in Table 3.1.

- Since creep and crack (in particular creep-induced cracking), were identified as the two most influential defects in historic masonry structures, the focus is on these two defects. A critical review of the previous models has also been given in Table 3.2. Moreover, a review of the need, and previous examples of simulating repair in historic masonry structures was also given in this section.

- It was concluded that the selected constitutive law should account for materials deterioration processes, such as reduction in stiffness and loss of section over time, with less emphasis on the post-cracking behaviour. Predicting the onset of the global failure of the structure is also considered as one of the main requirements of the adopted constitutive law.

- A comparison was carried out (in Table 3.3) between Burgers Rheological model and Empirical formulae (as the two common laws used in the literature to model creep and damage), to select the most suitable approach.

- Similar to Roca and Lourenco (Roca *et al*., 1998), this work has also established that tracing the entire response of a structure through macro-modelling (based on simple constitutive law) can give more insight into behaviour of structure; instead of using a highly sophisticated material response that does not result in a converged solution. Therefore, due to restrictions in obtaining the required material parameters from the literature, more sophisticated models have not been implemented. Thus, as suggested by (Bull, 2001) adoption of a simple elastic-plastic constitutive law is adequate for simulating behaviour of masonry structures.

- The adopted constitutive law can be named as discontinuum damage mechanics; creep power-law (time-hardening) and damage mechanics (using XFEM). This law uses the mechanical behaviour of model (creep and time-dependent behaviour) in combination with induced damage. When modelling creep, a linearly elastic,

homogenous material is assumed for masonry. Due to simultaneous presence of creep alongside crack formation in structure, a bi-linear analysis is adopted. As such, a linear initial response is used before the damage is initiated and a linear softening response is used to illustrate the damage evolution in the material.

- The use of this constitutive law and Abaqus software allows for:
  - A realistic presentation of the overall geometry, loading and mechanical behaviour of historic structures;
  - Application of arbitrary material properties to random sets/sections of the model, to represent defects such as gradual reduction in stiffness;
  - Accurate estimate of long-term creep pattern and behaviour;
  - Formation of single and multiple macro-cracks, predicting the crack initiation point and propagation path;
  - Combination of defects such as creep and creep-induced crack;
  - Application of pre-existing cracks in structure; to simulate damaged historic structures, as well as applying repair on historic masonry;
- The computational tool will simulate a simple and yet realistic behaviour of historic masonry structures, primarily exposed to creep defects. The use of a simple constitutive law in this tool, also allows for addition of other defects such as size reduction with time to represent weathering effects on historic masonry structures. This enables the user to focus on more important aspects of modelling historic masonry structures, that is, to estimate the in-service life-time of structure.

Chapter 4 : Development of the Computational Modelling Strategy

4.1 Introduction

In Chapter 3, an attempt was made to identify the most suitable strategies, techniques and software packages available for modelling historic masonry structures. It was concluded that the use of FEM and commercial software packages such as Abaqus offers great flexibility.

As explained previously, it is very important to have a realistic and accurate prediction of the performance of historic masonry structures. However, understanding, modelling and analysing such structures, due to their inherent complexity, are often very difficult (Lourenço, 2002). So, it would be extremely useful to have a computational tool, which is capable of predicting the behaviour of historic masonry structures from the initial or current state, through degradation and cracking to complete failure. Indeed, one of the objectives of this research work is to develop a robust numerical tool, with such capabilities. Only then, it is possible to monitor and predict the serviceability limit state, towards a comprehensive understanding of the failure mechanism and assess the safety of historic masonry structures (Lourenço, 1996).

Such complexity manifests itself in the simulation of structural damages, including material decay and a reduction in the material properties (thereby affecting the structural performance), creep and cracking; forming a disconnection between the different elements of construction (Roca, 2010). This is mainly due to the fact that the existing damage and their sources (natural or human interventions) are often unknown; therefore significant historical research is required (Gigla and Schlesinger, 2008). Moreover, many limitations exist in the study of historic masonry structures, most commonly seen in the form of (a) inadequate laboratory testing information, (b) rare or missing information on the geometry and the mechanical properties of the constitutive materials, (c) an inability to understand fully the mechanical properties of individual and combined masonry material types in historic structures, and (d) unknowns in the construction sequence and regulations and the difficulties in applying the existing codes of practice to these structures.

Although techniques such as non-destructive testing (NDT) (Bull, 2001; Binda, 1998b), or experiments carried out on specimens obtained from the collapse of some historic

structures can provide useful information on the material and mechanical properties of such structures, interpretation of these results is extremely difficult. Also, it would be very difficult to acquire most parameters required by the sophisticated constitutive models used in practice.

Clearly the above difficulties significantly limit the validation of the modelling and simulations. Such limitations are driven mainly by the variability of the masonry and the impossibility of reproducing the same masonry specimen, regardless of the structure size and test type. It is also difficult to perform advanced testing of ancient structures (e.g. long-term creep tests), due to the time and cost factors involved.

Therefore, from a practical point of view, it would be extremely difficult if not impossible, to establish a close-fit relation between a simulation model and the experiment results. Thus, the most sensible solution would be to offer a computational tool that can produce a similar trend and closest possible fit between the numerical and experimental results. More specifically, for a better interpretation and validation of the results of an FEM analysis of an old masonry structures, a combination of different analytical computations, structural models and, where required, hand calculations can be used (Bull, 2001).

This chapter illustrates the development of a computational tool by defining its constituent models and the validation of (a) the simulated deterioration (involving various materials) and (b) the model representing undamaged masonry (Section 4.3). In Section 4.4, the developed computational tool is presented and examined through various simulations to illustrate its ability in modelling the exfoliation of stone (loss of section) and the repair of the damaged zone, long-term creep behaviour and cracking. The loss of section aspects of the modelling applies to a range of different deterioration types including frost damage, erosion and salt crystallisation damage as well as the exfoliation of stones.

4.2 Model description

Model description is a process in which different aspects of the modelling of masonry are determined; aspects such as part, material properties, loads and boundary conditions, steps, mesh, etc., which are referred in simulation software packages as *modules*. Abaqus/CAE provides a consistent interface between the different modules of a model; these modules are briefly described below (Simulia, 2013).

Part and Assembly: The module 'part' is used to create the model geometry, through either Abaqus drawing tools or the import option from other CAD software. For recreating the geometry of historic masonry structures, a basic sketch of the structure is required. The 'assembly' module can then be used to create and modify the assembly of these geometry instances created in the part module.

Material properties: This is probably the most important and yet difficult part of modelling historic masonry structures. The existing material library contains numerous models for the inelastic behaviour of materials such as iron, soils, concrete, etc. However, masonry is not included in this library. As mentioned before, variance in properties and geometrical details of the constituting materials (such as variations in the thickness of mortar joints) adds to the inhomogeneity of the texture and hence inaccuracy of the material parameters under simulation. Moreover, difficulties in obtaining and interpreting information on the material properties of historic masonry structures means that very little information is available for this module. The general material models such as elasticity, plasticity, damage (crack initiation and propagation) and other mechanical models can be defined in this module. The principal material properties used for modelling the masonry assembly are density, elastic modulus, Poisson's ratio and tensile strength.

Step: This module can be used to create steps to indicate the analysis duration, specify output requests, analysis control and adaptive meshing for individual parts. These can be achieved through static, visco, dynamic, coupled temp-displacement, etc. step types. General loads can be applied to the structure via the *static* step and masonry defects such as creep can be simulated using the *visco* step. The choice of static or dynamic analysis mainly depends on the type of analysis (Boothby *et al*. 2006).

Interaction is a step-dependent module, which is available in the form of contact, fluid cavity, acoustic impedance, etc. and is used to define and manage (a) mechanical and thermal interactions between different parts, (b) mechanical properties of the interfaces, (c) constraints; tie, rigid body, coupling, and (d) crack initiation and propagation for modelling fractures.

Mesh: This module allows the user to generate mesh on parts. A variety of meshing techniques such as structured, swept and free meshing is offered in Abaqus, as the shape and size of the elements have an important impact on the solution. Depending on the

chosen technique, colour coding can be assigned to the structure. Similarly, based on the model requirements, different levels of automation and control, various seed size, mesh techniques and element types can be applied to the structure. Examples of mesh elements can be given as solid (3 dimensions) and brick (8-20 noded). Solid elements are known to be useful for modelling mass structures and so are useful for modelling historic masonry, though the use of large numbers of nodes makes them uneconomical. Brick elements have previously been commonly used for modelling masonry structures (Boothby *et al*. 2006), and have been advised to be used wherever possible as they give the best results for the minimum cost (Cecan, 2012; Simulia, 2013). Brick elements have therefore, been adopted to mesh the models in this thesis. It is also advised that for general analysis (using Abaqus/standard), quadratic elements can be used where large strains or complex simulations (e.g. simulations involving contacts) are not present.

Having the correct size of mesh is very important. A very coarse mesh can produce inaccurate solutions, while excessive run or program limits on the node/element numbers will arise when a very fine mesh is used. Fine and coarse mesh should be used in areas of low and high stress levels, respectively. Care should also be taken when meshing the angles of the corners; not to generate too acute or too obtuse angles. The aspect ratio of the elements should also be within the limits (no more than four and preferably less than 2). Depending on the nature of model, implicit or explicit analysis is used. When meshing creep models, the use of the accuracy tolerance parameter (CETOL) limits the time increment (Al-Chaar and Mehrabi, 2008).

Loads and boundary conditions are step-dependent modules. Loads can be applied to nodes in the structure in the form of concentrated force, moment, pressure, etc. to help produce a better model of the loading conditions in a structure. Boundary conditions (BC) also have different types (symmetry/antisymmetry/Encastre, displacement/rotation, etc.), which help represent a similar condition to the test specimens and can have a great influence on the computed results. Since most masonry structures are under compressive load, pressure is applied to the top surface of the specimen with a fixed base (to represent other masonry units and mortars at the bottom of the structure). Application of BC when modelling masonry depends on the structure's physical properties as opposed to clarity of the BC in say steel structures (Boothby *et al*. 2006).

In general Abaqus approaches the nonlinear problems by dividing the time steps into increments. Loads are also divided and applied in increments unless stated otherwise in the input file. The equations representing the response to the applied load at each increment are solved iteratively using the Newton-Raphson method (Wescott *et al*., 1999). While modelling a non-linear FEM, considerable care should be taken when undertaking the *step* and *mesh* module, as the time increment and mesh size have the most influence on the accuracy of the results. So, for an accurate and cost-effective model a compromise must be made between the calculation time and accuracy. In simulations such as creep, where some variables and stress need to remain constant over a long period of time, errors occur between the real response and the incremental model simulation. This can be overcome by application of small time increments, giving a more accurate and longer calculation time. Therefore, smaller time increments will be used during the primary creep phase (Verstrynge, 2010b).

When the designer moves from one module to another, modules are built, according to which Abaqus generates input files. These input files are then submitted to Abaqus/Standard or Abaqus/Explicit for analysis. Next, the analysed information is sent to Abaqus again for monitoring purposes and if all goes well, generating output files. Lastly, the output database is read, using the visualisation module in the Abaqus (viewer), in the form of graphical displays. This procedure can be explained in detail in (Liu and Quek, 2003).

4.3 Development of the computational tool

This section describes the gradual development of the computational tool. As mentioned in chapter two, masonry consists of different materials. The chosen masonry depends on the type of masonry the user aims to model, i.e. the precise type and combination of masonry units and mortar. Since the purpose of this research is to keep the models simple, the above features are presented as a very simple masonry specimen. The same approach can be used for different types of masonry.

The basic and main features of this tool are validated individually, either by applying the feature to an existing example, or in the form of simple engineering logics and hand calculations. A combination of these features is then presented in one model, to resemble the concept of combining masonry defects in one model. Further defects such as creep effects and cracking will then be added to the developed tool (see Section 4.4).

4.3.1 Stage 1- Validation of simulated deterioration (different materials)

Model validation counts as one of the most important steps in modelling. This is to enable the software users to have scientific proofs as to whether their models are correct. Models can be validated via different approaches, some of which include experimental results, hand calculations, simple engineering logic, etc.

Much of the existing historic masonry consists of 'outer' and 'hearting' masonry. The outer masonry refers to the facing masonry, exposed to climate change defects such as weathering, frost action, etc. Moreover, the hearting masonry refers to inner masonry with lower quality (consisting of rubble masonry with loose mortar). For better illustration and validation of this feature, presence of two different materials in one structure can be applied to a model of reinforced concrete. Once this feature is validated, a similar idea can be used in a masonry model, where more than one material exists in a structure, due to repair of the structure.

Moreover, as mentioned in Chapter 2, masonry deteriorates with time leading to gradual deformation or failure of the structure. This deterioration can be modelled in form of reduction in stiffness (E) of material; where the undamaged material gradually changes into a specimen that in terms of having stiffness and load bearing capacity barely exists (the material has deteriorated and the geometry exists but has the stiffness of 'foam'). Furthermore, the model will also be developed to illustrate the disappearance and removal of the deteriorated masonry, which will be shown in section 4.4.1. In addition, changes in temperature (e.g. as a result of climate change), are also causing damage in historic masonry structures. It is therefore, useful for the model to have the ability to accommodate a change in temperature as a feature. Change in E and temperature are therefore, shown in a model with two different material properties (model 2). It is important to note that the above mentioned features of the model will then be combined in one model, to show the combination of these effects as well as to present a more realistic behaviour of a historic masonry structure. A summary of the models mentioned above, and the features each aim to validate are given in Table 4-1.

Table 4.1: A list of models and basic features of the tool.

Original model	Model	Consistent Parameter	Changing parameter	Validating Approach
Two materials in a masonry specimen	Model 1: Reinforced Concrete Column	- Constant uniform pressure - On-going time	Two constant material properties	Hand calculation
Effect of temperature in a masonry specimen; 1 material	Model 2: Bimetallic Strip	- Two constant materials properties (Constant E) - One set of temperature - On-going time	Different expansion factors	Hand calculation

4.3.1.1 Model 1- reinforced concrete column

The concept of having two different material properties in one structure can be applied to a reinforced concrete (RC) column, where the column is reinforced with four steel bars (0.02m diameter each). Once the hand calculations have shown the feasibility of this model, the same concept can be applied to structures with masonry materials, where the user would only change the material properties.

Different material properties have been applied to the steel and the concrete. For each material, E has been kept constant throughout the simulation. Figure 4.1 illustrates the plan view of a RC column, where the load has been applied instantly to the top surface of the column that is fully fixed at the bottom, as seen in Figure 4.2, and the model properties are specified in Table 4.2.

Table 4.2: Characteristics of the two different materials of model 1.

Concrete	Steel
$E = 15000$ N/mm^2	$E = 200000$ N/mm^2
$v = 0.2$	$v = 0.2$
Density = 2E-6 Kg/mm^3	Density = 7.75E-6 Kg/mm^3
Pressure = 6.25 N/mm^2	Pressure = 6.25 N/mm^2
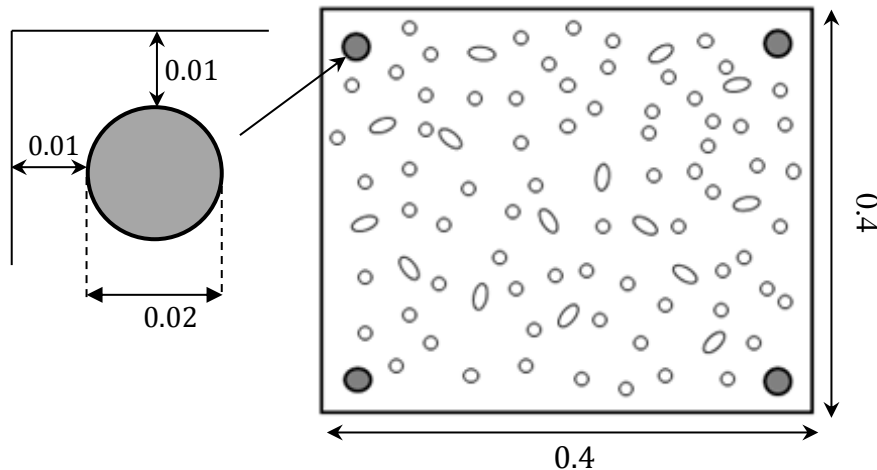
Figure 4.1: Plan of a reinforced concrete column (all dimensions are in metres).
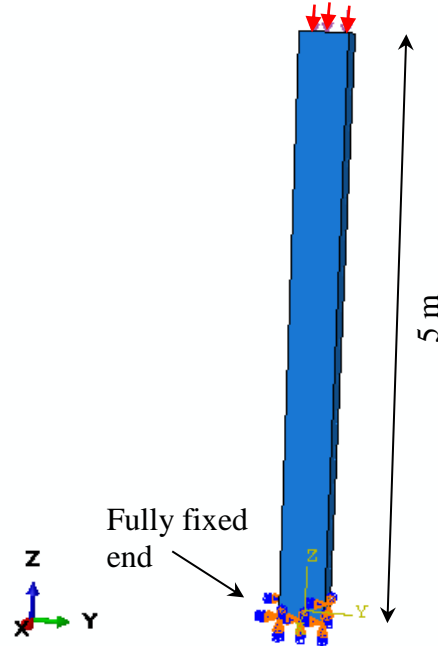
Figure 4.2: Reinforced concrete column subjected to uniform vertical stress at the top and fully encastered at the bottom.

The concrete and steel parts have been connected together using 'tie' joints in order to provide a more realistic simulation of the RC columns and also to avoid any slippage between the parts.

a) Hand calculations

This model is validated, using hand calculations, to calculate stress levels of concrete and steel, as well as the maximum deflection (axial shortening) value of the reinforced concrete model. So, the calculations give:

$$A_s = \Pi \times r^2 \tag{4.1}$$

$$A_s = 4 \times \Pi \times \left(\frac{20}{2}\right)^2 = 1257\text{mm}^2$$

$$A_c = (400)^2 - 1257 = 158743\text{mm}^2$$

where A_s and A_c are cross sectional areas of steel and concrete, respectively.

Therefore, stress values for Steel and Concrete can be calculated using (4.2)-(4.4) as:

$$S = \frac{E_s}{(A_c E_c) + (A_s E_s)} \cdot P \tag{4.2}$$

$$S = \frac{200000 \times 400 \times 400 \times 6.25}{(158743 \times 15000) + (1257 \times 200000)} = 76\text{N/mm}^2$$

$$C = \frac{E_c}{(A_c E_c) + (A_s E_s)} \cdot P \qquad (4.3)$$

$$C = \frac{15000 \times 1000 \times 10^3}{(158743 \times 15000) + (1257 \times 200000)} = 5.64 \text{N/mm}^2$$

The axial displacement of the reinforced concrete column can also be calculated as:

$$\delta = \frac{\sigma_c L}{E_c} = \frac{5.7 \times 5 \times 10^3}{15000} = 1.9 \text{mm} \qquad (4.4)$$

b) Result analysis

In order to validate this model, the calculated and simulation results are compared here. In the simulations, the load has been applied instantly to the model, at time increment 0.1 (where each step consists of 10 increments).

The steel bars are shown in Figure 4-3(a), where a stress value of 76.53N/mm^2 can be seen for the steel, which is very close to the hand calculated value of 76N/mm^2. As it can be seen from Figure 4-3(b), the column is fully compressed (blue colour in the contour with negative sign). There is no significant geometric non-linearity, as there is no bending. A stress value of 5.53N/mm^2 can be seen for concrete, which is quite close to the hand calculated value of 5.7N/mm^2. Figure 4-3(c) shows a deflection value of 1.913mm (the negative value corresponds to the direction of deflection), which matches the deflection value of 1.9mm, calculated above, confirming that the feature of presence of more than one material property in the model has been validated.
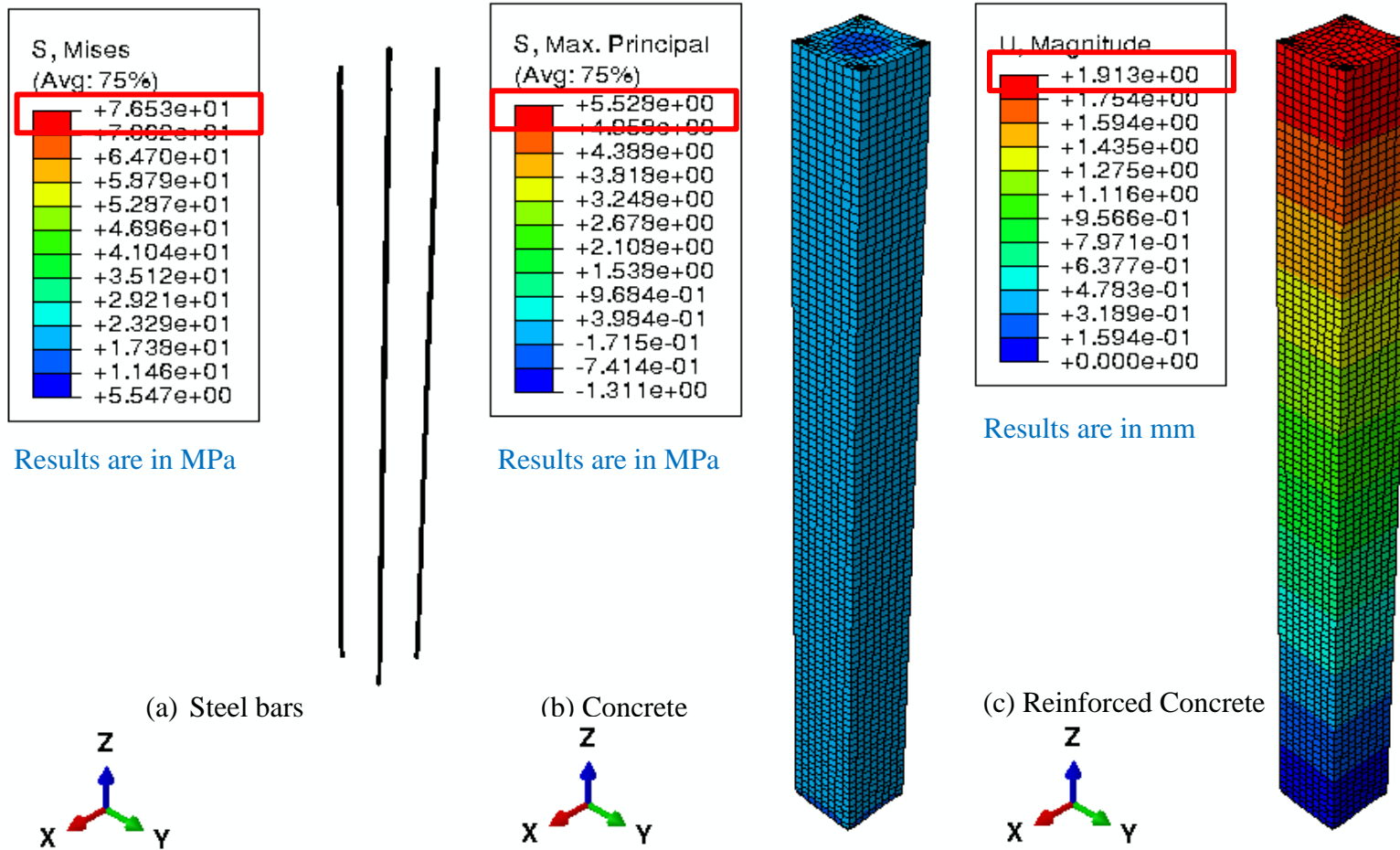
Figure 4.3: Stress in (a) steel, (b) concrete and (c) deflection of RC of model 1.

4.3.1.2 Model 2- bimetallic strip with different expansion factors

As it was explained in the previous model, the effect of temperature on steel plate (with constant material property throughout the simulation) was shown in the previous model to illustrate the ability of the tool to show effect of temperature. Here, this model aims to show the effect of temperature on a bimetallic strip with more than one material property (sample obtained from (Childs, 2001)). The dimensions, load and boundary conditions of the model are given in Figure 4.4.

Element type C3D8I was also used in this model which consists of two layers of different materials (with different coefficients of linear thermal expansion), which are bonded together. In order to show the effects of temperature and different expansion factors on these two materials, a 30mm long bimetallic strip is fixed at right end side to represent a cantilevered beam. The upper and lower layers are chosen to be 0.6mm thick Iron and Invar, respectively, each heated from 15°C to 40°C. As the Poisson's ratio was not given in the sample in the paper, ν is assumed to be 0.3. Properties of the Bimetallic Strip are shown in Table 4.3. Changes in temperature with time are also given in Table 4.4.

Table 4.3: Two different material properties in model 2 (Webster, J.G. 2000).

Material	Young's Modulus (N/mm^2)	Coefficient of Thermal Expansion (K^{-1})	Density
Iron	2.11E+11	1.21E-05	0.000778
Invar	1.4E+11	1.7E-06	0.008

Table 4.4: The temperature changing with time in model 5.

Time (days/years)	Temperature (°C)
0.1	15
0.2	18
0.3	21
0.4	24
0.5	27
0.6	30
0.7	33
0.8	36
0.9	39
1.0	40
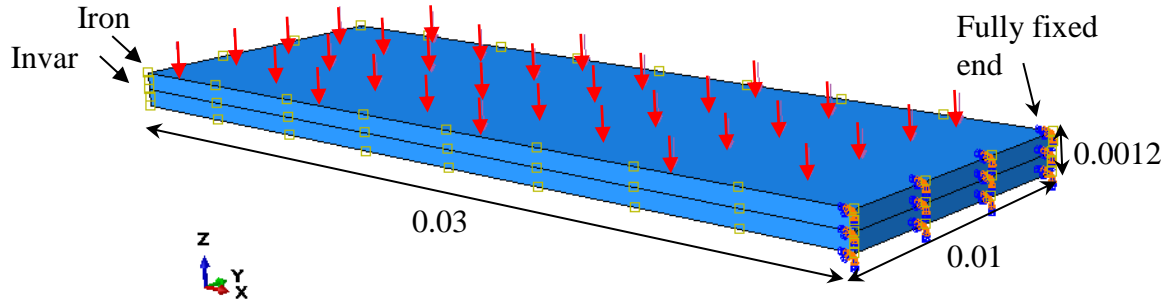
Figure 4.4: The bimetallic strip, subjected to a uniform vertical stress at the top and fully encastered at the bottom (all dimensions are in meters).

a) Hand calculations

Deflection of a cantilevered Bimetallic Strip can be calculated using (Webster, J.G. 2000):

$$\delta = \frac{3L^2(1+m)^2(\alpha_2-\alpha_1)(T_2-T_1)}{t[3(1+m)^2+(1+mm)(m^2+\frac{1}{mn})]}$$

(4.5)

Where α_1 and α_2 are coefficients of thermal expansion of the material with the lower (K^{-1}) and higher (K$_{-1}$) expansivities, respectively. Also, $n= E_1/E_2$ where E_1 and E_2 are the Young's moduli for the upper and lower layers.

$n= 0.664$

$m = t_1/t_2$, the overall thickness of the strip (m); $m =1$

$t = t_1 + t_2$

T_1 = initial temperature (K), T_2 = final temperature (K); so,

$$\delta = \frac{3(0.03)^2(1 + 1)^2(12.1 \times 10^{-6} - 1.7 \times 10^{-6})(40 - 15)}{0.0012 \times \left[3(1 + 1)^2 + (1 + 0.664)\left(1^2 + \frac{1}{0.664}\right)\right]} = 0.145\text{mm}$$

b) Result analysis

For illustration purposes, contour scaling factor of 50 has been used in the figures below. Once the Bimetallic Strip is heated, due to difference in expansion factor, it is expected to bend downwards, in the direction of the weaker material (with lower expansion factor).

Figure 4.5 depicts the strain distribution across the strip at different increments of times and a close-up view of the fixed end. As it can be seen from Figure 4.5(a) and (b), the top end surfaces of the two layers are in tension. Compressed areas are also visible at the bottom of each layer (shown as negative values). Moreover, a uniform pattern of compression and tension are visible at the bottom and top of each layer, respectively, as seen in Figure 4.5(c).

Figure 4.6 shows the maximum principal stress at both increments of 0.5 and 1.0; at the middle and end of simulation. The colours red and blue represent highest and lowest stress values. The highest stress levels can be seen at the top fixed end of the plate, as well as between the two layers of steel plate. Compressed areas can be seen at the bottom of each plate; shown as negative values. As there is no load applied to this model, the higher expansion factor of the Iron material (top layer) has caused the Iron plate to expand more, causing more stress on the bottom layer and hence bending the plate downwards. Difference in behaviour of the two plates, has evidently illustrated and confirmed temperature's effect, presence of two different materials with different expansion factors.

Figure 4.7 illustrates the deflection in this model, with blue and red colours representing maximum and minimum displacements of the bimetallic strip, respectively. The signs of the numbers in the contour also signify direction of the displacement (minus represents downwards displacements). Note that significant deflection can be seen at the free end of the steel plate. As seen in Figure 4.7(b), deflection value of 0.16mm is evident, which is very similar to the one calculated 0.145mm (using eq.4.5). This confirms validity of this feature of the proposed tool.

(a) Time increment0.5

(b) Time increment 1

(c) Fixed end of the strip
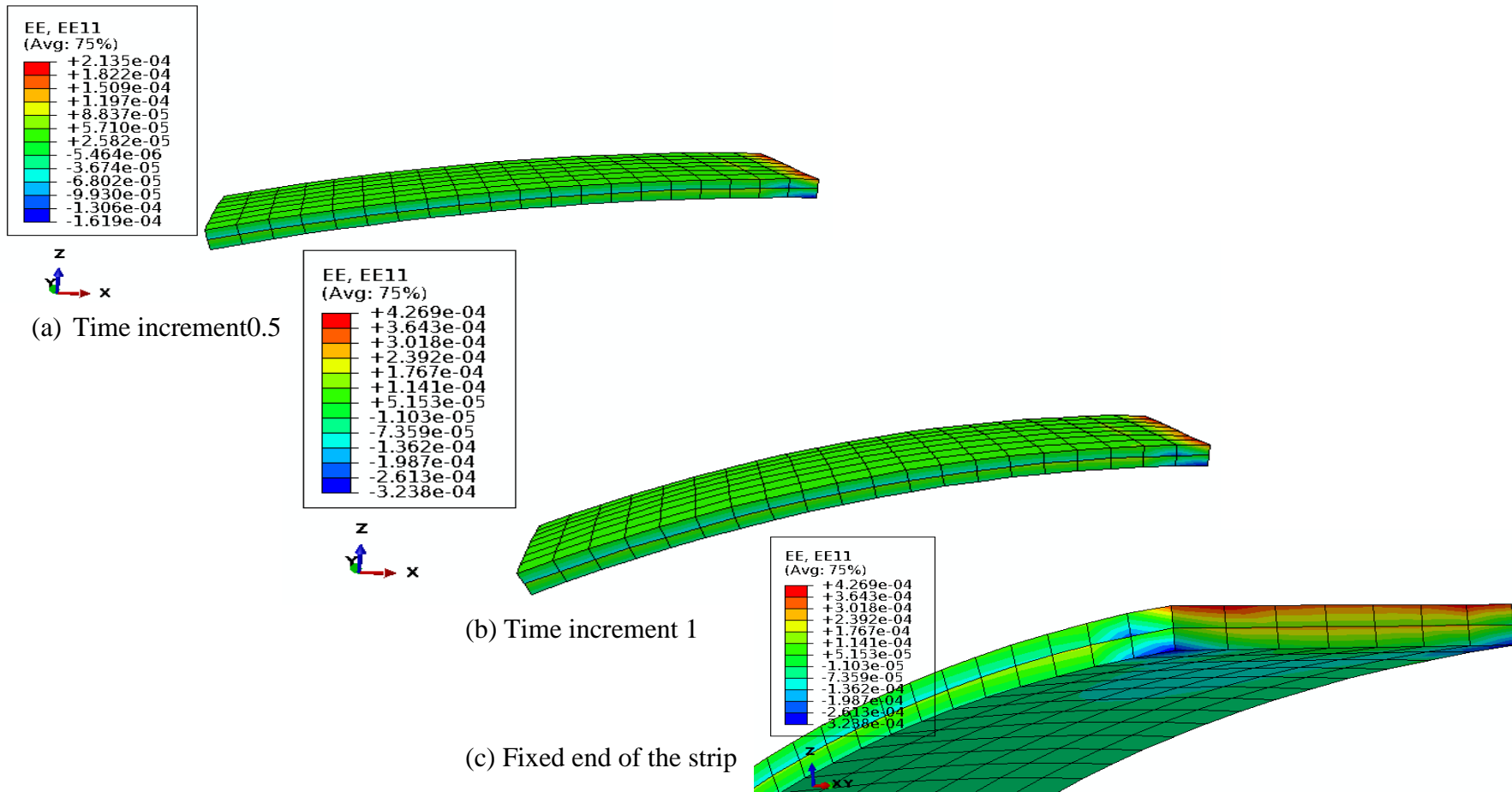
Figure 4.5: Strain in *X*-direction at increments (a) 0.5, (b) 1.0, and (c) at fixed end of the strip of model 5; contour results are in mm.

(a) Time increment 0.5   (b) Time increment 1
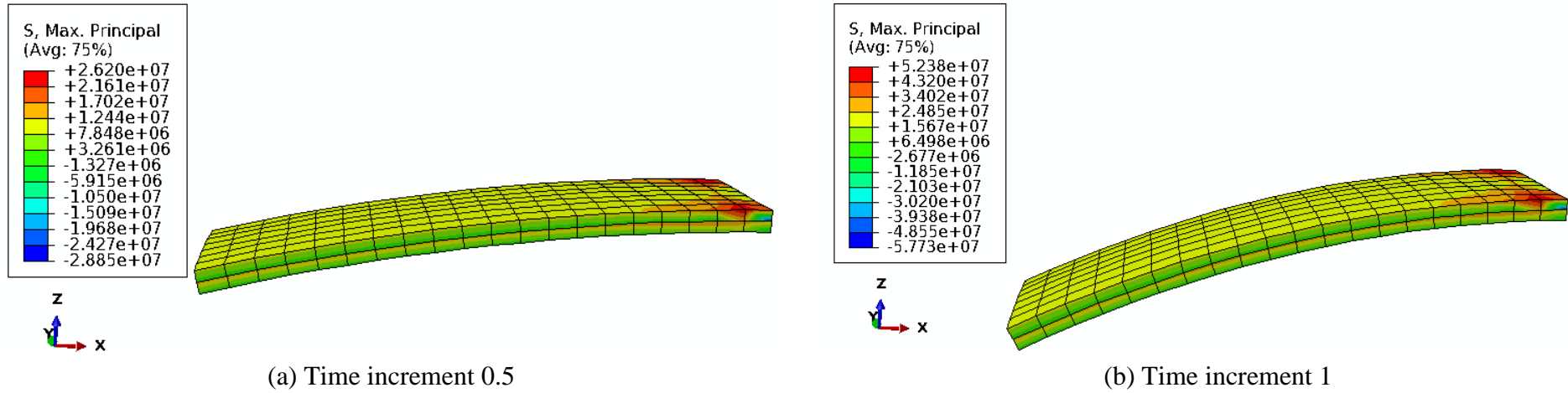
Figure 4.6: Stress at increments (a) 0.5, and (b) 1.0 in model 5; results are in MPa.

(a) Time increment 0.5   (b) Time increment 1
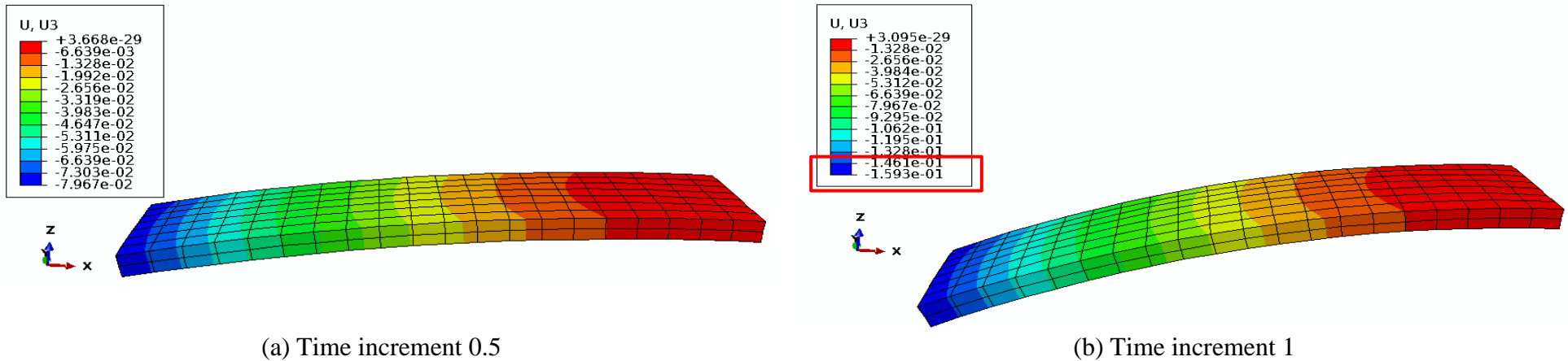
Figure 4.7: Deflection at increments (a) 0.5 and (b) 1.0 in model 5; contour results are in mm.

4.4 The developed computational tool (stage 2)

Gradual development of the computational tool was shown, validating its features by means of comparing the hand-calculations and simulations. In this section, the features validated previously will be used to apply the defects identified in Chapters 2 and 3 (exfoliation of outer layers, creep effects and cracking), to further develop the computational tool.

4.4.1 Localised damage: softening zone
4.4.1.1 Exfoliation of stone

As mentioned in the literature review (Chapter 2), the climate change consequences on structures, particularly historical structures, can be rooted down to a few parameters including temperature, moisture (in forms of rain, ice, snow and vapour clouds), soil conditions, radiation (in specific short-wave radiation) and wind. Presence of these parameters has consequences on historic masonry structures which appear in the form of erosion and exfoliation of the outer layers, weathering, salt crystallisation, efflorescence, and so on. Amongst these defects, erosion of historic masonry structures over time can be of great concern; for instance in a case where a slender column is not connected to any side arches despite being originally constructed that way. Such a slender column does not have any support when exposed to wind load, and mainly relies on the integrity of its mortar joints and is stable by uniform distribution of compressive stress due it its own weight. Gradual reduction in stiffness, erosion and exfoliation of the outer masonry, as well as wash-away of the mortar due to weathering effects, reduces the column's resistance to imposed pressure. As mentioned before, resistance is reduced with time to a value lower than the applied load and the overall distributing force, which in turn leads to collapse of the column. It is, therefore, very important for the tool to have the ability of modeling exfoliation of masonry structure with time.

Exfoliation of masonry has been previously described as "peeling, swelling or scaling of masonry or mineral surfaces in thin layers". It is gradual deterioration and erosion of masonry, leading to reduction in the structure size with time. Considering the above, a model is developed to simulate size reduction in masonry structures as a result of deterioration over time. Exfoliation can be modelled, using either a user-specified subroutine or via CAE.

The former allows for high flexibility in terms of selecting random and arbitrary elements (representing eroded or repaired areas on structure), specifying material properties and mechanical behaviours (e.g. deterioration rate), as well as enabling parametric simulation of scenarios to examine the effects of various changes (e.g. climate change) in the structure under investigation. The field variables of the model can be set so that the elements can be removed based on the stress or strain levels; details can be found in (Simulia, 2013). A dearth of experimental values for "deterioration rate" of masonry structures significantly limits the use of subroutines for this end. Therefore, a manual approach which affords a greater control and granularity must be adopted. This allows for the possibility of using a consistent rate of reduction in stiffness of historic masonry (details presented below), to remove the eroded material with time. The main benefit of this model is that it gives the user a realistic estimate of existing defects in historic masonry structures and a plausible estimate of their remaining lifetime. The model becomes even more realistic when the combination of other climate change defects such as creep and crack are simulated, shown in Section 4.4.2. This will provide a more realistic understanding of the present state of the historic masonry structures.

Exfoliation of stone can, therefore, be modelled as reduction in size of structure with time. The model presented in Figure 4.8 is a simple specimen of historic masonry, which is fully encastered at one end, with its upper surface under uniformly distributed load of $10N/mm^2$. It consists of three sets of different materials (shown as patches), given in Table 4.5, where materials 1, 2 and 3 represent ordinary, semi-eroded and eroded masonry materials, respectively. The eroded batches represent typical areas that are more exposed to erosion. A typical Poisson's ratio of 0.2 (for historic masonry structures) was used in simulation of this model.

To provide a framework example of the model, a specimen of masonry (500x250x102mm) consisting of three material types including original masonry, an initial repair and a subsequent repair (properties given in Table 4.5), are investigated. To run the simulation, hexahedral elements (type *C3D8R*) were used for meshing the model.

For each material, the Young's modulus, *E*, is reduced consistently with time, which depending on the situation, can take units of days, months or even years; though kept constant throughout the simulation. The patches of masonry that erode and peel off are

modelled as a material whose stiffness is reduced over time; that is, eroded materials are given very low stiffness values ($E = 50N/mm^2$). The material set with the lowest stiffness is given a material property similar to foam, resembling a patch with physical existence but no ability to carry the distributed load. Consequently, this would put more pressure on other patches, in turn increasing the chance of failure.
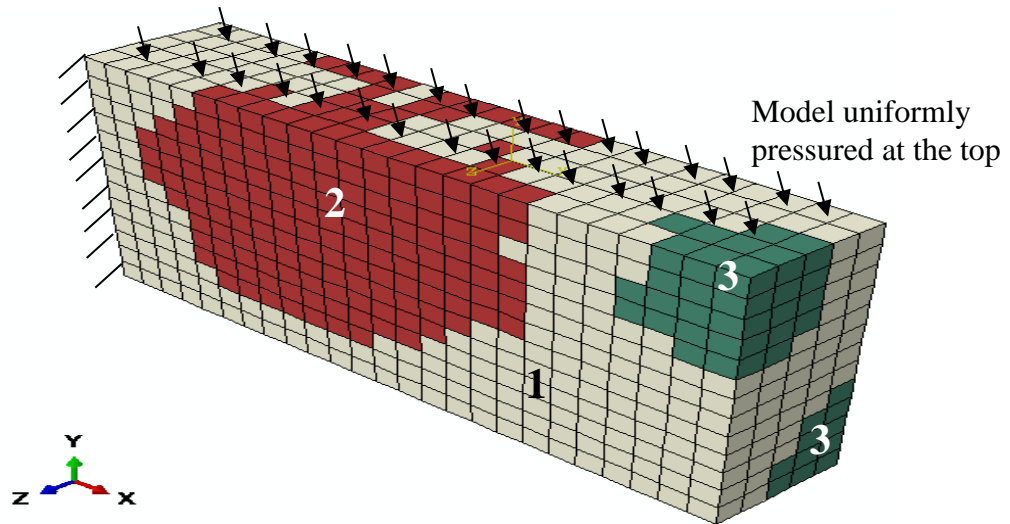
Figure 4.8: Examples of different sets of materials: (1) ordinary masonry, (2) semi-eroded masonry, and (3) eroded masonry.

Further analysis of Figure 4.9(a), reveals that the eroded material (set 3) reaches a low stiffness after 10 years indicating a potential exfoliation and so, the geometry of set 3 is removed to represent part of the masonry that has been most exposed to weathering. This is then followed by removal of semi-eroded material (set 2), after 20 years Figure 4.9(b). With removal of each batch of material, the stability of the stress/strain distribution across the masonry specimen is disturbed. Removal of eroded material helps the user better visualise this effect.
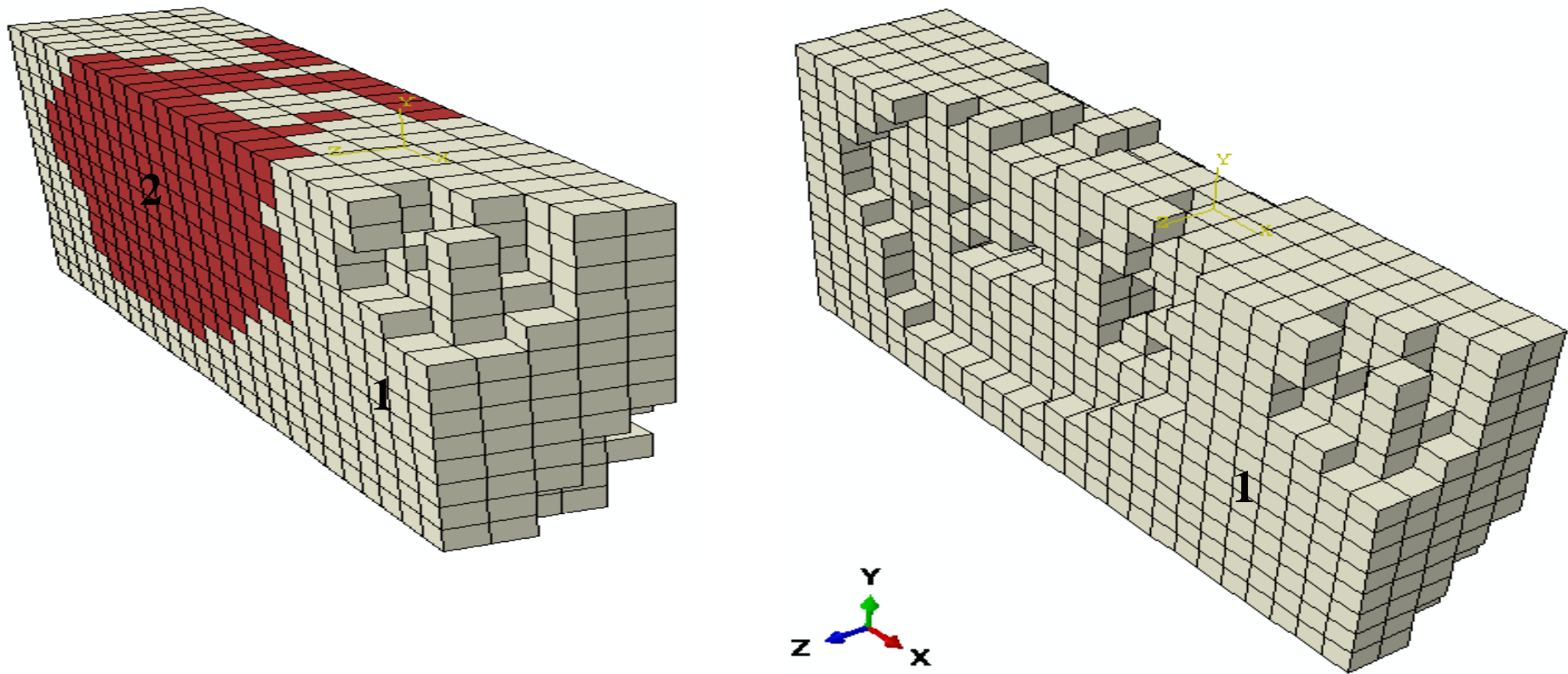
(a) Removal of eroded material   (b) Removal of eroded and semi-eroded material

Figure 4.9: Exfoliation of (a) eroded material, and (b) semi-eroded material**.**

Table 4.5: Material properties of different sets, indicating reduction in stiffness with time.

Ordinary masonry (Set 1)		Semi-eroded material (Set 2)		Eroded Material (Set 3)		Repaired material (Set 1)	
E (*N/mm²*)	*Time* (*years*)	*E* (*N/mm²*)	*Time* (*years*)	*E* (*N/mm²*)	*Time* (*years*)	*E* (*N/mm²*)	*Time* (*years*)
6000	1	4000	1	2000	1		
5800	2	3750	2	1750	2		
5600	3	3500	3	1500	3		
5400	4	3250	4	1250	4		
5200	5	3000	5	1000	5		
5000	6	2750	6	750	6		
4800	7	2500	7	500	7		
4600	8	2250	8	250	8		
4400	9	2000	9	150	9		
4200	10	1750	10	50	10		
4000	11	1500	11			7000	11
3800	12	1250	12			6800	12
3600	13	1000	13			6600	13
3400	14	750	14			6400	14
3200	15	500	15			6200	15
3000	16	400	16			6000	16
2800	17	300	17			5800	17
2600	18	200	18			5600	18
2400	19	100	19			5400	19
2200	20	50	20			5200	10
2000	21						
1800	22						
1600	23						
1400	24						
1200	25						
1000	26						
800	27						
600	28						
400	29						
200	30						

4.4.1.2 Repair of damaged zones

As it is known, repairing the eroded areas most often involves introducing new materials (with higher stiffness, *E*) to that area of the structure. Use of repair in the form

of incompatible patches shows that the application of such repair on any part of the structure can change the overall stress-strain distribution and could have adverse effects on its stability. Therefore, the developed computational tool proves to be very useful in modelling the application of suggested repairs on historic masonry structures, and analysing the effects of such repair. Depending on the results of such analysis, material properties of the patch can either be altered to better fit the existing structure, or alternatively, application of other repair techniques can be considered.

In the proposed model, the repaired material has been applied to the historic masonry specimen presented in Section 4.4.1.1. After removal of the eroded material, Set 3, the repaired material is applied to this set; details of the set are given in Table 4.5. The effect of repair on the existing materials (Sets 1 and 2) has been simulated in Abaqus for duration of 10 years (from 11 to 20 years).

Figure 4.10(a) and (b) show the maximum principal stress and maximum principal strain contours, respectively. It can be seen that the repaired sections have much lower deformation with application of load, in comparison with the semi-eroded set. The section between the semi-eroded material and ordinary masonry faces the highest level of deformation. In Figure 4.10(a), maximum and minimum stress levels are shown in colours red (areas in tension) and blue (areas in compression). The fixed end of the model is bearing the highest level of stress, while the least stress level is shown in the repaired section. The areas surrounding the repaired section are also bearing relatively low stress, as the improved strength of the new material has helped with better stress distribution in the masonry specimen.

Similar pattern of strain can be seen in Figure 4.10(b), where the highest and lowest levels of strain are shown in red and blue, respectively. The repaired areas are least strained, whereas the semi-eroded areas and the section between the semi-eroded area and ordinary masonry have the highest levels of strain; suggesting that the semi-eroded materials also need repair

.

<div align="center">(a) MAXPS   (b) MAXPE</div>
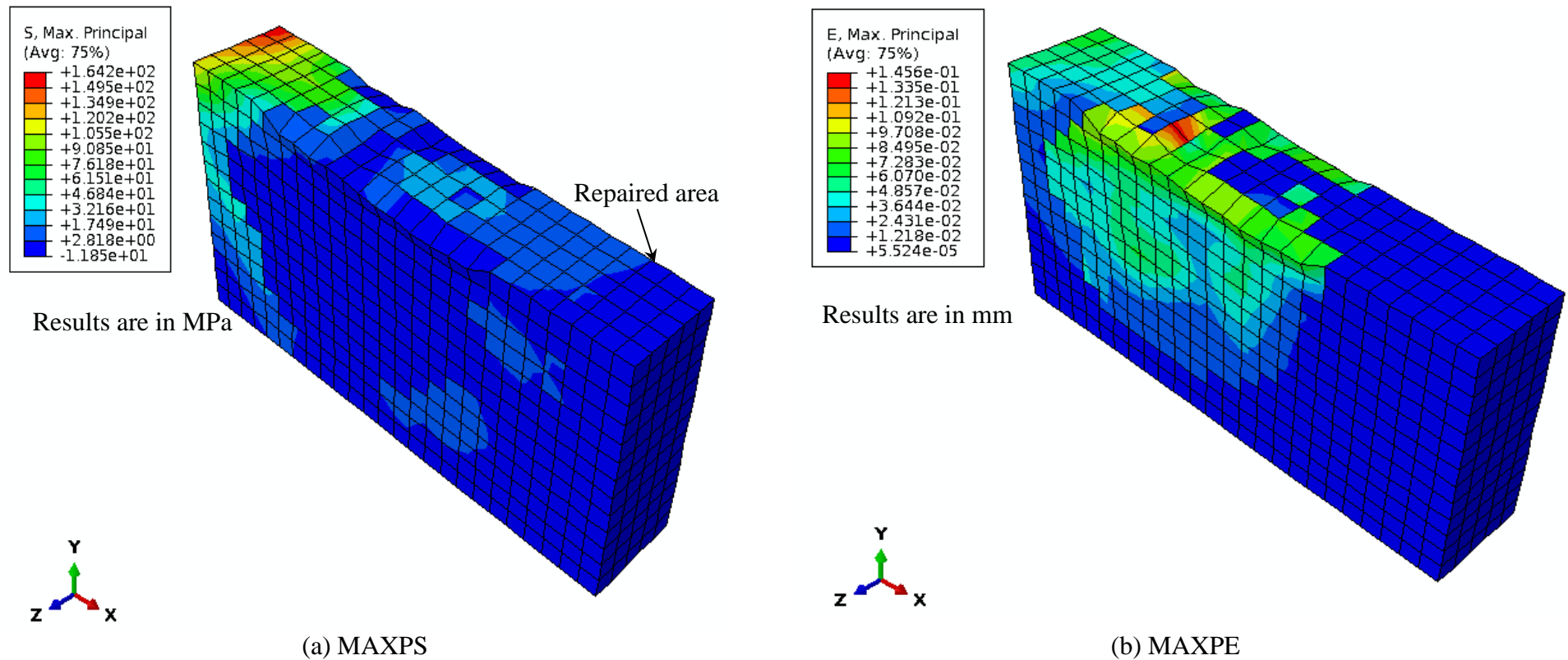
Figure 4.10: Effect of repair on, (a) maximum principal stress of the masonry specimen, and (b) maximum principal strain of the masonry specimen.

In such cases, various repair methods (with different stiffness values) can be applied to the structure and the best repair mechanism can be chosen by comparing their effects on stress-strain distribution of the masonry specimen. Existence of such defects in the structure, and others defects like creep, reduces the overall stiffness of structures. So, similar study from computational modelling viewpoint has been done for other defects including creep and creep-induced crack, as presented in the following sections.

4.4.2 Modelling creep

This section is concerned with analysis of creep behaviour on different types of masonry materials, as well as parametric study of effect of different variables on the creep behaviour.

As mentioned before, high cost of such tests and limitations in the availability of ancient masonry specimens, as well as the test time durations (≈ 500-1000 days), means that not many experimental results useful for the test are present.

Moreover, the realistic simulation of effect of long-term damages on historic masonry structures, still requires numerical developments. Nevertheless, in order to be able to model the behaviour of creep in various historic masonry structures, five different sets of creep experimental results, with similar test durations were chosen from the literature. The models' parameters were deduced from long-term creep test results presented in each paper. The models are not aiming to model the peak failure of the creep behaviour in historic masonry, but the main trend of strain accumulation with time, a linear line is therefore, being expected to count for increase in the strain level.

When creating the models, the pressure were initially applied, followed by the effect of creep. This effect was shown by using two steps of *Static and *Visco. For each time a new load was applied, the sequence of these two steps was repeated. The first step, represents the elastic behaviour of material, and the second step is used to obtain a transient static response in time-dependent analysis; creep. The explicit method was chosen in the Visco step, to avoid use of iterations. The CETOL value of 1E-08 (Simulia, 2013) was also chosen in all models, to count for limiting the time increment.

As creep is time-dependent, the simulation results are not influenced by the mesh size and element type, and hence it was not needed to carry out mesh sensitivity. This is only required when creep and crack are combined together in the following sections. The creep models have a total number of 3751 and 3000 elements (C3D8 linear hexahedron).

4.4.2.1. Simulating creep on different type of masonry

The following masonry types, classified according to their material properties, will be discussed in this section:

- Type A: Low strength clay brick and air-hardening lime mortar (accelerated carbonation);
- Type B: A sort of concrete made with layers of broken bricks and stone altered with layers of mortar; random rubble masonry;
- Type C: Historic brick masonry and hydraulic lime mortar;
- Type D: Historic brick masonry and hybrid lime-cement mortar;
- Type E: Modern masonry, Clay brick masonry and cement based mortar (1: ½: 4½ ; OPC: cement: lime).

Table 4.6, summarises details of the experimental tests carried out on the above types of masonry. A comparison of the creep results (vertical and horizontal creep experimental data) for four types of historic masonry is shown in Figure 4.16. Masonry type E was not presented in this graph, due to the large difference between the sets of results, which would have made comparison difficult.

Table 4.6: The 5 different types of masonry materials used for creep simulation

Masonry type	Test duration (days)	Specimen size (mm^3)	Test conditions	Reference
Type A	440	190 x 190 x 600	- Constant temperature of 20±1°C, - 60±5% relative humidity	Verstrynge, 2010
Type B	900	300 x 300 x 510	- Initial stress of 40-50% of compressive strength - Constant temperature of 20°C - 50% relative humidity	Anzani *et al*, 2000
Type C	950	290x 190 x 850	-Initial stress of 50% of compressive strength	Verstrynge 2008
Type D	950	290 x 190 x 850	-Initial stress of 50% of their compressive strength	Verstrynge 2008
Type E	850	$215 \times 214 \times 965$	-Initial stress of 1.5N/mm^2	Brooks *et al*., 1997

Looking through the literature and previous simulations used to validate the experimental results, there has been an approximate difference of 20% between the experiment and simulation strain values. Examples of this can be seen in results provided in Figure 4.11 of (Verstrynge, 2010b), where there is an approximate 600

difference in micro-strain value that is 20% of the experiment micro-strain results 3000. Therefore, the simulation results presented below are good and valid, if the micro-strain values are within a range of approximately 20% of the experimental results.

It is evident that all the creep responses of all four masonry types follow very similar trend, where there is an increase in strain values with time. These curves, however, have different initial strain values, which relates to a higher initial load (higher percentage of the material's compressive strength).

Note that these curves are not a true representation of creep behaviour in historic masonry structures, as these tests have been intentionally developed for the material to fail in desired time duration. This approach is adopted, because during the creep tests, specimens should be kept under controlled conditions of constant temperature, humidity (measured using thermo-hygrometric instruments) and load for a long period of time (Papa and Taliercio, 2000).

It is therefore, only understandable that in order to resemble creep effect (hence strain accumulation) over considerably long period, the creep tests presented in the literature and in the above figure, have been carried out under constant load steps of fixed amplitude and where possible duration.
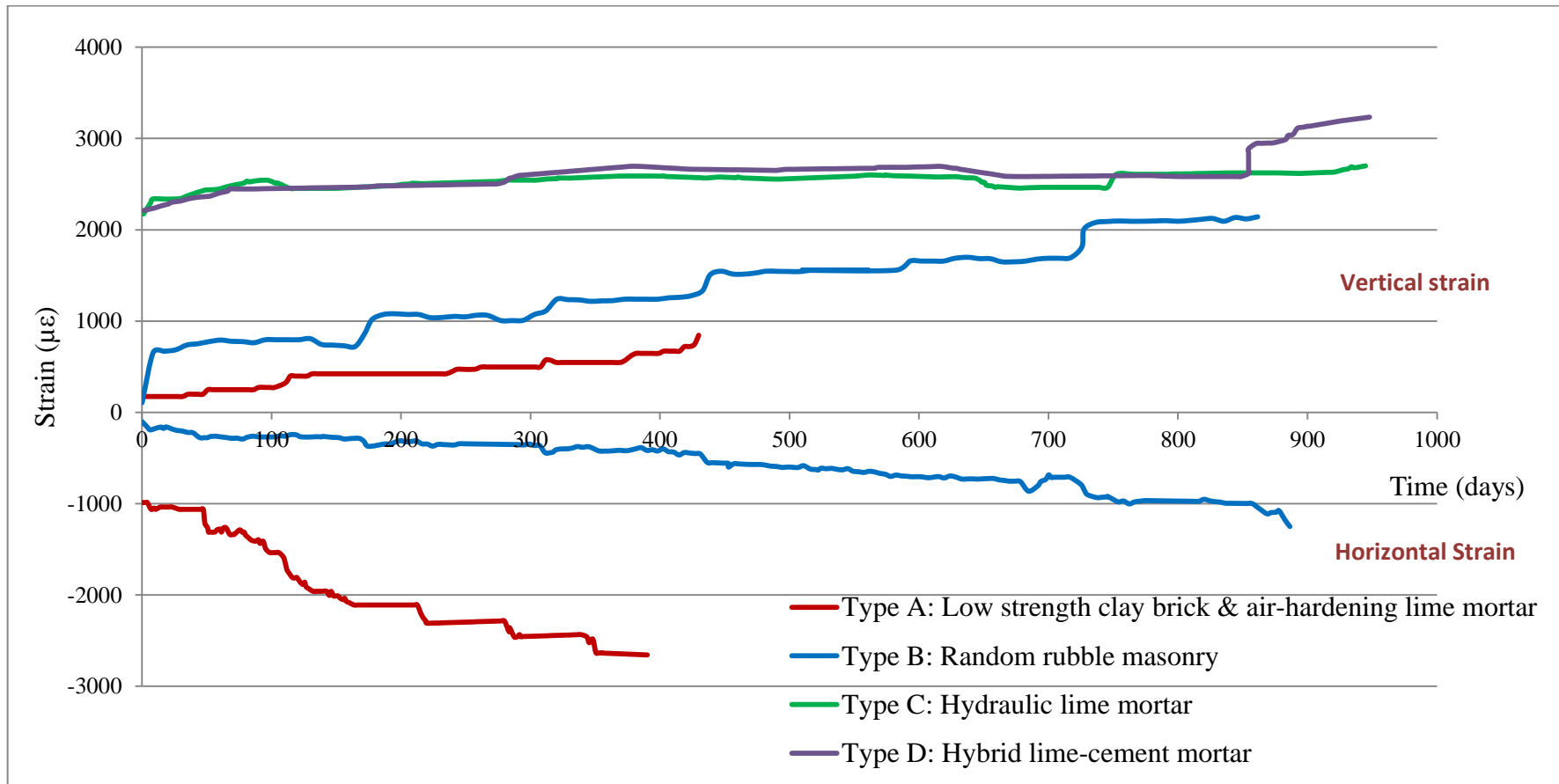
Figure 4.11: Comparison between long-term creep test results of different historic masonry materials.

For the same purpose, the initial load have intentionally been applied at say 50-80% of materials compressive strength, and gradually increased in small amounts, to meet failure at shorter time duration; usually in real historic masonry, the load is only applied during construction and majority of this load stays constant throughout the structure's life-time. The loads for all masonry types have been kept constant until a steady state is reached or creep strain has reached a constant value. It goes without saying that even though such tests do not replicate true creep effects, they are yet useful for studying the creep response of historic masonry structures; as they represent a real trend of creep behaviour in masonry (Papa and Taliercio, 2000). Although this is different in the case of masonry type E where one load has been applied throughout the simulation.

The present work takes a similar approach to the experiments of Figure 4.11, in terms of applying constant loads in steps at given time frames.

It was concluded in the previous chapter that the creep power law, and in particular time-hardening, should be used in Abaqus to model creep behaviour. Three parameters of *A, n,* and *m* should be obtained (assumed constants), to be used in the time-hardening power law. The range of parameters were obtained from the concept of creep and creep fracture, explained in (Ashby *et al*., 2009), as well as Abaqus documentation (22.2.4 Rate-dependent plasticity: creep and swelling (Simulia, 2013)), to be as follows:

$$-1 < m \leq 0, \qquad\qquad 3 < n \leq 8, \qquad\qquad A > 10^{-27}$$

Since the creep results provided in the referred articles illustrate only the measured strain-time curves, in order to reproduce similar results, the FindGraph software was used to extract the associated coordinates.

As mentioned in Section 3.4, the power-law model currently available in Abaqus uses the same equation (3.1). The creep strain values for each day can be obtained by integrations of (4.6); which represents the creep strain rate.

$$\varepsilon^{cr} = \frac{A}{m+1} q^m t^{m+1} \tag{4.6}$$

Equation 4.6 was used in the MATLAB code, to represent time-hardening power law for coordinates of each creep tests for every kind of Masonry type were used. Regression analysis and in particular Least Squares Fitting (LSF) method has been used in the form of MATLAB code (Appendix B), to find the best-fitting curve from these coordinates, in order to obtain optimal values for *A*, *m* and *n*. A typical of best fitted

curve has been plotted against the experimental curve for each types of masonry; seen in Figure 4.12.

Masonry type B
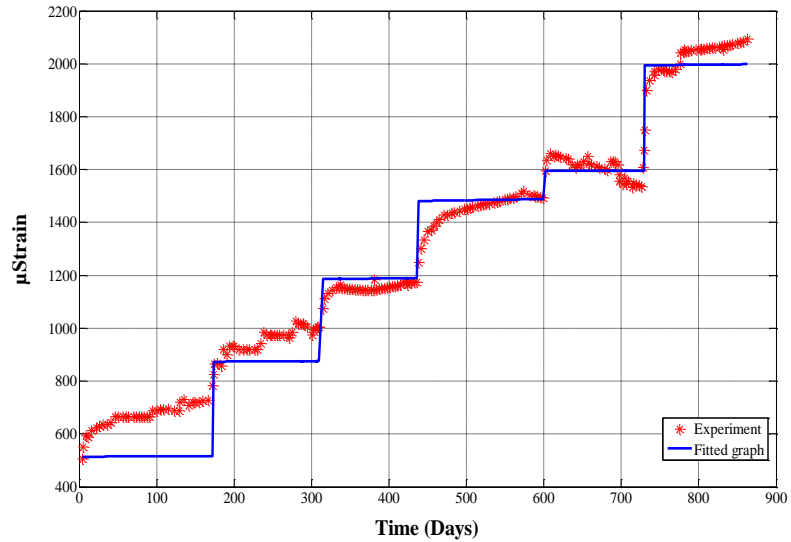
(a)

Masonry type D
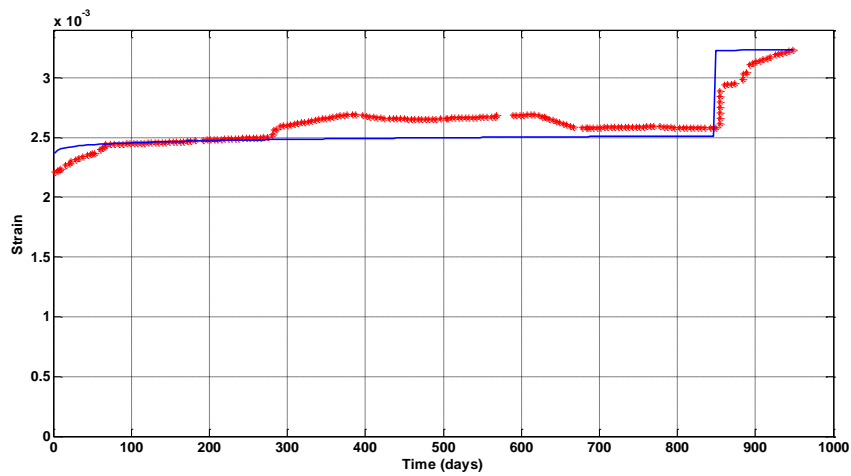
(b)

Figure 4.12: Samples of best fit LSF curve plotted against experimental creep curves.

A sensitivity analysis of ±10% (i.e. 27 different sets of *A*, *m* and *n* values) is carried out to provide a range of these parameters for each type of masonry, and to enable the user obtain information on effect of each variable on the curve trend – seen in Figure 4.18. These sets are also used in a parametric study to determine their effect of *A*, *m* and *n*, on the shape of the creep curves (hence strain values); which will be discussed in the next section
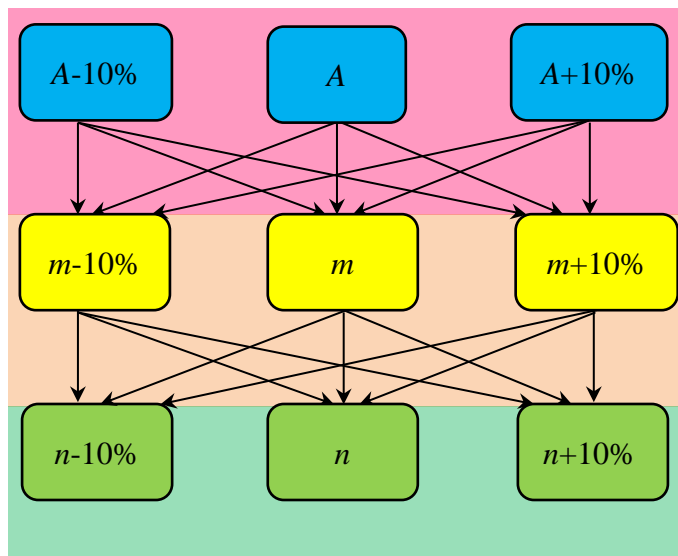
Figure 4.13 : Sensitivity analysis for 27 cases of creep parameters

These values are input to Abaqus (as creep parameters) together with material properties for each masonry type, and simulated under exact tests conditions as in the experiment. This result into 27 creep curves, which are compared against the experiment results (obtained from the literature) and the closest fit, is chosen as the most suitable set of creep parameters.

Creep simulation results can be validated by using any of these set of A, m and n values within this parameter boundaries obtained from each sensitivity analysis, can be used for any historic masonry structure which is similar to that specific masonry type.

It is also important to note that the presented models are not trying to capture failure due to creep, and only aim to replicate the creep trend.

4.4.2.2. Parametric study

A parametric study is performed in this section to give more insight into the influence of input variables such as *creep parameters*, *Poisson's ratio*, *density* and *elastic modulus*, on the resulting creep simulation; curvature of the graph and strain results. For each study, 9 cases of simulation have been considered (referred to as C1-9), based on combination of parameters in defined in tables of each section.

A. Effect of creep parameters

Figure 4.14 illustrates the creep behaviour for a typical masonry structure. A parametric study can be carried out to investigate the effect of the individual creep parameters (*A*, *m* and *n*) on the shape of the strain-time plots, within the above given range.

In this graph, *n* is kept constant, but *A* and *m* are changed ±10% of their calculated value from the LSF method by MATLAB, as shown in Table 4.7.

Table 4.7: Colour and marker notation for effect of *A* and *m* results.

Colour notation	Marker
Green → *m* + 10%	Triangle → *A* + 10%
Red → *m*	Square → *A*
Blue → *m* – 10%	Circle → *A* – 10%

As it can be seen, the resulting strain-time curves have interesting trends. Note how the curves with the same colour (and *m* values) have bunched together on different strain levels. Also note the green, red and blue colour sequence which can relate to reduction of the *m* values.

It is also interesting to note that in every bunch, the curves have found their place according to their *A* values, with the highest being at the top. It is also evident that higher the m value, steeper the creep curve.
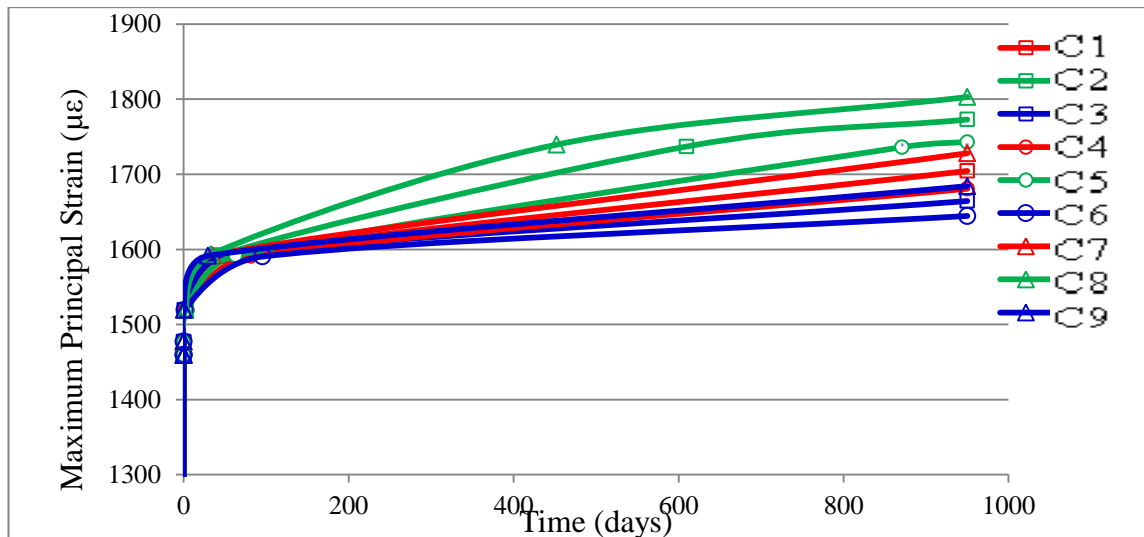
Figure 4.14: Illustration of the effect of different *A* and *m* parameters on creep results.

139

In this graph, A is kept constant, but m and n are changed $\pm 10\%$ of their calculated value from the LSF method by MATLAB, as shown in Table 4.8.

Table 4.8: Colour and marker notation for effect of m and n results.

Colour notation	Marker
Green → n + 10%	Triangle → m + 10%
Red → n	Square → m
Blue → n – 10%	Circle → m – 10%

Similar to the above figure, some interesting trends are also evident in Figure 4.15. The curves with the same colour (and n values) have bunched together on different strain levels; in the order of green, red and blue relating to reduction of the n values. Again, in every bunch, the curves have found their place according to their m values, with the highest being at the top.
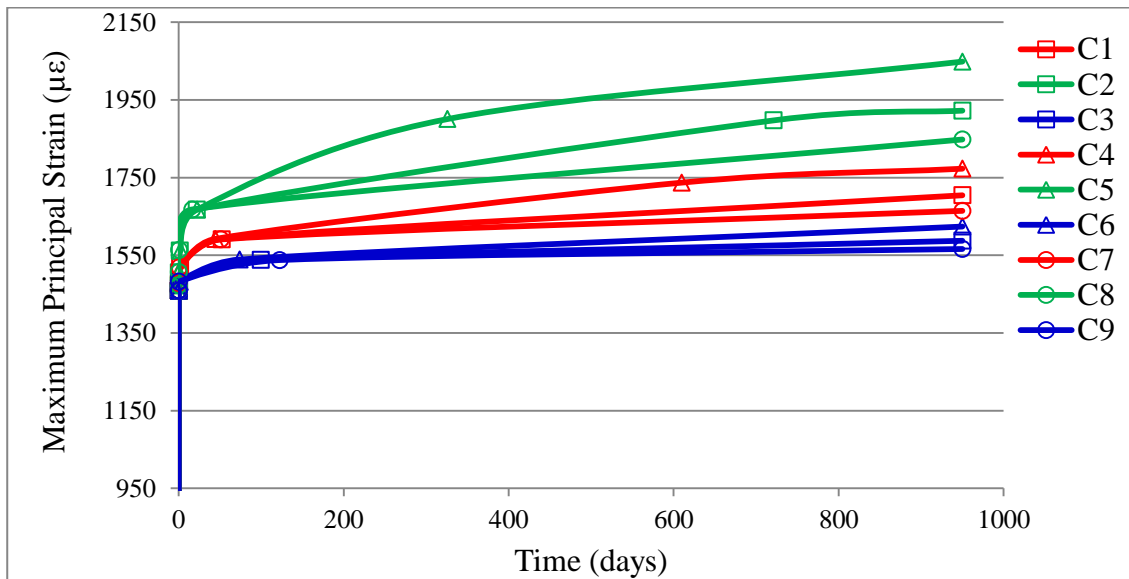
Figure 4.15: Illustration of the effect of different m and n creep parameters on strain-time simulation results.

It is observed that changing the n values causes a much larger difference to the strain values than changing m. Although one could establish relations between change in A, m and n, on an individual basis, understanding the combined effect of change in these parameters is a tedious task that is better left to computer tool; hence the use of LSF in the following sections. In addition, this method can be used to obtain a range of values for 'design guide' of each masonry type. A set of values within the design guide can be

used for other masonry types with similar material properties, to predict the creep behaviour.

B. Effect of Poisons ratio

Figure 4.16 illustrates the effect of changing the Poisson's ratio while other input variables are kept constant. The resulting strain values from three different simulations are shown in Table 4.9.

Table 4.9: The effect of change in Poisson's ratio on strain results.

Poisson's ratio, v	Strain value, ε	Label
0.05	-0.00084	P1
0.12	-0.00083	P2
0.4	-0.00076	P3
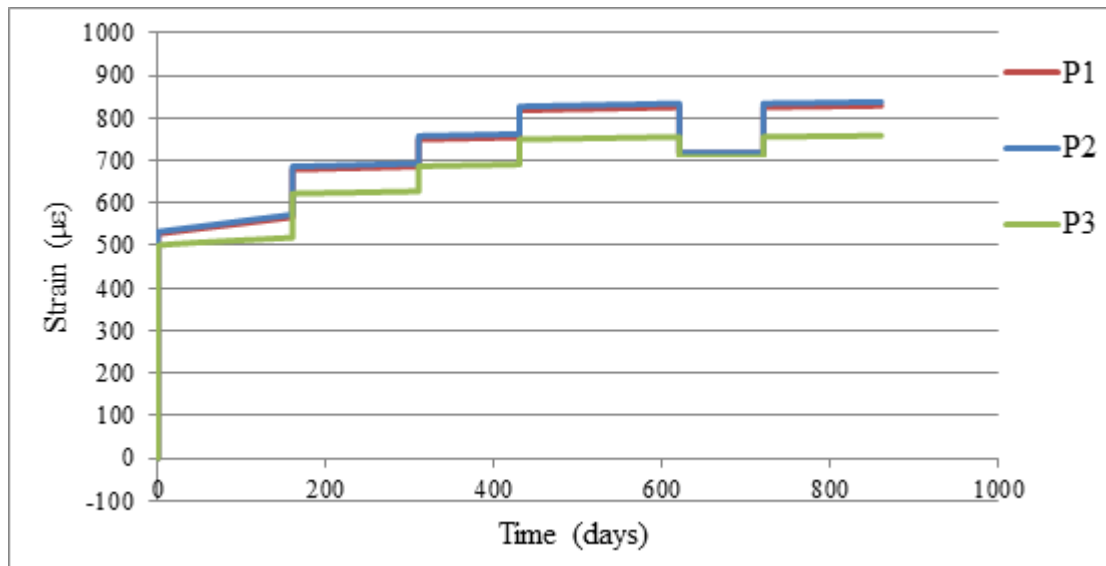
Figure 4.16: Effect of Poisson's ratio on creep curves.

As it can be seen from Table 4.9 for a small increase in Poisson's ratio value (from P1 to P2), a small change in strain value is observed. Interestingly enough, a larger change in the Poisson's ratio value (from P2 to P3), also produced a small change of 0.0001 in ε. So, it can be said that the effect of change in Poisson's ratio on change in strain value is not significant. Moreover, it is observed that increase in Poisson's ratio value decreases the creep induced strain result, though the change may not be significant.

141

C. Effect of density

Figure 4.17 shows the strain-time plot for creep in masonry and examines the effect of density on strain rate. Note that increase in density value (from 2E-06 to 2E-04Kg/mm^3) does not seem to have visible impact on the strain rate.
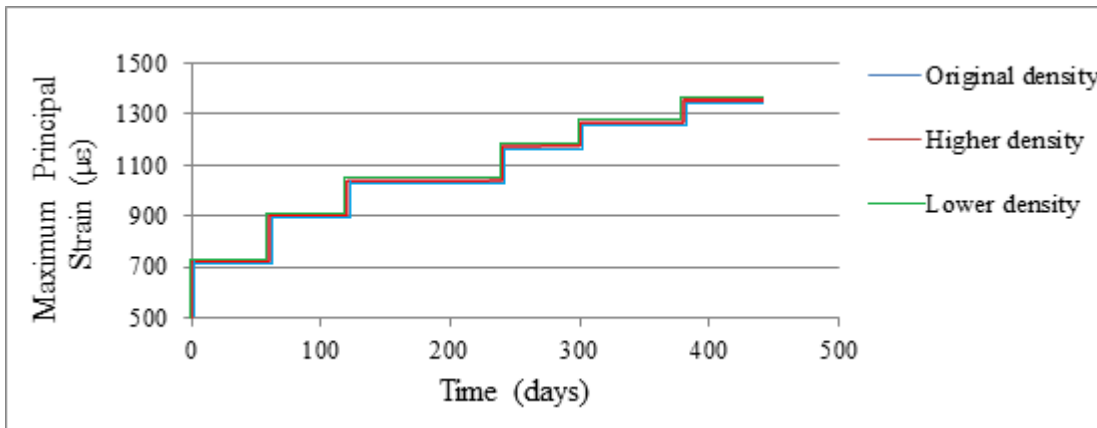
Figure 4.17: Effect of density on creep curves.

D. Effect of elastic modulus

The effect of elastic modulus on creep behaviour is examined here. Table 4.10 provides three sample values for *E* and their associated strain values obtained from Abaqus simulations. As it can be seen from both Table 4.10 and Figure 4.18, the higher the *E* value, the lower the strain value; which is due to the material's higher stiffness and resistance to the applied load. This result is as expected, which confirms the reliability of the tool in predicting creep behaviour.

Table 4.10: Effect of elastic modulus on creep results.

Parameter	Elastic modulus, E (N/mm^2)	Strain, ε
Higher E	2500	0.00118
Mean E	2184	0.00135
Lower E	1868	0.00158

142
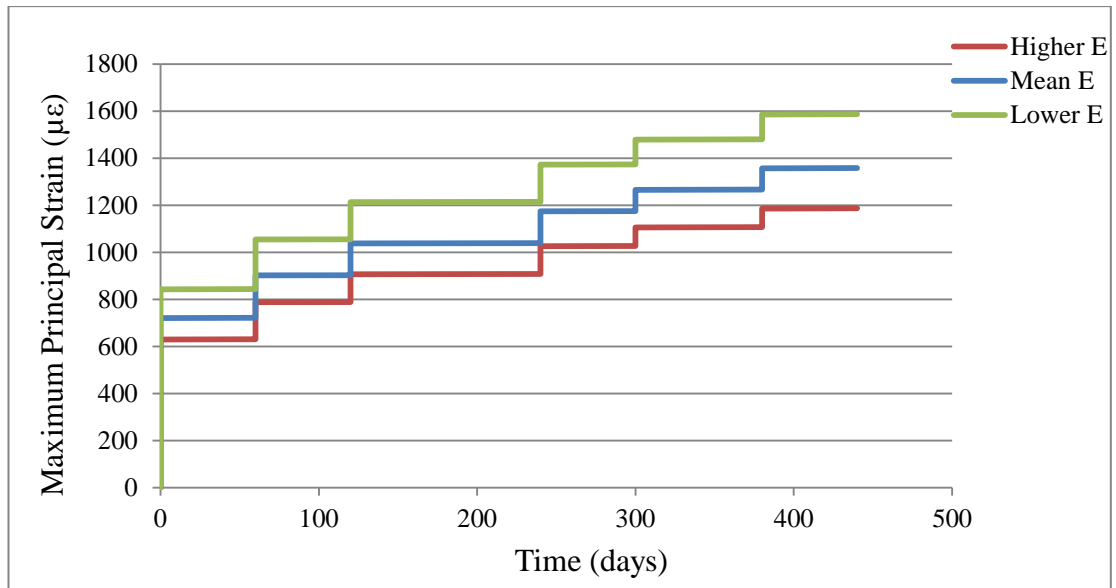
Figure 4.18: The strain-time plot for various elastic moduli.

4.4.2.3. Masonry type A

Figure 4.19 shows the results of accelerated creep test (ACT) being carried out on masonry columns with dimensions of approximately 190 x 190 x 600 mm^3, presented in (Verstrynge, 2010). According to this article, low strength clay brick masonry was used with air-hardening lime mortar (where the mortar was fully carbonated) for this test, and the specimens were stored under constant temperature of 20±1°C, and a relative humidity of 60±5% for three months before ACT was started. The paper, illustrates the vertical and horizontal strain results as negative and positive, respectively. However, this is opposite the way the results are published in the current research. The vertical and horizontal strain-time results are therefore, shown as positive and negative.
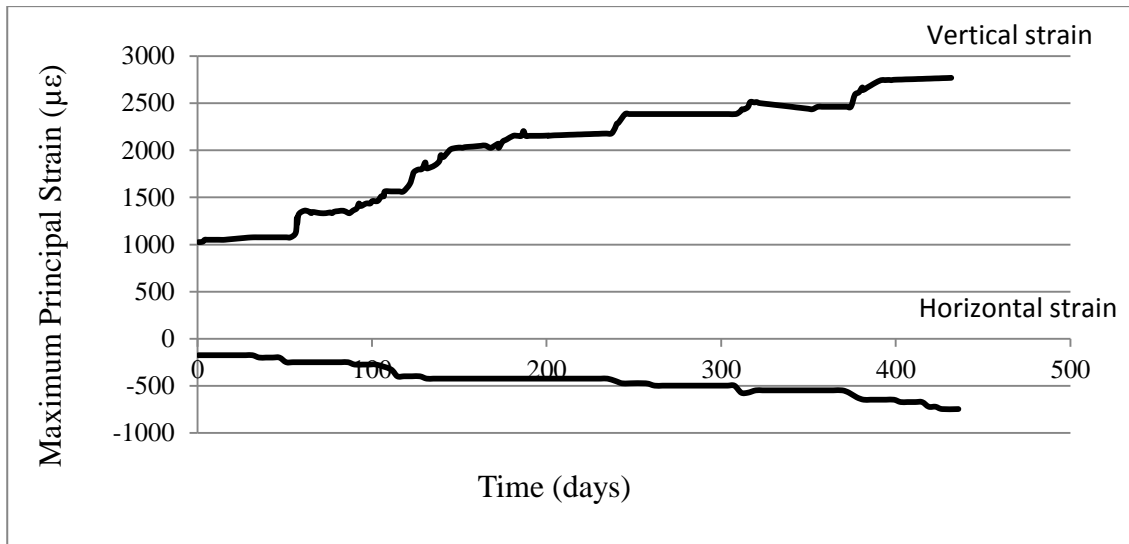
Figure 4.19: Accelerated creep test results for masonry type A; presenting vertical and horizontal strain over time (Verstrynge, 2010).

An initial stress of 1.7N/mm^2 (50% of the anticipated compressive strength), has been applied to the specimen. The stress was applied and increased in subsequent steps (in 5-10%) and kept constant for durations of approximately 2 months; as depicted in Figure 4.20.
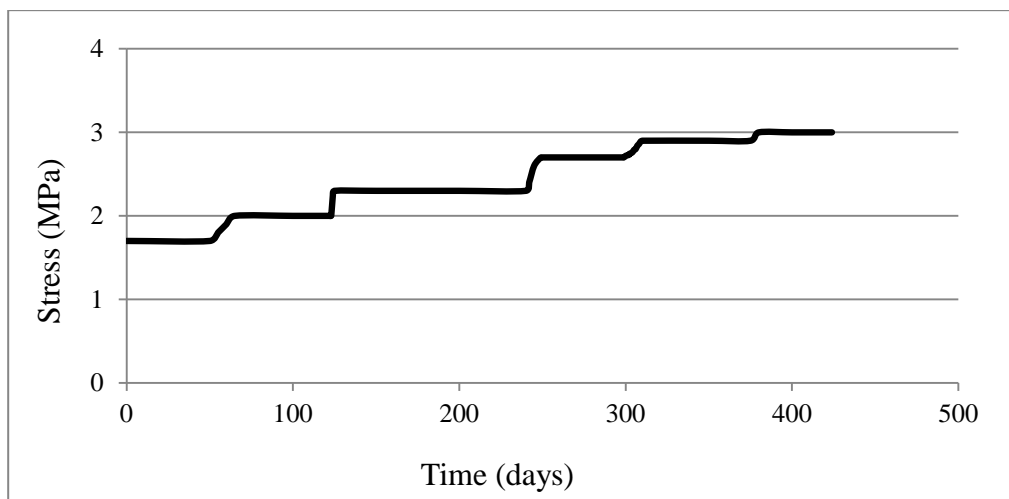
Figure 4.20: Stress applied to masonry type A (Verstrynge, 2010).

A. Sensitivity analysis

The creep power-law parameters were obtained using the same approach, giving the creep parameters of m = -0.9, n = 8, A = 1.7144e-8. The curve-fitting for masonry type

A, is shown in Figure 4.21. As it can be seen, there is a close agreement between the experiment and LSF plot, confirming the reliability of the employed MATLAB code.

In order to carry out the sensitivity analysis, ±10% of the creep parameters values has been calculated (shown in Table 4.11) and imported into Abaqus to run 27 creep simulations.
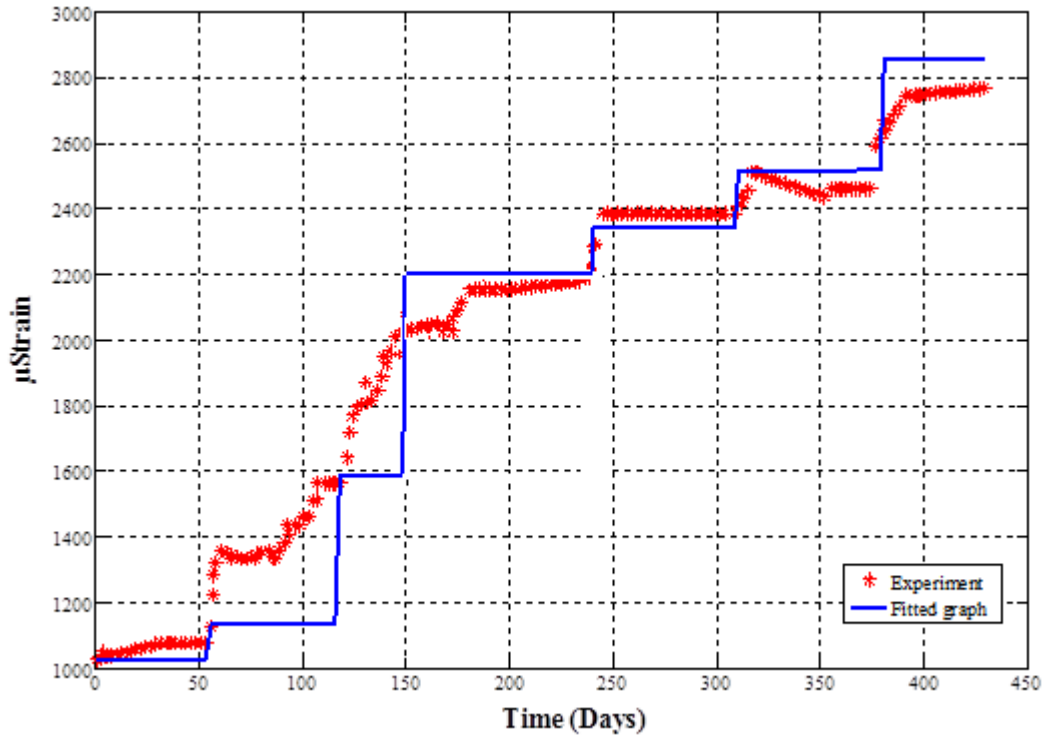
Figure 4.21: Comparison of experimental and LSF method results for long-term creep tests on masonry type A.

Table 4.11: Different sets of *A, m* and *n* values used in 27 simulations for masonry type A.

A values	*m* values	*n* values	Label
1.7144 E-8	*-0.9*	*8*	A1
		8.8	A2
		7.2	A3
	-0.81	**8**	A4
		8.8	A5
		7.2	A6
	-0.99	**8**	A7
		8.8	A8
		7.2	A9
1.8858 E-8	-0.9	**8**	A10
		8.8	A11

		7.2	A12
		8	A13
	-0.81	8.8	A14
		7.2	A15
		8	A16
	-0.99	**8.8**	A17
		7.2	A18
		8	A19
	-0.9	**8.8**	A20
		7.2	A21
		8	A22
1.5429 E-8	-0.81	8.8	A23
		7.2	A24
		8	A25
	-0.99	**8.8**	A26
		7.2	A27

B. Simulation of the creep results

The following material properties for masonry type A have been used in Abaqus:

$E = 2184\text{N/mm}^2$, $v = 0.2$. An Elastic Modulus value was not given for the specimen used in this test. Instead, average of the two given values of E^k (E of the Kelvin model) and E^m (E of the Maxwell model), were used for Abaqus simulation (Verstrynge, 2010).

The strain-time plot for masonry type A is shown in Figure 4.21, where a good trend between theoretical and experimental results can be seen. Figure 4.22 presents the simulation results of the 27 creep parameter sets for vertical and horizontal creep curves, against the experimental results for the sensitivity analysis explained above. As it can be seen, the creep experiment and simulation results for masonry type A are in good agreement; this is evident in both vertical and horizontal creep curves. The response initiates with primary creep and a steady state is reached approximately from day 120 to day 300, representing the secondary creep. The stepwise increase in the strain path is continuous, until the tertiary creep phase is reached where failure gradually occurs. As seen, the final vertical creep strain value predicted by the model is 2780 με, which is close to the experiment's strain value of 2760 με (shown in bold) and within the range of 20% of 2760 (2215 ↔ 3321 με), confirming the reliability of the proposed tool, despite presence of numerous unknowns, resulting from complex nature of masonry and estimation of the material properties.

A good agreement is also visible between the horizontal strain curves. The curves signify lateral tension in the specimen. As the curve reaches tertiary creep phase, it gradually reaches the critical strength of the softening zone and cracks would form. As

mentioned before, the model is not trying to capture the peak failure of creep curves, but their actual trend.

The final vertical strain values for all the curves fit within the 20% range. The parameter ranges for *A*, *m* and *n* are all the values specified in Table 4.12, amongst which the curves which best fit the experimental results for masonry type A, have the parameter ranges of *A*, *m* and *n* (values shown in bold):

A: 1.5429E-8 , 1.7144E-8, 1.8858E-8

m: -0.99, -0.9, -0.81

n: 7.2, 8, 8.8

In this case, all the curves except A5, A14, and A23 present a good simulation fit with the experimental curve.
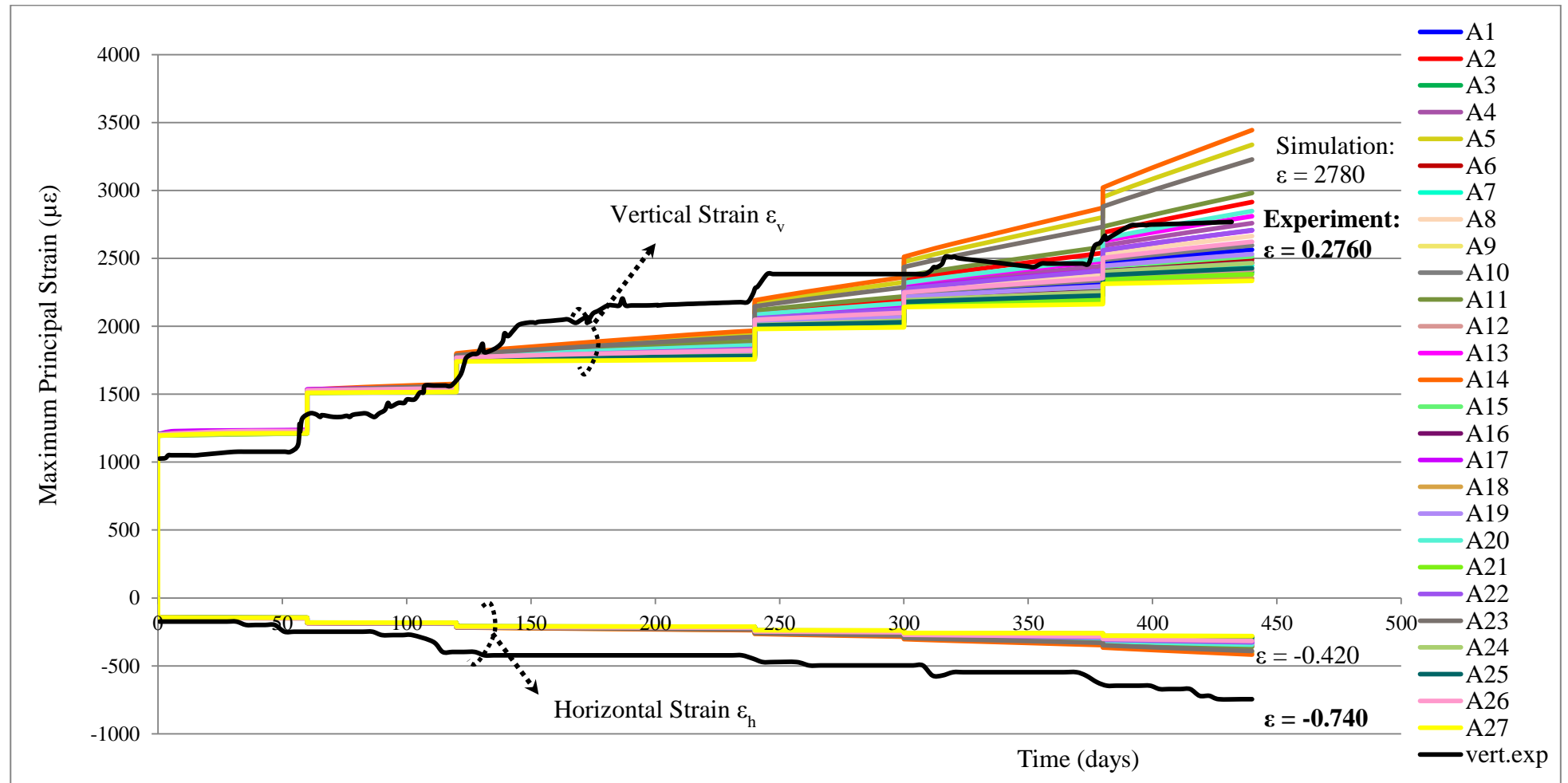
Figure 4.22: Theoretical and experimental predictions (vertical and horizontal) for creep curves of masonry type A- (27 creep parameter set).

4.4.2.4. Masonry type B

This section focuses on the creep test results presented in (Anzani *et al*, 2000), which have been obtained from the tests carried out on the specimens recovered from the internal wall of the Civic Tower of Pavia, in Italy.

According to this paper, the construction of the tower was carried out in four phases, between years 1060-1598. The tower's belfry was built with granite blocks and its walls had multiple leaves with the following material properties:

- Two external leaves; thin regular brickwork
- Internal leaf; Random rubble masonry

Since the internal leaf constituted thick layers of mortar, creep is more likely to have formed in that leaf, hence the long-term creep tests on the internal leaf of the tower. An initial stress of 40-50% of the static strength of the material (estimated by sonic tests) has been applied to the specimens (Anzani, 2009; 2000).

Figure 4.23 presents long-term creep tests, carried out for six blocks of masonry with dimensions of 300x300x510mm^3. The specimens have been kept under controlled conditions of 20°C and 50% RH. Hydraulic machines and LVDTs[37] were used to keep conditions constant, and to take strain readings (horizontal and vertical strains), respectively.
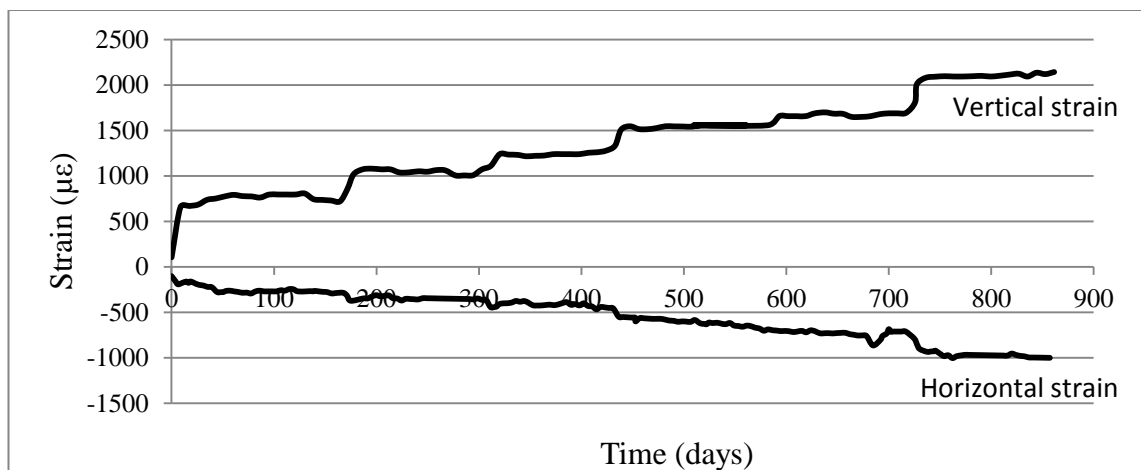
Figure 4.23: Average (vertical and horizontal) strain components (Anzani *et al*, 2000).

---

[37] A transduced that converts a linear displacement into information that provides direction and distance information.

As mentioned, the load was initially increased and then kept constant, as seen in Figure 4.24 (Anzani, 2000). As seen, the vertical strain curve shows increase in strain with time (due to compressive stress). The horizontal strain curve represents transverse strain, where the negative values replicate dilation, resulted from crack formation in specimen. Specimen labelled 102A has been chosen for simulating the results in Abaqus.
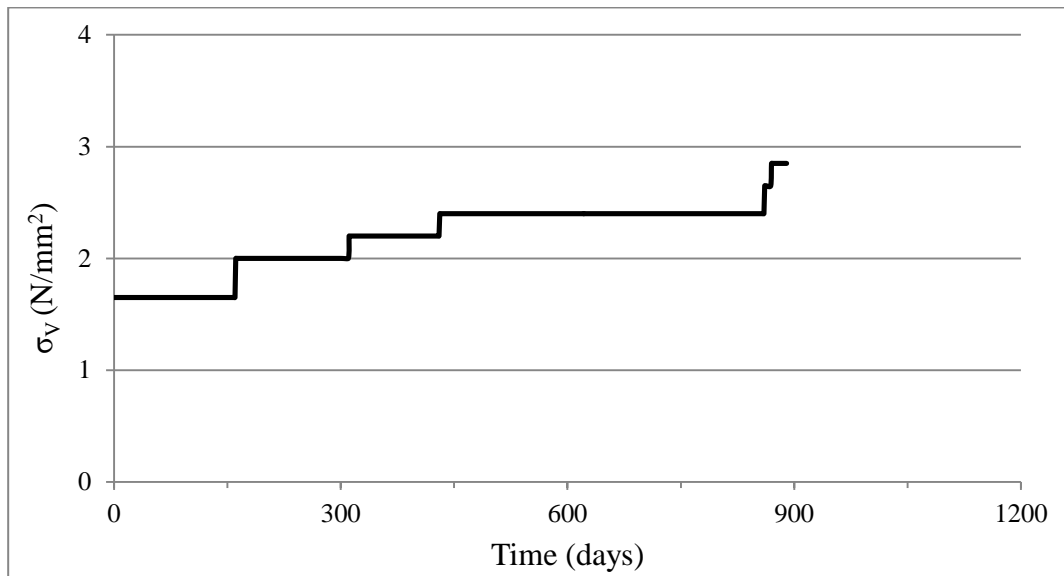
Figure 4.24: Nominal stress versus time for specimen 102 A (Anzani *et al*, 2000).

A. Sensitivity analysis

Figure 4.25 illustrates the curve-fitting for masonry type B, and the obtained creep parameter values are found to be *m* = -0.9, *n* = 8, *A* = 8.5682E-7. Different sets of creep parameters, using the LSF method, are given in Table 4.12.
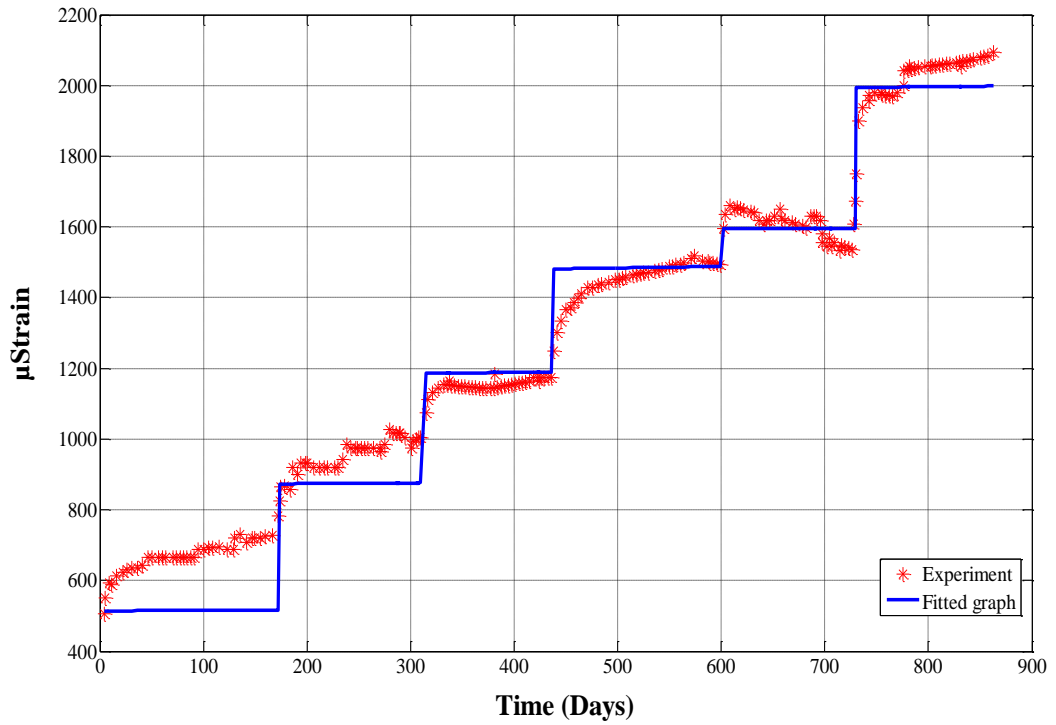
Figure 4.25: Comparison of experimental and LSF results for long-term creep tests on masonry type B.

Table 4.12: Different sets of *A, m* and *n* values, used in 27 simulations for masonry type B.

A values	*m* values	*n* values	Label
8.5682 E-7	*-0.9*	*8*	B1
		8.8	B2
		7.2	B3
	-0.81	8	B4
		8.8	B5
		7.2	B6
	-0.99	**8**	B7
		8.8	B8
		7.2	B9
9.42502 E-7	-0.9	**8**	B10
		8.8	B11
		7.2	B12
	-0.81	8	B13
		8.8	B14
		7.2	B15
	-0.99	**8**	B16
		8.8	B17
		7.2	B18
7.71138 E-7	-0.9	**8**	B19
		8.8	B20
		7.2	B21
	-0.81	8	B22

		8.8	B23
		7.2	B24
		8	B25
	-0.99	8.8	B26
		7.2	B27

B. Simulation of the creep results

The following material properties for masonry type B have been used in Abaqus (Anzani, 2000): $E = 3080\text{N/mm}^2$, $v = 0.2$. In this case, the Elastic Modulus value was not provided for the specimen, and as such the value was calculated using an approximated initial strain value from the creep curve[38].

Figure 4.26 compares the vertical creep experiment results and the simulated results obtained from the LSF method. As it can be seen, vertical strain-time curves of both simulation and experiment are in reasonable agreement, as they have very similar steps where the loads are applied. The initial strain levels are directly influenced by the material's response to the applied load. A reasonably clear primary, secondary and tertiary creep phase can be seen in the simulation curve. There is a small discrepancy between strain values of the two curves, which can be reduced by using a more precise Elastic Modulus value. As expected, the simulation results agrees with the experimental behaviour well, as both have a similar general trend with the final ε values being just 0.0002 apart.

The horizontal creep strain-time experimental results are plotted in Figure 4.27. Like before, a similar trend is visible between the two curves.

The experimental and theoretical predictions (of the 27 sets) for the strain-time plots are shown in Figure 4.28. A general increase in the strain trend can be seen in the curves, which represents true creep behaviour; accumulation of strain with time under constant load. It can be seen that the load has been applied in subsequent steps and kept constant in each step, until the creep strain reached a constant value, or steady state has been reached. A sudden drop in strain values can be seen in the simulation curves (between days 620-700), which indicates unloading of the specimen. It is interesting to note that even though a considerable part of the total strain is regained during this phase (due to its elasticity), small amount of the strain values remain, indicating the irreversible creep strain in masonry. The curve picks up as expected when applying load after day 700,

---

[38] $E = 1.65/0.54 \times 10^{-3} = 3080 N/mm^2$

where the tertiary creep is visible and continues until the failure in tertiary phase is reached. At this phase, materials dilate under the compressive stress (shown as negative values) due to presence and rapid increase of horizontal strain. With rapid increase in strain rate, failure of the material is obtained.
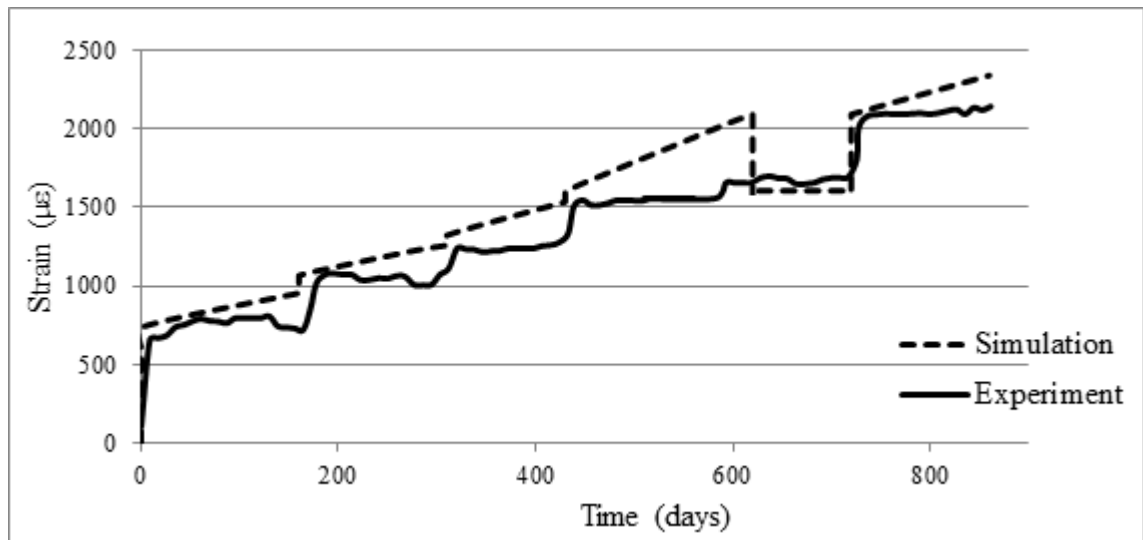
Figure 4.26: Strain-time plots from simulation and experimental results of specimen 102A, masonry type B.
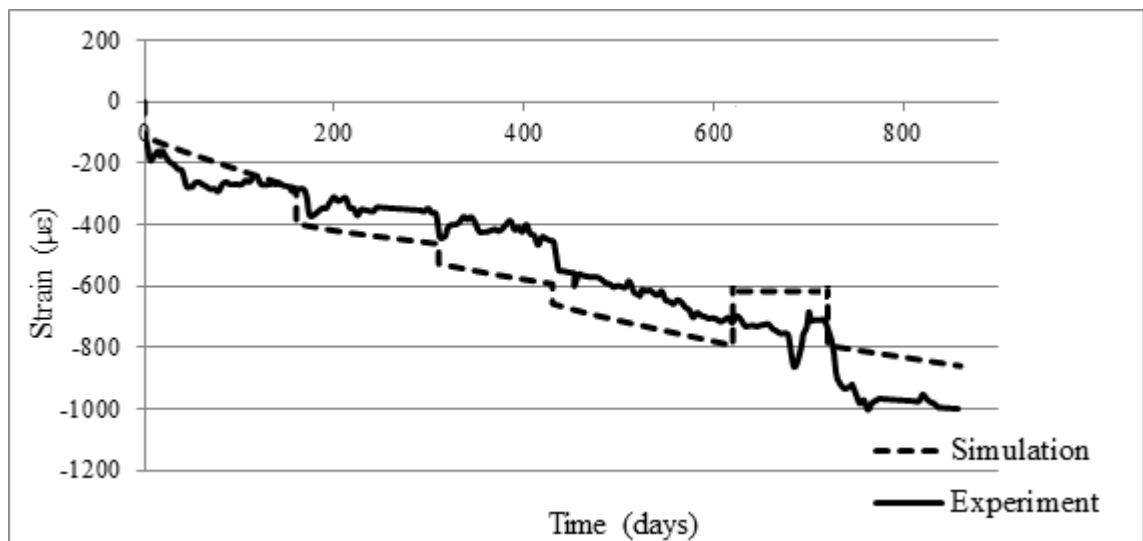
Figure 4.27: The creep strain-time plot from simulation and. experimental results masonry type B.
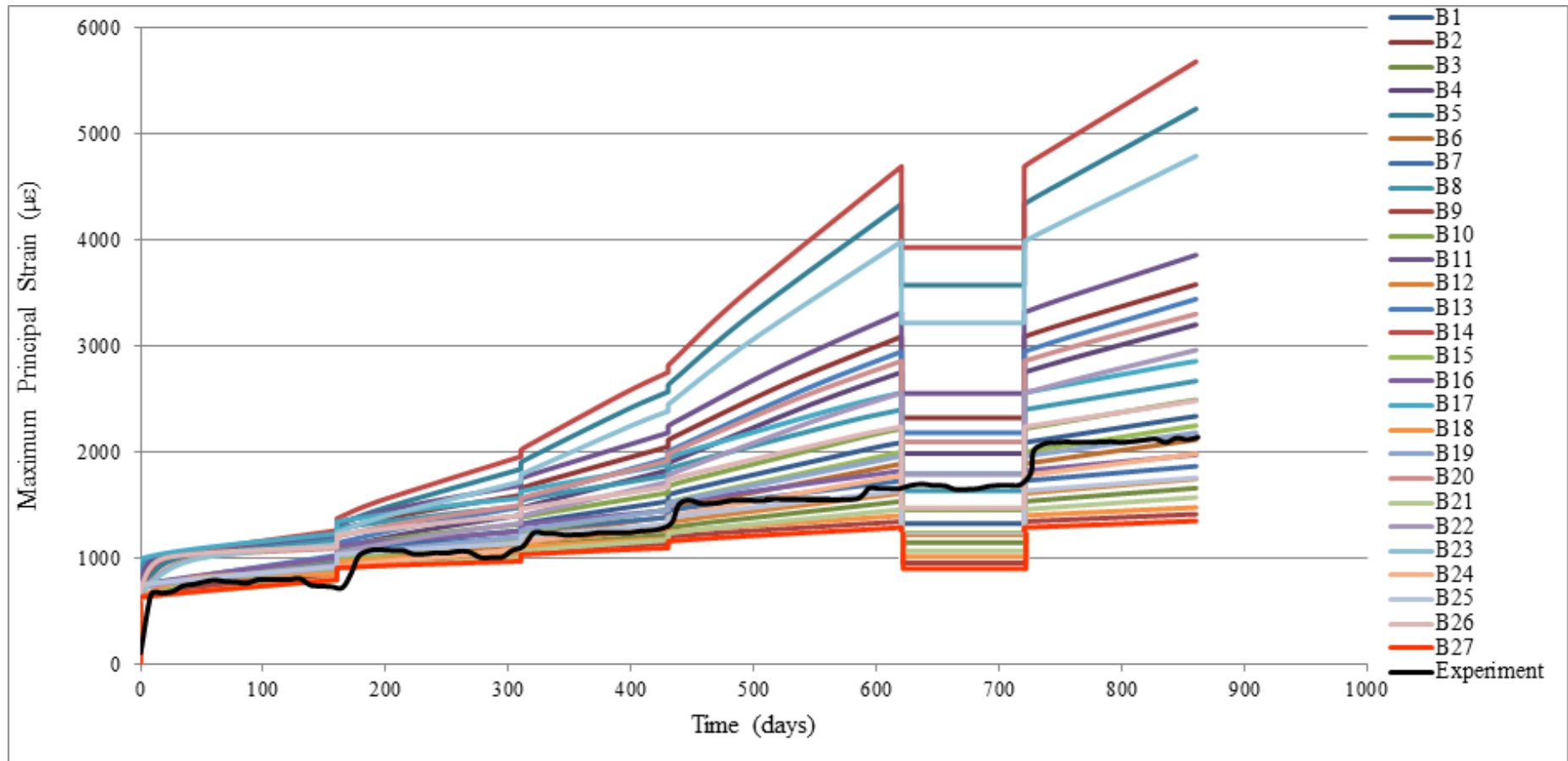
Figure 4.28: The vertical theoretical and experimental predictions for creep curves of masonry type B (27 parameter sets).

As it can be seen from the results, presented in Figure 4.28, the curves which best fit the experimental results for masonry type B, have the parameter ranges of *A*, *m* and *n* (values shown in bold in Table 4.12):

A: $7.71138E - 7$, $8.5682 E - 7$, $9.42502E - 7$

m: -0.81, n: 7.2

m: -0.9, n: 8 , m: -0.99, n: 8

4.4.2.5. Masonry type C

The article (Verstrynge 2008) assesses the long-term behaviour of masonry under creep, for one single type of historic brick masonry, that has been combined with the following three types of mortar; representing the historical masonry encountered in Belgium:

- o Hydraulic lime mortar
- o Cement mortar
- o Hybrid lime-cement mortar; referred to in the paper as air hardening lime mortar and a cement-lime mortar.

The creep tests were carried out on wallets of masonry with dimensions of 0.29x0.19x0.85m, where 14 layers were placed on top of each other; each layer having 3 bricks (0.19x0.09m) in a rectangular layout.

The experimental results for the creep tests on these masonry wallets are presented in Figure 4.29. The percentage values in the bracket refer to the specimens being initially loaded at 50, 65 and 80 percent of the material's compressive strength, which are obtained by averaging the results of the monotonic tests (Verstrynge, 2008).

As the majority of historic masonry had been constructed using both hydraulic lime and air hardening mortars, the model was tested on both creep results for these two types of mortar, to find a range of creep parameters for this type of masonry. The vertical strain-time curves are marked as (a) and (b), respectively in Figure 4.30. Both these two curves were chosen to have the same initial loading of 50% of their compressive strength, to illustrate the effect of different mortars on creep in masonry. The horizontal strain results were not provided for these tests.

The creep tests presented for historic brick masonry and hydraulic lime mortar (50%), are discussed in this section, and referred to as masonry type C. Moreover, the results for hybrid lime-cement mortar (50%) will be discussed in the next section, titled Masonry type D.
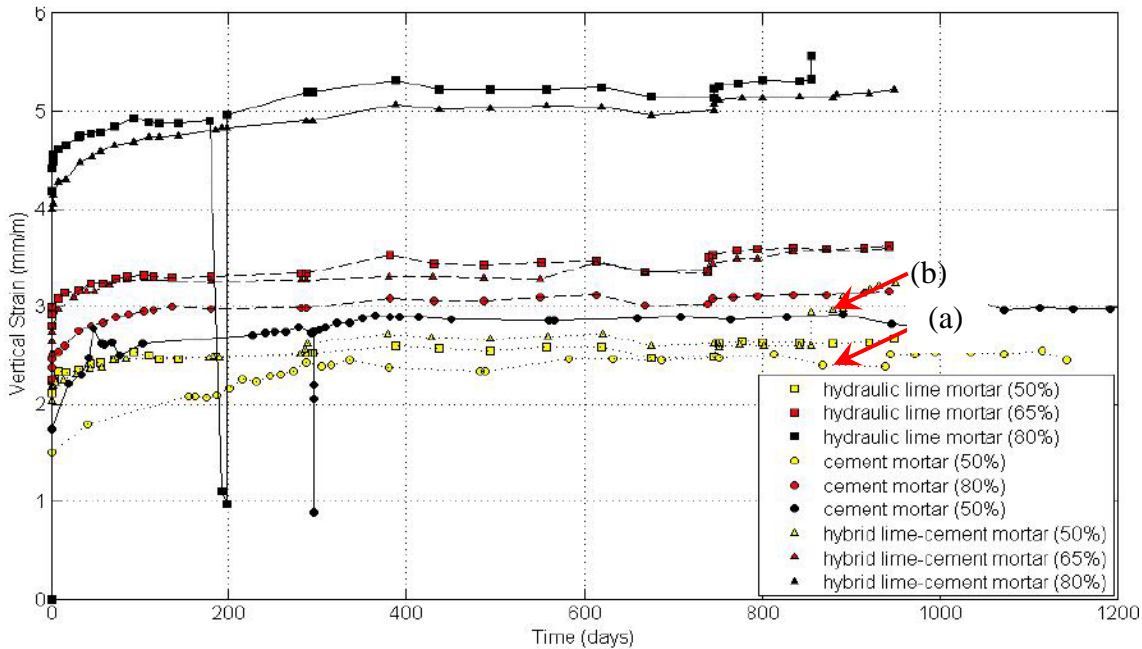
Figure 4.29: Vertical deformations during long-term creep tests (Verstrynge, 2008).

Details of the stress levels applied to the wallets are given in Table 4.13. There is a small increase in the stress level (5% of the compressive strength), around period of 750 days (Verstrynge, 2008). As expected, the initial stress and strain are directly proportional.

Table 4.13: Stress applied to masonry type C.

Stress (N/mm^2)	Duration (days)
3.15	1-750
3.5	750-950

A. Sensitivity analysis

The creep power-law parameters were again obtained using MATLAB, and are given in Table 4.14. Curve fitting is also done for creep test on masonry type C (Hydraulic lime mortar 50%), giving the following range of:

156

A = 6.8737 E-9, m = -0.9, and n = 8

Table 4.14: Different sets of *A, m* & *n* values, used in 27 simulations for masonry type C.

A values	*m* values	*n* values	Label
6.8737 E-9	*-0.9*	*8*	C1
		8.8	C2
		7.2	C3
	-0.81	**8**	C4
		8.8	C5
		7.2	C6
	-0.99	8	C7
		8.8	C8
		7.2	C9
7.5611 E-9	-0.9	**8**	C10
		8.8	C11
		7.2	C12
	-0.81	**8**	C13
		8.8	C14
		7.2	C15
	-0.99	8	C16
		8.8	C17
		7.2	C18
6.1863 E-9	-0.9	8	C19
		8.8	C20
		7.2	C21
	-0.81	**8**	C22
		8.8	C23
		7.2	C24
	-0.99	8	C25
		8.8	C26
		7.2	C27

B. Simulation of the creep results

The following material properties for masonry type C have been used in Abaqus, in Table 6.7 in (Verstrynge, 2010b): E = 2025N/mm^2, v = 0.12. As the value of the Elastic Modulus, E, was not given for the specimen used in this test, average of the two given values of E^k (E of the Kelvin model) and E^m (E of the Maxwell model), were used for Abaqus simulation.

As expected, the simulation results agrees with the experimental behaviour well, as both have a similar general trend with a difference of 20% between the final ε values; seen in Figure 4.30.
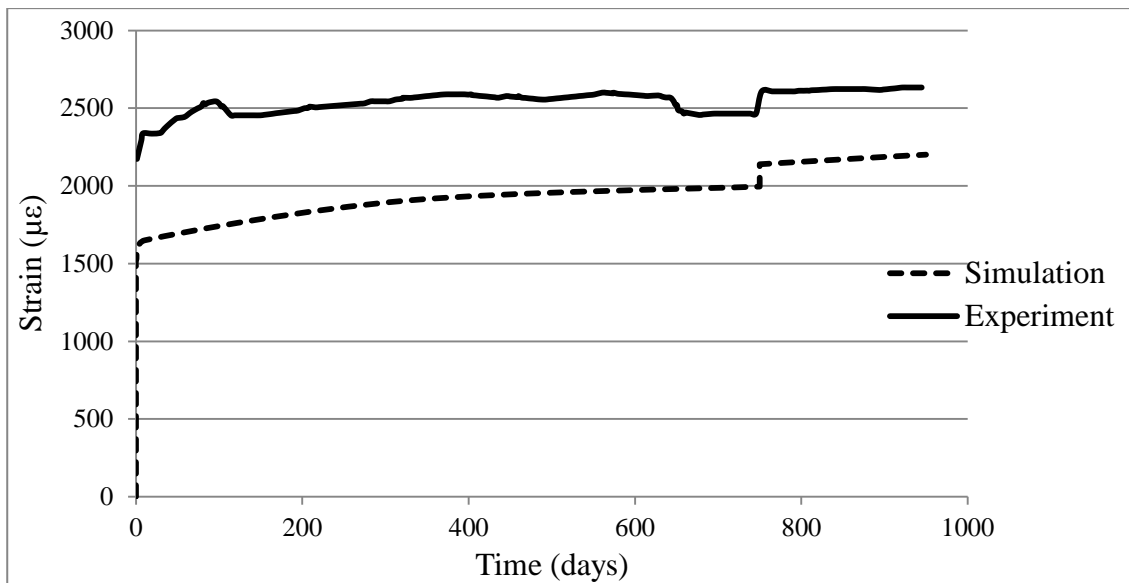
Figure 4.30: Strain-time plots from simulation and experimental results masonry type C.

Figure 4.31 presents the horizontal and vertical strain-time plots of the 27 sets outlined in the sensitivity analysis section, and the experimental data (thick black line) given in (Verstrynge, 2008). As it can be seen, not only there is a similar trend between the simulation and experimental data, but also the experimental curve fits in the middle of the theoretically calculated creep set range. Note that almost identical strain values are observed at the point where there is an increase in stress (i.e. day 750), and afterwards where the tertiary creep phase begins.

As it can be seen, the parameter ranges for *A*, *m* and *n* that fit well with the experiment results are:

A: 6.1863 E-9 ,6.8737 E-9,7.5611 E-9

m: -0.9   *n*: 8.8 , *m*: -0.81   *n*: 8 , *m*: -0.99   *n*: 8.8

It can therefore, be said that the suggested range of creep parameters gives an accurate prediction of the creep behaviour and so can be used for other masonry structures with similar material properties.
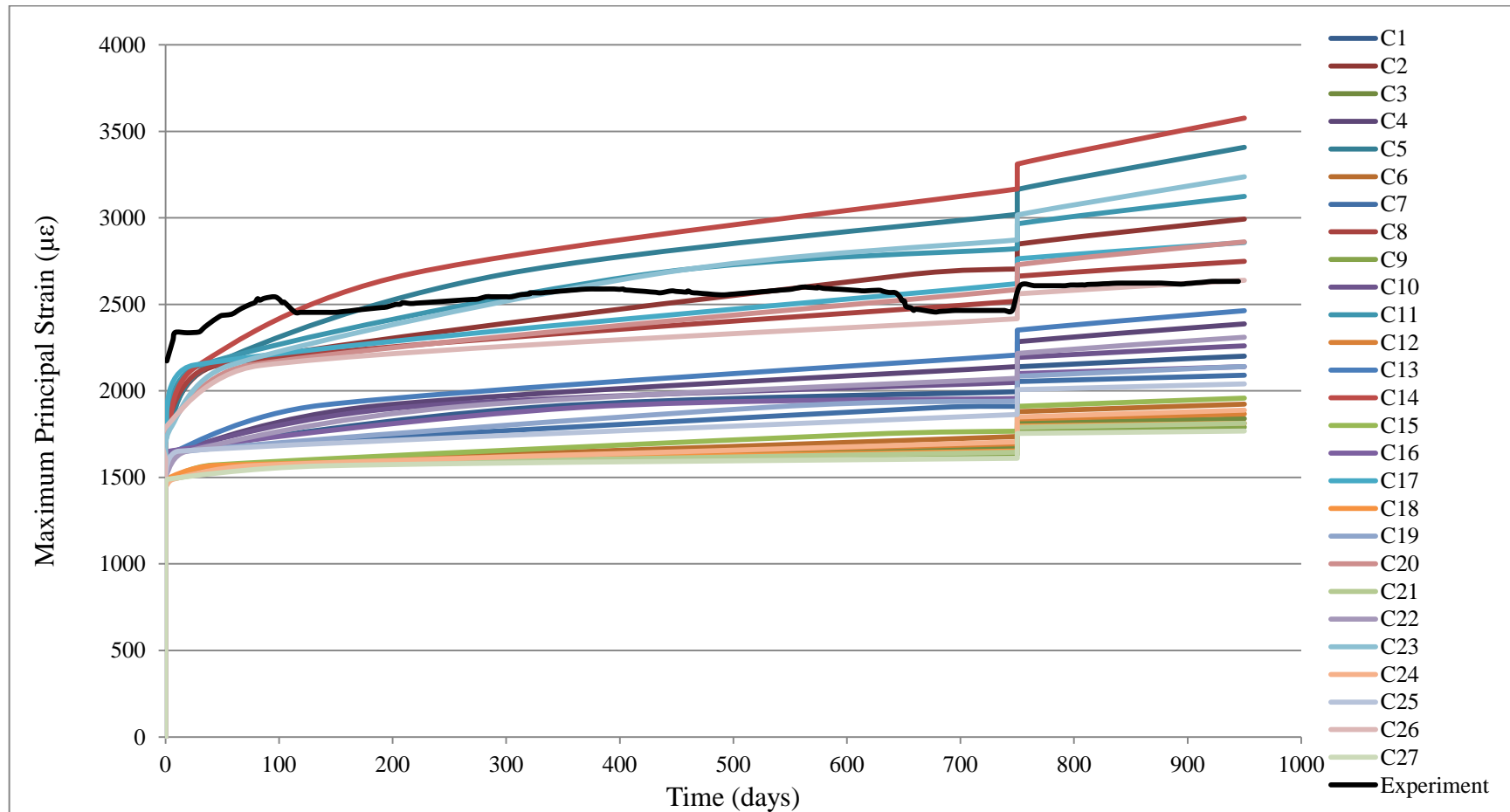
Figure 4.31: Experimental and theoretical predictions (vertical and horizontal) for creep curves of masonry type C (27 parameter sets).

4.4.2.6. Masonry type D

As mentioned in the previous section, the following is concentrating on Masonry type D, where historic brick masonry is combined with hybrid lime-cement mortar. The specimens are initially loaded at 50% of their compressive strength. There is also a small increase in the stress level (5% of the compressive strength), around period of 850 days (Verstrynge, 2008); details are given in Table 4.15.

Table 4.15: Stress applied to masonry type D.

Stress (N/mm^2)	Duration (days)
3.65	1-850
4	850-950

A. Sensitivity analysis

The obtained creep parameter values are found to be A = 8.8755 E-9, m = -0.9, and n = 8. The creep parameters for 27 cases are shown in Table 4.16.

Table 4.16: Different sets of A, m and n values, used in 27 simulations for masonry type D.

A values	m values	n values	Label
		8	D1
	-0.9	8.8	D 2
		7.2	D 3
		8	D 4
	-0.81	8.8	D 5
8.8755 E-9		7.2	D 6
		8	D 7
	-0.99	8.8	D 8
		7.2	D 9
		8	D 10
	-0.9	8.8	D 11
		7.2	D 12
		8	D 13
9.7631 E-9	-0.81	8.8	D 14
		7.2	D 15
		8	D 16
	-0.99	8.8	D 17
		7.2	D 18
		8	D 19
7.9880 E-9	-0.9	8.8	D 20
		7.2	D 21

		8	D 22
	-0.81	8.8	D 23
		7.2	D 24
		8	D 25
	-0.99	8.8	D 26
		7.2	D 27

B. Simulation of the creep results

The following material properties for masonry type D have been used in Abaqus (Verstrynge, 2008): $E = 2025\text{N/mm}^2$, $v = 0.12$. As the value of the Elastic Modulus, E, was not given for the specimen used in this test, average of the two given values of E^k (E of the Kelvin model) and E^m (E of the Maxwell model), were used for Abaqus simulation.

As depicted in Figure 4.32, the simulation results agree very well with the experimental results, as both have a very similar trend with the difference between the final ε values being as small as 50, almost the same.
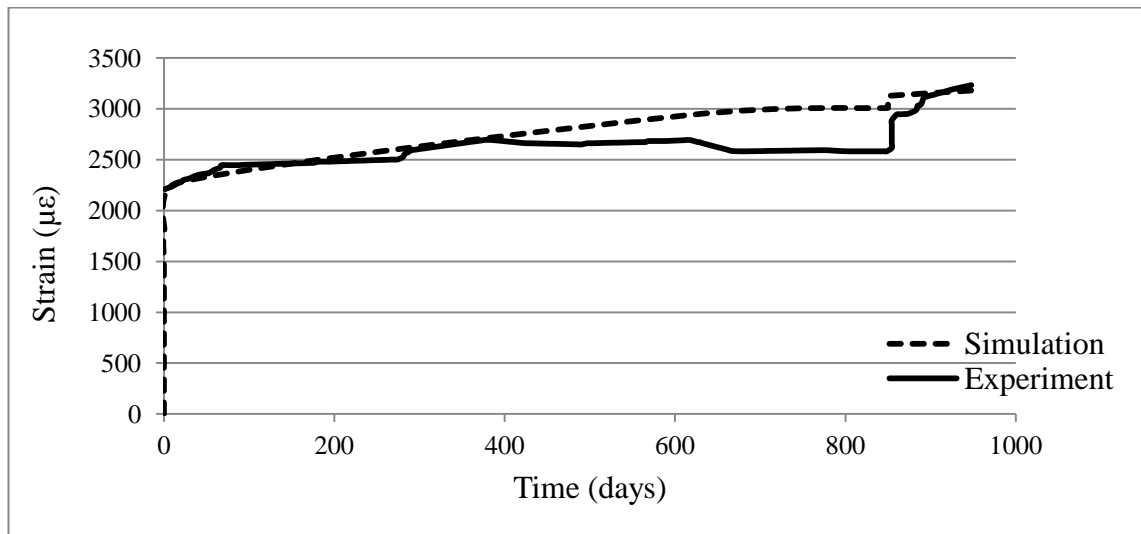
Figure 4.32: Strain-time plots from simulation and experimental results of masonry type D.

Figure 4.33 presents the horizontal and vertical strain-time plots of the 27 sets identified above, against the experimental results for masonry type D, where a good agreement is evident between the curves. The results seem to be divided into three batches. The top batch consist of curves D2, D14, D23, etc., where *n* has the highest value of its range (n

= 8.8). The second and third batch also follow with similar trend, having $n = 8$ and $n = 7.2$, respectively. This means that a high n value, increases the strain values.

The general response of the curves (in Figure 4.33) initiate with primary creep and a steady state is reached approximately from day 300 to day 800, representing the secondary creep. The stepwise increase in the strain path is significant at day 850, where there has been a slight increase in stress and also when the specimen reaches the tertiary creep. As seen, the final creep micro-strain value predicted by the model is 3210, which is almost the same as the experiment's strain value of 3220. This is an excellent fit which confirms the reliability of the proposed tool. As observed from the figure, the parameter ranges for *A*, *m* and *n* are:

A: 7.9880E-9, 8.8755E-9, 9.7631E-9

m: -0.99, -0.9, -0.81

n: 8
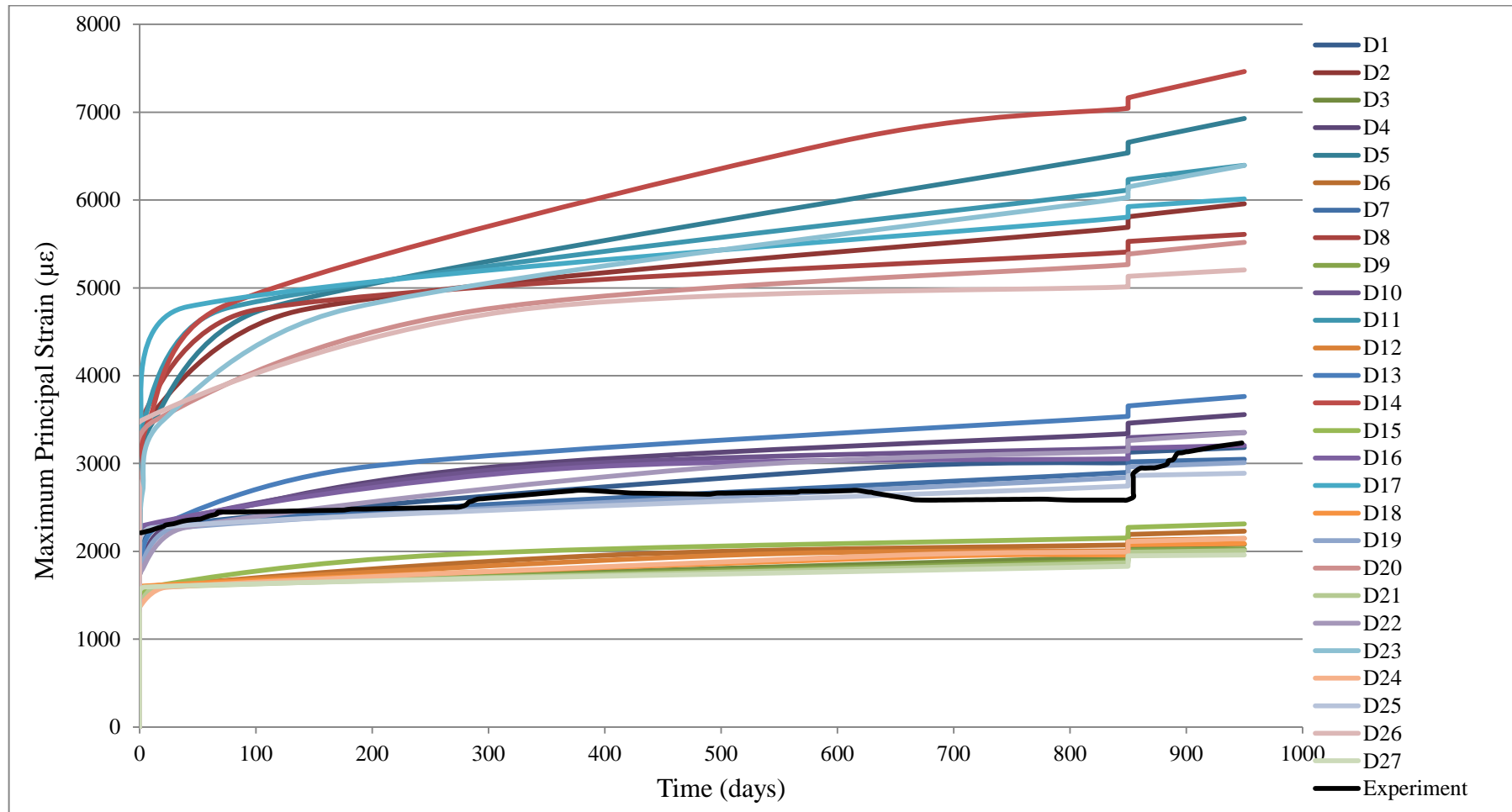
Figure 4.33: Experimental and theoretical predictions (vertical and horizontal) for creep curves of masonry type D (27 parameter sets).

4.4.2.7. Masonry type E

The type of masonry covered in this section is not considered as historic masonry. This type of masonry is being simulated, as it has similar material properties as the pier used for validation of this computational tool in the next chapter.

Three types of clay brickwork were tested in this paper, out of which Class B clay brick were adopted for this test, as they were the same type of masonry used in the Larpool Viaduct piers. A cement based mortar, namely, a 1: ½: 4½ (OPC: cement: lime) mortar mix, was used in the construction of these piers.

The tests were carried out on 5 piers, each being loaded at either of 3, 7, 14, 28 or 56 days. As the Larpool viaduct has taken a long time to cure, the pier that was loaded at 56 days was chosen for simulation in this section. Figure 4.34 shows the results of long-term creep tests on a pier of masonry, constructed of; 2 brick wide and 13 course high. Mortar thickness of 10mm was assumed to be used between the bricks. The overall dimensions of $215 \times 214 \times 965 mm^3$ was adopted in this simulation (Brooks *et al*., 1997).
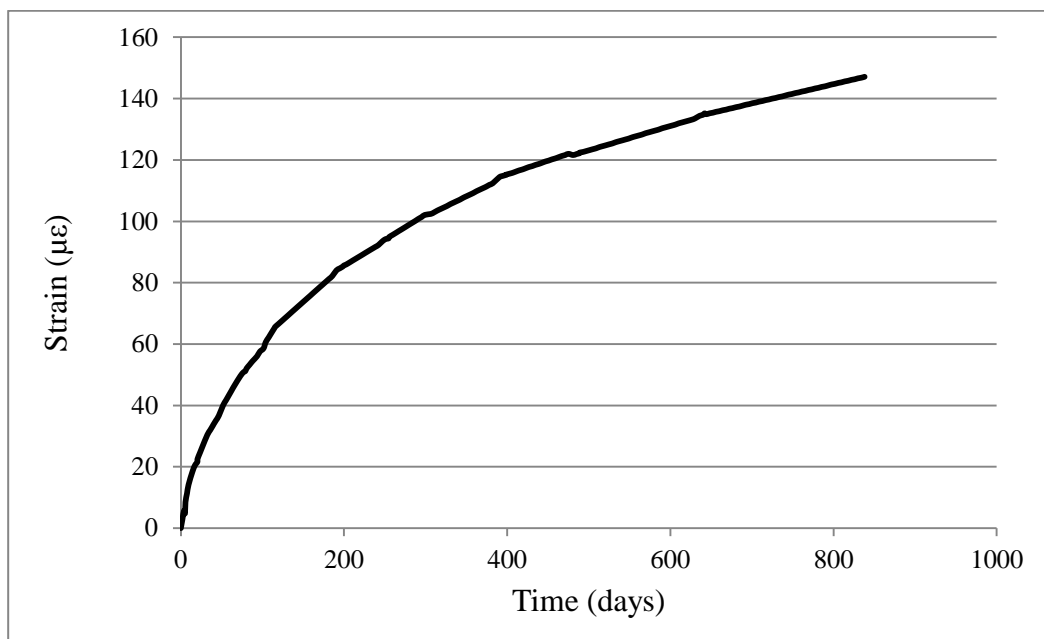
Figure 4.34: Strain-time curve for class B clay-brick masonry; masonry type E (Brooks *et al*., 1997).

An initial stress of 1.5N/mm^2 (during the first day) has been applied to the pier and kept constant during the experiment. The test was carried out for an approximate duration of 838 days.

A. Sensitivity analysis

The creep power-law parameters were again obtained using MATLAB, and are given in Table 4.17. Curve fitting is also done for creep test on masonry type E.

$A = 1.5806$ E-7, $m = -0.6$, and $n = 8$

Table 4.17: Different sets of *A, m* & *n* values, used in 27 simulations for masonry type E.

A values	*m* values	*n* values	Label
1.5806 E-7	*-0.6*	*8*	E1
		8.8	E2
		7.2	E3
	-0.54	**8**	E4
		8.8	E5
		7.2	E6
	-0.66	8	E7
		8.8	E8
		7.2	E9
1.7387 E-7	-0.6	**8**	E10
		8.8	E11
		7.2	E12
	-0.54	**8**	E13
		8.8	E14
		7.2	E15
	-0.66	8	E16
		8.8	E17
		7.2	E18
1.4225 E-7	-0.6	**8**	E19
		8.8	E20
		7.2	E21
	-0.54	**8**	E22
		8.8	E23
		7.2	E24
	-0.66	8	E25
		8.8	E26
		7.2	E27

A. Simulation of the creep results

The following material properties for masonry type E have been used in Abaqus, (Brooks *et al.*, 1997): $E = 15460\text{N/mm}^2$, $v = 0.22$. The pier masonry has compressive strengths of 98.3 N/mm^2 and 9.6N/mm2, for brick and mortar respectively. As the value of the Poisson's ratio, was not given for the specimen used in this test, an average value of the typical mortars used in such construction was used in Abaqus simulation.

The results in the paper have also shown that the pier has exhibited a small and yet slow moisture expansion; since it is negligible can be ignored in simulating the creep in this pier.

Figure 4.35 presents the vertical strain-time plots of the 27 sets outlined in the sensitivity analysis section, and the experimental data (thick black line) given in (Brooks *et al.*, 1997). As expected, the simulation results agree with the experimental behaviour well, as both curves have very similar trend. In addition, the experimental curve fits in the middle of the theoretically calculated creep set range.

As it can be seen, cement-based brick masonry have much lower strain values over time in comparison with historic masonry that mostly lime-based masonry, indicating their higher resistance to long-term creep in cement-based masonry structures. However, despite such resistance moisture seepage and creep in cementations materials, attributes to crack growth, as under sustained loading (which is the case for the experiment in this set of experiments) forced moisture redistribution in masonry pores over time causes de-bonding and re-bonding of the cracks, leading to further creep and crack growth in structure.

As it can be seen, the parameter ranges for *A*, *m* and *n* that fit well with the experiment results (within the ±20% range of the final experimental strain) (147.1) are:

A: 1.5806E-7, 1.7387E-7, 1.4225E-7

m: -0.6, *n*: 8, *m*: -0.54, *n*: 8, *m*: -0.66, *n*: 8.8

It can therefore, be said that the suggested range of creep parameters gives an accurate prediction of the creep behaviour and so can be used for other masonry structures with similar material properties.
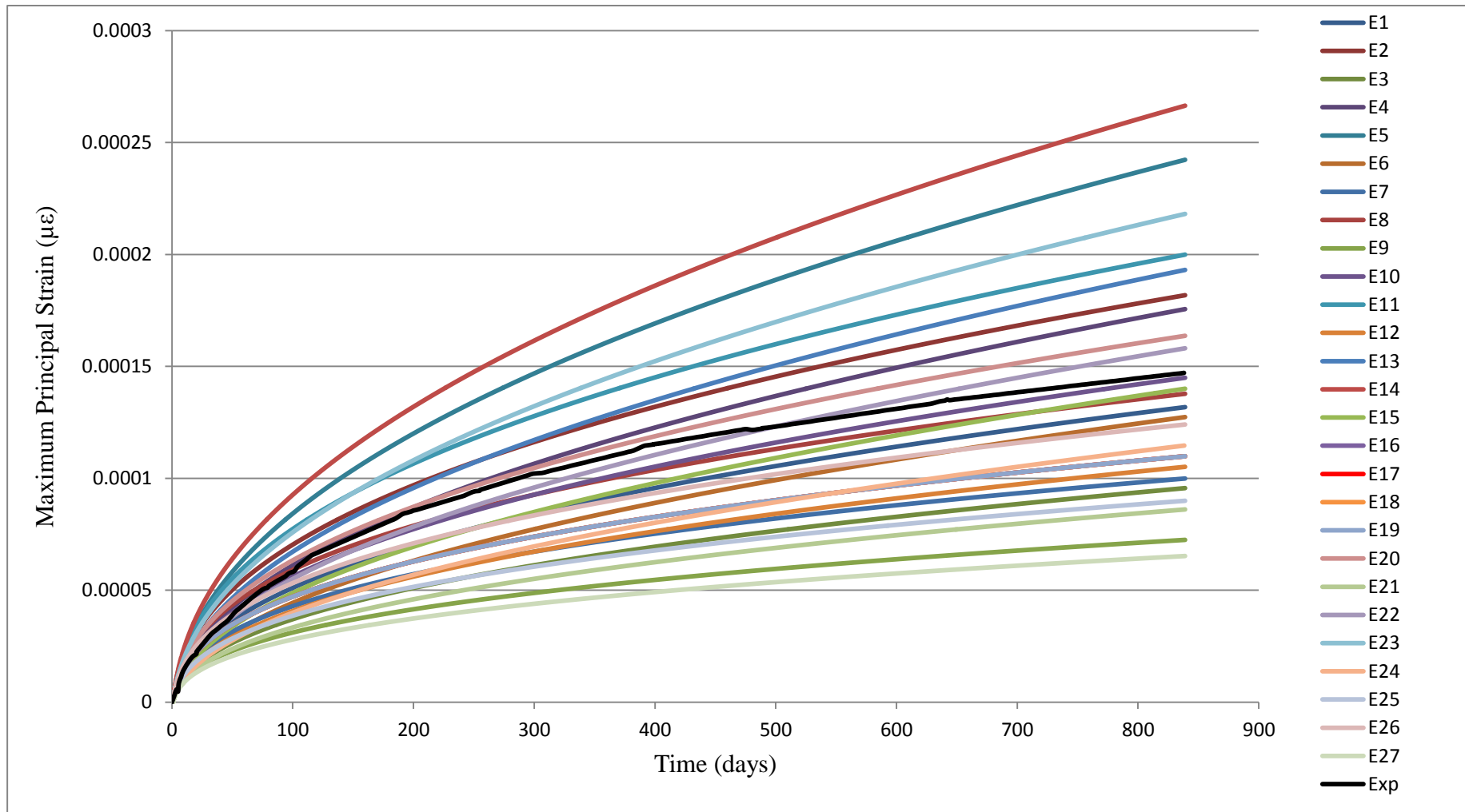
Figure 4.35: Theoretical and experimental strain-time plots for masonry type E.

4.4.2.8. Tuning

As it was shown in the parametric study in Section 4.4.2.2, the value of elastic modulus, *E*, can have considerable effect on the creep results. Since, a precise value of *E* cannot be given for historic masonry, a range of upper and lower values for this parameter can be used to obtain a closer fit between the theoretical and experimental results. This process of iteration and improvement is referred to as tuning, which can be applied to any parameter whose optimal value is not known.

4.4.3 Cracking

As it was explained in previous chapters, crack (in particular creep-induced crack) is another important defect, which has been the subject of many research works. These studies have tried to assess the long-term effect of creep on crack initiation and propagation in brittle structures, such as historic masonry. The results could be used to estimate the life time of the structure, and where possible predict and prevent failure of structure, by means of adequate repair.

4.4.3.1. Mesh dependency

In the computational tool developed, when both creep and creep-induced crack defects are present, if damage criteria are met, damage will occur at specific points in the material, gradually increasing the crack growth will localise in a narrow band. The crack bandwidth mainly depends on the mesh size. A considerable level of mesh refinement is required to give acceptable simulation results, and so, a mesh sensitivity analysis is done to find the dependency of result accuracy to the element size on time-dependent historic masonry models (Simulia, 2013). A 'block' of masonry (representing a typical masonry specimen consisting of units and joints) is simulated for 8 different mesh sizes. A uniform pressure is applied to the top surface of the model, which is fully encastered at the bottom surface (shown in Figure 4.36). Since loading and boundary conditions of the model are uniform across the model, a quarter of the masonry specimen is modelled and hence two sides of the specimen are fully fixed by symmetrical boundary conditions in X and Z directions. Propeties of the block are given in Table??
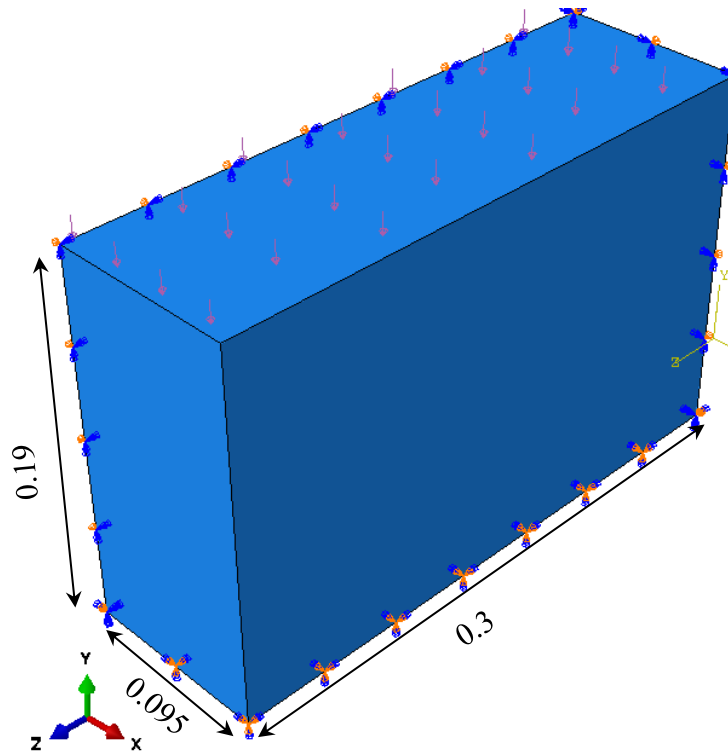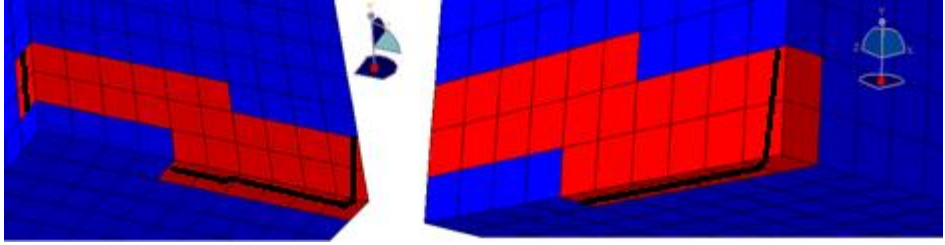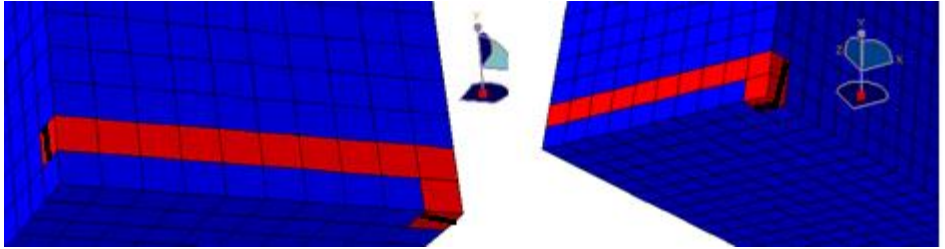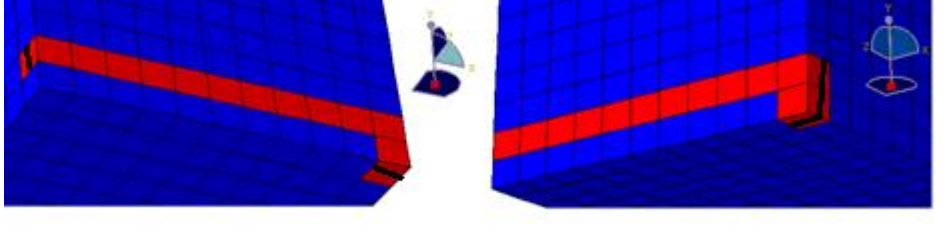
Figure 4.36: A quarter of masonry specimen, pressure at the top and encastered at the bottom (all dimensions are in metres).
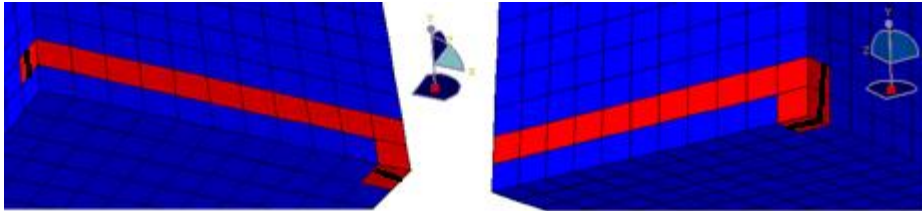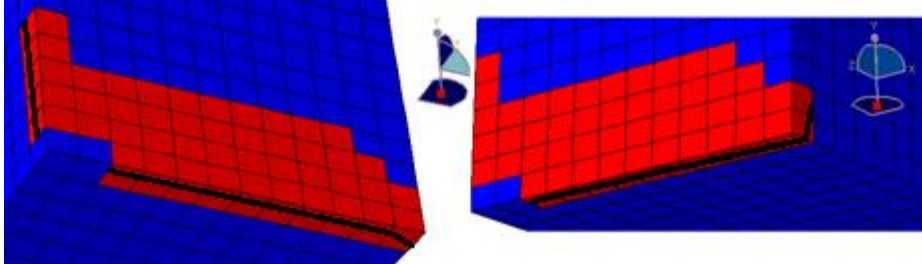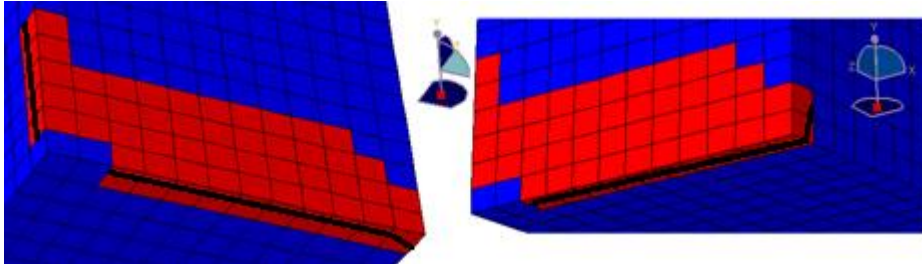
Table 4.18: The material properties of the block.

Material parameters	Values
Young's Modulus (E)	800N/mm^2
Poisson's Ratio (v)	0.2
Density	2E-0kg/mm^2
Pressure	2N/mm^2

Since the crack location is not predefined, and with crack initiating and propagating from the middle of elements, the crack tip cannot be selected and so, stress or strain levels at the crack location cannot be identified. Thus, mesh sensitivity analysis is carried out by comparing the crack pattern, damaged zones and crack formation time in each model (given in Table 4.18), in addition to the change in maximum principal strain value of each model with element number (shown in Figure 4.37). The data provided in this table, will be used to identify the most suitable mesh size for use in modelling historic masonry structures.

169

Table 4.19: Mesh sensitivity analysis to identify changes in crack pattern with number of elements.

Model no.	Number of elements (mesh size)	Crack formation time (second)	Damaged zone and crack pattern
1	6400 (max 10, min 9)	9.1507E-4	
2	6930 (max 10, min 8)	7.9213E-4	
3	9108 (max 10, min 7)	7.5997E-4	

Model no.	Number of elements (mesh size)	Crack formation time (second)	Damaged zone and crack pattern
4	10944 (max 10, min 6)	7.4299E-4	
5	13858 (max 10, min 5)	7.4299E-4	
6	20010 (max 10, min 4)	7.4299E-4	
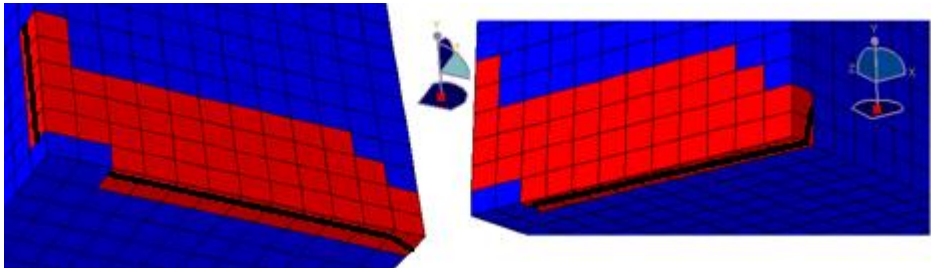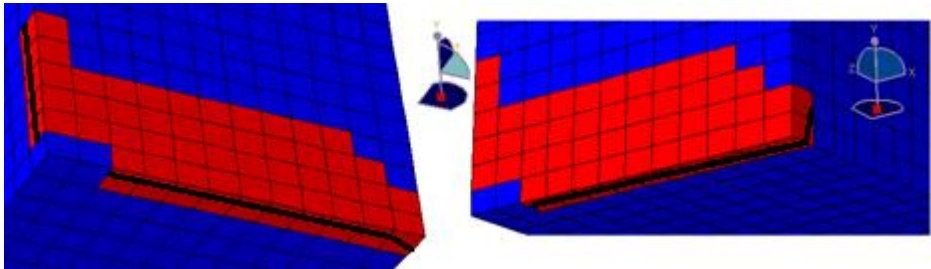
171

Model no.	Number of elements (mesh size)	Crack formation time (second)	Damaged zone and crack pattern
7	21150 (max 8, min 5)	7.4299E-4	
8	27456 (max 8, min 4)	7.4299E-4	

Table 4.18 indicates the total element number, crack initiation and path for the models simulated for mesh sensitivity analysis. In this table, for each model the total numbers of elements are specified. As the model is compressed and fully fixed at the bottom, majority of the cracks are expected to take place at the bottom of the model, reasonably fine seed size are applied to 4 vertical edges of the model and the upper parts of the edges are meshed using coarse elements (larger seed numbers); for each model this is given in the forms of maximum and minimum numbers in the second column. Screenshots of the crack formation time, damaged zones and crack patterns (from different angles) for each model are also shown.

172

The red areas in each model indicate damaged zones, where crack is likely to form. Multiple cracks are also visible in most of the models. As it can be seen from this table, an increase in the number of elements reduces the crack formation time. This is a confirmation that the strain distribution can be predicted more accurately when higher number of nodes are present; leading to a reduction in crack formation time.

It is evident from Table 4.18 that all models have a damaged area in the same part of the model. While the first 4 meshes show considerable variation in crack patterns, the results begin to converge from model 5. Therefore, it can be said that models 5 to 8 have the optimum number of mesh elements where the results converge by consistent crack formation time, damage zone and crack pattern. This indicates that the mesh sizes adopted for either of these models is good enough and can be applied to simulation of future structures, without the need for a finer mesh. The mesh sensitivity is further confirmed by plotting a maximum principal strain value against element number for the models, as seen in Figure 4.37.
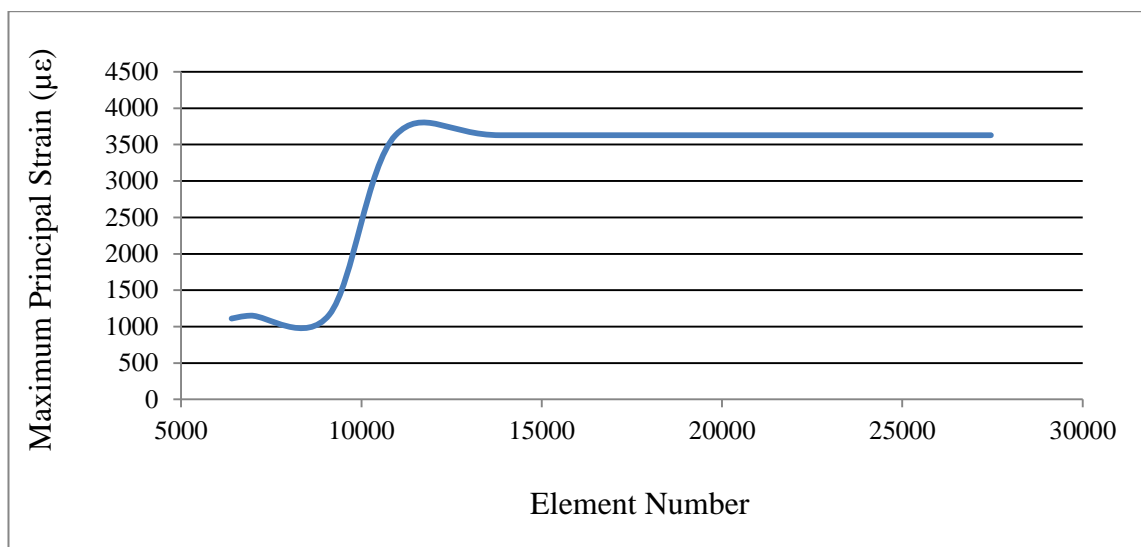
Figure 4.37: Change in maximum principal strain values with element numbers.

It is expected that as the total number of elements in a model increases (i.e. size of an element decreases), the maximum strain level would approach a constant value; this is evident in Figure 4.37, confirming convergence of the model.

Use of finer mesh sizes, beyond those of models 5-8 has also been considered. However, the maximum storage space available by the university do not allow for finer mesh; due to the difficulties in writing the input file for the model (e.g. huge file size, processing and buffer limitations, etc.) and the resultant inaccurate crack predictions.

So, it can be deduced from the above observations that, to avoid the complexities (rising room size of the model, longer analysis duration of the finer sizes and the need for simulating bigger sized structures), the mesh size specified for model 5, i.e. respective maximum and minimum seed numbers of 10 and 5, will be used for coarse and fine mesh. In other words, the seed number used for meshing the model should vary between 1.7% to 3.3% of the size of the model.

4.4.3.2 Modelling cracks

This section is concerned with modelling crack formation in masonry structures. As has been mentioned in the literature, in historic masonry structures that suffer from creep under stress), the thin existing micro cracks propagate and form macro-cracks; a behaviour that can be modelled as crack formation. It was also mentioned in previous chapters that creep induces slow crack growth redistributing the stress in structure. This can lead to offload of the cracked section and the load being applied as excess load on un-cracked sections of structure as well as different rate of material creep. This in turn leads to further disturbance in stress distribution, over-stressing some sections and further crack propagation, until gradually a significant macro-crack is observed.

Fracture is illustrated in a time-dependent model in the form of geometrical discontinuity. A crack initiates and propagates from a flaw, when the conditions are satisfied. The flaw(s) in the material behaviour are represented by specified damage that have threshold of tensile strength, according to which crack will be formed in parts of the structure where the tensile strength reaches and exceeds the limit state value. Although micro-cracks are known to exist in the structure, it is assumed that they will not have major effect on failure; an assumption that is made until it effects the maximum tensile strain threshold (failure strain), after which macro-cracks are formed.

An example of crack formation in a simple cantilevered masonry specimen (consisting of both unit and mortar) is presented in Figure 4.38, where an initial point for crack has not been defined; i.e. crack initiation point is estimated by the tool, based on the threshold specified in the damage model. As it can be seen, the model is fixed at one end and subjected to constant, uniform pressure at the top surface. Material properties of the model are listed in Table 4.19. Since in majority of masonry structures, creep-induced cracks form in structures that are subjected to compressive stress (presented in the following chapter), a typical and simple masonry specimen (consisting of both unit

and mortar) modelled in this section was also fixed at one end to represent crack formation in historic masonry subjected to flexural stress.

Table 4.20: The material properties of the crack model.

Material parameters	Values
Young's Modulus (E)	800N/mm^2
Poisson's Ratio (v)	0.2
Density	2E-0kg/mm^2
Pressure	2N/mm^2
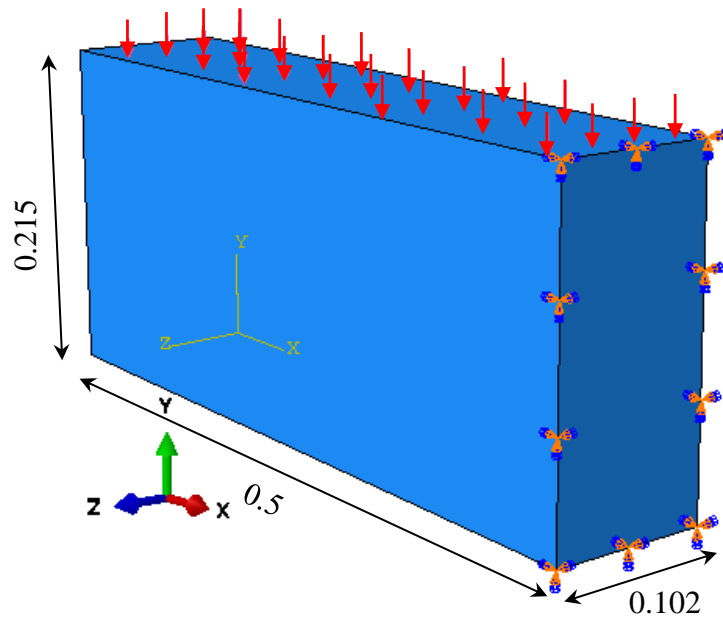
Figure 4.38: A cantilevered historic masonry specimen pressured at the top and fully fixed at one end (all dimensions are in metres).

A damage criterion has been specified for damage to initiate at elements with the maximum principal strain (MAXPE) value of 0.008. Since the creep-induced crack is the main type of fracture considered in this research, this strain value was chosen based on average strain values of the points beyond which historic masonry specimen (subjected to creep[39]) entered tertiary creep phase (the phase where crack mainly occurs). Moreover, the weaker the materials, the lower the failure criterion, as the maximum principal stress and strain are lower.

---

[39] Creep tests simulated in Section 4.4.2.

In a cantilever system, the maximum moment occurs at the fixed end of the material, and tensile crack is mostly expected to be within the top surface of the fixed end as it is subjected to tensile stresses while the base is under compression. So, the two vertical edges were meshed with finer seed sizes on the upper side, compared to the bottom edge of the model.

The load was applied to the model and simulated for time period of 1 day; the load was divided and distributed throughout the increments of the simulation. Screenshots of the simulation results for this model are presented in Figure 4.39, where crack initiation and propagation on fixed-side of the specimen are illustrated. Highest levels of strain are seen on the top fixed corner of the model are seen in the first image of this figure. The MAXPE value reaching the damage threshold is marked on the colour coded legend in Figure 4.39(b). The area pointed on the image also illustrates damaged zone, where the elements have reached the damage threshold and failed elements have already cracks (crack lines are visible). With time and as more load is applied to the model, rise in the MAXPE value in each contour (marked in black), propagation of the damaged zones and further opening of crack is evident in Figures 4.39(c)-(d). The results shown below confirm that the tool is capable of simulating fracture (single or multiple-crack) in masonry structures, by means of crack initiation, propagation up to failure of structure.

When using XFEM feature in this tool, the STATUSXFEM output helps illustrate a good representation of the status of elements, with a value between 0 and 1 (1 indicating that the element is cracked), based on damage criteria specified in the model.

(a) After load application   (b) After damage initiation   (c)Damage propagation   (d) Failure of masonry
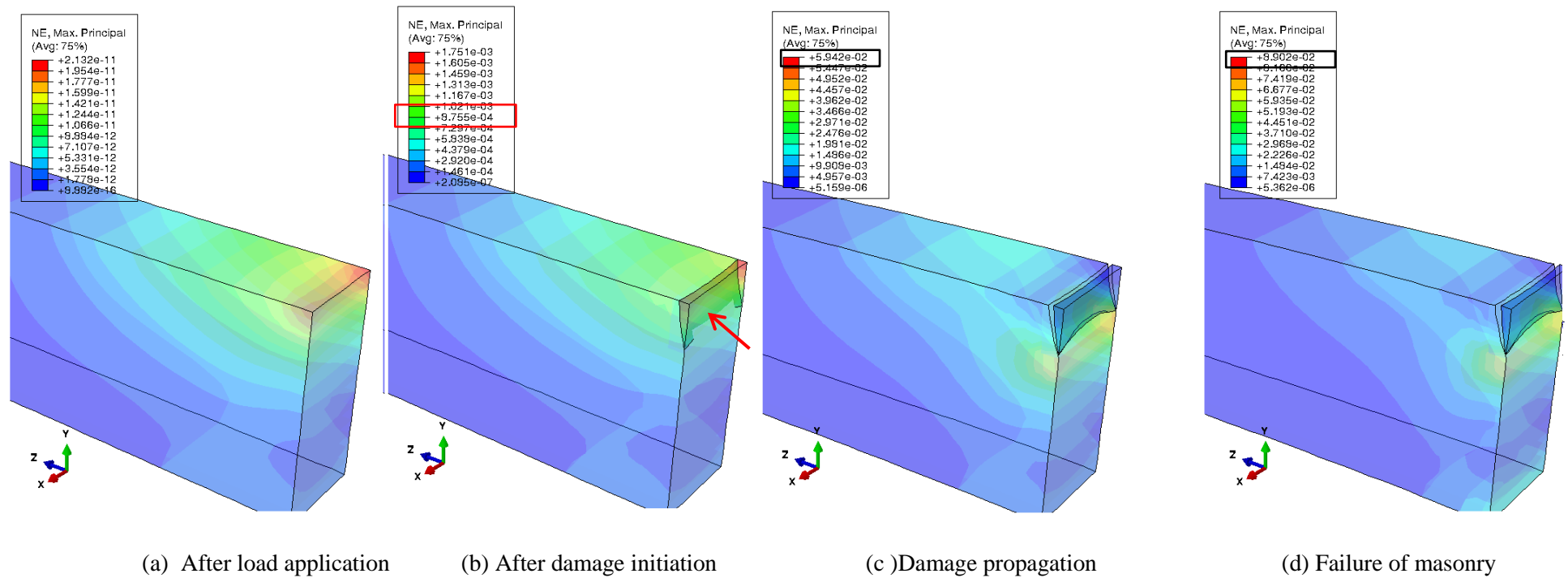
Figure 4.39: Illustration of a time-dependent model (a) after application of load, (b) after damage criterion is met and crack initiated and (c) damage propagation, leading to (d) failure of masonry specimen at the fixed end; contour results are in mm.

4.5 Summary

This chapter adopted the techniques and modelling strategies identified in Chapter 3 in order to develop a computational tool (using Abaqus), which can not only be used to model the existing defects in historic masonry structures, but also to predict their future structural behaviour and lifespan. Towards this, several difficulties have been identified including the complex nature of masonry and limitations in obtaining accurate data on material properties. Validation of the model proved to be even more difficult, and it was recognised that a reliable computational tool should have the ability of estimating a reasonably similar trend to the existing experimental results.

From a software point of view, the Abaqus modules, including part and assembly, material properties, step, interaction, mesh, load and boundary conditions have all been taken into account and addressed appropriately. Creating a model for each simulation, produces input data which describes the structure (by means of geometry, material properties, mesh, loads and boundary conditions), producing desired and specified output data; stress, creep and overall strain, and deformation. The total number of nodes and elements (depending on mesh size, etc.), determines the speed and storage of the simulation.

The principle and mechanism of operation of the proposed computational tool were introduced in Section 4.3 through validating the effect and variation of the main modelling variables i.e. time, temperature, Elastic modulus, material properties, etc.

The following features and capabilities of the tools were developed and validated:

- *Deterioration in masonry with time*: the ability of the tool in reducing the material stiffness with time was illustrated, to resemble deterioration in masonry. The idea of coexistence of more than one material in a structure, from different construction phases was implemented.

- *The ability for surface layers to exfoliate thereby reducing the size of the masonry component*: Existing defects in historic masonry, such as exfoliation of the outer layer were shown by removal of different batches with time.

- *Repairing the damaged zone*: Existence of the more than one material in a structure, such as a repaired section was modelled to analyse the change in stress-strain distribution over time.

- *Creep in four different types of masonry*: LSF method was used to obtain a range of creep parameters to be used in the Abaqus software for each masonry type. The experimental creep results obtained from four different long-term creep tests were compared with the simulation results, and very good agreement was seen between the results (horizontal and vertical strains).

- *Mesh sensitivity in modelling cracking in masonry*: The extended finite element method (XFEM) was used to model creep-induced cracking in masonry. As crack formation is stress-dependent, a mesh sensitivity analysis was carried out to find the effect of different mesh types and size on the stress levels in the structure. A consistent cracked zone, crack formation time and maximum principal strain values were evident for few mesh sizes. It was summarised that according to size of the structure that needs to be modelled, a maximum and minimum seed size of 8-10 (2.6-3.3% of size of the model) and 4-5 (1.3-1.7% of size of the model) can be used as coarse and fine mesh, respectively.

- *Cracking*: The structure was modelled using the identified mesh. Fracture in a typical historic masonry specimen was modelled using the XFEM features in Abaqus (based on the MAXPE damage criterion), and crack initiation, propagation of the crack and failure of the model over time was illustrated.

From the simulations of creep and crack defects, it was found that:

o Creep is significantly present in the form of an accumulation of strain over time under constant stress, where the applied stress affects the strain growth in the structure. Stepped and gradual increases in the applied load increase the strain levels and crack propagation up to the failure point;

o The low tensile strength of historic masonry is the predominant factor affecting crack initiation and damage growth that are mainly labelled as horizontal strain. These are shown on the strain-time graph as negative values;

o The percentage of mortar present in historic masonry has shown to have a significant influence on the tensile strength and ultimate loading capacity of structures; e.g. brick masonry has higher creep levels in comparison to stone masonry, as it contains a higher percentage of mortar.

o As expected, creep simulations carried out on cement-based mortar have much lower creep strain levels in comparison with lime-based mortars.

In summary, it was found that presence of several of unknown parameters significantly influences and limits the simulations and analysis of historic masonry structures. Sensitivity analysis on the main creep parameters also illustrated the importance of simulating the upper and lower boundaries of the main fundamental parameters, as scatter on the material parameters influences the final predictions. However, despite this, the proposed tool proved to be able to suggest suitable creep parameters for various types of masonry (mainly historic masonry), predicting creep behaviour over long durations.

In addition, the fact that large range of masonry material types, long construction periods, masonry patterns, loading, workmanship and so on, makes each and every masonry structure unique, also suggests that there are many unknown parameters affecting the structural performance of historic masonry structures. Therefore, while using this tool, appropriate safety margins should be considered when assessments and decisions concerning the long-term stability of such structures are made.

In the next chapter, validation models will be presented to illustrate the effectiveness and reliability of the proposed tool in dealing with a combination of the defects individually simulated in this chapter. The initial validation has been carried out using the results of tests performed in the laboratory on small samples of masonry. The tool was then further validated using one of the piers of a clay brick masonry railway viaduct constructed in the UK in 1883.

Chapter 5 : Validation of the Computational model

5.1 Introduction

As described in Chapter 4, the computational tool has been developed by the author to simulate individual defects in historic masonry, including the exfoliation of eroded sections, creep and creep-induced cracking. There are, hereafter, referred to as the features of the computational tool. In this chapter, a combination of these features will be applied to specific models, with the aim of illustrating the ability of the tool in predicting the creep behaviour and possible creep-induced crack in a simple masonry specimen; replicating existing long-term creep tests on historic masonry specimen. Creep and creep-induced crack are simulated together since the latter is a gradual consequence of the former. In other words, long-term effect of creep induces crack initiation and gradual crack propagation. In addition, the tool's ability in replicating exfoliation of masonry over time, alongside creep and creep-induced cracking is examined on a real-life masonry structure. These validation cases will be used to illustrate how the proposed tool can be employed to assess the long-term behaviour of historic masonry subjected to time-dependent defects. Moreover, simulation of the applied repair on the real-life structure exemplifies how use of the tool can fit into the larger framework of maintenance and restoration projects.

5.2. Validating the creep and cracking features of the model

In this section, the 'creep feature' of the tool is used to predict the long-term creep behaviour of a historic masonry specimen, and the results are validated against the experimental test results for that specimen given in the literature. The 'crack feature' is then combined with the validated creep feature on the same model (in Section5.2.2), to (a) illustrate formation of creep-induced crack, and (b) validate these crack patterns through comparison with the real sample.

5.2.1 Validating the creep feature

As explained in Section 4.4.2, a range of creep parameters were identified for each type of masonry. The simulation results confirmed that good creep parameters were given by the LSF method, which in turn helped obtaining reasonably accurate creep-induced

strain rate predictions for masonry structures. Although the results of the creep simulations from Chapter 4 confirm the reliability of the proposed approach, this section attempts to validate both the techniques employed and the tool developed in this research work, by using the experimental data given in other research papers that have used masonry specimens with similar material properties. In doing so, the experimental results reported by Lourenço and Pina-Henriques (2008) are adopted, which represent samples collected from the ruins of the belfry of the Pavia civic tower (referred hereafter as masonry type F). As masonry type F consisted of regular coursed bricks, similar to masonry type B[40], the same creep parameter range has been used for the creep simulation of type F masonry.

Lourenço and Pina-Henriques (2008) describe long-term creep tests carried out on masonry specimens sized $(200\pm5)\times(200\pm5)\times(330\pm20)$ mm^3. Load had been applied to the specimen in successive steps and kept constant for given periods of time. The initial pressure was given as 4.10 N/mm^2 (60% of its compressive strength), and was increased slightly by 0.65 N/mm^2 (10% of compressive strength) for each step; details are given in Table 5.1. The loads are applied at a *static* step, and kept constant for the duration of time given in Table 5.1 under a *visco* step. The material properties used in Abaqus for masonry type F are: $E = 5055$ N/mm^2 and $v = 0.09$ (Lourenço and Pina-Henriques ,2008). Figure 5.1 shows the load and boundary condition on this masonry specimen.
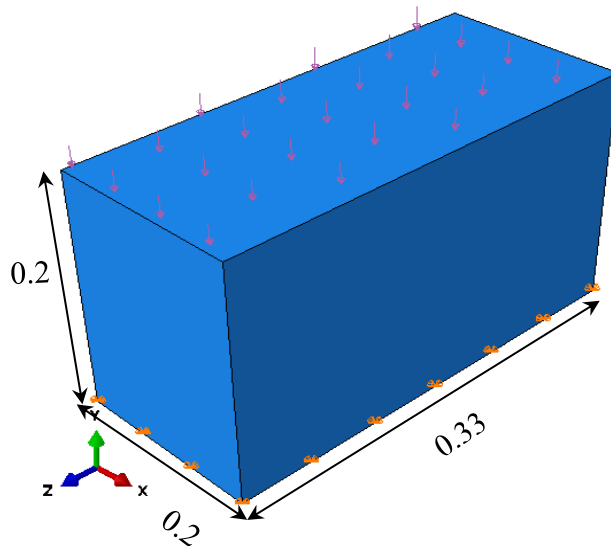
Figure 5.1: A masonry masonry specimen subjected to a uniform vertical compressive stress on the upper face, fully fixed on the lower surface (all dimensions are in metres).

---

[40] Used in construction of the internal leaf of the wall.

Table 5.1: Stress applied to masonry type F in steps.

Applied Vertical Stress (N/mm^2)	Time (days)
4.10	0-184
4.8	185-371
5.4	372-559
6.1	560-739

Figure 5.2 illustrates the Strain-time graph of the experimental results presented in Lourenço and Pina-Henriques, 2008. The creep parameter range (*A*, *m* and *n*) for masonry type B was identified to be as follows, where any *A* value can be used with the given *m* and *n* sets:

A = 7.71138E-7, 8.5682E-7, 9.42502E-7

m = -0.81, *n* = 7.2

m = -0.9, *n* = 8

m = -0.99, *n* = 8

So, if *A* = 7.71138E-7, any one of these *m* and *n* sets can be used with it: (*m* = -0.81, *n* = 7.2), (*m* = -0.9, *n* = 8), and (*m* = -0.99, *n* = 8) as the creep parameter set, to simulate the behaviour of the specimen subjected to creep behaviour.

The vertical strain results were plotted against the experimental data of Lourenço and Pina-Henriques (2008), shown in Figure 5.3. As seen, the primary, secondary and tertiary creep phases and a general increase in strain rate are visible in the figure. Also the theoretical and experimental vertical strain-time curves are in very good agreement and a very similar step path representing an increase in load are evident. Note that there is a very small discrepancy of approximately 300 between the closest micro-strain values of the numerical results (e.g. F23) and the experimental data. Also the difference between the final strain values of the upper and lower simulation curves (i.e. the maximum strain difference between F23 and F24) is approximately 100, which is an indicator of good accuracy of the suggested creep parameter range for each masonry type.

It is therefore proposed that the tool developed by the author can be used to give a reasonably accurate prediction of the long-term creep behaviour in different masonry structures.

A summary of the suggested creep parameters (obtained using the LSF method) for each type of masonry are hence given in Table 5.2. The relative compressive strength and maximum principal strain values used are also given in the table.

Each type of masonry has a different range of compressive strength values, and a relation cannot be identified between these. Although the MAXPE values for these types of masonry are relatively close, a relation cannot be seen between the MAXPE value of these masonry types. It seems that for better simulation results, experiments in the laboratory should be carried out to identify more representative material properties and a better damage threshold for each type of masonry. These values should then be used for predicting the creep-induced crack pattern in masonry.
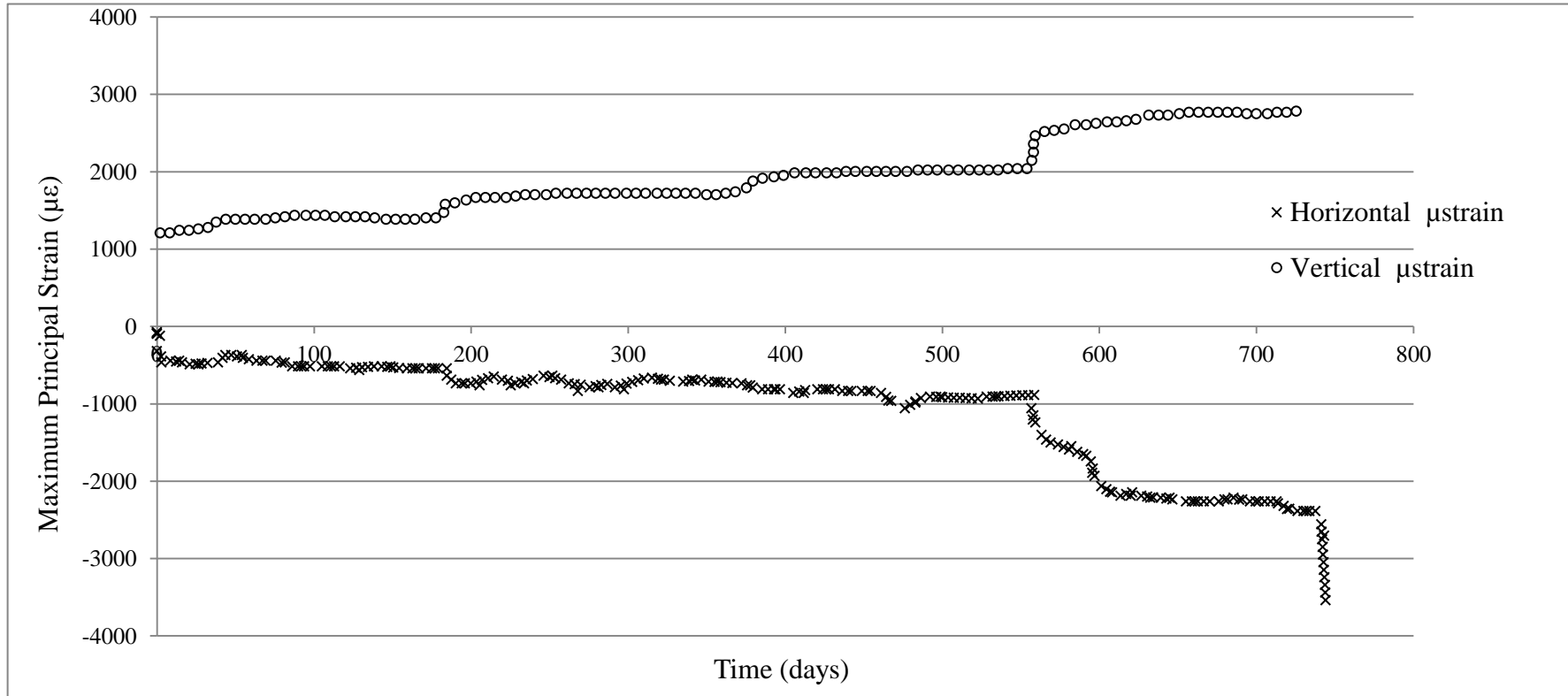
Figure 5.2: The strain-time graph of the experimental results of masonry type F (Lourenço and Pina-Henriques, 2008).
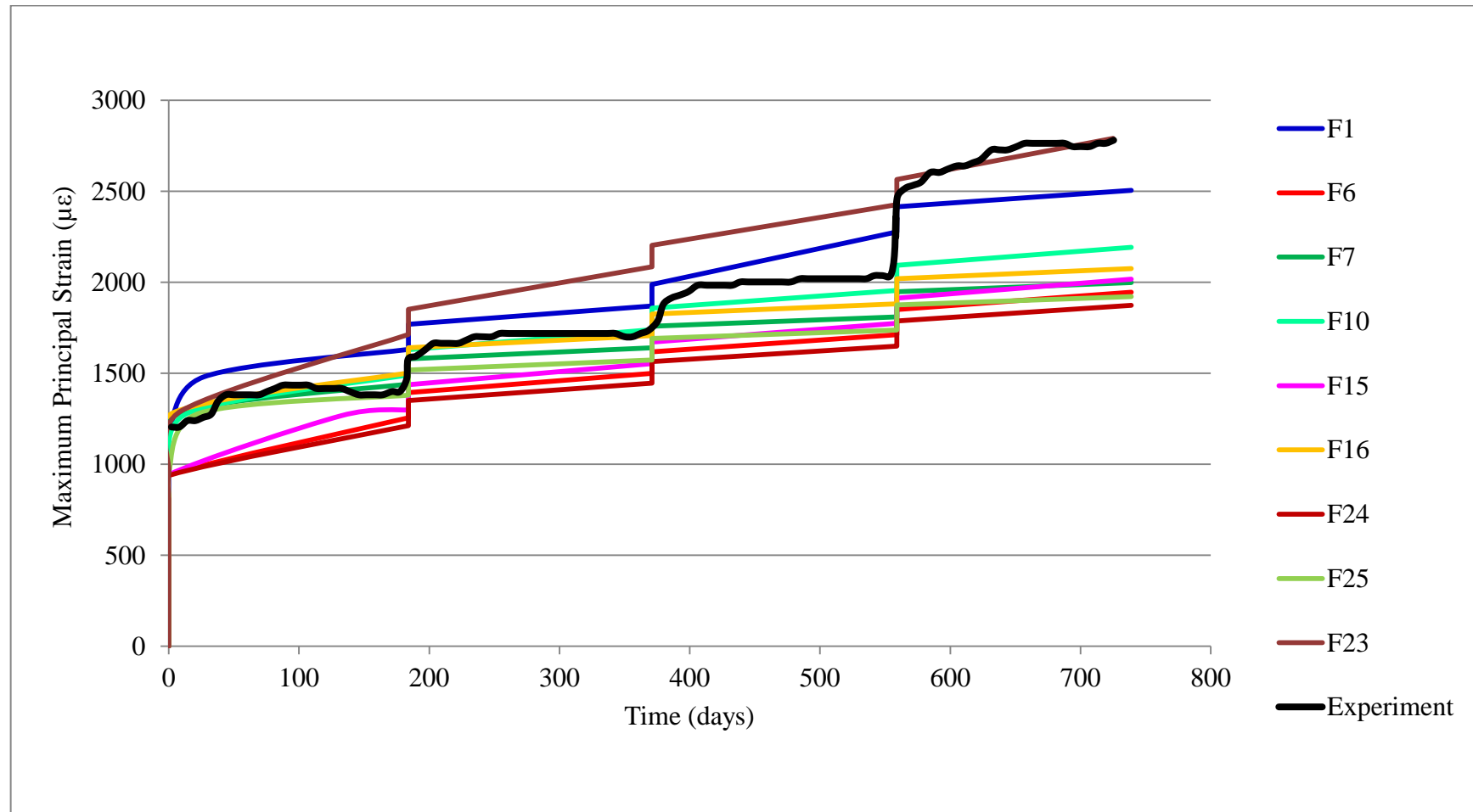
Figure 5.3: The theoretical and experimental vertical strain-time predictions for masonry type F.

Table 5.2: Type of masonry, suggested creep parameter range and compressive strength range used for types A-F.

Masonry type	Suggested creep parameter range	Compressive strength range (N/mm^2)	MAXPE
Type A: Low strength clay brick masonry used with air-hardening lime mortar	A: 1.5429E-8 , 1.7144E-8, 1.8858E-8 m: -0.99, -0.9, -0.81 n: 7.2, 8, 8.8	3.4	0.0005
Type B: Random rubble masonry: a type of concrete made with layers of broken bricks and stone altered with layers of mortar	A: 7.71138E-7, m: -0.81, n: 7.2 A: 7.71138E-7, m: -0.9, n: 8 A: 7.71138E-7, m: -0.99, n: 8 A: 8.5682E-7, m: -0.81, n: 7.2 A: 8.5682E-7, m: -0.9, n: 8 A: 8.5682E-7, m: -0.99, n: 8 A: 9.42502E-7, m: -0.81, n: 7.2 A: 9.42502E-7, m: -0.9, n: 8 A: 9.42502E-7, m: -0.99, n: 8	2.6 ± 0.9	0.0007
Type C: Historic brick masonry and hydraulic lime mortar	A: 6.1863E-9, m: -0.9, n: 8.8 A: 6.1863E-9, m: -0.81, n: 8 A: 6.1863E-9, m: -0.99, n: 8.8 A: 6.8737E-9, m: -0.9, n: 8.8 A: 6.8737E-9, m: -0.81, n: 8 A: 6.8737E-9, m: -0.99, n: 8.8 A: 7.5611E-9, m: -0.9, n: 8.8 A: 7.5611E-9, m: -0.81, n: 8 A: 7.5611E-9, m: -0.99, n: 8.8	6.3 ± 0.9	Not available

Type D: historic brick masonry and hybrid lime-cement mortar	*A*: 7.988E-9, *m***:** -0.9, *n***:** 8 *A*: 7.988E-9, *m***:** -0.81, *n***:** 8 *A:* 7.988E-9, *m***:** -0.99, *n***:** 8 *A*: 8.8755E-9, *m***:** -0.9, *n***:** 8 *A*: 8.8755E-9, *m***:** -0.81, *n***:** 8 *A:* 8.8755E-9, *m***:** -0.99, *n***:** 8 *A*: 9.7631E-9, *m***:** -0.9, *n***:** 8 *A*: 9.7631E-9, *m***:** -0.81, *n***:** 8 *A:* 9.7631E-9, *m***:** -0.99, *n***:** 8	7.3 ± 0.3	Not available
Type E: Clay brick and cement based mortar	*A*: 1.5806E-7, *m*: -0.6, *n*: 8 *A*: 1.5806E-7, *m*: -0.54, *n*: 8 *A:* 1.5806E-7, *m*: -0.66, *n*: 8.8 *A*: 1.7387E-7, *m*: -0.6, *n*: 8 *A*: 1.7387E-7, *m*: -0.54, *n*: 8 *A:* 1.7387E-7, *m*: -0.66, *n*: 8.8 *A*: 1.4225E-7, *m*: -0.6, *n*: 8 *A*: 1.4225E-7, *m*: -0.54, *n*: 8 *A:* 1.4225E-7, *m*: -0.66, *n*: 8.8	6.83	Not available
Type F: Random rubble masonry: regular coursed brick / granite blocks	*A*: 7.71138E-7, *m***:** -0.81, *n***:** 7.2 *A*: 7.71138E-7, *m***:** -0.9, *n***:** 8 *A:* 7.71138E-7, *m***:** -0.99, *n***:** 8 *A*: 8.5682E-7, *m***:** -0.81, *n***:** 7.2 *A*: 8.5682E-7, *m***:** -0.9, *n***:** 8 *A:* 8.5682E-7, *m***:** -0.99, *n***:** 8 *A*: 9.42502E-7, *m***:** -0.81, *n***:** 7.2	6.25 ± 0.25	0.0009

	A: 9.42502E-7, *m*: -0.9, *n*: 8		
	A: 9.42502E-7, *m*: -0.99, *n*: 8		

5.2.2 Validating combination of creep and creep-induced crack features

As it has been explained in previous sections, existence of creep in a masonry structure over a long period of time, leads to formation and propagation of cracks in the structure. The masonry sample used for validation of creep (Lourenço and Pina-Henriques, 2008), can be used as an example of failure in a masonry specimen; indicating creep-induced crack initiation and propagation in masonry. The same data can, therefore, be used to validate a model where both creep and crack features are present.

As such, the crack feature of XFEM is used together with the above validated creep feature to simulate formation of creep-induced crack over time in this specimen. In doing so, the same material properties and creep parameter range were used, to simulate the creep behaviour. As it has been explained in previous sections, the user has an option of pre-defining the initial crack point (based on existing crack patterns on structure), or allowing for prediction of crack pattern by the tool. Since prediction of crack pattern is vital for validation of this tool, location of crack is not predefined in this model. Linear hexahedral elements of type *C3D8R* were used in meshing the model, where mesh sized 10mm was used, giving the total number of 10500 elements for meshing the masonry model.

According to Figure 5.2[41], and as mentioned in (Lourenço and Pina-Henriques, 2008), the maximum principal strain (MAXE) of masonry type F is 800, which can be used as the threshold for damage and crack formation in the simulations.

A sample crack pattern of the masonry specimen from experiments is selected and marked as red in Figure 5.4(a) (Lourenço and Pina-Henriques, 2008). In order to compare and validate crack predictions of this tool, simulation results of this masonry specimen are also shown in Figure 5.4(a-b), where initiation and propagation of the cracks are depicted, respectively. As can be seen damage zones are highlighted in blue, and crack patterns are visible on the specimen. In this model symmetrical loading and BC are assumed, and so symmetric numerical solution is generally expected; this is seen

---

[41] The damage threshold (MAXPE) is selected from the strain point, where the experimental curve enters tertiary creep phase.

in the form of two large vertical cracks after crack initiation (Figure 5.4(b)). In the experimental results, however, the crack pattern is not symmetrical. This can be due to the non-symmetrical architecture of the bricks, as well as uneven pattern of the mortar in masonry.

In the experimental results, crack propagation is seen in the form of patterns, which are mostly evident in the mortar and at the unit-mortar interface. These patterns are, however, not visible in the simulation results (Figure 5.4(C)), as the masonry specimen (consisting of both unit and mortar) is assumed to be homogeneous. Nevertheless, micro-cracks are seen in the simulation results (joining the large vertical cracks together), due to the fact that the use of elastic modulus for masonry specimen, obtained from (Lourenço and Pina-Henriques, 2008), roughly takes into account the overall presence of micro cracks across the model.

It is important to note that it is very difficult to predict exact crack patterns in such specimen based on limited information provided in the published papers. This is due to the nature of masonry (particularly historic masonry), uncertainty on constituent materials, inaccurate information on applied BC, and inability of taking into account humidity and temperature effects, and so on.

The horizontal strain-time curves of the simulation (crack model) and experiment results are plotted in Figure 5.5, where a very similar trend to vertical strain (Figure 5.3) is visible. Also a gradual increase in transverse strain with time is evident in both curves. As has been mentioned before, positive and negative signs are adopted for vertical and horizontal strains, respectively.

The horizontal strain values represent dilation of material under compression; hence, formation of minor tensile cracks in the horizontal direction. Accumulation of the strain level over time is also observed with increase in load at the steps. Note that as the horizontal strain of the experimental curve reaches the tertiary creep phase around days 560-570, there is a considerable increase[42] in the strain values of the experimental data.

The general pattern of simulation curves of the suggested creep parameter rang is very similar, and few curves overlap. These curves follow a very similar loading pattern to the experimental curve; that is a consistent increase in strain with applied new load. Although there is a difference of 500 between initial micro-strain value of experiment

---

[42] Approximately from -8.9E-4 to -0.0004, i.e. 63%.

and simulation curves, the curves cross around day 560, giving very similar strain results. The slight discrepancy in the strain values can be due to (a) each simulation curve being an average maximum principal strain value for all elements of the model, and (b) uncertainty and lack of accuracy on values of parameters such as fracture energy for this type of masonry.

(a) Experimental specimen
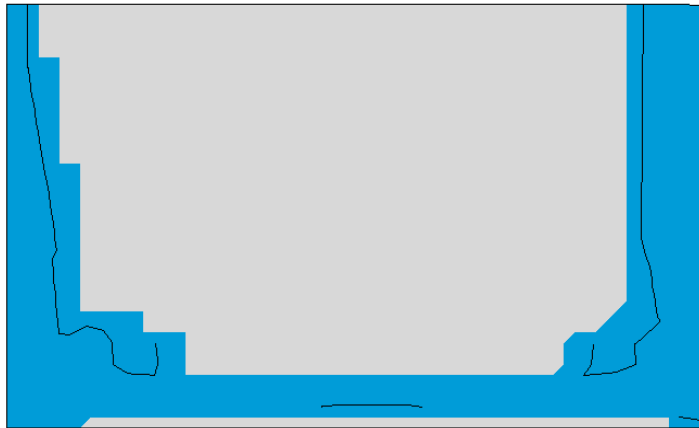
(b) Damage and crack initiation

(c) Damage and crack propagation

Figure 5.4: The creep-induced crack patterns for masonry type F in (a) experimental specimen (Lourenço and Pina-Henriques, 2008), and simulation model for (b) initiation, and (c) propagation.
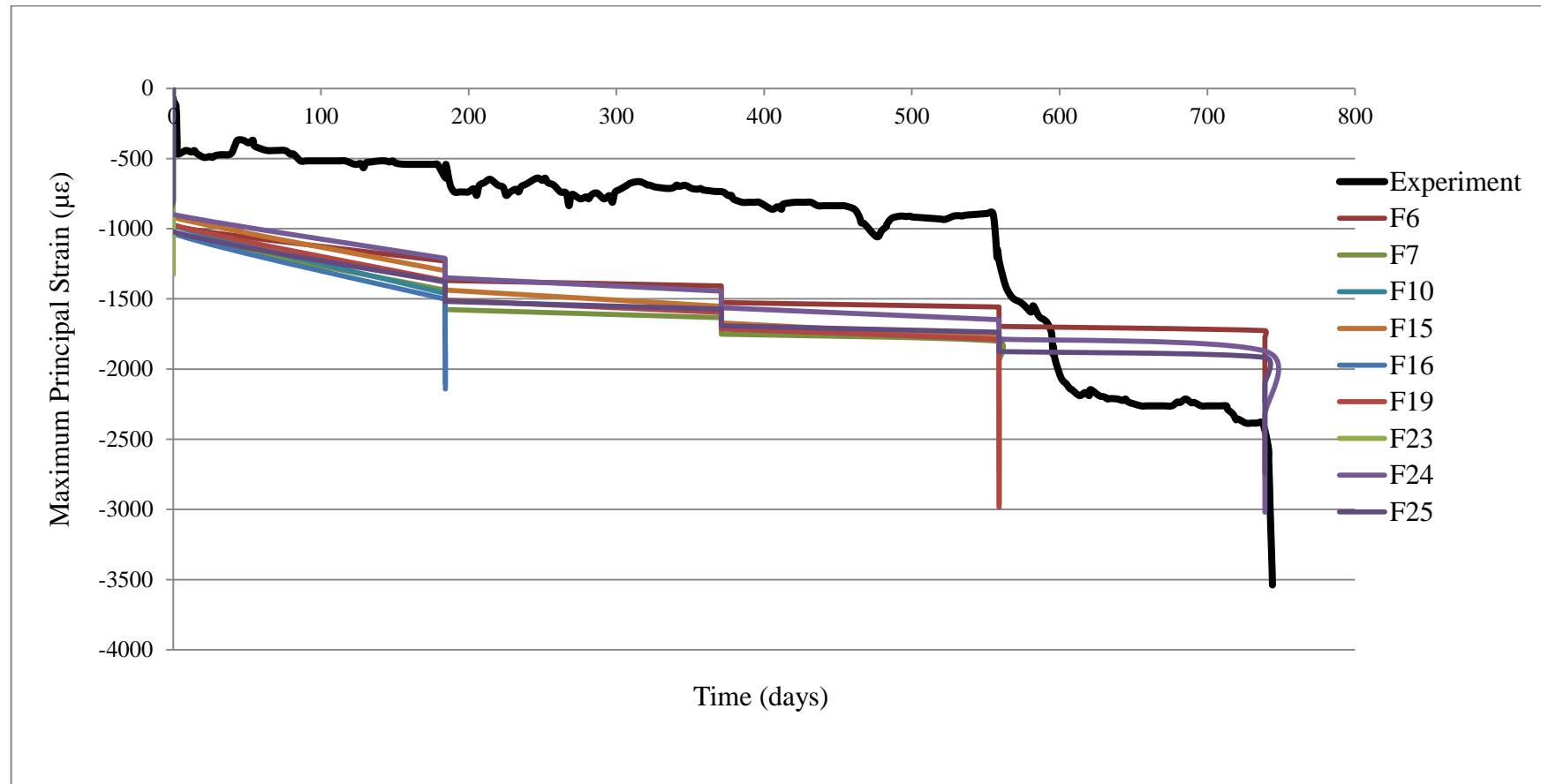
Figure 5.5: Theoretical and experimental horizontal strain-time predictions for masonry type F (selected parameter sets from table 5.2).

5.3. Validating the model on a real-life masonry structure

As was mentioned in Chapter 2, previous examples of structural collapse confirm that tall, relatively slender forms of construction are vulnerable to creep-induced cracking and collapse. It was noted that the majority of these structures also undergo time-dependent weathering defects such as exfoliation of the eroded sections. Therefore, it is essential to be able to simulate and predict such trends to estimate the lifetime of the structure, and where possible, foresee and prevent their failure by means of adequate repair. Indeed, this is a very useful feature and functionality of the proposed tool, which is used to combine the effects of weathering (or exfoliation), creep and creep-induced cracking.

5.3.1. Larpool Viaduct

One of the piers (pier 4) of a former railway viaduct, the Larpool viaduct, was used by the author to further validate the model. It was built between 1882 and 1884 to carry the Scarborough and Whitby railway in North Yorkshire, England, and is a 13 span, grade II listed, red clay brick viaduct (with multi-ring arch construction) located approximately 2km south of the centre of Whitby. The plan and elevation of this viaduct are seen in Figure 5.6 (Garrity, 2008). Detailed sections and elevations of one of the piers of the viaduct are presented in Appendix C.
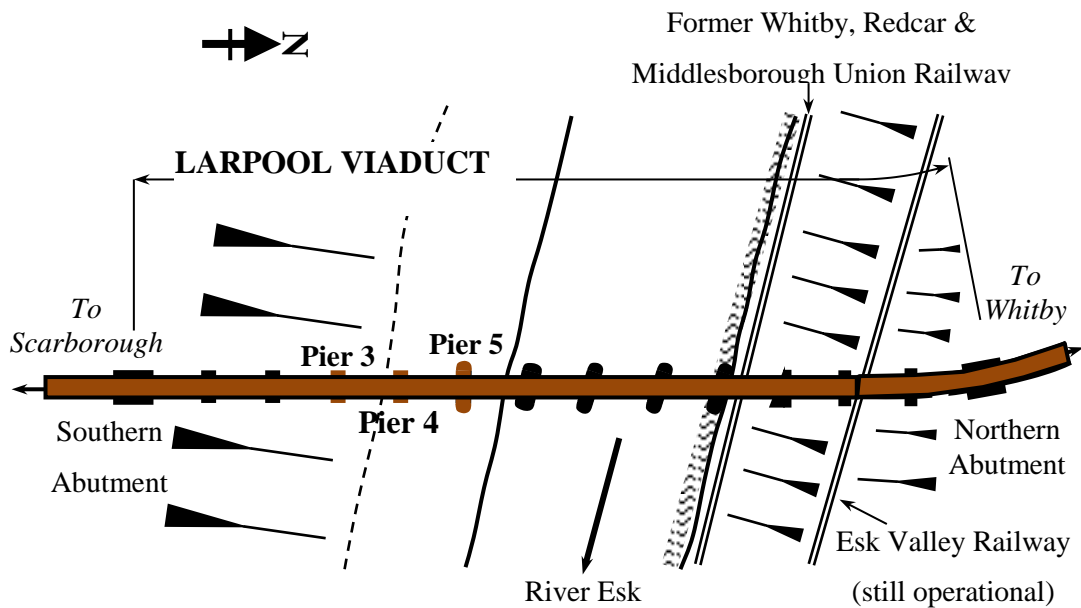
.

Figure 5.6: Outline plan of Larpool Viaduct, illustrating piers 3, 4 and 5 (Garrity, 2008).

5.3.1.1. Defects

An inspection of the viaduct was carried out in 2006 by Garrity (2008) on behalf of the viaduct owners, Railway Paths Limited (RPL). The inspection revealed that all of the original brickwork is of solid construction, consisting of clay bricks laid in 1:4 (OPC: sand) mortar. A 0.125m diameter cast iron pipe had been used for draining the ash fill above the brickwork haunching, which was connected to a vertical drain that was originally fixed to the external face of the pier.

The inspection also identified that some piers 3, 4 and 5 of the viaduct were in urgent need to repair as numerous pieces of clay brickwork were spalling from the viaduct onto houses below. Much of the deterioration was observed around the drainage of the piers. Moreover, long-term exposure to weathering (driving rain, wind, and repeated freeze-thaw cycles) had resulted in severe spalling, frost-induced deterioration, and hence peeling-off and exfoliation of the outer layer brickwork on upper section of the pier (see Figure 5.7). Therefore, exfoliation is also envisaged as a feature of the proposed computational tool to enable modelling of this defect in historic masonry structures.
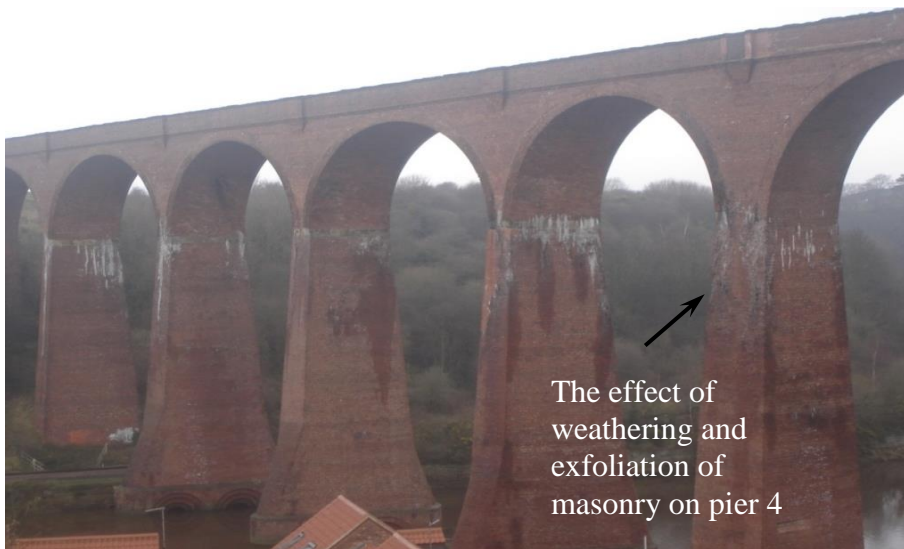
Figure 5.7: Weathering and exfoliation of the eroded masonry evident on piers of Larpool Viaduct.

Different parts of the pier are exposed to different intensities of weathering, and so, the water ingress and the bond strength vary in different sections of the pier. A sample of this is shown in Figure 5.7, where the white patches indicate zones with higher water ingress and extensive lime bloom.

At the most recent site visit carried out by the author in October 2014, it was decided that pier 4 would be an ideal candidate for demonstrating all three mentioned defects; Figure 5.8 is a 3.D model of this pier. As seen in this figure, Faces 1, 2, 3 and 4 represent the South, East, North, and West faces of the pier. In addition, for the purpose of validating the computational tool, sketches of the current state of each face of the pier (noting any damage, cracks and existing repair works) were made. These are summarised in Figures 5.9 and 5.10. Although no signs of other damage such as salt crystallisation or chemical attack were evident, considerable moisture and surface dampness were visible on the upper section of the pier.
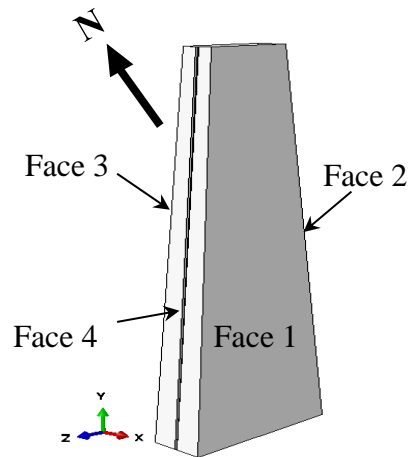
Figure 5.8: Illustration of the four sides (faces) of pier 4.

As seen in Figure 5.9(a), continuous vertical cracks were noted to run through bricks and mortar in damaged and undamaged zones of face 1 of the pier. These cracks cannot be considered to have been induced as a result of settlement, since, according to the as-built drawings of the viaduct, a concrete foundation extending down to shale bedrock was used for this pier. Furthermore, there was no visual evidence of any differential settlement (such as distorted bed joints). All of these defects and signs suggest that the presence of creep in the pier has caused redistribution of stress and excessive tensile strain in the brickwork, which has, in turn, resulted in the formation of cracks. Considering that creep and creep-induced cracking coexist with exfoliation in the pier, the proposed tool has been developed so that it is able to model the combination of these defects.
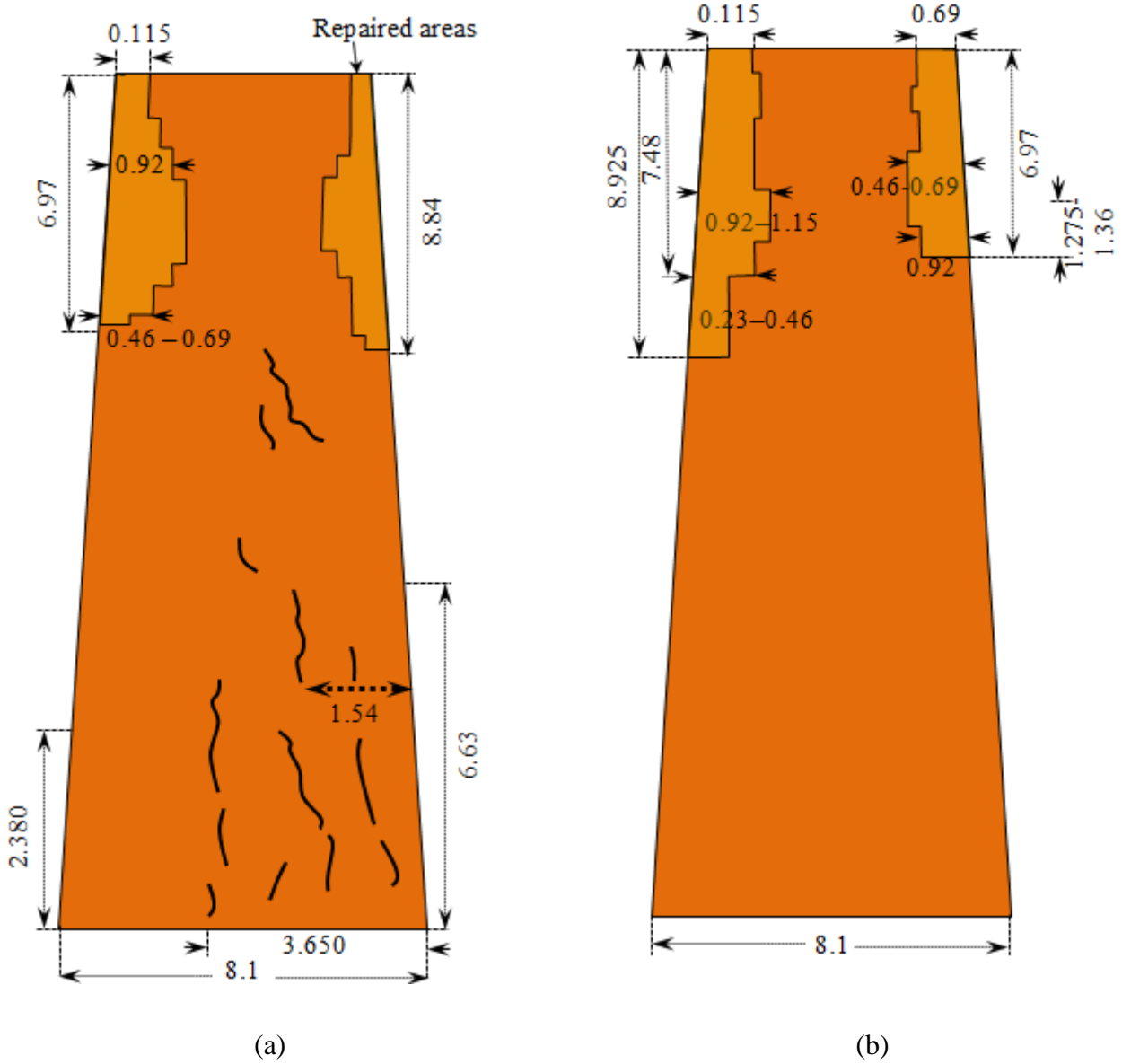
Figure 5.9: Pier 4 of Larpool Viaduct, (a) face 1, and (b) face 3 (all dimensions are in meters).
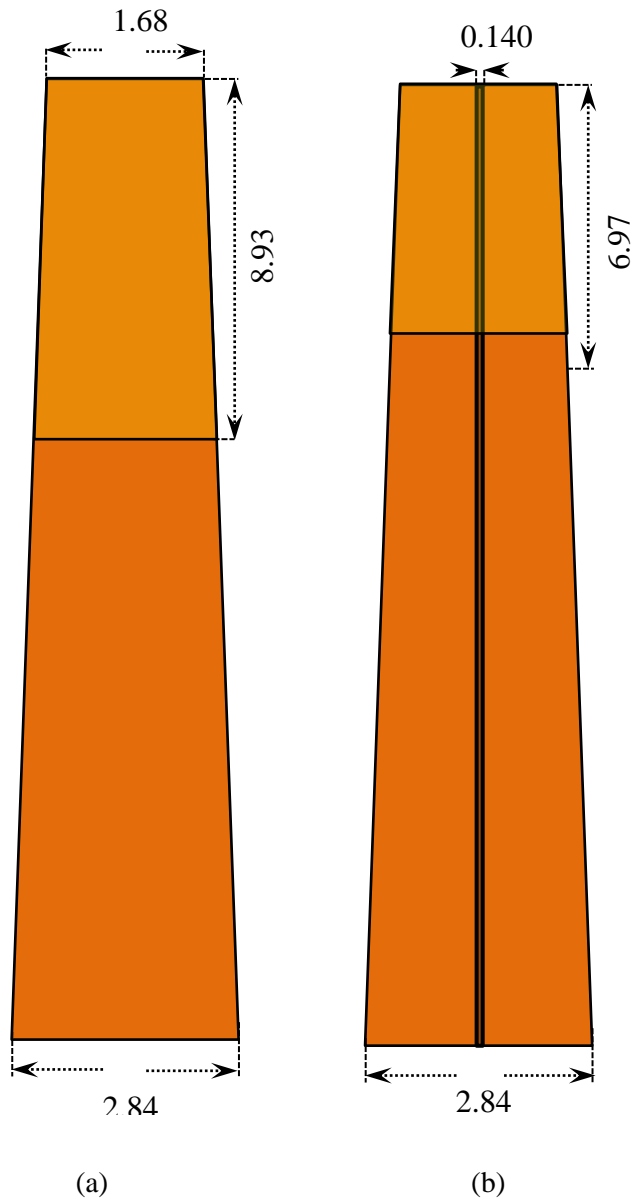
Figure 5.10: Pier 4 of Larpool Viaduct, (a) face 2, and (b) face 4 (all dimensions are in meters).

5.3.1.2. Repair

According to Garrity (2008), piers 3, 4 and 5 of the viaduct were repaired by removing the outer skin of damaged brickwork and replacing it with new brickwork bonded into the existing brickwork substrate. The new brickwork was red class B engineering brick laid in 1: ½ : 4½ (OPC: lime: sand) mortar. The bricks had maximum water absorption of 7% (to withstand future water ingress) and a minimum compressive strength of 50 N/mm^2. The repaired areas on each face are shown in Figures 5-9 and 5-10. The new brickwork was chosen to match the original construction material as closely as possible. Further views of pier 4 are shown in Appendix F.

Figure 5.11: Pier rehabilitation works on Larpool Viaduct.

A clear difference between the repaired and eroded sections of the pier is evident in Figure 5.11, highlighting the importance of carrying out repair on such structures.

The above points were the essence of the observations of the inspection of Larpool viaduct. In the following section an attempt will be made to use this information to model and simulate the pier 4 defects in Abaqus in order to evaluate the capability of the developed computational tool to analyse the overall stress-state of the pier, from an assumed initial construction time (undamaged state) up to its present state, a period of approximately 130 years. In addition, the repair works already implemented on the pier will be included in the Abaqus model to simulate the repair of the deteriorated sections, and to structurally analyse its compatibility with the original material and its effect on the stress-strain distribution of the structure. It is also hoped that the tool could be used to predict the structure's expected life-time and its resistance to the effect of ongoing creep damage of the original and perhaps repaired material. (Such a prediction is considered to be outside the scope of this thesis).

5.3.2. Modelling of pier 4 of Larpool Viaduct

In order to validate the computational tool in predicting the structural response of an existing real-life masonry structure, pier 4 of Larpool Viaduct was modelled in Abaqus, where there is evidence of the pier being exposed to extreme weathering conditions and a combination of creep and creep-induced cracking. Presence of cracks in piers of this viaduct, and the piers being slanderous under heavy loads, suggests existence of creep

in the piers (as stated in Section 2.4.2-i). It is, therefore, important to model creep and creep-induced crack in the structure for simulations with durations of 130 years; both with and without repair.

5.3.2.1. The entire pier

As mentioned in the previous section, the viaduct is constructed with class B clay brick work and cement-based mortar, and so, masonry type E material parameters are used for simulation of the pier; i.e. Engineering class B clay brick laid in 1: ½: 4½ (OPC: cement: lime) mortar; details are given in Section 4.4.2.7.

Since there is no indication of material properties of the pier under study in the literature, properties of a very similar masonry type is used; these features are presented in Tables E-1 and E-2, in Appendix E. As is evident from these tables, there is a wide range of elastic modulus values associated to this type of masonry. Due to the large number of uncertainties in the properties of constituent masonry materials of the viaduct, and for better presentation of the proposed tool in this thesis, materials with reasonably low stiffness have been chosen for simulation of the pier. These parameters are selected from within the range of experimental data given in the literature. The material properties listed in Table 5.3 have, therefore, been used in Abaqus model to simulate material properties of the pier. As the value of the Poisson's ratio was not known for the specimen used in this model, average value of the typical masonry used in such construction was used in the simulation. Dimensions of the pier, as well as its model in Abaqus are also shown in Figure 5.11, illustrating the surfaces at which the load and boundary conditions are applied to the model. As evident, the structure dimensions are huge and it is expected that modelling and simulations would be computationally extensive.

Table 5.3: The material properties used in simulation of pier 4 of Larpool viaduct.

Material property	Value	Reference
Elastic modulus	5600 N/mm^2	(Brencich *et al*., 2002)
Poissons ratio	0.22	(Narayanan *et al.,* 2013)
Density	2E-06 N/mm^2	(Sarhosis *et al.,* 2010)
Maximum principal strain	0.00031	(Hughes and Harvey, 1995)

The self-weight of the arch and parts of the viaduct above the pier are identified as the most critical load affecting structural performance of the pier. Therefore, only the pier is modelled and the weight of the corresponding arch and parapets are imposed on the model to account for the overall arch weight, giving the total pressure of 0.778 N/mm^2 to be applied on the top surface of pier above the springing level (calculations are given in Appendix D.1). The self-weight of the pier is taken into account by including the density parameter in the model.

Trains have crossed over the viaduct for almost 80 years to date, and undoubtedly together with other factors have imposed further load and strain on the pier. However, due to lack of data on such loads, the transient nature[43] of such loads, and since this research is not taking into account dynamic loading (such as wind); therefore, the train load is not considered in the load calculations of this study.

The vibrations caused by train movements are also thought to only affect upper parts of the viaduct (i.e. the arches) and not the pier; and so, it is believed that their effect won't be proportionally significant to trigger the propagation of micro-cracks across the pier, and in particular the bottom few meters of the pier. It is, therefore, safe to assume that the transient train and pedestrian loads are negligible and hence can be ignored.

It is also assumed that the spans between the two arches of piers are equal; otherwise eccentric load was to be considered; as shown in Figure 5.12(c).

---

[43] The load being present for a short period of time.
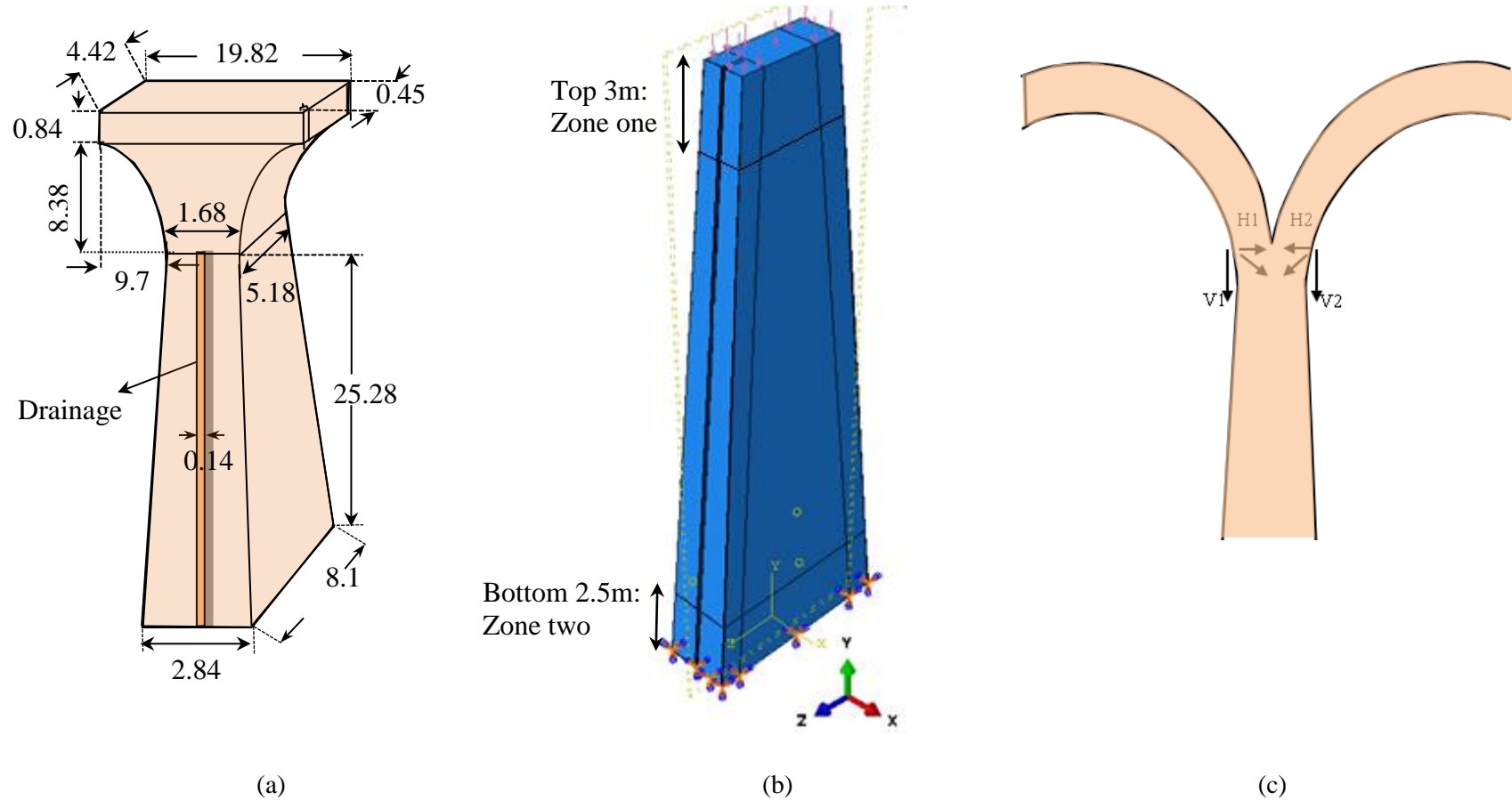
(a)

(b)

(c)

Figure 5.12: (a) Pier 4 and arch dimensions, (b) pier fully pressured at the top and fixed at the bottom, and (c) eccentric loads distribution on the pier from the arch (all dimensions are in meters).

As it has been highlighted in previous research (Verstrynge, 2010b), to identify the border between safe situation and failure in a structure, it is very difficult to set a reasonably accurate limit state for masonry. In addition, since creep and creep-induced cracks are the two main defects considered in this approach, a maximum principal strain threshold (MAXPE) is used to identify the safety zone and the time at which cracks appear. In other words, in this approach, a situation is considered unsafe, when the maximum principal strain[44] exceeds the critical specified threshold; though in previous research, failure and non-convergence of the finite element computations were considered as failure criterion (Verstrynge, 2010a).

Moreover, as the exact time of crack formation (i.e. tensile fracture) is not known, both features of creep and crack are enabled from the beginning of simulation. Although, ultimately, a comprehensive computational tool would be able to model the entire pier structure (height: 25.28m, and volume: 386m^3) while taking into account the combined effect of the three defects in a single model, due to the limitations in computational resources present, this is not possible. As such, the following assumptions and simplifications are made:

- There are cases where a combination of the three defects in large scaled models with large number of elements, leads to the 'illegal memory' error. This is a system error, where the nodal level set values might not be correct for the elements. After flagging up this error to Dassault Systèmes Simulia Corp.[45], enormous effort went into finding the root-causes and trying to solve the issues. After technical consultations with their UK and US HQ offices, they have confirmed that Abaqus code is structurally unable to handle such simulation; and the error has resulted from either of the following (both of which are believed to be present in simulating the entire pier):

  o Intersection or merging of two separate cracks,

  o A single crack front impinging on two or more sides of an element.

  In other words, the underlying error is generated when the 'level set' of one element interacts with that of another. This means that as long as the underlying issue exists, it is currently impossible to simulate the entire pier in Abaqus.

---

[44] Mainly influenced by time-dependent creep calculated for each increment

[45] Dassault Systèmes Simulia Corp. acquired Abaqus, Inc. and announced SIMULIA in October 2005.

- Trial and error in simulations showed that the above-mentioned error can be avoided to some degree with the use of smaller size models, i.e. modelling and simulating parts of the pier rather than the whole structure. This inherently poses a much tougher challenge in simulation and data handling towards a fully optimised tool. Nevertheless, it is the only solution.

In doing so, the pier model was systematically divided into smaller parts, based on observed defects on top 3m and cracks at the bottom 2.5m of the pier; as illustrated in Figures 5.13 and 5.31. The top 9m of the pier was also initially modelled, for a better presentation of the deteriorated/ repaired sections of the pier. However, to meet the computational limitations[46], to shorten the simulation time, and as an illustration of the main approach of this thesis, it was decided to only model the top 3m (Figure 5.14) and bottom 2.5m (Figure 5.31) of the pier; which are hereafter referred to as zones one and two, respectively. To reduce the total element number and hence computation time, it was also decided to adapt coarse mesh in most parts of the model. Fine mesh was used according to requirements of each section of the model.

---

[46] Limitation on usage of cpus, Abaqus licenses, duration and prioritisation of jobs on super computers.

Eroded and
repaired areas
(shown in green)

(a) Model of the entire pier   (b) Eroded and repaired area on Face 1   (c) Eroded and repaired area on Face 3
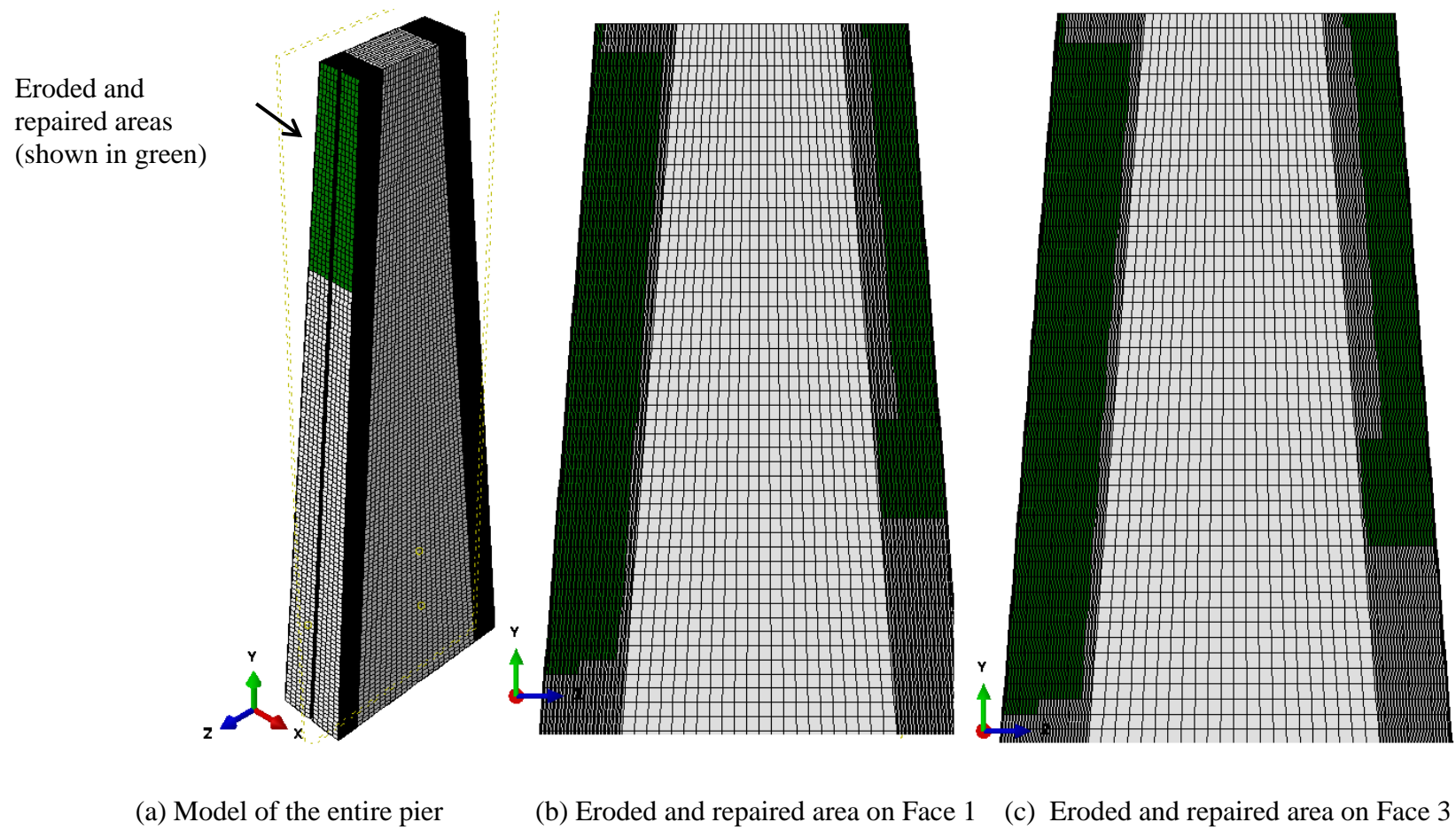
Figure 5.13: The eroded and repaired area on (a) entire pier, (b) Face 1, and (c) Face 3.

5.3.2.2. Top 3m of the pier: zone one

The defects and repair of zone 1 of the pier, as well as results of these simulations are presented in this section.

A: Modelling the defects

As it has been explained before, zone one of pier, has combination of the three defects. The uniform pressure is applied to top surface of the model, taking into account the effect of the arch above the pier (Figure 5.14(a)). All three defects of exfoliation, creep and creep-induced crack are combined in this model.

The bottom surface of the model is also fully fixed, representing continuity of the pier below this section. Linear hexahedral elements of type *C3D8R* were used to mesh the whole model with total of 2755 elements. As it can be seen from Figure 5.14(a) and (b), fine sized mesh was only used in the partitioned are of the model, where 3 layers of 0.01m and 0.02m elements are selected and removed with time (for better illustration of exfoliated and repaired areas). The rest of the model was meshed with seed size of 0.2m.

In addition, the effect of exfoliation of the pier's outer surface is assumed to have initiated around the year 1925 (chosen arbitrary, as there was no evidence to suggest otherwise). Exfoliation of the pier has been shown in terms of peeling off three 10mm-thick layers of masonry[47], when the elastic modulus of the layer is linearly degraded to 100 N/mm^2. This is to illustrate the concept of very low stiffness on defected areas, fitting the purpose of this research. In other words, elastic modulus *E*, of the material is reduced to that of foam[48].

Layers of elements (linearly) reaching such low *E* are then removed, representing linear[49] exfoliation of masonry layers, according to the relations presented in Figure 5.16; giving an indication of rate of reduction of *E* for each exfoliated layer with respect to time. As it can be seen from this figure, these layers are removed at the years of 1925, 1965 and 2005, i.e. 41, 81 and 121 years after construction, respectively. Note that the ability to control the degradation rate of *E*, and layers' exfoliation is provided in this

---

[47] The pattern of these layers is selected manually in the model, based on observed defects of the pier (shown in Figures 5.9 and 5.10).
[48] Where the geomety exists, and is not able to undertake any load. i.e. no stress or strain are present in these areas.
[49] Each exfoliation layer is modelled to erode and exfoliate linearly, as there was no evidence to suggest otherwise.

tool, so it can be adapted to different sites and situations based on available historic and climatic records. For instance, if the structure has been exposed to natural defects such as flooding or earthquake, due to which parts of the structure have been removed, this sudden change can be reflected on time-duration of removing the affected sections. Details of exfoliation and the exact values of *E* have been given in Table G.1 in Appendix G.

As the outer layers of the pier are more exposed to weathering effects, different material properties have been considered for the three eroded layers (shown in different colours in Figure 5.15). A different material property is applied to the rest of the pier, indicating ordinary masonry[50] used in construction of the pier. In practice, the pattern and number of the layers can be selected arbitrarily, depending on the defected or repaired area of the structure.

A total of 262 steps have been used in each simulation. As the tool has time unit of 'days'[51], each year is divided into two steps, named as 'year 1-1' and 'year 1-2', each representing period of 6 months (182 and 183 days, respectively). A *static* step was used to apply the initial load, which was followed by 261 *visco* steps, representing creep behaviour in the pier. Each visco step was divided into 100000 increments (higher increment values helps with convergence problems), with initial, minimum and maximum sizes of 1E-30, 1E-35 and 182, respectively. A creep strain error tolerance of 1E-5 was used.

The pressure was applied to the top surface of the pier. With removal of each layer, the surface area (where the pressure is applied to) is reduced, and hence, a new pressure is calculated to take into account the effect of the new load distribution over smaller area (Appendix D.2). Although the total change in load with removal of each layer is very small, calculated to be 0.005 N/mm^2 so as to become negligible, but for sake of accuracy it has been taken into account and applied in this model.

---

[50] The ordinary masonry represents the original masonry using which the pier was constructed.
[51] Selecting days (rather than years) as unit of time was necessary, as the creep parameters identified in Chapter 4 were obtained from long-term creep experiments given in 'days'.
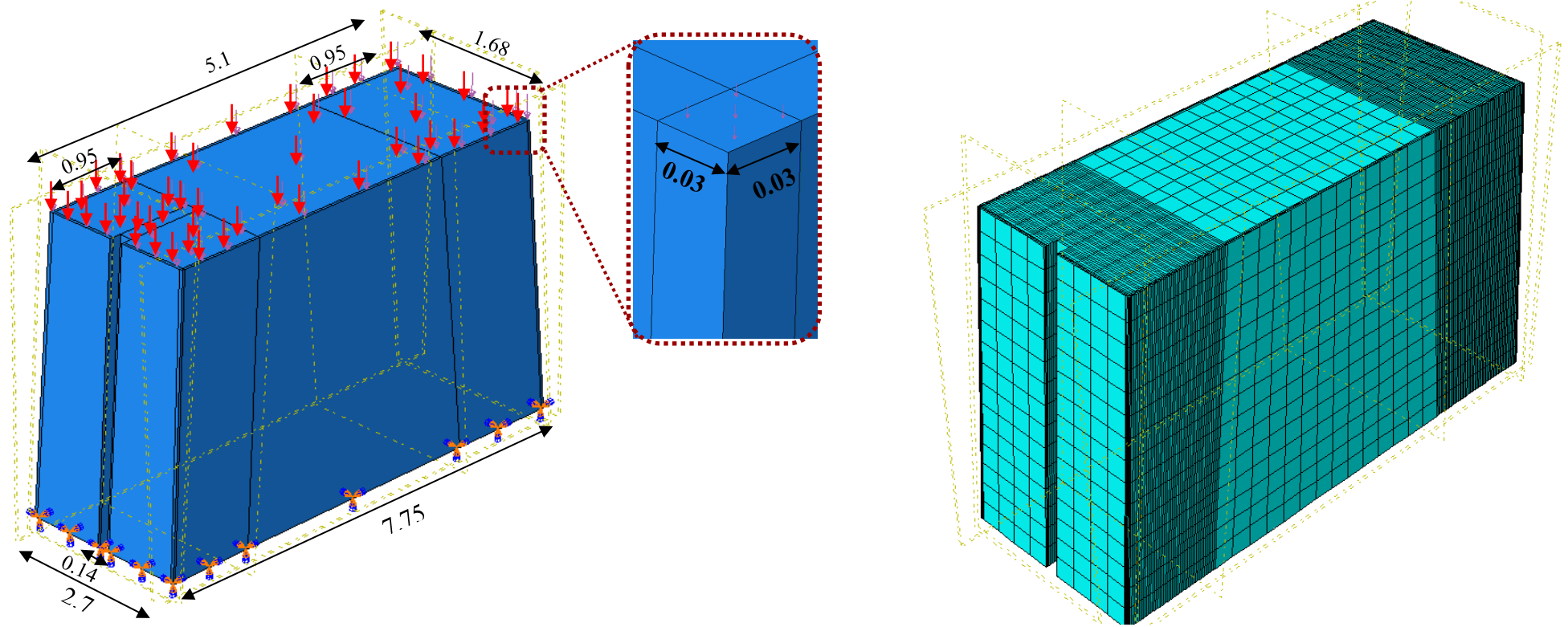
(a) Load and boundary condition on zone one model

(b) Mesh on the zone one model

Figure 5.14: Zone one model of the pier (a) subjected to a uniform vertical stress at the top and fully encastered at the bottom, and (b) showing the fine mesh used in the central 2m wide zone (all dimensions are in metres).

Green: Layer 1
Red: Layer 2
Navy: Layer 3
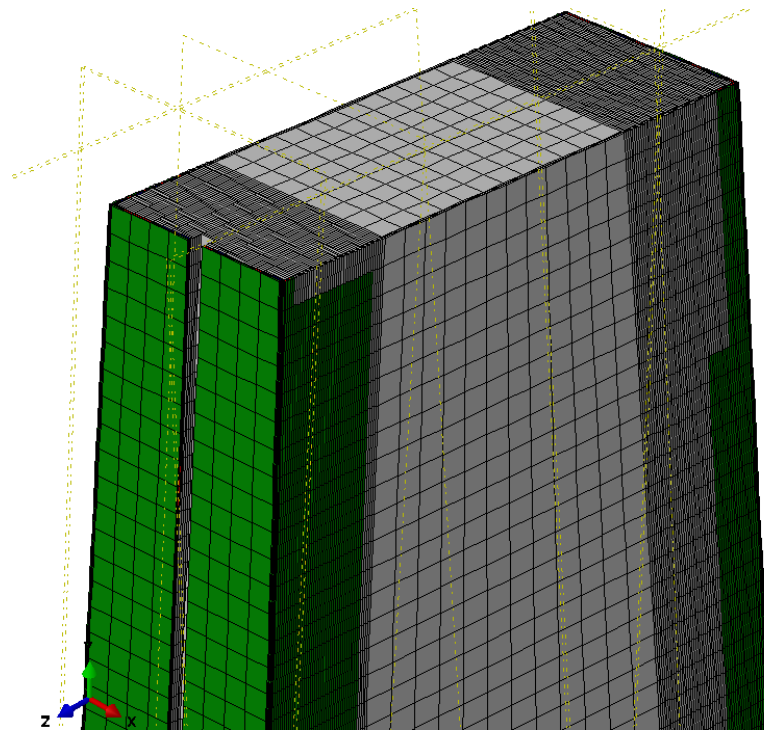
(a) Eroded and repaired areas on zone one   (b) Colour coded materials on eroded areas
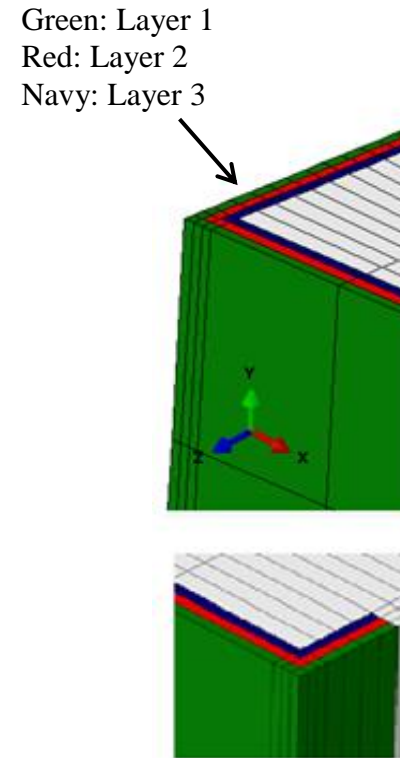
Figure 5.15: (a) Eroded and repaired areas on the zone one model, and (b) colour coded materials.

Figure 5.16: Linear relations indicating deterioration rate of each layer of zone one.

The zone one model was simulated to illustrate the two cases of (a) defects and (b) repair, which are explained below.

a) Simulation results of the defect model
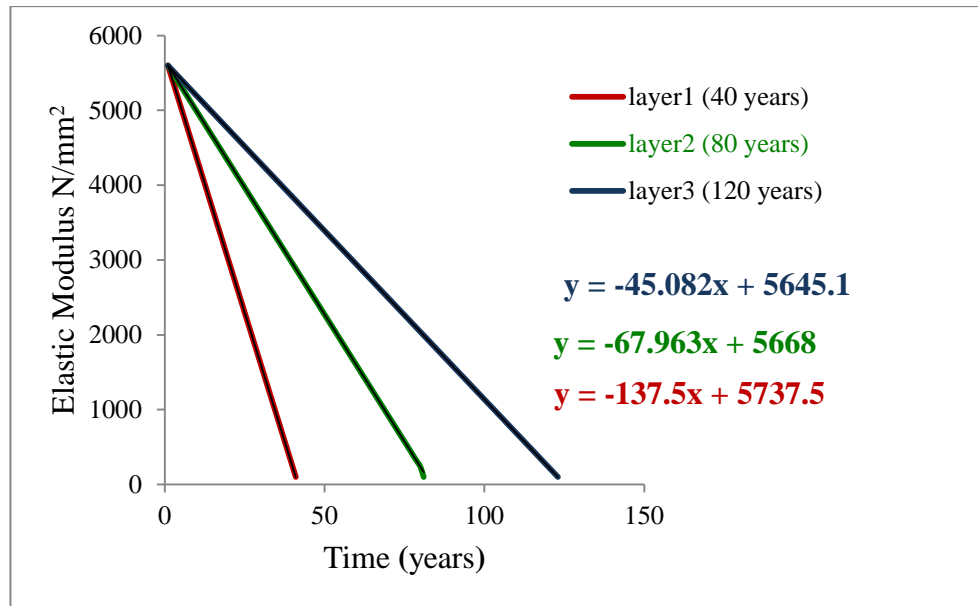
As explained above, the material properties of the eroded layers are reduced and the layers are removed accordingly. The model is simulated for the total duration of 130 years, and the results are presented below.

As it was mentioned in Section 5.3.2.2, the damage threshold of MAXPE = 0.00031 has been specified for this model. Figure 5.17 is, therefore, illustrating the crack initiation as the specified threshold is reached. As it can be seen in this picture, initial cracks have been generated in the second six months of year 26, at the bottom corner of the 'block' (zone one model of the pier), between faces 2 and 3 of zone one. The damaged zone is shown in orange, and the damage threshold has been marked on the legend.
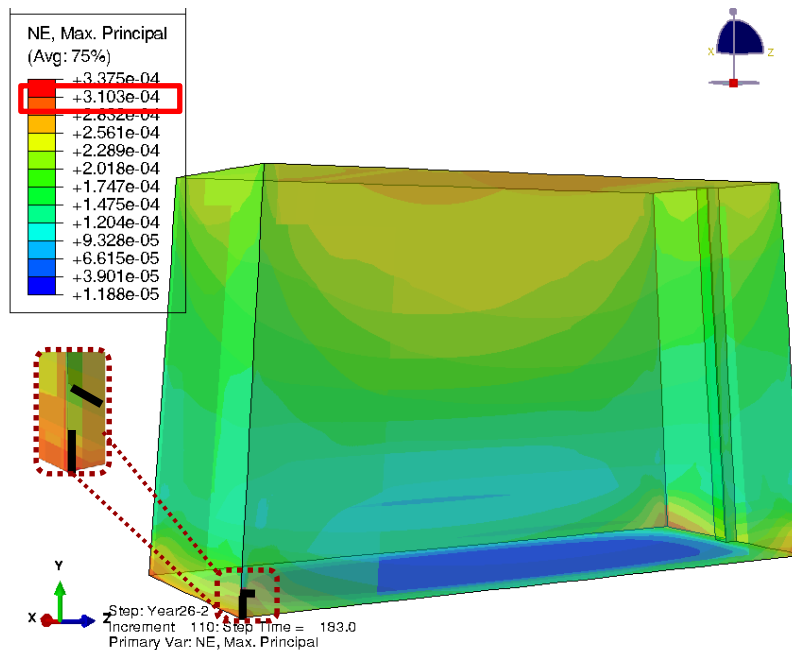
Figure 5.17: Crack initiation at the bottom corner of the zone one model, between faces 2 and 3.
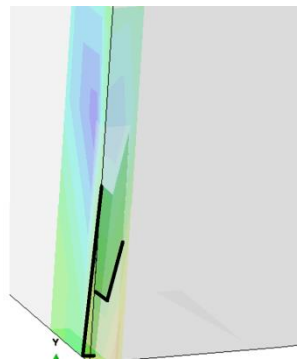
In addition, maximum levels of strain are evident at the top surface of the pier, where the load is applied, as well as in the corners of the block; shown in orange and red colours. Very low tension levels are also visible in blue at the bottom surface of the block.

As the creep defect is enabled from the beginning of the simulation, creep-induced strains are increasing with time, causing formation of creep-induced cracks. This is presented well in Figure 5.18(a)-(g), where the three phases of creep are shown in the form of crack formation, at years 26, 31, 42, 82, 104, 122 and 130. Cracks at years 42, 82 and 122 are illustrating crack patterns in the model, after removal of exfoliation layers. An overall image of the zone one of the pier, after removal of the first layer (at the year 42) from each face of the zone one model is shown in Figure 5.19. As seen, on each face of the pier, the damage and repaired zones (previously highlighted in Figures 5.9 and 5.10) are removed at year 1925 (when the Viaduct is 41 years old). For better illustration of these zones, the damaged areas on faces 1 and 3, are highlighted in pink.

It is known that exfoliation of layers of masonry from the pier, causes disturbance to stress-strain distribution across the pier. A sample of this is hence, shown in Figure 5.20, where Von-misses stress distribution across the model at years 1 and 130, are presented in Figures 5.20.
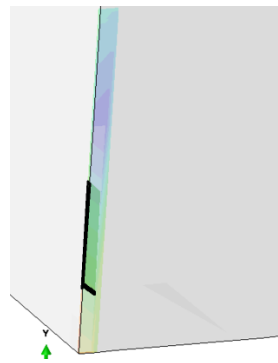
(a) 1910 (Viaduct 26 years old) (b) 1915 (Viaduct 31 years old) (c) 1926 (Viaduct 42 years old) (d)1966 (Viaduct 82 years old)
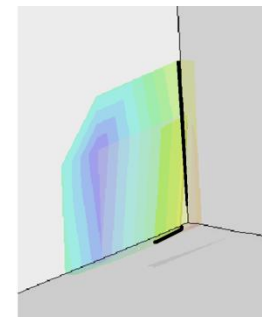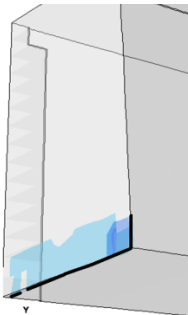
(e) 1988 (Viaduct 104 years old) (f) 2006 (Viaduct 122 years old) (g) 2014 (Viaduct 130 years old)
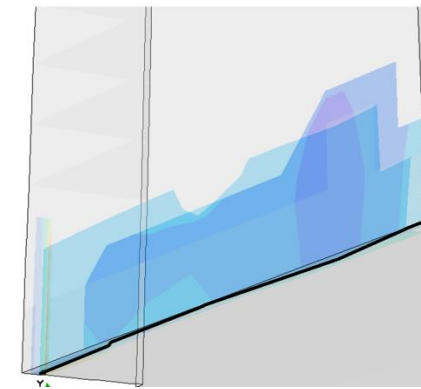
Figure 5.18: Zone one model, illustrating creep-induced crack, (a) initiation, (b)-(d) propagation, and (e)-(g) failure at the bottom corner of the model
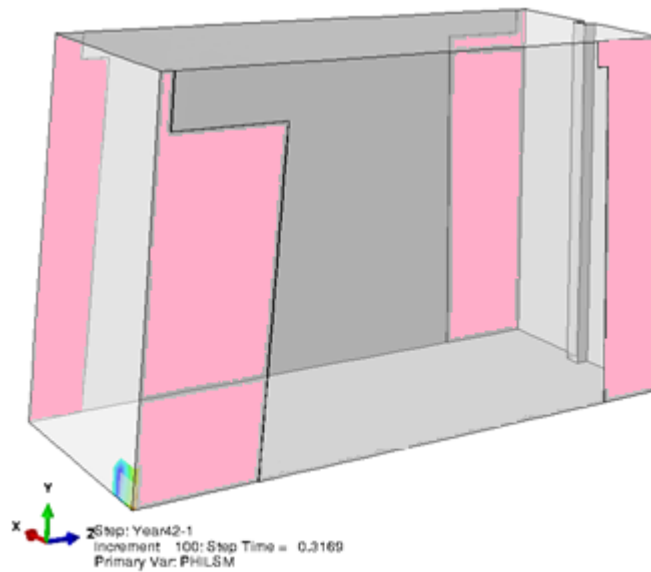
Figure 5.19: Zone one of pier at year 42, after exfoliation of the first layer from all 4 faces of zone one model.

The colour pattern shown across the block, illustrate the stress level at each particular point of the model. All the values on the contour are positive, presenting tensile stress. Red and blue colours also represent maximum and minimum tensile stress levels, respectively. As it can be seen, the stress distribution has considerably increased across the model, where the middle and upper parts of the block are in tension and shown in light green, orange, yellow and red colours.

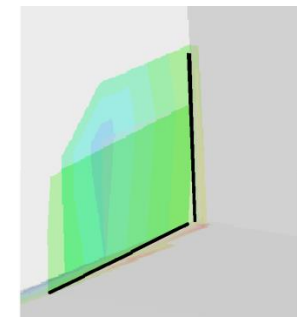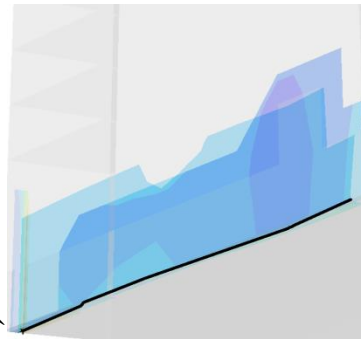Furthermore, stress distribution after removal of each layer, at years 43, 83 and 123 are shown in Figure 5.21. As it is evident, the yellow, orange and red zones around top corner of the block, where the elements have been removed, are significantly increasing with time presenting increase in the stress levels across these areas. This can be explained, by decrease in elastic modulus of the elements and hence physical removal of each layer of elements reduces the surface area over which load is distributed. This applies more pressure on the areas surrounding the damaged zone, hence increasing stresses in these areas. A close-up image of top corner of the model, at year 123, after removing three layers of masonry, is shown in Figure 5.22. As can be seen, the remaining layers on the outer face of the block have the lowest stress levels, as shown in blue and pointed to on Figure 5.21(a). With removal of elements (show in Figure 5.22), a very high stress is shown in areas surrounding these elements, which are shown in yellow, orange and red.

214

(a) 1884 (Viaduct 1 years old) (b) 2014 (Viaduct 130 years old)
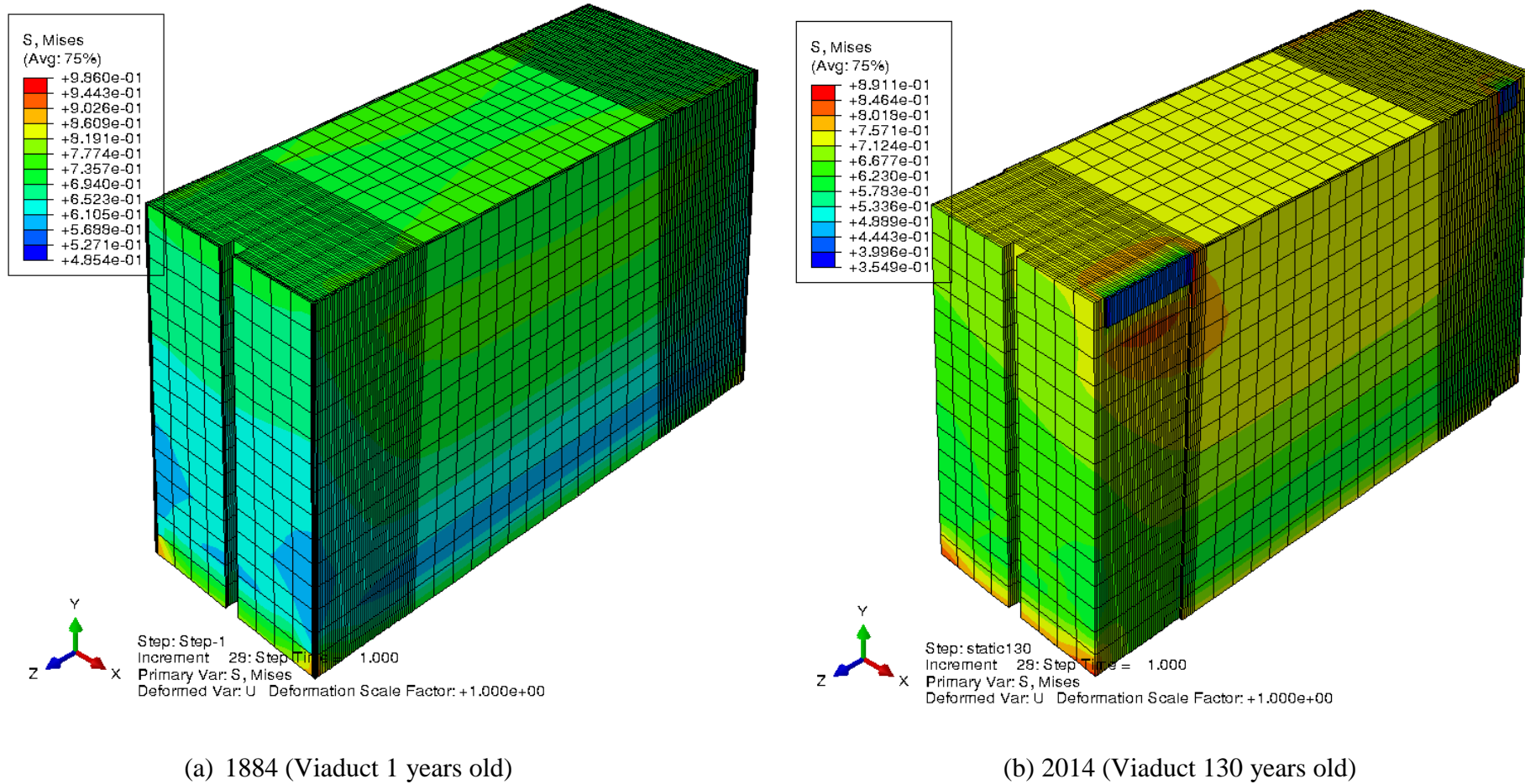
Figure 5.20: Von Mises stress distribution across the model, (a) prior to exfoliation, and (b) after exfoliation of three masonry layers (results are in MPa)
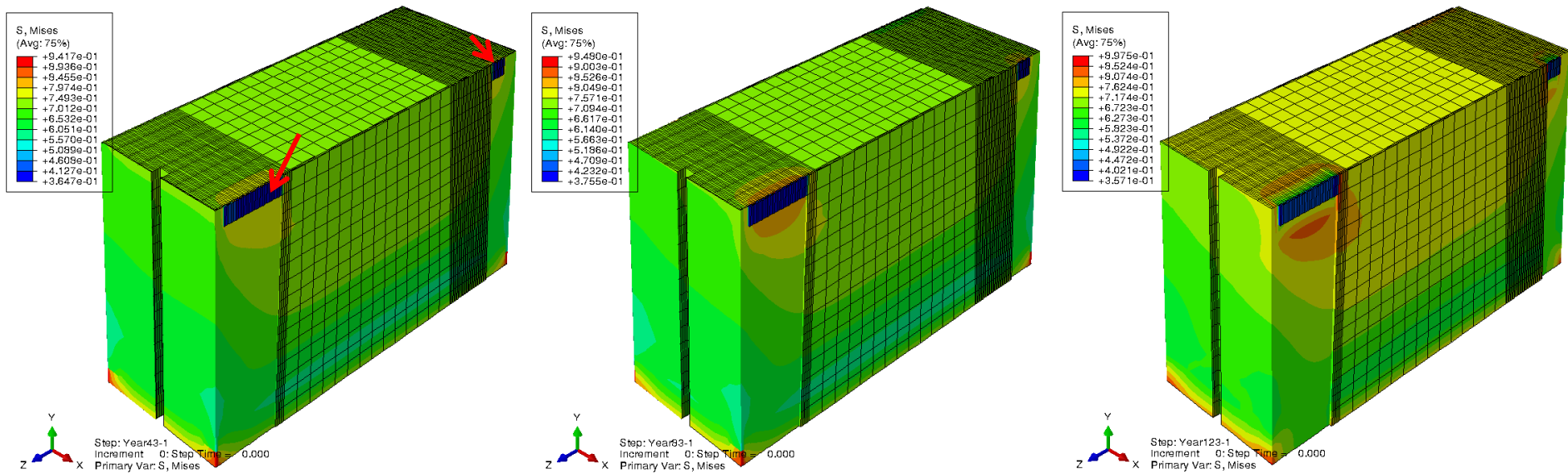
(a) 1927 (Viaduct 4 3 years old)   (b) 1967 (Viaduct 43 years old)   (c) 2007 (Viaduct 123 years old)

Figure 5.21: Von Mises stress across the model showing increase in stress distribution after exfoliation of masonry layers; after removal of (a) first layer, (b) second layer and (c) third layer (results are in MPa)
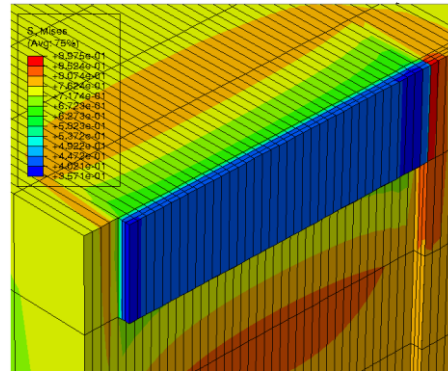
Figure 5.22: Stress distribution around a top corner of the block, after exfoliation of all three layers; at year 123 (results are in MPa)

a) Simulation results of the repaired model

Repair of zone one of the pier is modelled in this section. As explained in Section 5.3.1, before the repair process begins (whereby new material is applied to the pier), the damaged surface brickwork was fully removed. In addition, parts of the substrate masonry are also removed to achieve the optimum repair[52]; a typical example of this and application of such repair on piers of Larpool viaduct are shown in Figure 5.23 and Figure 5.24, respectively. Since the author of this work had not visited the site before repair was carried out on the viaduct (in year 2007), and as the existing repaired batch represents combined volumes of both damaged and substrate brickwork, there is an uncertainty as to how much of the batch represents damaged brickwork only. As such, 20mm of zone one (i.e. 2 layers) is considered to be the damaged zone, and a further 10mm (third layer) as the substrate. The former is removed at years 41 and 81, and the latter removed[53] just a year before the repair is applied to these three layers. Further details of the repair have been described by (Garrity, 2008). The total of 18 years, after removal of the third layer, represent the years after the repair up to the time of inspection of the site by the author.

In the context of repairing the exfoliated sections of a model, it was illustrated in Section 4.4.1.2 that when the simulation of the damage model is complete, simulation can be restarted and repair can then be applied to the model. This way, the existing strain and stress levels (from the damaged model where crack is not present) can be

---

[52] Locating the ties, filling the new mortar and toothing the new brickwork into existing undamaged brickwork, at repair boundaries.
[53] Representing the rehabilitation process.

imported into the repair model, while the element set (representing exfoliated materials) are given high *E* values to represent repaired materials. However, to present the 'concept of repair' on a block already affected by exfoliation and creep, and where cracks are present, it is very difficult to restart the repair simulation. More specifically, the difficulty lies in replacing the removed elements in models with cracks, as they require importing the existing strain and stress values from the defected model into the repair model. This is currently not possible in the current version of Abaqus, as simulations abort with the 'illegal memory error'; which as explained the current code in Abaqus cannot handle.
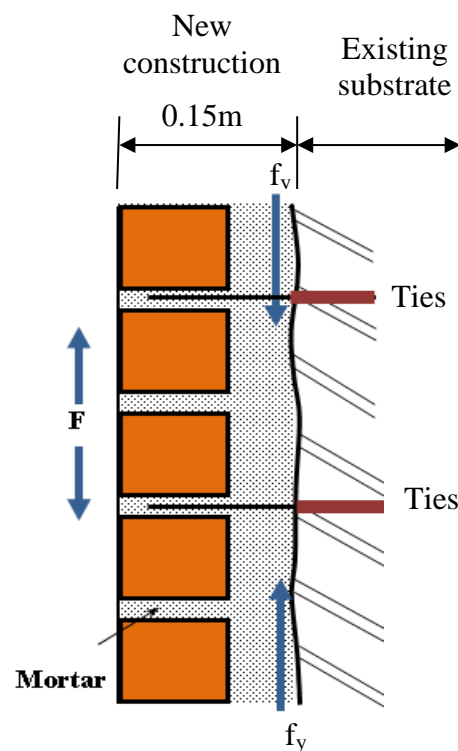
Figure 5.23: Typical repair approach for existing structures (Garrity, 2008).

Figure 5.24 : Repair of the brickwork on piers of Larpool Viaduct, illustrating ties.

This difficulty can, however, be overcome by mimicing 'the repair effect' in the model. That is, the elastic modulus *E*, of each layer can be reduced to represent he material's deterioration, and kept constant to represent the years after exfoliation; similar to the defected model. The effect of the repair feature is then shown in the form of a rapid increase in the *E* value of each layer (to a very high value), to represent sudden replacement of damaged masonry with repaired material in the Pier 4 of Larpool Viaduct; this is further ellaborated in Appendix G. The features of creep and XFEM will remain active after application of the repair, to the simulate continous presence of creep in the structure, as well as the possibility of crack formation after changes in strain distribution with application of repair.

In such a model, where layers are not physically removed, a gradual reduction in the density value of these layers should be considered. A linear reduction in the density can be assumed to describe this effect. However, in the zone one model, as the overal volume of the three exfoliated layers is only 1.24%[54] of the total volume of zone one, it is fair to say that, such a small value has almost negligible impact on the strain result. It is, thus, safe to assume that removal of these layers will not have a considerable affect on the density of the pier.

---

[54] Overall volume of three exfoliated layers: $0.537m^2$.

The strain-time graphs shown in Figure 5.25 present a comparison between the maximum principal strain for models with (model I) and without (model II) exfoliation effects (subjected to the original calculated load in Appendix D.1). As mentioned, the repair effect has been applied to the model without physical removal of elements.

As evident, the two curves overlap in the primary creep phase, where an increase in strain levels in the block is observed. However, abrupt drops can be seen in the strain level at years 41 and 120. Correlations to Figure 5.26(a), at year 41, the element with the highest maximum principal strain value of 41.63 με, is pointed at using the red arrow and is located adjacent to the crack, at the bottom corner of the block (between faces 2 and 3). Exfoliation of the first layer, removes this element, and hence the sudden drop in the maximum principal strain value, to 38.87 με. As shown in Figure 5.26(b), at year 42, location of the element with maximum principal strain value is changed to corner of Face one (between faces 1 and 4), and is pointed at using the red arrow. It is interesting to note that throughout the simulation, the element with maximum principal strain was located in the exfoliation layers. Such rapid changes in the strain values are, however, not visible in the curve of the model without the exfoliation defect-repair[55]. This further highlights the effect of erosion of masonry on the strain distribution across the model.

Crack propagation is observed with increase in the strain level in both models; this is followed by further increase in the strain level across the block, mainly due to the fracture energy caused by each crack in the model. Moreover, the significance of taking exfoliation defects into account is also highlighted by comparing the maximum principal stress-time response, in models with and without the exfoliation defect-repair.

---

[55] The effect of repair has been taken into account in the model without exfoliation defect.
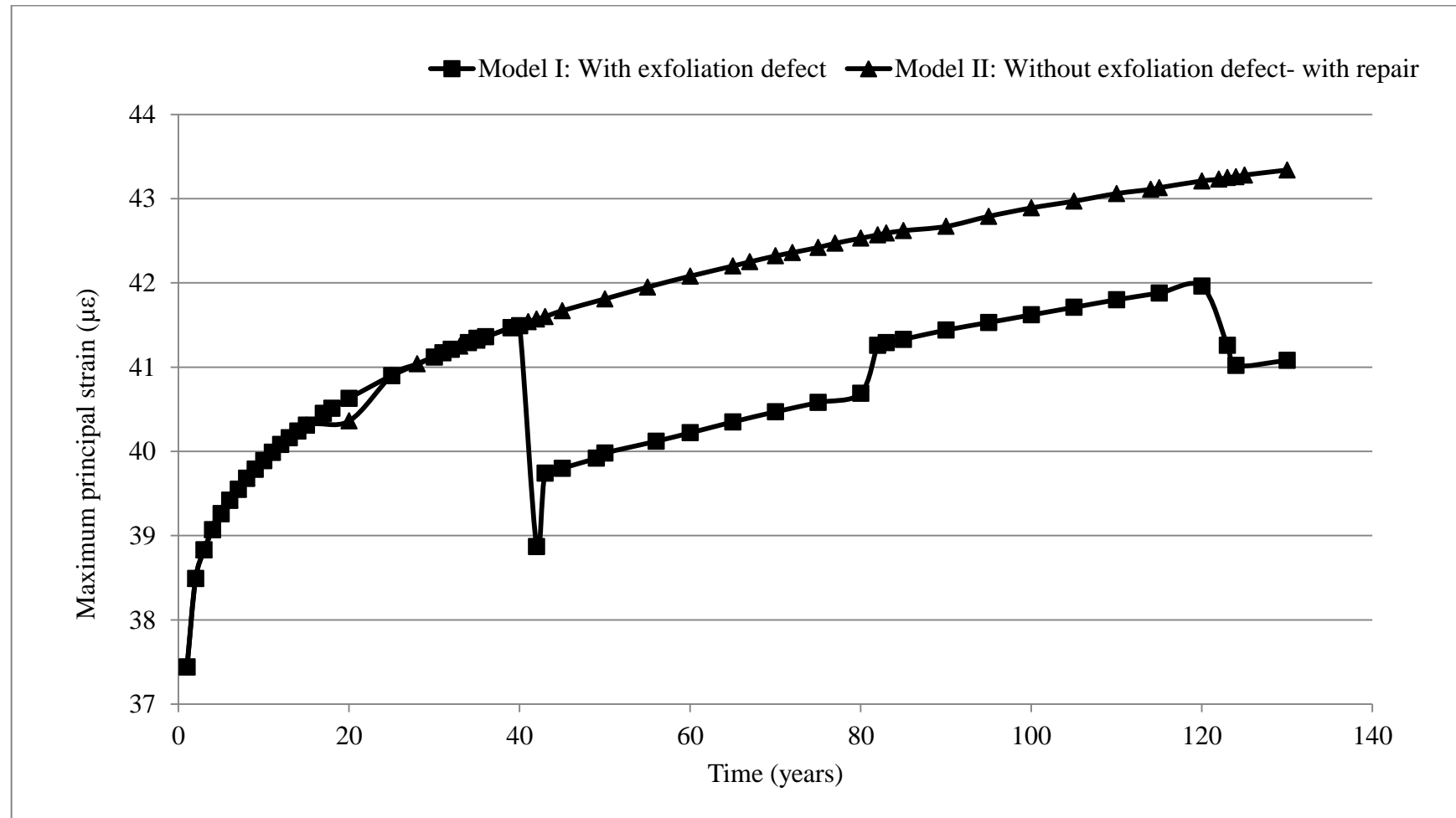
Figure 5.25: Strain-time graph, comparing the models with and without the exfoliation defect-repaired.

(a) 1925 (Viaduct 41 years old – prior to exfoliation)　　　(b) 1926 (Viaduct 42 years old –after exfoliation)
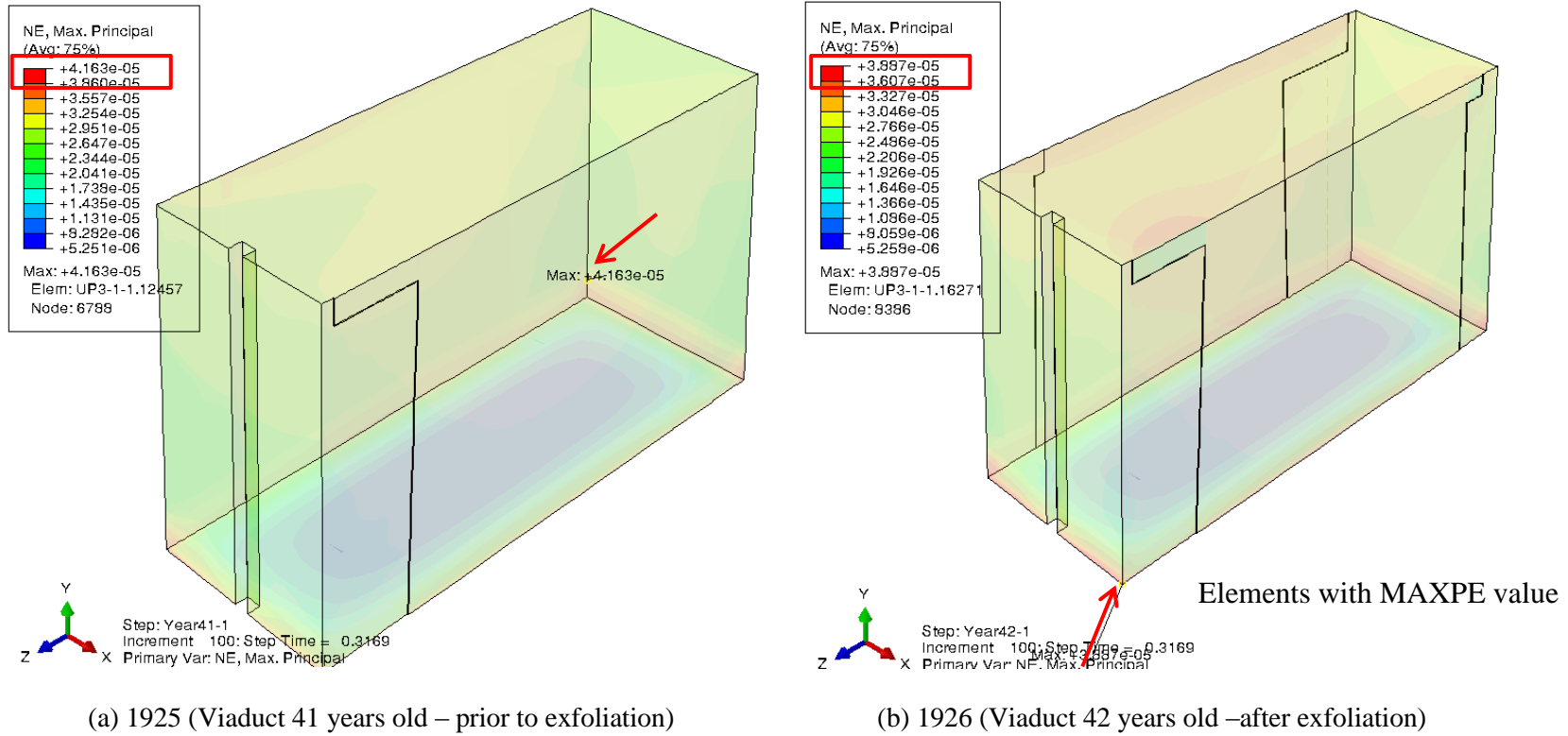
Figure 5.26: Drop in maximum principal strain, due to the exfoliation of layers, from 41.63 to 38.87 (με); contour results are in mm.
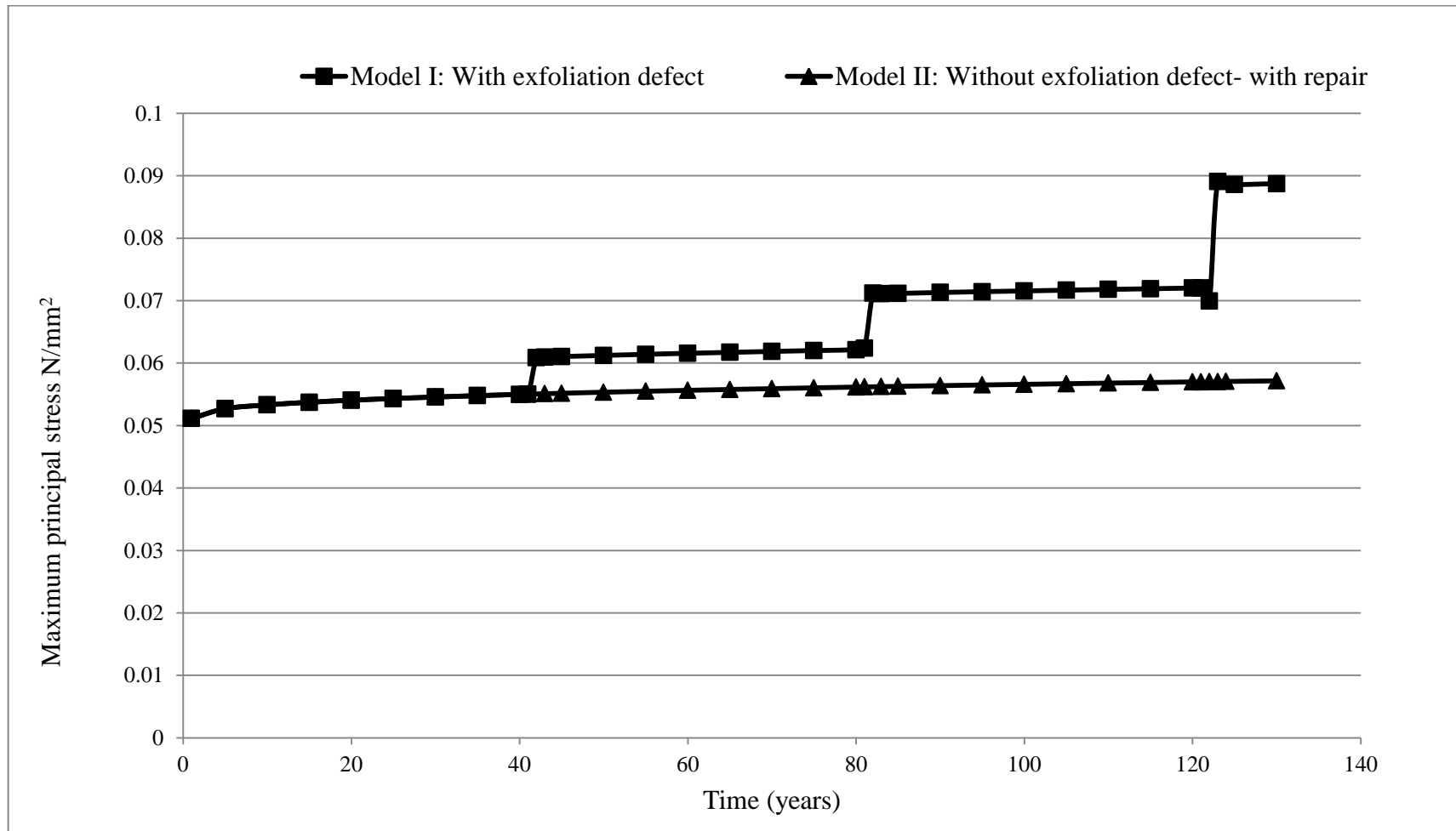
Figure 5.27: Stress-time graph, comparing the models with and without the exfoliation defect-repair.

In order to analyse effect of exfoliation in masonry, plot of maximum principal stress or both models, with and without exfoliation (but with repair), is plotted in Figure 5.27, where a constant increase is seen in the maximum principal stress level of the block. An overlapping response is evident in the curve of the two models up to year 41, where the first deteriorated layer is removed. Similarly, an increase in the maximum principal stress is seen at years 41, 81 and 121, with the removal of each layer in the model (due to the exfoliation defect), indicating increased stress across the model with removal of each eroded layer. This causes further crack propagation and subsequent change in the stress distribution across the block.

It is also interesting to note that applying the repair to model II has led to an even further increase in the maximum principal strain across the model. The change in the maximum principal strain ($613.9\mu\varepsilon$ to $636.9\mu\varepsilon$) and the maximum principal stress (0.93 to 2.34 N/mm^2) levels across the model is evident from year 123 to 130, in Figures 5-28 and 5-29. The effect of repair on crack propagation is also analysed by comparing the damage zones and crack pattern before and after repair. As it can be seen from Figure 5.30, new damage zone and crack lines are seen after repair is applied; pointed at using red arrows. This is expected as increase in the maximum principal strain value was evident in Figure 5.25.

Simulating the repaired pier allowed for assessment of the structure's performance after repair, and up to the present date. This is significant, as creep effect continues to occur in the original material, as well as the new repaired material. Evidently, the maintenance and repair applied to the pier seems to have increased the strain across the model, and thus increasing the further crack initiation. This has further highlighted importance of modelling repair.
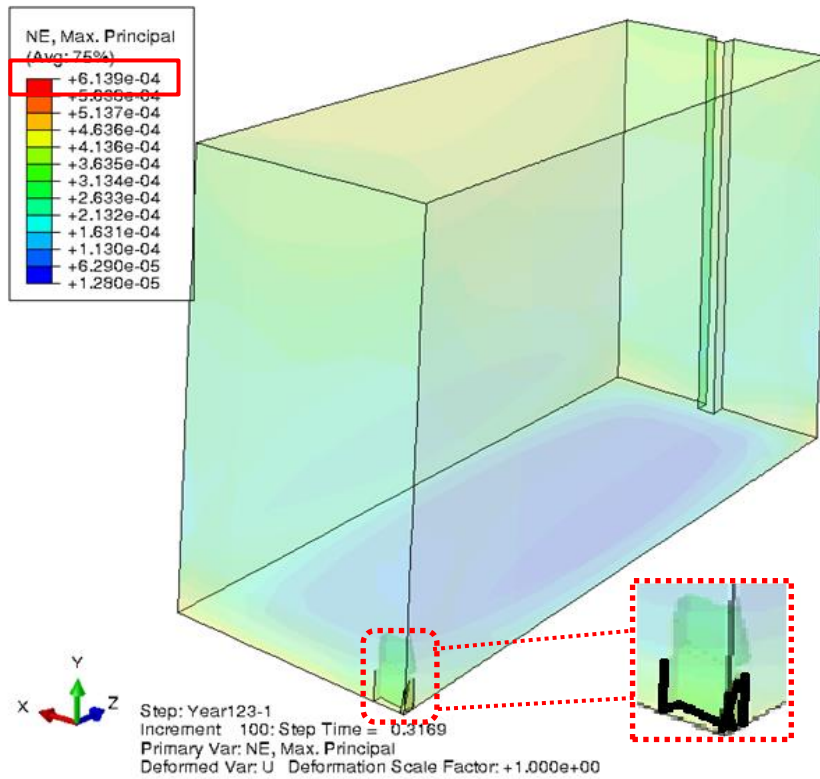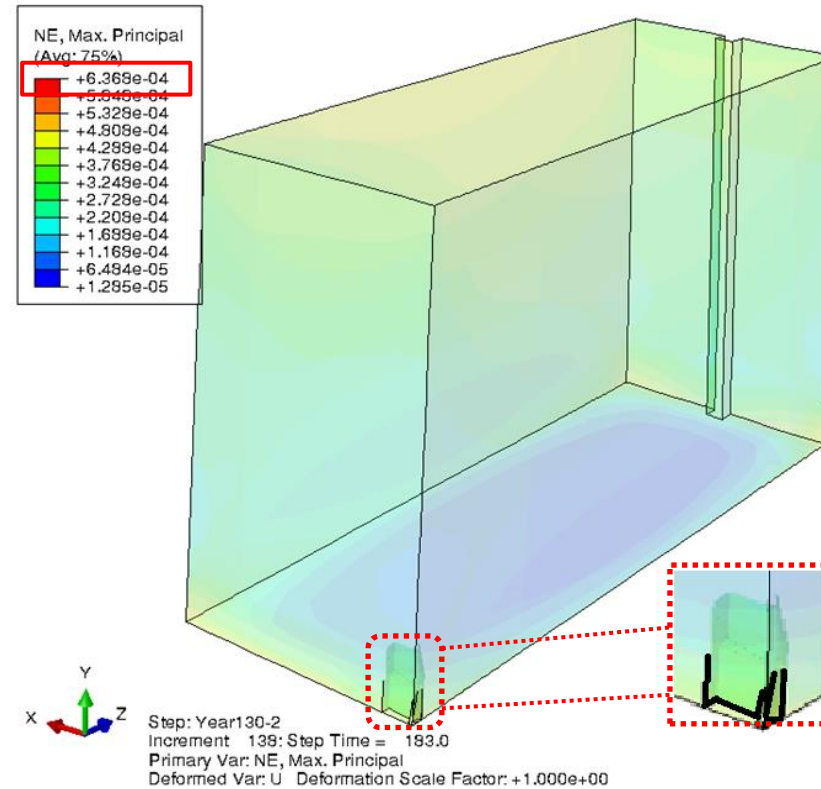
(a) 2006 (Viaduct 123 years old – prior to repair) (b) 2014 (Viaduct 130 years old – after repair)

Figure 5.28: Change in maximum the principal strain value in the model (a) prior to and (b) after repair; contour results are in mm.
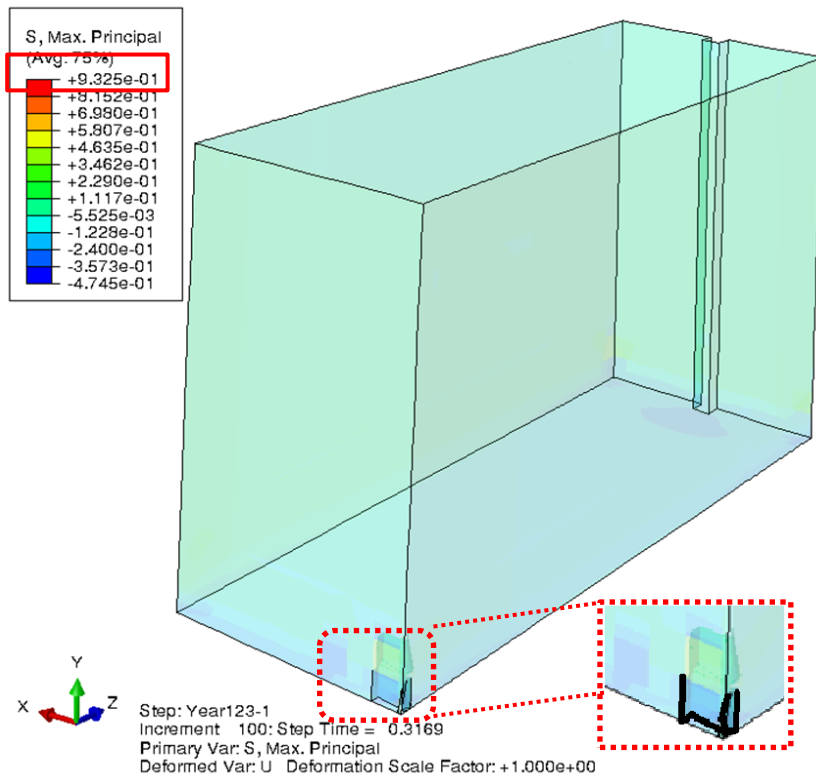
225

(a) 2006 (Viaduct 123 years old – prior to repair)   (b) 2013 (Viaduct 130 years old – after repair)

Figure 5.29: Change in maximum principal stress value in the model (a) prior to and (b) after repair (results are in MPa).

(a) 2006 (Viaduct 123 years old – prior to repair)   (b) 2013 (Viaduct 130 years old – after repair)

Figure 5.30: Crack propagation and increase in damage zone, (a) prior to, and (b) after repair on model of zone one.

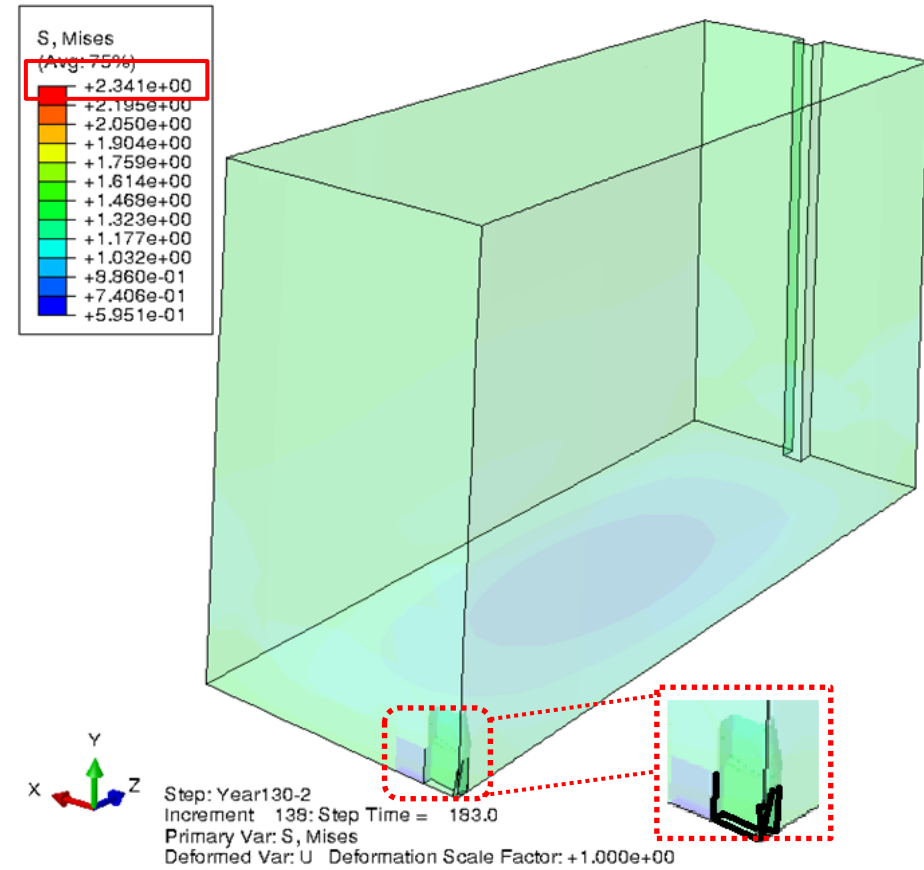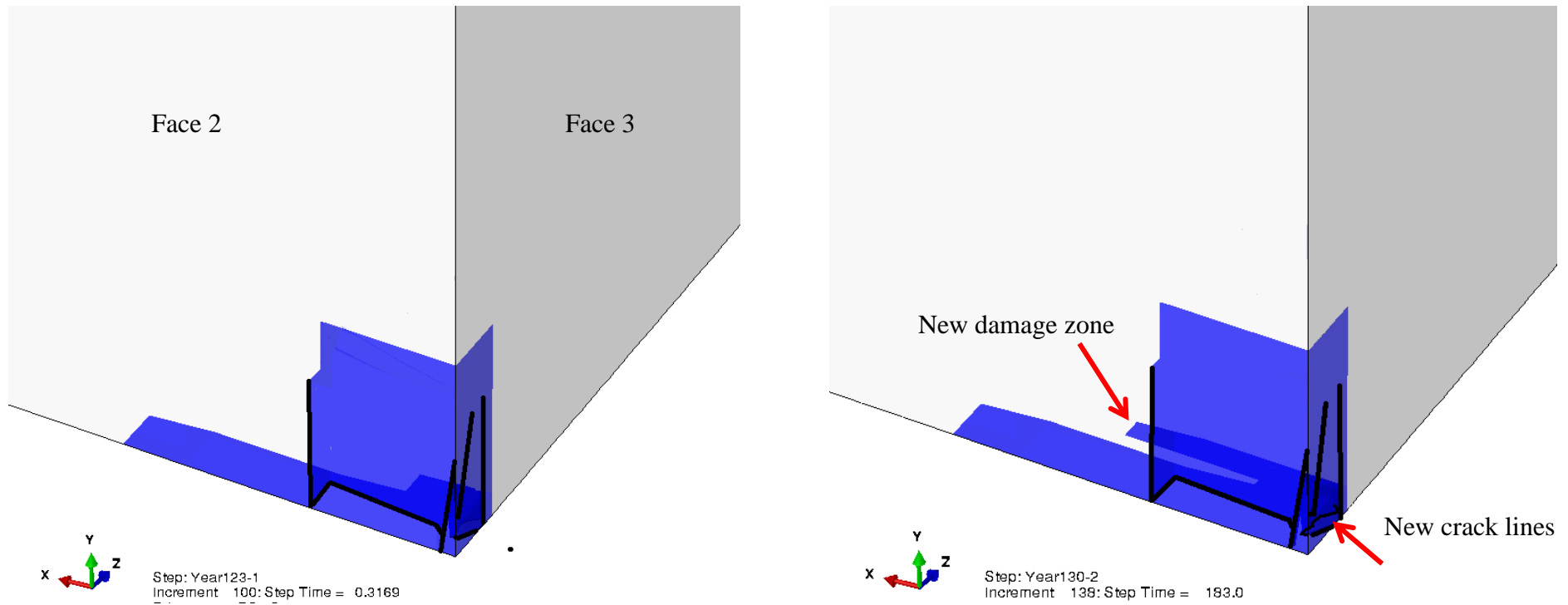### 5.3.2.3. Bottom 2.5m of the pier: zone two

Zone two of the pier was modelled separately to illustrate the combined effect of the two defects of creep and creep-induced crack. Although no exfoliation is present at the bottom of the pier, the exfoliation effect (geometry removal) at top of the pier has been taken into account in the form of change in the applied load, when modelling the bottom section of the pier. In the on-site inspections carried out from the pier, many cracks were observed mainly around the middle 2m of zone two, which was chosen as the crack enrichment zone of the model. Therefore, a fine mesh was used[56] in associated sections of the pier model in Abaqus, in order to pick up and illustrate a reliable and consistent pattern of the cracks. Moreover, to reduce the computational time, a very coarse mesh size of 1500mm was used for the rest of the zone two. The height of this model is also meshed using seed size of 200mm. Therefore, a total of 9542 linear hexahedral elements (of type *C3D8R*) were used for meshing the entire block.

From the load point of view, it can be seen from Figure 5-31 that the block is stressed at the top surface, fully constrained at the bottom surface and fine-meshed in the middle two metres of the model.

Also at the site inspections of the pier, no significant exfoliation or cracks were evident in the middle 19.78m of the pier (see Figures 5.9 and 5.10), and so, it was decided not to model this part of the pier. Instead, its effective presence was assumed by adding its weight to the initial load (from the arch above the pier) and applied to the top surface of zone 2 (calculations given in Appendix D.2). As such, it is assumed that the sum of the initial calculated pressure and the self-weight of this 19.78m pier, gives an approximate effective load as the entire pier. It is important to note, that due to lack of data, live loads induced by passengers and transient stresses induced by train movement over the period of 80 years have not been taken into account.

The effect of the concrete foundation of the pier can be modelled by fixing the bottom surface of model of zone two. A previous inspection of the site by Garrity (2008) revealed that the upper parts of the foundation were in good condition with no obvious signs of bed joint deviation, indicating that there was no visual evidence of subsidence or settlement-related damage to the pier. This surface should, therefore, be fixed in *Y*-direction. It was also thought that movement in *X*- and *Z*-directions should be allowed.

---

[56] (50 mm- based on the mesh dependency carried out in Section 4.4.3.2)

However, it is believed that having such boundary condition produces significant instability and convergence problems in the model. The base of the pier is assumed to be fixed and, therefore, any possible base movements are neglected. As such, a fully fixed boundary condition is applied to the bottom surface of the pier.

The remaining section of the pier above zone two (19.78m) would pose a constraining effect on transverse movements (resulting from friction) of the top surface of the model. Therefore, to take into account the continuity of the pier (to take into account the physical presence of the rest of the pier); constraints[57] should be applied to the edges at the top surface of the block. In this context, as the width of top edges of faces 2 and 4 (in *X*-direction) are approximately one-third of that of faces 1 and 3 (in *Z*-direction), all these edges are fixed in the *X*-direction (no movement allowed), and so the block can be considered as a thin-plane. This is done to simplify the analysis, by assuming the block under plane stress[58]. Since constraints in Abaqus do not *allow* for movement within a given value[59] , but rather *force* the edge to move in given directions, it is fair to say that such assumption is reasonable. Nevertheless, it is expected that the reality falls somewhere in between the unconstrained and fully constrained edges. Note that no constraint has been defined in the *Y*-direction, as the direction in which loadings of the block are exerted, and compressive forces are imposed.

In order to validate the employed methodology and the ability of the proposed tool to provide realistic prediction of existing crack patterns in the pier, the results of the simulations presented below are compared to the actual crack patterns on the bottom 2.5m of the pier (as shown in Figure 5.9).

For a better illustration of the results, an overall view of the crack patterns and damaged zones are shown across the block, in Figure 5.32. The real crack patterns on each face are then shown separately, for detailed comparison between simulation and observed cracks on the pier.

---

[57] Constraint is a boundary conditions that partially or fully eliminates degrees of freedom of a group of nodes.
[58] i.e. the stress vector is assumed zero in the *X*-direction.
[59] In Abaqus, the user-specified constraint for each direction is not a range, but a value indicating displacement.
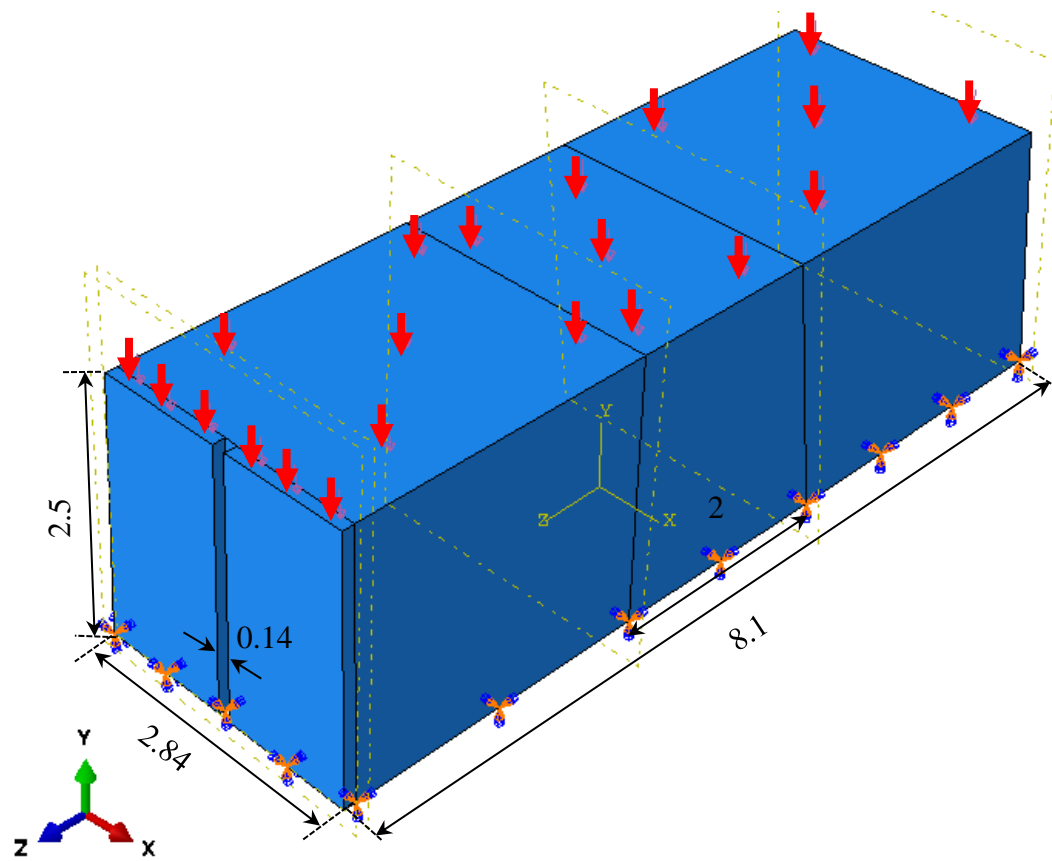
(a) Load and boundary condition on zone two
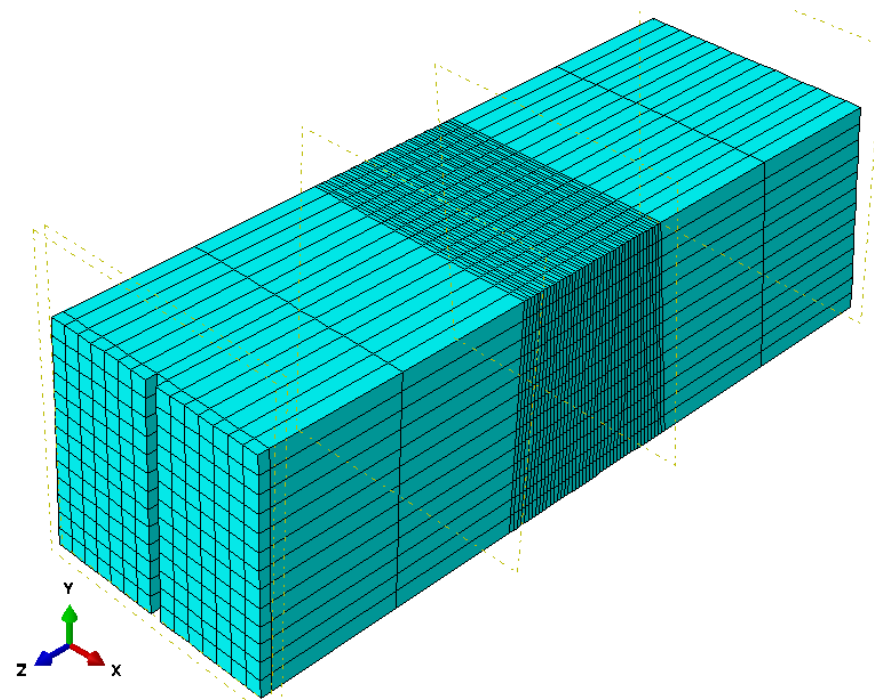
(b) Zone two model meshed

Figure 5.31: Zone two of the pier (a) subjected to a uniform vertical stress at the top and fully encastered at the bottom, and (b) showing the fine mesh used in the central 2m wide zone (all dimensions are in metres).

In these generated figures from Abaqus, the damaged zones are shown in blue, and the cracks on the outer faces of the block are shown in black solid lines. As mentioned in Section 3.3.2, the elements in the damaged zone have reached the damage threshold, but have not yet cracked (linear damage softening response in Figure 3.8). Figures 5.33 to 5.37 show the propagation of damage and cracks over time. Strains in the middle 2m of the block were seen to increase with time and this is reflected in the growth of the cracks and damaged zones.

Different faces of the block, explained in this section are labelled as F1-6, where F stands for Face. As one can see from Figure 5.33, a small patch of damaged zone is evident on faces 1 and 3, which have not reached the specified damage threshold. The elements of the damage zones on face 6 have, however, reached the specified threshold, where the tensile stress acting on these damaged elements, leads to their dilation in the *X*-direction, and thus crack formation in the *Z-Y* plane. As seen these vertical cracks occurred closer to the side of the block that included the drainage channel (on face 6 rather than face 5). This may be due to the drainage channel being closer to face 6, and thus the effect of, the sharp edges that define it, and also use of smaller mesh size on this face.

 The damage seen in Figure 5.33 is characteristic of a mode-I fracture, where the crack surfaces are pulled open, due to the presence of tensile stresses perpendicular to the crack surface. A typical mode-I fracture is shown in Figure 5.32, where the crack is opening with respect to the *Z-X* plane.
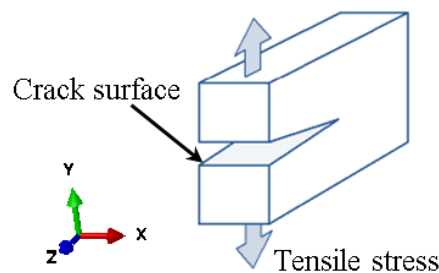
Figure 5.32: Fracture mode-I; tensile stress acting perpendicular to the crack surface.

The maximum principal strain values of 3.01E+02 and 2.275E+02 are recorded in *X*- and *Z*-directions, respectively, and are tensile strains. Higher tensile strains in the *X*-direction (as the edges are constrained in this direction), causes damage to extend in the *Z*-direction (higher degree of freedom are allowed in the *Z*-direction), as evident in

(Figure 5.34(a)). The high strains in the *Z*-direction also induce symmetrical damage zone and crack formation in the *Z-Y* plane, on two sides of face 6 (Figure 5.34(b)).

In Figure 5.33 (a), as expected, a strip of damage zones are can be seen across both faces 1 and 3, where a crack initiation is also evident in the *Y-Z* plane. In addition, further damage and crack propagation in the *Y*-direction (with respect to the *Z-Y* plane) is evident on face 6 in Figure 5.35(b). This results from the maximum strain values of *Y*-direction 1.063E+02, being smaller than those of the Z-direction. Propagation of the damaged zone across faces 1 and 3, consequently results in further increase of strain in the adjacent elements, and so formation of damage zone and crack lines on face 5.

As was reported in Section 2-4-2-i, propagation of vertical cracks leads to increase in strain and lateral deformation of structure with time. Moreover, with further creep accumulation and, consequently, higher strain levels in the secondary phase a gradual increase in the horizontal strain values leads to dilation of masonry in the *Z*-direction; seen in Figure 5.36. As time collapses and with further accumulation of creep effect, these horizontal damage zones develop in the form of a vertical bar (finger) in the *Y*-direction, the damage evolves and leads to failure and formation of cracks with respect to the *Y-Z* plan e. These cracks were located near the top constrained edges of faces 1and 3, at the top surface of the block Figure 5.36.

As seen in (Figure 5.37(a)), with passage of time, and at the end of the simulation (representing the time that the site was visited by the author of this work), the damaged zones extend deep in the *Y*-direction, propagating a vertical crack on the faces 1 and 3 (increase of approximately 380 mm in the crack length). The vertical cracks represent a typical creep-induced crack, shown in Section 2.4.2. Further accumulation of creep and crack-induced strain and crack-induced strain, leads to additional propagation of damage zone and appearance of crack lines at the top edges of the block.

As it can be seen from Figure 5.37(b), and as expected, the cracks seen on the outer faces of the middle 2m of the block, represent damage formation in the form of spalling of the outer layers, examples of which were also evident on the pier (shown in Figure F-8 of appendix F). Both mentioned crack patterns are typical behaviour masonry under compression.

Although the damaged zone, vertical bars and cracks (Figure 5.37(b)) propagated to achieve an approximately symmetrical distribution (at the middle of the block in the *Z*-direction), more damaged regions were evident on face 6, being the closest side to face

4; where the drainage channel is located. As explained earlier, use of smaller mesh size on face4, results in an increase in the strains in the elements on face 4, compared to those on face 2, and, therefore, increased likelihood of cracks forming in this half of the block. This can be shown by comparing the maximum principal strain values of elements at top corner of face 4 and 2, giving the strain values of 1.73E+02 and 1.14E+02, respectively. Detailed crack patterns on both faces 1 and 3 (at the end of year 130) are visible in Figure 5.38.

The exact number of cracks recorded from the pier itself could not be reproduced in the simulation. A good representation of the direction and pattern of the actual vertical cracks on the pier was achieved, however (Figure 5.9). The differences between the pier and computational model can be attributed to the various simplifications and assumptions that were required in order to produce the computational model. These include the load calculations, which did not account for the live load imposed on the pier (i.e. train load over the 80 years of its use, passengers, and weathering load); and so, the actual load is believed to be higher than the one used in the model. Given a more accurate loading profile it would be expected that the cracks may combine to form macro-cracks at the top edges, and further damage propagation and vertical crack lines appear in the *Y*-direction (up to the bottom edge of the block). A similar pattern to those at the top edges is also expected to form at the bottom edge of the block. For better illustration of this, higher load was applied to the same model; shown in Figure 5.39.
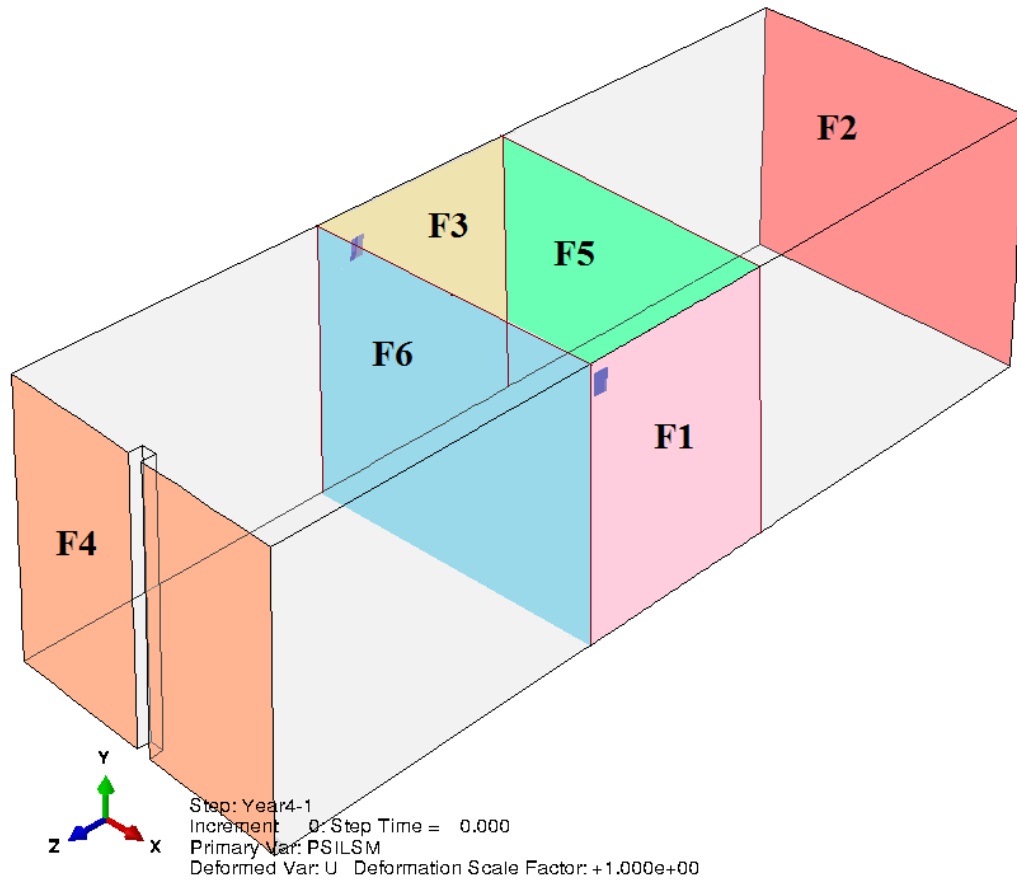
(a) 1888 (Viaduct 4 years old), the entire zone 2   (b)1888 (Viaduct 4 years old), middle section of zone 2
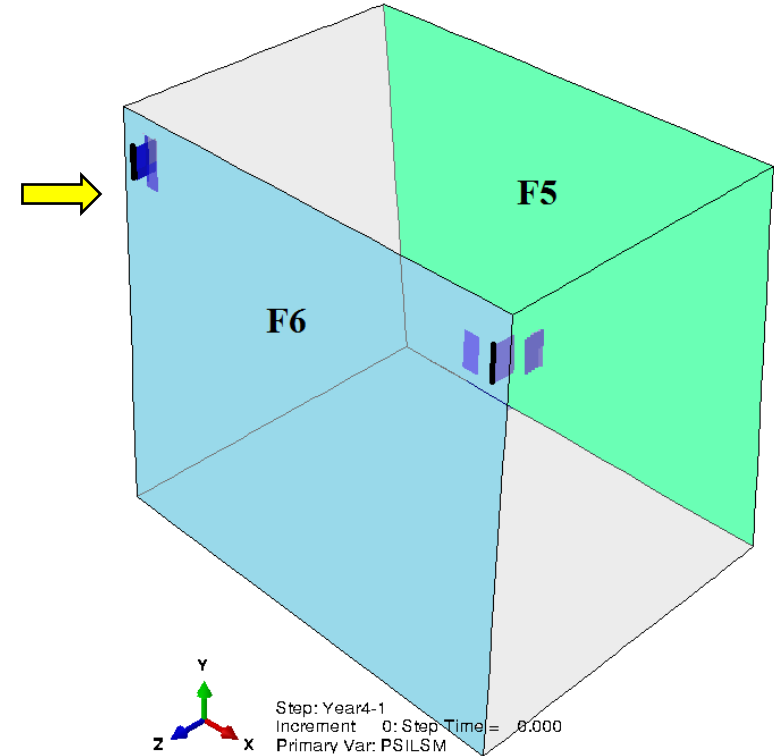
Figure 5.33: Creep-induced cracking initiation on (a) the entire block, and (b) middle 2m of the block.
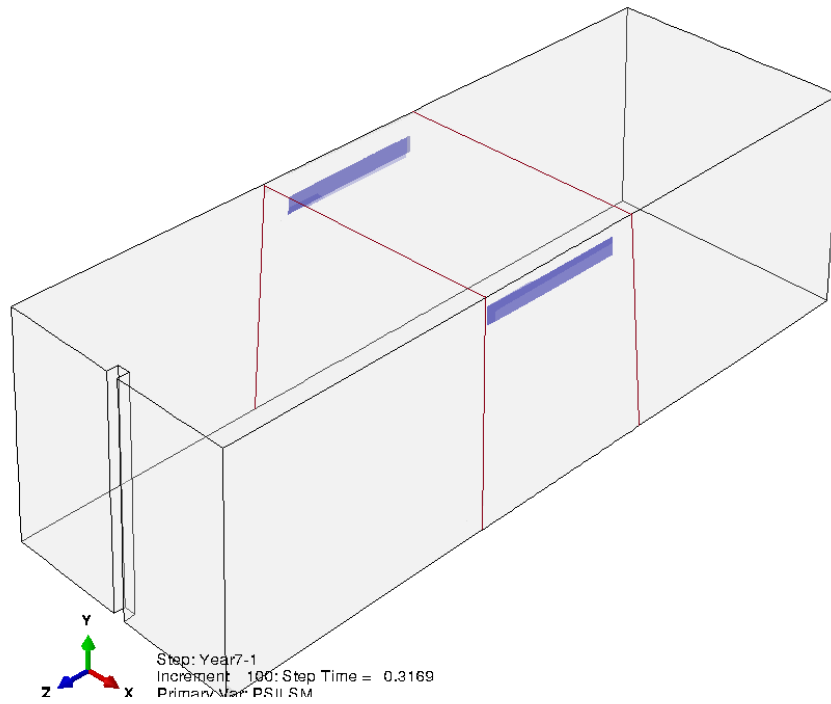
(a) 1891 (Viaduct 7 years old), the entire zone 2   (b) 1891 (Viaduct 7 years old), middle section of zone 2
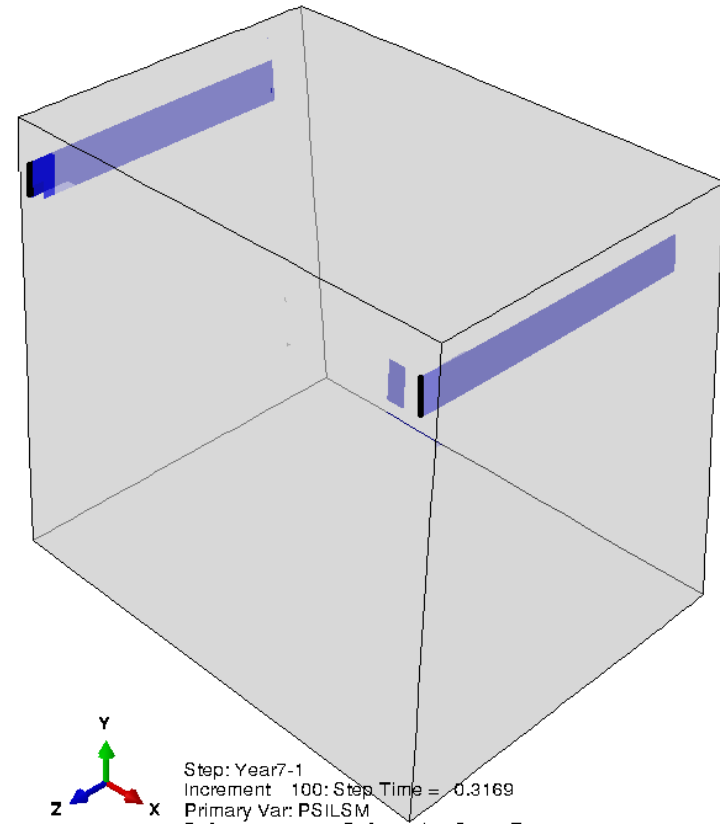
Figure 5.34: Crack propagation in the *Z-Y* (vertical) plane, on (a) the entire block, and (b) middle 2m of block.
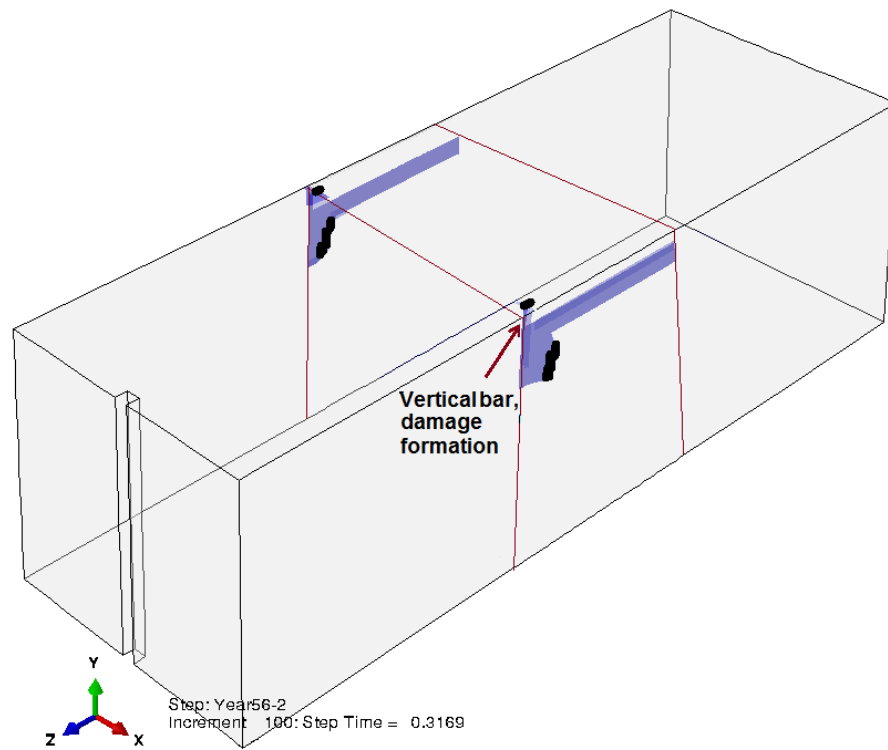
(a) 1940 (Viaduct 56 years old), the entire zone 2   (b) 1940 (Viaduct 56 years old), middle section of zone 2
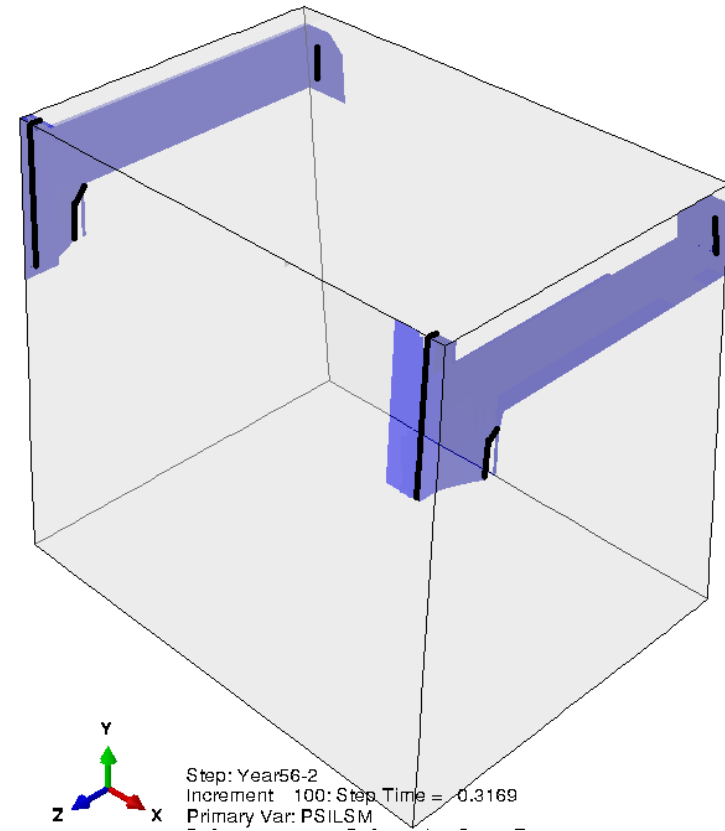
Figure 5.35: Vertical crack formation on (a) the entire block in the *X-Y* plane, and (b) middle 2m of block in the *Z-Y* (vertical) plane.

(a) 1965 (Viaduct 81 years old), the entire zone 2   (b) 1965 (Viaduct 81 years old), the entire zone 2
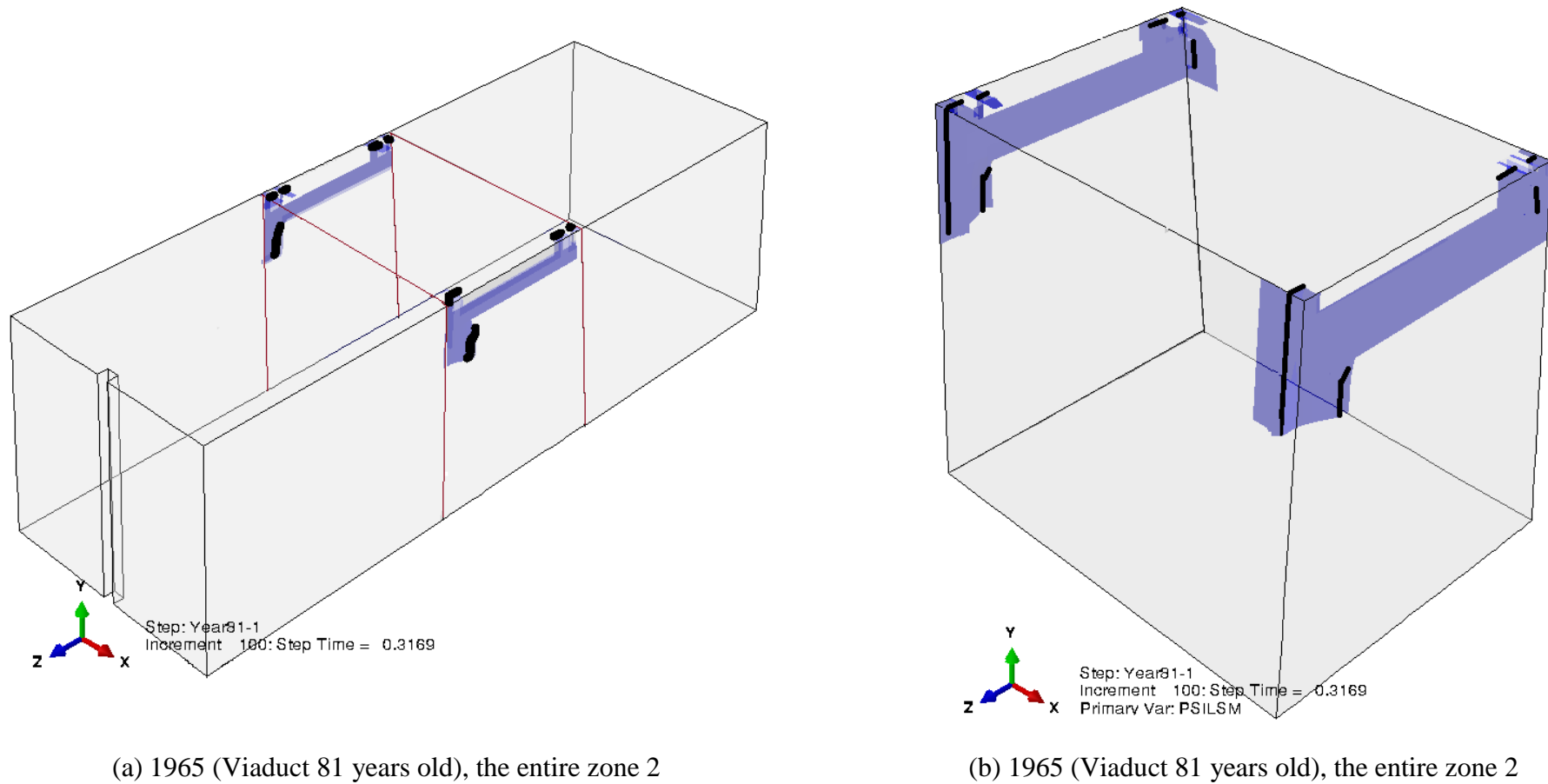
Figure 5.36: Crack formation on vertical damage bar zone on face 1 and 3 (a) entire block, and (b) middle 2m of block..
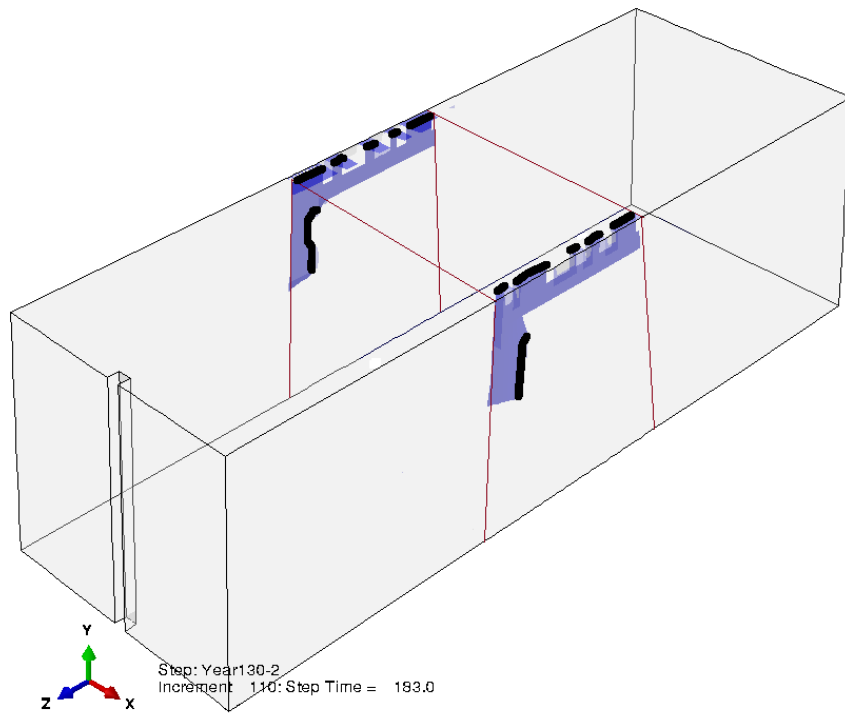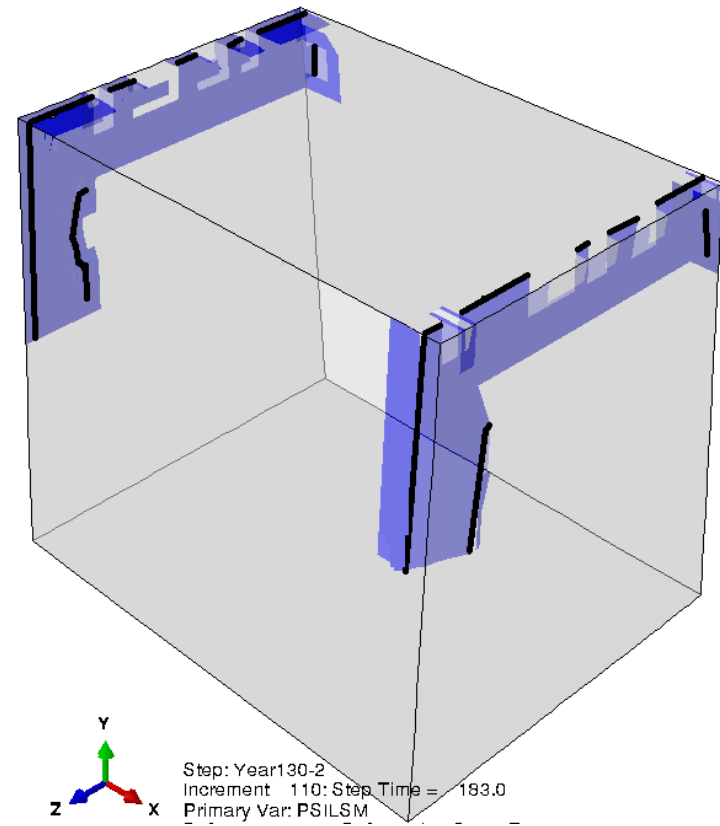
(a) 2014 (Viaduct 130 years old), the entire zone 2   (b) 2014 (Viaduct 130 years old), the entire zone 2

Figure 5.37: The overall crack pattern on outer face of block at the end of the year 130.
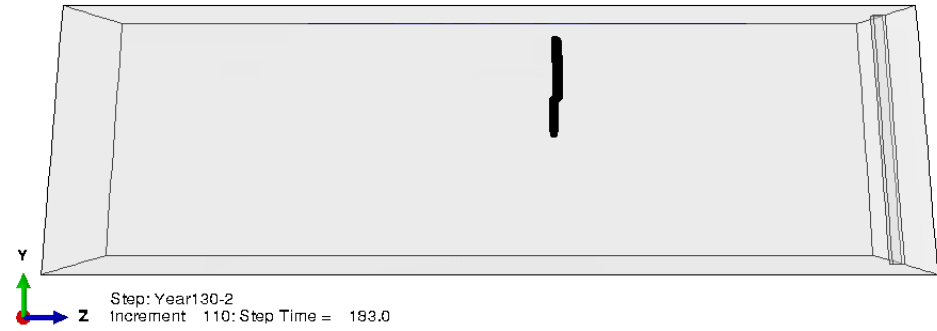
(a) 2014 (Viaduct 130 years old)   (b) 2014 (Viaduct 130 years old)

Figure 5.38: Crack pattern on (a) face 1, and (b) face 3 of the block, at the end of year 130.
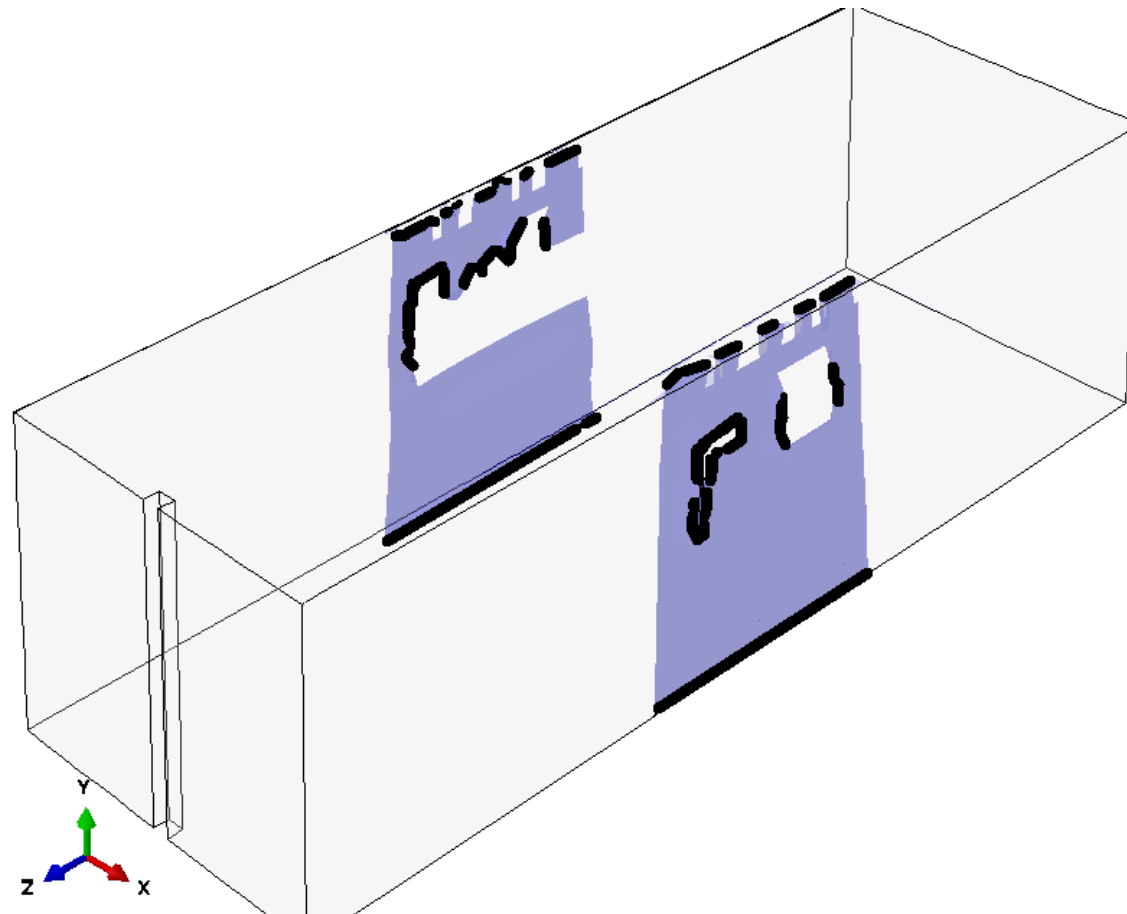
Figure 5.39: Crack pattern on face 1 and 3 of model, subjected to higher vertical load.

For better analysis of creep behaviour in the form of strain accumulation over time and to illustrate the importance of creep effect in a simulation, two models are compared, whereby "creep and XFEM" are enabled in one model and "creep is not present" in another. To do so, the strain-time graph of the model was plotted in Figure 5.40. Hereafter, the two models are referred to as 'case one' and 'case two', respectively. In 'case one', the XFEM feature is only enabled in the model to pick up the load-induced cracks at the beginning of the simulation. The initial maximum principal strain in the block is 106 $\mu\varepsilon$. The strain level stays constant with the constant load, which is expected for there being no creep and creep-induced strain present in the simulation.

In 'case two', both creep and XFEM features are enabled at the beginning of the simulation (in static and visco steps). In this case, continuous increase in strain level is seen once the load is applied.

Analysis of the simulation results reveal that cracks are not formed under initial loading. The peak point of MAXPE is highlighted in Figure 5.40, where the load was applied at year 1 and a crack formed at year 3, marked as points A and B, respectively. The MAXPE value increased with time, from 108 to 303, over this period when creep properties were included in the model (as shown in Figure 5.41). This further highlight that crack formation was due to a gradual increase in creep-induced strain with time.

There is an obvious difference in the strain level compared to response of case 1 model, highlighting the importance of taking into account the presence of creep feature in a simulation. The large difference between the recorded final strains in the models with and without the effects of creep highlight the importance of creep strain as a driver for masonry fracture. The three phases of creep are marked in Figure 5.40. When creep is present in the simulation, in phase I (primary creep phase) an increase in strain level is seen at year 3 due to formation of the damage zone.
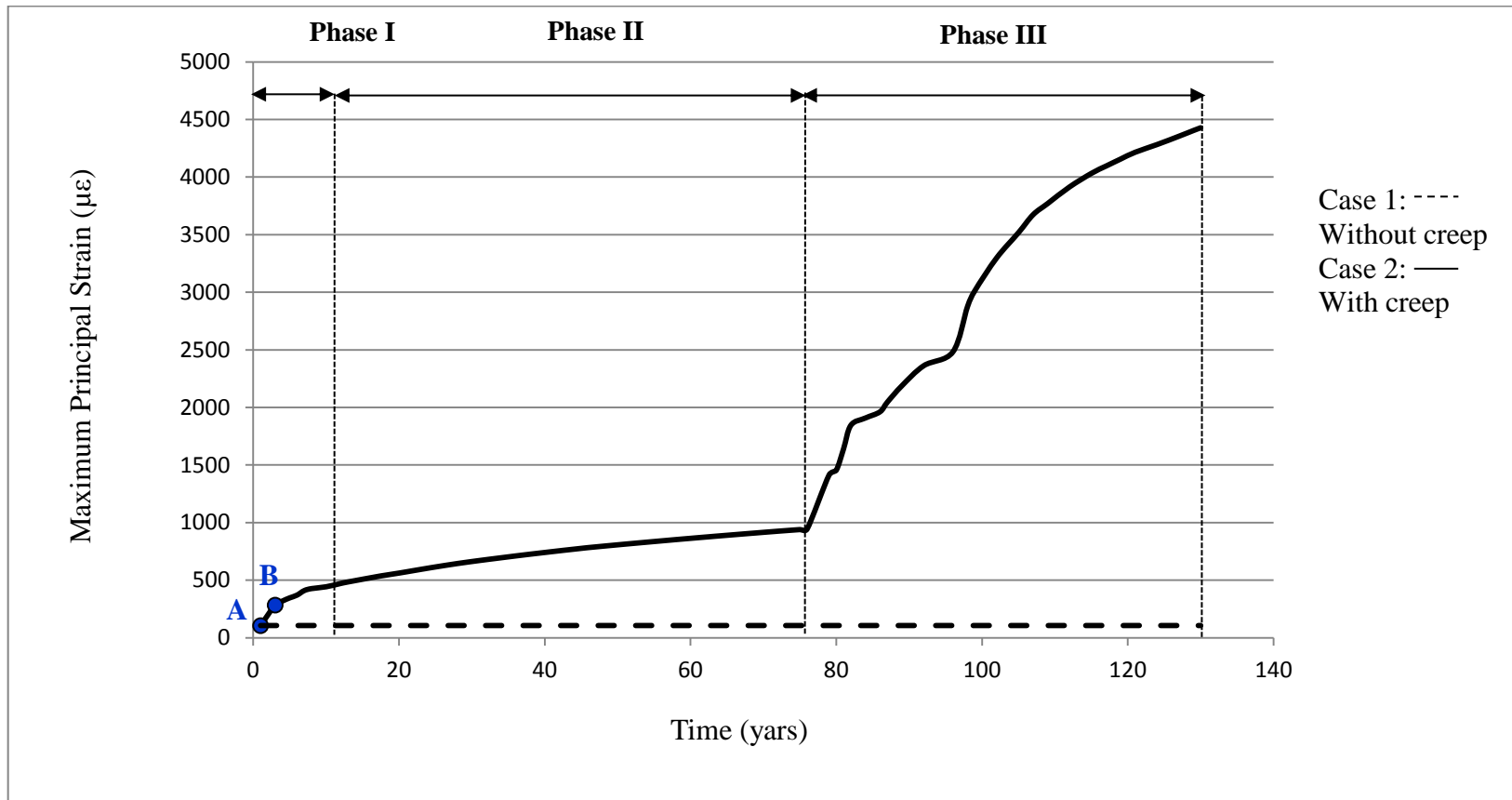
Figure 5.40: Comparison between simulations for models with and without creep effect.
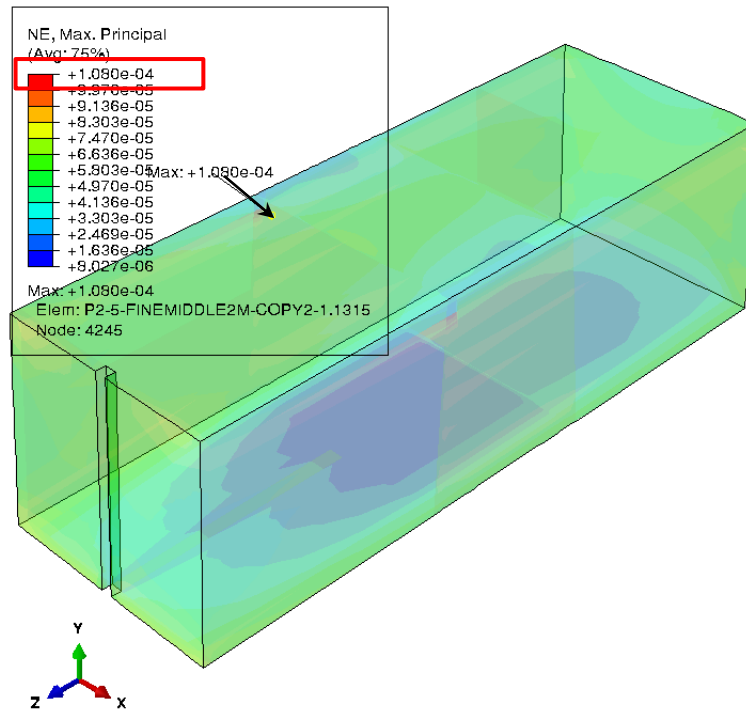
(a) 1884? (Viaduct 1 years old- after applying the load)   (b) 1887 (Viaduct 3 years old- prior to damage formation)
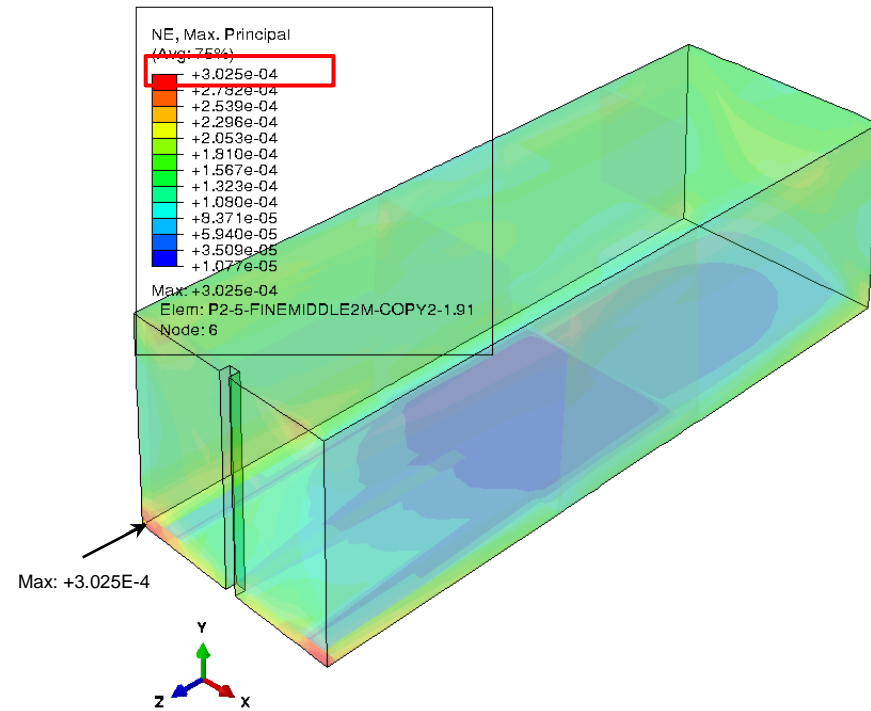
Figure 5.41: Increase in maximum principal strain (a) after applying load, and (b) prior to damage formation is evident, due to increase in creep-induced strain with time; contour results are in mm.

Crack formation in the third year of the simulation supports the expectation highlighted in the literature review of this thesis (Section 2.4.2-i) that the majority of initial cracks form within the first few years after construction. Expectedly, the strain has an almost linear response at phase II, indicating gradual increase in creep-induced strain with time, and thus an increase in the damage zone and crack propagation in the zone two model.

Tertiary creep phase starts around the year 77, where a rapid jump in the strain level is evident. This is related to a sudden increase in damage zone propagation and the development of vertical bars. The accumulated strain from previous phases leads to development of further damage zones. This led to cracks extending to meet the outer surface of the block, resulting in visible external cracks in the pier block.

5.5 Summary

This chapter adopted the computational model developed in Chapter 4, to illustrate the abilities that the proposed tool offers and its significant potential in changing the architectural, civil engineering, conservation and restoration industries.

Towards this, abilities of the tool in predicting the *individual* feature of long-term creep effect, as well as *combination* of features including creep and creep-induced cracks in historic masonry structures have been examined and validated. Primarily, these features were validated by using the creep parameter range identified in Section 4.4.2, to predict the long-term creep behaviour of historic masonry. Long-term creep experimental results given in the literature (obtained from ruins of belfry of the Pavia Civic tower) were then used to verify this prediction. In addition, the maximum strain value from experimental results was used to specify the damage threshold for the model to be used in the 'crack feature' of the tool. The crack patterns obtained from simulation results were then validated through comparison with creep-induced crack patterns of the same experiment in the literature. With successful validation of tool's ability in predicting individual and combined effect of defect-oriented behaviour of a small masonry specimen, it was essential to demonstrate the tool's ability in modelling a complete structure whose constituent materials are not properly known.

Pier 4 of Larpool viaduct was, therefore, chosen as a structure that meets all the required criteria, where the three defects of exfoliation, creep and creep-induced crack are present and evident. The proposed tool was used to reproduce and simulate the combined effects of these defects in Abaqus over time. The results were then verified through a comparison with existing defects on pier 4 of Larpool viaduct.

In order to overcome the computational limitations, to shorten the simulation time, and as an illustration of the ultimate functionality of the proposed tool, it was decided to model only the top 3m and bottom 2.5m parts of the pier (referred to as zones one and two, respectively). The presence of creep and creep-induced cracks were taken into account in modelling of both zones, with exfoliation also present in zone one. The effect of repair was also simulated in zone one model, without presence of exfoliation defect. These models were simulated for the pier's lifetime; i.e. a total duration of 130 years.

In zone one of the pier, linear degradation and sudden increase of elastic modulus, *E*, of materials was used to simulate exfoliation and repair, respectively. The ability to control the degradation rate of *E*, exfoliation of selected erosion layers, and the specified damage criteria, offer the flexibility of adapting this tool to different site and situations based on available historic and climatic records.

The effect of removal of each layer on the stress and strain distribution across the model was examined. Analysis of exfoliation defect indicates significant increase in both stress and strain levels in zone one. This leads to gradual increase in the MAXPE value of the model, increase in damage zone, further crack propagation, and hence subsequent change in stress-strain distribution of the block. As expected, application of repair also seemed to disturb the stress-strain distribution, and increase the MAXPE value of the zone one, causing further damage and crack propagation.

It was deduced from the results that reduction in size of the structure and appearance of cracks in the pier lead to reduction in resistance of the damaged/cracked areas to stress, which in turn lead to redistribution of stress, and over-stressing the undamaged areas. The structure then becomes more susceptible to further damage and fracture, and over a long-period of time leading to eventual collapse of the structure. Such phenomenon usually begins in a small zone and spreads over time, under influence of other defects.

Therefore, it is of significant importance to be able to model combination of various defects, and to concisely simulate patterns of the eroded area, in order to estimate and identify the time and sources of potential crack formation.

Zone two of the pier was also modelled, taking into account both creep and creep-induced crack features. The effect of exfoliation of the layers at top of the pier was also considered, in terms of the applied pressure to zone two. Micro-cracks are formed over time with respect to the *Y-Z* plane, near the constrained edges of faces 1 and 3 at the top surface of the block. Vertical creep-induced cracks have also extended in the *Y*-direction, with respect to *X-Y* and *Z-Y* planes. As expected, the vertical cracks are seen

on the outer faces of the middle 2m of the block. Vertical cracks are also seen on the side faces of this section, damage formation in the form of spalling of the outer layers, examples of which were also seen on the pier. Both mentioned damages are typical of the behaviour masonry under compression.

Although the proposed tool considers the effects of weathering combined with creep and damage, as expected, the exact number of cracks is not obtained in the simulation. This is since transient stresses induced by train movement over the period of 80 years (and so, higher load than the one used in the model), as well as temperature and moisture movements have not been considered in the proposed tool, and, therefore, the process of creep, deboning of units and extension of cracks are more accelerated in real-life structures than in simulations by the tool. From a computational perspective, the simulation results could have also been affected by:

- High number of elements in finite element meshing increases the strain levels in a model. Due to the aforementioned limitations in available computational resources and consequently extended simulation time, coarse mesh and hence lower number of elements have been used in the model. This offers less degree of freedom and so, low strain levels are inevitable.

- FEM simulations are known to over-estimate the stiffness and under-estimate the strain levels.

- Fixed boundary conditions at the bottom surface of the model allow for zero movement, ignoring the possible movements in the *X-* and *Z*-direction and thus inducing very low (or no) stress and strains in the model.

Therefore, given the correct considerations, it is expected that the micro-cracks are joined to form macro-cracks at the top edges, and further damage propagation and vertical cracks lines appear in the *Y*-direction (up to the bottom edge of the block). Crack patterns similar to the top edges are also expected to form at the bottom of the block.

This is a confirmation of the fact that the methodology employed and the proposed tool are capable of modelling zone two of the pier under specified criteria - a significant achievement, considering the number of unknowns involved in the process.

It is important to highlight that the main aim and emphasis of this research has been to develop and validate the proposed methodology and computational tool, based on similarities in direction and pattern of cracks, rather than producing an exact crack replica of defects on the real-life structure. In other words, the emphasis here is on

producing cracks in a realistic manner, based on the implied constraints, boundary conditions, load and geometry, etc.; that is, without knowledge and data on constituent materials, damage threshold, construction and weathering conditions. Needless to say that the pier can only be validated and realistically simulated, where the exact material properties, loads, and constraints applied on the sample of masonry used in the pier are quantified, by means of experimental measurements.

Therefore, success of the tool in analysis of the long-term defects, and its ability in simulating the effect of such defects on current state of a real structure, is a guarantee of a correct prediction of structure's safety and durability. In addition, ability of modelling and simulating the desired repair before its application to real structure, gives an insight into use of the most suitable repair to be applied to the structure. These are facilities that this tool provides for architecture, structural engineering or restoration industries. It can, thus, be concluded that the proposed tool can be used as a way of predicting the structure's behaviour subjected to the three defects of exfoliation, creep and creep-induced crack; under various loading scenarios and weathering conditions.

Chapter 6 : Conclusions and Future Work

The main aim of conducting this research was to develop a computational modelling strategy and to propose a novel tool to examine structural behaviour of masonry and in particular historic masonry, through analysis of structural damage, examination of the effects of reconstruction and repair on such structures; and also to offer safety, stability guidelines for their maintenance. The conclusions drawn, limitations highlighted and recommendations offered for future research are outlined in this chapter.

6.1 Conclusions

Objective 1 was achieved through a review of the published literature on masonry units and their mechanical properties (with a particular focus on historic masonry structures and their defects), maintenance and repair. The findings of this review are outlined below:

- The published literature and experimental studies seem to have a consensus on the complexity of assessing the structural capacity of masonry as a composite material. This complexity arises from variance of masonry mechanical behaviour including brittle response in tension, relatively high resistance to compression, frictional response in shear, and anisotropy.

- Historic masonry structures are affected by short-term and long-term natural and human intervention. Lack of maintenance due to neglect of structure or inappropriate repair are human imposed damages on historic masonry structures. The latter can be overcome by adequate knowledge of masonry constituting materials, guiding the conservation industry to take appropriate and effective (internal and/or external) repair measures.

- These structures are exposed to climate change effects, often translated to a combination of defects such as creep, deterioration, etc., which make prediction of life expectancy of such structures very difficult. Study of numerous structural damage reveals that the presence of one or more defects in a masonry structure contributes to its failure. This is mainly due to the growth and propagation of internal micro-cracks, which can occur in the mortar, at the unit-mortar interface, in the masonry unit, or a combination of these. Combined actions of

time-dependent defects such as creep and gradual exfoliation of masonry layers, in structures under sustained stress lead to stress redistribution and development of damaged zones; hence formation of cracks in historic masonry. Although attempts have been made to model individual defects, to the author's knowledge, no computational tool has been provided to model and structurally simulate a combination of these defects (exfoliation, creep, and creep-induced crack).

- It was found that although significant effort has gone into characterisation and mathematical description of masonry in terms of its mechanical behaviour and response, inherent variations in constituent materials and elements, construction process (sequence and geometry) and workmanship of historic masonry, and combination of time-dependent and weathering defects in structures (visible and hidden damages) add to their complexity and makes prediction of their life expectancy very challenging. Consequently, it would be difficult to identify and simulate such damages to offer an accurate prediction of the long-term deformation of historic masonry. In spite of all these difficulties, the present research work has developed an efficient computational tool that provides reliable simulation and lifetime predication of historic masonry structures; herein lies the main novelty of this work.

To achieve **objective 2**, a review of the literature on the computational modelling of masonry, in particular historic masonry was carried out. The different computational modelling strategies were reviewed and critically evaluated as follows, with a view to identifying an appropriate modelling strategy for historic masonry.

- Review of the masonry *modelling approaches* revealed the availability of many *computational techniques* whose choice of selection mainly depends on the accessible information and the desired level of accuracy and simplicity. Since the computational tool proposed in this research mainly aimed to provide simple and reasonably accurate analysis, a macro-scale strategy is adopted. Similarly, homogeneity is assumed in majority of the models, to simplify the properties of the constituting materials. Heterogeneous material is also adopted where repair is applied, to represent presence of more than one material in a structure. Similarly, critical evaluation of the available computational techniques confirms that FEM technique and Abaqus software package are preferred for predicting the pre- and post-failure behaviour of masonry structures. The proposed

approach allows for simulation and analysis of the overall effect of various damages on stress state of structure using both continuum and discontinuum modelling.

- Review of the constitutive laws for modelling each of the three mentioned defects, their characteristics and abilities, as well as records of previous modelling in historic masonry show that the selected constitutive law should account for material's degradation and loss of section over time; with less emphasis on post-cracking behaviour. Predicting the onset of the global failure of the structure should also be considered as one of the main requirements of the adopted constitutive law.

- Having compared previous creep and crack models (and keeping simplicity in mind), an empirical formulae in the form of simple elastic-plastic constitutive law was chosen to be adequate for simulating behaviour of historic masonry. Therefore, a discontinuum damage mechanics, i.e. time-hardening creep power-law together with bi-linear damage law (using XFEM feature in Abaqus), was adopted as the constitutive law in this computational tool. Simplicity is achieved by assuming a linear initial response before damage initiation, and a linear softening response, to illustrate the damage evolution in the material. Depending on the masonry material, maximum principal strain (MAXPE) and fracture energy values are selected as the main criteria for damage initiation threshold, and indication of damage evolution of the material.

Towards satisfying **objectives 3 and 4**, results from the literature reviews were used to develop a computational modelling tool, to capture the behaviour of masonry including the time-dependent damage (resulting from the effects of weathering and creep). In doing so, the following features of the tool were developed and validated:

- The presence of more than one material property in the model; also used for illustration of repair of a damaged zone in the masonry,

- A reduction in the stiffness of the masonry with time, to present a softening zone and the controlled degradation of masonry to a low stiffness material. This feature helps simulate the mechanical effects of the gradual loss of masonry, due to different types of deterioration with time,

- Exfoliation (surface peeling) of the external (exposed) faces of the masonry specimen; indicating the gradual loss of thickness and reduction in size of

historic masonry, due to wind erosion, chemical reactions, etc., over a long-term period of time,

- Long-term creep behaviour: A simple block of masonry is then used to validate repairs, creep and creep-induced cracking using the results from laboratory-based creep tests carried out on 5 different types of masonry (referred to as types A-E). The ability and reliability of the computational tool was verified through comparison between the mentioned test results and simulation for the following cases: low strength clay brick and air-hardening lime mortar, random rubble masonry, historic brick masonry and hydraulic lime mortar, historic brick masonry and hybrid lime-cement mortar, and clay brick masonry and cement based mortar. The Least Squared Fitting (LSF) method and sensitivity analysis were used to identify specific ranges of creep parameters (A, m, and n) for each masonry type; with the logic that these parameter ranges could be applied to any other masonry structure with similar material properties. Abaqus simulations and experiment results for each masonry type were in good agreement, and the three creep phases (primary, secondary and tertiary) were evident, verifying that the tool predicts the creep trend well. As an illustration and to further verify the accuracy of the proposed creep parameter sets, these parameters were used to simulate and predict the creep behaviour of another masonry specimen (referred to as type F), with material properties similar to masonry type B. Comparison of the creep simulation and experimental results showed good fit between the response curves. Therefore, the creep behaviour of any historic masonry, with material properties similar to either of the above five masonry types, over a long period can be predicted, only with given primary material properties (E, v and density) and without the need for carrying out long-term experimental creep tests; a major achievement.

- Creep-induced cracking: the long-term effect of creep induces crack initiation and gradual crack propagation; redistributing stress in the structure. This can lead to offload of the cracked section, and exertion of excess load to un-cracked sections, which in turn leads to a change in creep rate of materials in cracked and un-cracked zones. Subsequently, this leads to further disturbance in stress distribution, over-stressing some sections and further crack propagation until a significant macro-crack is formed. Therefore, this tool simulates and predicts such trends, in order to estimate the lifetime of a structure, and where possible,

foresee and prevent its failure by means of adequate repair. Indeed, this is a very useful functionality of the proposed tool, which has been examined for combination of creep and creep-induced crack on the simulated model for masonry type F. Needless to say that due to changing environmental conditions (moisture, temperature, etc.) and thus unaccounted defects such as weathering, simulating the real-world sites are more complex than simulations carried out on small specimen from creep tests in the literature.

o Parametric studies are then carried out for the creep simulations as part of the model development process, to analyse the effect of creep parameters and material properties on creep simulations. The concept of 'tunning' was also suggested, where parameters could be changed (or tuned) independently based on parametric studies to achieve the optimal creep response.

- **Objective 4**, that is validation of the tool, was completed by using the model to simulate the loading history and predict the structural response of one of the piers of an existing 130 years old multi-span clay brick railway viaduct, i.e. pier 4 of the Larpool Viaduct in Whitby, Northern England. The viaduct had been constructed from clay brick masonry (with cement-based mortar), with 13 piers. The reason for this selection was the fact that all the three mentioned defects are present and visible in the pier (from site-inspection), and that more repair data was available (compared to other masonry structures) from the maintenance carried out by the supervisor of this work. The procedure involved, limitations, and the findings of the validation (objective 4) are outlined below:

    o To meet the computational limitations, to reduce the simulation time, and to illustrate the main approach of this thesis, only parts of the pier were modelled, where the mentioned defects were visible (i.e. top 3m and bottom 2.5m sections - referred to as zones one and two).

    o Linear degradation and exfoliation, and sudden increase of elastic modulus, *E*, of materials was used to represent exfoliation of three layers and repair in zone one of the pier, respectively. Deterioration of pier 4 of the viaduct over 130 years was shown using the exfoliation of its outer layers. Creep and crack features of the tool were also used simultaneously to illustrate the creep damage and onset of creep-induced crack when the damage criteria is met.

o   Analysis of simulation results for *exfoliation* defect in zone one model indicates that exfoliation of the eroded masonry significantly increases both stress and strain levels. This leads to gradual increase in the MAXPE value of the model, increase in damage zone, further crack propagation, and hence subsequent change in stress-strain distribution of the block. It was also deduced from the results that reduction in size of the structure and appearance of cracks in the pier, leads to reduction in resistance of the damaged zones, which in turn results into redistribution of stress, and thus, over-stressing the undamaged areas. The structure then becomes more susceptible to further damage and fracture, over a long-period of time. Such phenomenon usually begins in a small zone and spreads over time, under the influence of other defects. Therefore, it is of significant importance to be able to model combinations of various defects, and to concisely simulate patterns of the eroded area, in order to estimate the time and identify the sources of potential crack formation.

o   Simulating the *repaired* part of the pier allowed for assessment of the effect of repair on pier's structural performance. As expected, application of repair in the zone one model seemed to disturb the stress-strain distribution and increase the MAXPE value, causing further damage and crack propagation. This helped visualising that even after repair, the creep effect can continue to occur in the original material and may even initiate in the new material, confirming that repair in materials can be destructive if not properly accounted for in simulations; and thus highlighting the importance of simulating the proposed repair before applying it to structure. Moreover, the proposed computational tool can be utilised to model structures that have already undergone repair, in order to identify the signs, effects, causes and consequences of deterioration and repair; and subsequently help with development of an efficient retrofitting maintenance strategy that can prevent further damage and collapse of historic masonry structures.

o   Zone two of the pier was also modelled, taking into account both *creep* and *creep-induced crack* features. The width, height and length of the model are aligned to *X*, *Y* and *Z* directions, respectively. Since the width of the pier (in *X*-direction) is approximately one-third of its length (*Z*-

direction), the continuity of the pier can be taken into account by assuming the block under plane stress, whereby all the top edges are constrained (i.e. no movement allowed) in the *X*-direction. Damage initiates as soon as the specified damage threshold is reached. Cracks are formed over time with respect to the *Y-Z* plane, near the constrained edges at the top surface of the block. A vertical creep-induced crack has also extended in the *Y*-direction, propagating on faces 1 and 3; with respect to the *X-Y* plane. The high strains in the *Z*-direction also induce symmetrical damage zones and crack formations in the *Z-Y* plane. Accumulation of creep-induced cracks and presence of damage and cracked zones on faces 1 and 3 of the block, leads to formation of damage zones and crack lines on face 5 over time.

o   In spite of the inherent variability of masonry and the outlined uncertainties of the model, the model identifies the formation of vertical creep-induced cracks close to the lower portion of the pier (i.e. the section just above foundation level). Good correlation is evident between simulation results and observed cracks on the Larpool Viaduct pier. More specifically, the direction and pattern of vertical cracks in the outer faces of the zone two model were very similar to those observed on bottom 2.5m of the pier. This further reinforces the initial validation of the model carried out using a small representative block of masonry. This is a confirmation of the fact that the employed methodology and the proposed tool are capable of modelling zone two of the pier under the specified criteria - a significant achievement, considering the number of unknowns involved in the process.

o   However, as expected, a slight discrepancy in the number of cracks between simulation and the real pier is observed. This is thought to emanate from the assumptions made in the load calculations, and the lack of accurate data on the live load imposed on the pier (i.e. train load over the 80 years of its use, passenger and weathering loads); and so, the actual load is believed to be higher than the one used in the model. From a computational perspective, the simulation results could have also been affected by: (a) use of coarse mesh, and so, low number of finite element meshing, which offers less degree of freedom and low strain levels, (b)

> nature of FEM simulations that over-estimate the stiffness and under-estimate the strain levels, and (c) fixed boundary conditions at the bottom surface of the model that allow for no movements in the *X* and *Z*-directions, and thus less stress and strains levels.

> o It is important to highlight that the main aim and emphasis of this research has been to develop the proposed methodology and validate the computational tool, based on the similarities in direction and pattern of cracks, rather than producing an exact crack replica of defects on the real-life structure. In other words, the emphasis here was on producing cracks in a realistic manner based on the implied constraints, boundary conditions, load and geometry, etc.; that is, without the knowledge of, and access to data on constituent materials, damage threshold, construction and weathering conditions. Needless to say that the pier can only be validated and realistically simulated, where the exact material properties, loads, and constraints applied to the sample of masonry used in the pier are quantified, by means of experimental measurements.

The above analysis clearly confirms that the objectives set out in the thesis have been completed and the goals achieved. It is hoped that the computational tool would enable the practicing engineers to use their fundamental understanding of the original design and mechanical behaviour of masonry elements, alongside the analysis of the results obtained from simulation, and their observation of historic masonry structures. The proposed computational tool was developed to be simple to use, allowing the user to adjust the deterioration rate of elastic modulus in the materials according to various rates of change in the environment, and to input the creep parameters and tensile strength of masonry for creep and crack damage to take place.

Success of the tool in analysis of the long-term defects and its ability in reproducing the effect of combination of such defects on current state of a real structure is a guarantee of correct prediction of structure's safety and durability. In addition, the ability of modelling and simulating the desired repair before its application to real structure gives an insight into the use of the most suitable repair to be applied to the structure. The proposed tool can, thus, be used to predict a structure's behaviour subjected to the three defects of exfoliation (peeling of external surface caused by freeze-thaw action, salt crystallisation damage and exfoliation), creep and creep-induced crack; under various

loading scenarios and weathering conditions. These are facilities that this tool can offer to construction, conservation and restoration industries. It may, therefore, be concluded that this study can be considered as a corner stone for characterisation of mechanical behaviour and damage response of slender historic masonry structures.

As the final remarks, this study has clearly identified significant differences between the theoretical and real-world constraints in developing the computational tool. These limitations are outlined below and suggestions on the possible future work are also offered:

- Abaqus is very powerful modelling software that has found applications in many areas of engineering, but it is not very user-friendly and has a very complicated user manual. Moreover, a comprehensive understanding of the software's underlying principles is assumed, which makes it not so suitable for end-user researchers.

- To develop a comprehensive and detailed constitutive law for masonry, user-defined subroutines seem to be a better choice. This, however, requires good knowledge and experience of programming languages such as FORTRAN and Python.

- Computational modelling is very processor-intensive, time consuming and expensive (for licenses, etc.), particularly when mesh sensitivity or parametric studies are required.

6.2 Recommendations for future work

The results of previous studies and the potential benefit of the research described in this thesis have confirmed the promising future for computational tools in the modelling and structural analysis of historic masonry structures. To extend and improve the computational tool developed by the author, the following future work is suggested:

Suggested improvements to the modelling of individual and combinations of defects:

- Due to the limitations in the available computational resources, structures as big as pier 4 of Larpool Viaduct cannot be modelled as a single structural entity. Instead, other approaches such as the use of multi-scaling modelling should be considered, where the entire structure can be modelled as a whole, allowing for

analysis of the overall stress-strain distribution and creep strain throughout. Smaller sized modelling could then be carried out on a localised section of the structure, where mesh-dependent defects such as cracking are expected. Finer mesh sizes can be used on the smaller model, representing a good illustration and prediction of the likely crack pattern across the zone. Further details on this approach have been described by Bull (2001).

Other suggestions for improvement include:

- Other computational approaches such as mesoscale modelling (which uses partitioned modelling) could be adapted from the computational strategy presented by Macorini (2013), where the possibility of combining the proposed bi-linear constitutive law with meso-scale modelling is investigated. To improve the reliability of the proposed tool, research can also be carried out to extend the applicability of the tool to other masonry materials including those made from soft masonry units such as adobe or tuff.

- The temperature feature embedded in the proposed tool can be used to investigate the effects of weathering and cyclic temperature on historic masonry structures where such climatic data are available.

- A user-defined subroutine could be developed to include the rate of reduction in the elastic modulus and the removal of surface elements from the exposed faces of the masonry with the pre-defined elastic modulus values. This can be used to represent exfoliation of the weathered masonry and a reduction in size over time. Parameters such as temperature can also be included in the subroutine to take into account the effects of climate change.

- A more complex constitutive law can be developed to better represent creep behaviour in masonry. For instance, a UMAT subroutine could be developed for the 3D rheological creep model, which could also take into account the 'swelling' effects of frost heave to represent a more complex and detailed behaviour of historic masonry subjected to long-term creep effects.

- Pre-existing cracks (and other existing physical defects) could be included in the modelling strategy to provide a better representation of the behaviour of historic masonry.

- The research could also be extended to cover the resulting effect of seismic activity, fatigue, as well as other dynamic load effects on historic masonry structures.

- Further experimental work could be undertaken on a wide range of historic masonry types (rigid, as well as soft masonry units such as adobe and tuff), with the aim of offering a more reliable and realistic set of material and creep parameters; and thus, improving the reliability of the proposed tool. Such parameters provide good representation of the characteristics of historic masonry subjected to a combination of creep and weathering defects. This data can be used for an improved characterisation of the materials in the computational simulations and as a basis for designing more compatible repair materials.

- Accelerated weathering tests could be carried out on samples of historical masonry using a range of deterioration rates and formulations describing such behaviour. These can then be used as part of the formulations in the subroutine or as a python script, alongside fracture in structures.

- Detailed layout of bricks and mortar could be modelled.

Propositions for improvements in future computational tools

The computational tool developed in this research has offered a novel and useful approach for structural analysis of historic (unreinforced) masonry structures. However, from a practical point of view, and for this tool to have maximum beneficial impact to the construction and conservation industries, and world-heritage organisations, it is vitally important that an interface is created through which information and requirements are constantly exchanged between the users and modellers/developers. The interface can be a simple form outlining the objectives, priorities and main requirements of each project. For example, in a maintenance project, where the tool has been used to simulate the effects of alternative forms of repair on the damage to historic masonry, the estimated lifetime and safety levels of the structure and the analysis of the results should be stated by the modeller. Moreover, since a wide range of masonry materials is used across the world, the approach proposed in this thesis can be extended to include a wider range of creep parameter sets, which can be obtained through creep tests on small samples of masonry.

References

Abdou, L., Ami Saada, R., Meftah, F., and Mebarki, A. 2006. Experimental investigations of the joint-mortar behaviour. *Mechanics Research Communications.* **33**(3), pp.370-384.

Abuku, M., Janssen, H., Roels, S. 2009. Impact of wind-driven rain on historic brick wall buildings in a moderately cold and humid climate: Numerical analyses of mould growth risk, indoor climate and energy consumption. *Energy & Buildings.* **41**(1), pp.101-110.

Al-Chaar, G.L. and Mehrabi, A. 2008. *Constitutive models for nonlinear finite element analysis of masonry prisms and infill walls*. DTIC Document: Engineer Research and Development Centre-Construction Engineering Research Laboratory.

Amjad, M.A.B.A. 1990. *Elasticity and strength of masonary, units and mortar*. PhD Thesis, Department of Civil Engineering, University of Leeds.

Anand, S.C. and Gandhi, A. 1983. A finite element model to compute stresses in composite masonry walls due to temperature, moisture and creep. *In: Proceedings of the 3rd Canadian Masonry Symposium,* Edmonton, Alta. pp.34-1.

Andreaus, U. 1996. Failure criteria for masonry panels under in-plane loading. *Journal of Structural Engineering.* **122**(1), pp.37-46.

Anzani, A., Binda, L., Mirabella, R.M. 1993. Time dependent behaviour of masonry: Experimental results and numerical analysis, *Structural Repair and Maintenacne of Historical Buildings III,* STREMA, Bath, pp.415-422.

Anzani, A., Binda, L., Ramalho, M., 2005a. Historic multi-leaf masonry walls: Experimental and numerical research. *Masonry International.* **18**(3), pp.101-114.

Anzani, A., Binda, L., Taliercio, A. 2005b. Application of a damage model to the study of the long term behaviour of ancient towers. *In: 1st Canadian Conference on Effective Design of Structures,* McMaster University Hamilton, Canada.

Anzani, A., Binda, L., Roberti, G.M. 1995. A numerical interpretation of long-term behaviour of masonry materials under persistent loads. *Structural studies of*

historical buildings IV. Volume 1: architectural studies, materials and analysis. Computational Mechanics Publications, pp.179-186.

Anzani, A., Binda, L., Roberti, G M. 2000. The effect of heavy persistent actions into the behaviour of ancient masonry. *Materials and Structures.* **33**(4), pp.251-261.

Anzani, A., Roberti, G.M. 2003. Experimental research on the creep behaviour of historic masonry. *Struct. studies repairs and maintenance of heritage architecture VIII,* WIT Press: Southampton and Boston, pp.121-130.

Anzani, A., Garavaglia, E., Binda, L. 2009. Long-term damage of historic masonry: A probabilistic model. *Construction and Building Materials.* **23**(2), pp.713-724.

Ashby, M.F. and Jones, D.R.H. 2005. *Engineering materials 1: An introduction to properties, applications and design.* Oxford: Butterworth-Heinemann.

Ashurst, J. 2007. *Conservation of ruins.* Oxford: Butterworth-Heinemann.

Brick Industry Association. 2006. Efflorescence- causes and prevention, *Technical Notes on Brick Construction, 23A*.

Avallone, E.A., Baumeister, T., Sadegh, A.M. 1996. *Marks' standard handbook for mechanical engineers.* McGraw-Hill New York etc.

Bangert, F., Grasberger, S., Kuhl, D., and Meschke, G. 2003. Environmentally induced deterioration of concrete: physical motivation and numerical modeling. *Engineering Fracture Mechanics.***70**(7), pp.891-910.

Bekker, P. 1999. Durability testing of masonry: Statistical models and methods. *Masonry International.***13**(4), pp.32-38.

Berto, L., Saetta, A., Scotta, R., and Vitaliani, R. 2002. An orthotropic damage model for masonry structures. *International Journal for Numerical Methods in Engineering.* **55**(2), pp.127-157.

Binda, L., Anzani, A., Gioda, G. 1991. An analysis of the time dependent behaviour of masonry walls. *In: Proceedings of the 9th International Brick/Block masonry conference.* Berlin, pp.1058-1067.

Binda, L., Gatti, G., Mangano, G., Poggi, C., and Landriani, G.S. 1992. Collapse of the civic tower of pavia: A survey of the materials and structure. *Masonry International.* **6**(1), pp.11-20.

Binda, L. and Anzani, A. 1993. The time-dependent behaviour of masonry prisms: An interpretation. *The Masonry Society Journal.* **11**(2), pp.17-34.

Binda, L., Anzani, A., Mirabella, R. 1997. The failure of ancient towers: Problems of their safety assessment. *In: International IABSE Conference on Composite Constructio- Conventional and Innovative,* Zurich, pp.699-704.

Binda, L. 1998a. Method for triaxial compression tests on mortar specimens taken from bed joints, *In: Materials and Structures.* **31**(210), pp.363-377.

Binda, L., Lenzi, G., Saisi, A. 1998b. NDE of masonry structures: use of radar tests for the characterisation of stone masonries. *NDT & E International.* **31**(6), pp.411-419.

Binda, L., Garavaglia, E., Molina, C. 1999. Physical and mathematical modelling of masonry deterioration due to salt crystallization. *In: Eighth International Conference on Durability of Building Materials and Components, 8 dbmc.* pp.527-537.

Binda, L., Anzani, A., Roberti, G.M. 2000. Tall and massive ancient masonry buildings: Long term effects of loading. *In*: *Proceedings of the G. Penelis International Symposium on Concrete and Masonry Structures,* Thessaloniki, pp.273-284.

Binda, L., Saisi, A. Messina, S., and Tringali, S. 2001. Mechanical damage due to long term behaviour of multiple leaf pillars in Sicilian Churches. *In: Proccedings of 3rd International Historical Constructions*. pp.707-718.

Binda, L. 2008. *Learning from failure: Long-term behaviour of heavy masonry structures.* Advances in Architecture, Vol 23 WIT Press, Southampton.

Binda, L., Schueremans, L., Verstrynge, E., Ignoul, S., Oliveira, D.V., Lourenço, P.B., Modena, C. 2008. Long term compressive testing of masonry-test procedure and practical experience. *In: 6th International seminar on structural analysis of historical constructions,* Bath. pp.1345-1355.

Binda, L. and Saisi, A. 2009. Knowledge of the building, on site investigation and connected problems. *In: Proc. Of the Workshop "Eurocode 8 prespectives from the Italian Standpoint".* Napoli. pp.213-224.

Binda, L., Cardani, G., Cantini, L., and Tiraboschi, C. 2010. Long term effects of floods on masonry walls: NDTs to measure the drying rate. *In: 8th International Masonry Conference* Dresden, pp.653-662.

Bingel, P.R. 1993. *Stress relaxation creep and strain under varying stress in masonry.* PhD thesis, Department of Civil Engineering, University of Leeds.

Bisagni, C. 2000. Numerical analysis and experimental correlation of composite shell buckling and post-buckling. *Composites Part B: Engineering.* **31**(8), pp.655-667.

Bodner, S.R. and Chan, K.S. 1986. Modeling of continuum damage for application in elastic-visco-plastic constitutive equations. *Engineering Fracture Mechanics,* **25**(5), pp.705-712.

Boothby, T.E., Atamturk, H.S., and Erdogmus, E. 2007. Manual for the assessment of load bearing unreinforced masonry structures. *NCPTT.*

Bowler, G.K. and Fisher, K. 1989. Soluble salt analysis and indexation of sulphation risk. *Masonry International-Journal of the British Masonry Scoiety.* **3**(2), pp.62-67.

Bremner, A. 2002. *The origins and effects of cryptoflorescence in fired-clay masonry.* PhD thesis, Department of Civil Enginering, University of Leeds.

Brencich, A., Corradi, C., Gambarotta, L., Mantegazza, G., and Sterpi, E. 2002. Compressive strength of solid clay brick masonry under eccentric loading. *In: Proceeding of the sixth International Masonry Confrence*, pp.37-46.

Brimblecombe, P., Gross, C.M., Harris, I. 2006. Climate change critical to cultural heritage. *In: Heritage, weathering and conservation*, Taylor & Francis Group, pp.387-393.

Brocken, H. and Pel, L. 1995. Moisture transport over the brick/mortar interface. In: National Research Council Canda (NRCC). *In: International Symposium on Moisture Problems in Building Walls*. pp.397-401.

Brocken, H. and Nijland, T.G. 2004. White efflorescence on brick masonry and concrete masonry blocks with special emphasis on sulfate efflorescence on concrete blocks. *Construction and Building Materials.* **18**(5), pp.315-323.

Brooks, J., Abdullah,C., Forth, J., and Bingel, P. 1997. Effect of age on the deformation of masonry. *Masonry International.* **11**(2), pp.51-55.

Brooks, J.J. and Amjad, M. 1988. Elasticity and strength of clay brickwork test units. *Brick and Block Masonry(8 th IBMAC) London, Elsevier Applied Science,* 1, pp.342-349.

Budiwati, I.A.M. 2009. Experimental Compressive Strength and Modulus of Elasticity of Masonry. *Jurnal Ilmiah Teknik Sipil.* **13**(1).

Bull, J.W. 2001. *Computational modelling of masonry, brickwork and blockwork structures.* Saxe-Coburg Publications, Stirling.

Butterworth, B. 1933. The florescence test and the chemical examination of florescences. *Trans. British Ceramic Society.,* Vol. **36**(6), pp.270-283.

Caddemi, S. 1992. The global cracking laws for a finite-element model of no-tension material. *International journal of non-linear mechanics.* **27**(1), pp.63-73.

Veterans Affaris Canada. 2005. *Masonry in Cenotaphs/ monument*, The cenotaph/monument restoration program, Conservation Guildelines. [Accessed 26/03/2014] Available from: http://www.veterans.gc.ca/public/pages/memorials/cenotaph/restor_guide.pdf.

Casolo, S., and Pena, F. 2007. Rigid element model for in-plane dynamics of masonry walls considering hysteretic behaviours and damage. *Earthquake engineering and structural dynamics.* **36**(8), pp.1029-1048.

Cecan, D. 2012 *Assessment of reinforcing methods for masonry arch bridges*. Masters Disertation, Department of Civil Engineering, University of Leeds.

Cervera, M., Pelà, L., Clemente, R., and Roca, P. 2010. A crack-tracking technique for localized damage in quasi-brittle materials. *Engineering Fracture Mechanics,* **77**(13), pp.2431-2450.

Chaimoon, K. and Attard, M.M. 2007. Modeling of unreinforced masonry walls under shear and compression. *Engineering structures.* **29**(9), pp.2056-2068.

Chapelle, D. and Bathe, K.J. 2003. The finite element analysis of shells: fundamentals*, Springer*.

Chen, W.F. and Han, D.J. 2007. *Plasticity for structural engineers.* J Ross Pubications.

Chen, S., Moon, F.L., Yi, T. 2008. A macroelement for the nonlinear analysis of in-plane unreinforced masonry piers. *Engineering Structures.* **30**(8), pp.2242-2252.

Childs, P.R. 2001. *Practical temperature measurement.* Oxford: Butterworth-Heinemann.

Chin, I. R. and Petry, L. 1993. Design and testing to reduce efflorescence potential in new brick masonry walls. *Masonry: design and construction, problems and repair,* ASTM STP 1190, pp. 3-20.

Choi, K., Lissel, S.L., Reda T.M. M. 2007. Rheological modelling of masonry creep. *Canadian Journal of Civil Engineering.* **34**(11), pp.1506-1517.

Clifton, J. R. 1986. Cleaning stone and masonry: a symposium sponsored by ASTM Committee E-6 on Performance of Building Constructions, Louisville, KY, 18 April 1983. ASTM International.

Collepardi, M., Collepardi, S., Troli, R. 1994. Salt weathering of masonry walls. The venice experience. *In: 3rd ACI/CANMET Conf. on Concrete Durability.* France, pp.497-501.

Consulting, F.E.A.F. 2009. *FE analysis evolution.* Available from: http://www.fea-consulting.com/pages/evolution.htm [Accessed 23.09.2014].

Council of Europe. 1985. Convention for the protection of the architectural heritage of Europe. European Treaty Series No. 121 (Granada 3.X.1985). Strasbourg : The Council of Europe.

Crisafulli, F. J. 1997. Seismic behaviour of reinforced concrete structures with masonry infills, PhD thesis, University of Canterbury.

Cullinane, J.J. 2012. *Maintaining and repairing old and historic buildings.* Wiley.

De Borst, R., Feenstra, P.H., Pamin, J., and Sluys, L.J. 1994. Some current issues in computational mechanics of concrete structures. *In: computers modelling of concrete structures.* pp.283–302.

De Vent, I.A.E., Rots, J.G., Hobbelman, G.J. 2009. Finite element analyses help develop a diagnostic aid for masonry. *Computational Modeling on Concrete, Masonry and Fiber-reinforced Composites*, Delft, Netherlands, pp53-56.

Dialer, C. 1990 *Fracture and deformation behaviour of stress, biaxial tests on scale model masonry,* MSc Dissertation, Technical University of Munich.

Drysdale, R.G., Heidebrecht, A.C., Hamid, A.A. 1979. Tensile strength of concrete masonry. *Journal of the Structural Division.* **105**(7), pp.1261-1276.

Eklund, J.A. 2013. *Biological growth on masonry: Identification & understanding.* Available from: http://conservation.historic-scotland.gov.uk/bio-growth-masonry-inform.pdf [Accessed 17.06.2013]

Fan, T.J.J., Kim, M.M., Reda Taha, M.M., and Shrive, N.G. 2009. A three dimensional finite element model simulating damage and creep interaction in masonry *In: Proceedings of 11th Canadian Masonry Symposium.* Toronto, Canada pp.551-558.

Fan, T., Kim, J.J., Reda Taha, M.M., Shrive, N.G. 2010. Simulating creep and damage interaction in masonry columns considering interface debonding. *In: Proceedings of the 8th International Masonry Conference.* Dresden, Germany pp.1791-1800.

Feilden, B.M. 2003. *Conservation of historic buildings.* 3rd Edition, Routledge. London.

Ferretti, D. 2006. Stability of ancient masonry towers: Stress redistribution due to drying, carbonation, and creep. *Cement and concrete research.* **36**(7), pp.1389-1398.

Flickr, 2013. *Maagdentoren, Zichem.* Available from: http://www.flickr.com/photos/shakespier/2859956064/ [Accessed 02/09/2013]

Forth, J.P. and Brooks, J.J. 2000. Cryptoflorescence and its role in the moisture expansion of clay brick masonry. *Masonry International.* **14**(2), pp.55-60.

Fouchal, F., Lebon, F., Titeux, I. 2009. Contribution to the modelling of interfaces in masonry construction. *Construction and Building Materials.* **23**(6), pp.2428-2441.

Fudge, C. 2009. Sustainable construction to mitigate and anticipate climate change, *European autoclaved aerated concrete association.*

Gambarotta, L. and Lagomarsino, S. 1997a. Damage models for the seismic response of brick masonry shear walls. Part I: the mortar joint model and its applications. *Earthquake engineering & structural dynamics.* **26**(4), pp.423-439.

Gambarotta, L. and Lagomarsino, S. 1997b. Damage models for the seismic response of brick masonry shear walls. Part II: the continuum model and its applications. *Earthquake engineering & structural dynamics.* **26**(4), pp.441-462.

Garavaglia, E., Lubelli, B., Binda, L. 2002. Two different stochastic approaches modelling the decay process of masonry surfaces over time. *Materials and structures,* **35**(4), pp.246-256.

Garavaglia, E., Anzani, A., Binda, L. 2006. Probabilistic model for the assessment of historic buildings under permanent loading. *Journal of Materials in Civil Engineering.* **18**(6), pp.858-867.

Garrity, S.W. 2008. Rehabilitation of the piers of a 125 year old clay brick railway viaduct. *In: Proceedings of the 14th International Brick/Block Masonry confrence,* The University of Newcastle, Callaghan NSW, 2308, Australia.

Gazzola, E.A., Drysdale, R.G., Essawy, A. S. 1985. Bending of concrete masonry walls at different angles to the bed joints. *In: Proceedings of 3rd North American Masonry conference Arlington,* Arlington, Texas, Paper 27.

Genna, F., M., Di Pasqua, M., Veroli, M., and Ronca, P. 1998. Numerical analysis of old masonry buildings: a comparison among constitutive models. *Engineering structures.* **20**(1), pp.37-53.

Gentile, C., Saisi, A., Binda, L. 2002. Dynamic investigation of a historic masonry Bell Tower. *In: Proceedings of the 6th International Masonry Confrence.* London, pp.192-199.

Gigla, B. and Schlesinger, F. 2008. Investigation into the sustainability of industrial fixing systems for the repair of historic masonry. *In: Proceedings of the 14th International Brick and Block Masonry Conference.* 13-20 February Sydney.

Giordano, A., Mele, E., De Luca, A. 2002. Modelling of historical masonry structures: comparison of different approaches through a case study. *Engineering structures.* **24**(8), pp.1057-1069.

Goodwin, J.F. and West. H. 1982. A review of the literature on brick/mortar bond. *In: proceeding of british ceramic society.* **30**(23), pp23-27

Grazzini, A. 2006. Experimental techniques for the evaluation of the durability of strengthening works on historical masonry. *In: Masonry International.* **19**(3), p113-126.

Groot, C., Asheall, G., Hughes, J. 2004. Characterisation of old mortars with respect to their repair: A state of the art. *In: State of the art report of RILEM Technical Committee 167-COM*, pp.1-10.

Hardesty, J.M. 1944. Disintegration of face brick by dissolved salts. *Bell Laboratories Record.* **22**(5), pp.222-224.

Harrison, H.W. and De Vekey, R.C. 1998. Walls Windows and Doors. *BRE Building Elements series.*

Hendry, A.W. 1978. A note on the shear strength of brickwork in combined racking shear and compression. *In: Proceedings of the British Ceramic Society.* pp.47-52.

Hendry, A.W. 1990. *Structural masonry.* Macmillan Education, London.

Hendry, A.W. 1998. *Structural masonry.* 2nd edition. Palgrave Macmillan. London.

Hendry, A.W. and Khalaf, F.M. 2001. *Masonry wall construction.* Taylor & Francis.

Hendry, A.W., Sinha, B.P., Davies, S.R. 1997. *Design of masonry structures.* Taylor & Francis.

Hendry, A.W., Sinha, B.P., Davies, S.R. 2004. *Design of masonry structures.* Taylor and Francis. London, UK.

Heritage Victoria 2005. *Cleaning masonry* [online]. Available from: http://www.dtpli.vic.gov.au/__data/assets/pdf_file/0007/219346/CleanMasonry.pdf [Accessed 5 September 2014] .

Hofmann, P. and Stockl, S. 1986. Tests on the shear-bond behaviour in the bed-joints of masonry. *MASONRY INT. Masonry International.* (9), p1.

Hong, S.H., Ridley, I. and Oreszczyn, T. 2003. A hygrothermal monitoring and modeling of a historic roof. *In: Proceedings of 8th International IBPSA Conference*, Netherlands. **1**, pp.515-522.

Huebner, K.H., Dewhirst, D.L., Smith, D.E. and Byrom, T. G. 2008. *The finite element method for engineers.* John Wiley & Sons.

Huebner, K.H., Dewhirst, D.L., Smith, D.E., and Byrom, T.G. 2009. *The finite element method for engineers.* A1bazaar.

Hughes, T. and Harvey, R. 1995. Creep measured in a brick masonry tower block. *Masonry International.* **9**(2), pp.50-56.

Hutton, D.V. 2003. *Fundamentals of finite element analysis.* McGraw-Hill Science/Engineering/Math.

ICOMOS. 1931. *The Athens Charter* First International Congress of Architects and Technicians of Historic Monuments, Athens.

Iigo, A.C. and Vicente-Tavera, S. 2002. Surface-inside (10 cm) thermal gradients in granitic rocks: Effect of environmental conditions. *Building and Environment,* **37**(1), pp.101-108.

Isfeld, A. and Shrive, N. 2013. Finite element modelling of contact in rubble stone masonry. *In: Digital Heritage International Congress.* The Eurographics Association, pp.637-640.

Isfeld, A. and Shrive, N. 2014. Finite element analysis of grout Injection on multi-wythe stone masonry walls. *In: 9th International Masonry Conference,* Guimaeaes.

James, J. A. 1973. Investigation of the effect of workmanship and curing conditions on the strenght of brickwork. *In: 3rd International Brick Masonry Confrence.* Essen, Germany, pp.192-201.

Jing, L. and Stephansson, O. 2007. *Fundamentals of discrete element methods for rock engineering: Theory and applications.* Elsevier Science Ltd.

Johnson, F. B. and Thompson, J.N. 1969. Development of diametral testing procedures to provide a measure of strength characteristics of masonry assemblages. *Designing, engineering and constructing with masonry products,* Ed. FH Johnson, Gulf Publishing Company, Houston, Texas, pp.51-57.

Jukes, P. and Riddington, J.R. 1997. Review of masonry joint shear strength test methods. *Masonry International.* **11**(2), pp.37-43.

Karimian, H., Fallah, M., and Karimian, S. 2013. Methods of protection, reconstruction and restoration of troglodytic rocky architecture of Kafer Keli- Central Alborz, Iran. *In: 1st international troglodytic architecture conference,* Kerman, Iran.

Kim, J.J., Fan,T., Reda Taha, M.M., and Shrive, N.G. 2012. The effect of damage and creep interaction on behavior of masonry columns considering interface debonding and cracking. *Materials and Structures.* **45**, pp.15-29.

Kim, J. J., Fan,T., Reda Taha, M.M., Mahmoud, M. and Shrive, N. 2014. Warning signs of impending failure of historical masonry structures. *In: 9th International Masonry Conference,* Guimarães.

Kjaer, E. 2010. Bond strength: What is influencing the bond strength? In what way the bond strength influencing the masonry properties. *In: Proceedings of the 8th International Masonry Confrence.* Dresden, Germany.

Knutsson, H. and Nielsen, J. 1995. On the modulus of elasticity for masonry. *Masonry International,* **9**(2), pp.57-61.

Kralj, B., Middleton, J., Pande, G.N. 1991. Numerical model for the prediction df frost damage to brickwork. *Masonry International.* **4**(3), pp.89-93.

Kvande, T. and Lisø, K.R. 2009. Climate adapted design of masonry structures. *Building and Environment.* **44**(12), pp.2442-2450.

Lawrence, S.J. and Cao, H.T. 1987. An experimental study of the interface between brick and mortar. *In: Proceedings 4th North American masonry conference,* Dublin. pp.194-204.

Lawrence, S. J., Sugo, H.O., Page, A.W. 2005. Masonry bond strength and the effects of supplementary cementitious materials. *In: Australian Structural Engineering Conference 2005.* Engineers Australia, p.876

Leif, E.M. 1982. Moisture migration in buildings. *Editors: M. Leif, County college of Morris, H. R. Trechsel,* Trechsel Associates.

Lemos, J.V. 2004. Modeling stone masonry dynamics with 3DEC. *In:1st International UDEX/3DECSymposium: Numerical modelling of Discrete Materials in Geotechnical Engineering, civil Engineering and Earth Sciences,* Bochum, Germany, Taylor & Francis, pp.7-13.

Lenczner, D. 1965. Design of creep mechanism for brickwork. *In: Proceedings of the British Masonry Society.* pp.1-8.

Lenczner, D. 1969. Creep in model brickwork. *Proceedings of designing engineering and construction with masonry products,* Houston, Texas, US.

Lengweiler, P. 2000. *Modelling deposition and resuspension of particles on and from surfaces*. PhD thesis, Swiss Federal Institute of Technology Zürich.

Levén, M. and Daniel, R. 2012. Stationary 3D crack analysis with Abaqus XFEM for integrity assessment of subsea equipment, Master's thesis, Chalmers University of Technology.

Lipfert, F.W. 1989a. Air pollution and materials damage. *Air Pollution.* Springer, pp.113-186.

Lipfert, F.W. 1989b. Atmospheric damage to calcareous stones: comparison and reconciliation of recent experimental findings. *Atmospheric Environment (1967),* **23**(2), pp.415-429.

Liu, G.R. and Quek, S.S. 2003. *The finite element method: a practical course.* Butterworth-Heinemann.

Lotfi, H.R. and Shing, P.B. 1991. An appraisal of smeared crack models for masonry shear wall analysis. *Computers & Structures.* **41**(3), pp.413-425.

Lotfi, H. R. and Shing, P.B. 1994. Interface model applied to fracture of masonry structures. *Journal of Structural Engineering.* **120**(1), pp.63-80.

Lourenço, P.B. 1994. Analysis of masonry structures with interface elements. Delft University of Technologie, Delft.

Lourenço, P.B. 1995. Two approaches for the analysis of masonry structures: micro and macro-modelling *Heron Journal.* **40**(4), pp.313-340.

Lourenço, P.B. 1996. *Computational strategies for masonry structures*. PhD thesis, Delft University of Technologie, Delft.

Lourénço, P.B., De Borst, R., Rots, J. G. 1997. A plane stress softening plasticity model for orthotropic materials. *International Journal for Numerical Methods in Engineering.* **40**(21), pp.4033-4057.

Lourenço, P.B. and Rots, J.G. 1997. A multi-surface interface model for the analysis of masonry structures. *Journal of Engineering Mechanics.* **123**(7), pp.660-668.

Lourenço, P.B., Rots, J.G., Blaauwendraad, J. 1998. Continuum model for masonry: parameter estimation and validation. *Journal of Structural Engineering.* **124**(6), pp.642-652.

Lourenço, P.B. 2002. Computations on historic masonry structures. *Progress in Structural Engineering and Materials.* **4**(3), pp.301-319.

Lourenco, P., P. Roca, C. Modena and S. Agrawal, 2006. Experimental Investigation on the Structural Behaviour and Strengthening of Three-Leaf Stone Masonry Walls. *In: Proceedings of the 5th International Conference on Structural Analysis of Historical Constructions: possibilities of numerical and experimental techniques.* Macmillan, p.817-826.

Lourenço, P.B. and Pina-Henriques, J. 2006. Validation of analytical and continuum numerical methods for estimating the compressive strength of masonry. *Computers & structures.* **84**(29), pp.1977-1989.

Lourenco, P.B., Milani, G., Tralli, A., and Zucchini, A. 2007. Analysis of masonry structures: review of and recent trends in homogenization techniques. *Canadian Journal of Civil Engineering.* **34**(11), pp.1443-1457.

Lourenço, P.B., Pina-Henriques, J. 2008. *Collapse prediction and creep effects.* WIT Press: Southampton.

Macchi, G. 2001. Diagnosis of the facade of St. Peter's Basilica in Rome. *Proceedings of Historical Constructions: possibilities of numerical and experimental techniques, Guimaraes*, pp.309-318.

Maekawa, K. and Ishida, T. 2002. Modeling of structural performances under coupled environmental and weather actions. *Materials and Structures.* **35**(10), pp.591-602.

Maier, G. and Nappi, A. 1990. A theory of no-tension discretized structural systems. *Engineering structures.* **12**(4), pp.227-234.

Maier, G., Nappi, A., Papa, E. 1991. Damage models for masonry as a composite material: a numerical and experimental analysis. *Constitutive laws for engineering material: Theory and application*, pp.427-432.

Maier, G., Papa, E., Nappi, A. 1991. On damage and failure of brick masonry. *Experimental and numerical methods in earthquake engineering*, pp.223-245.

Mann, W. and Muller, H. 1982. Failure of shear-stressed masonry. An enlarged theory, tests and application to shear walls. *In: Proceedings of British Ceramic. Society.* **30**, pp.223-235.

Massart, T.J., Peerlings, R.H.J., Geers, M.G.D. 2007. An enhanced multi-scale approach for masonry wall computations with localization of damage. *International journal for numerical methods in engineering.* **69**(5), pp.1022-1059.

Mckenzie, W. 2001. *Design of structural masonry.* Palgrave.

Melbourne, C., Mckibbins, L.D., Sawar, N., and Sicillia Gaillard, C. 2006. Masonry arch bridges: condition appraisal and remedial treatment, CIRIA Report C656, London.

Middleton, J., Pande, G.N., Liang, J.X., and Kralj, B. 1991. Some recent advances in computer methods in structural masonry. *Computer methods in structural masonry, J. Middleton and GN Pande, eds., Books and Journals International, Swansea, UK*, pp.1-21.

Milani, G. 2007. A simple equilibrated homogenization model for the limit analysis of masonry structures. *WSEAS Transactions on Applied and Theoretical Mechanics.* **2**(5), pp.119-125.

Mirabella, R.G., Binda, L., Anzani, A. 1997. Experimental investigation into the effects of persistent and cyclic loads on the masonry of ancient towers. *In: Proceedings of Structural Faults & Repair*, pp.339-347.

Modena, C., Valluzzi, M.R. Tonogini Folli R., and Binda, L. 2002. Design choices and intervention techniques for repairing and strengthening of the Monza cathedral bell-tower. *Construction and Building materials.* **16**(7), pp.385-395.

Naguib, E.M.F. and Suter, G.T. 1991. Stresses in a running bond brick masonry 3-D finite element model under axial compression. *Masonry International.* **5**(2), pp.48-54.

Oan, A. and Shrive, N.G. 2011. Influence of axial stress on shear performance of concrete masonry walls. *In: 9th Australasian Masonry Conference.* Queenstown, NewZealand.

Ostergaard. 2010. *The influence of the grain size distribution on the mortar and masonry properties*. Denmark: Danish Technological Institute.

Page, A.W. 1978. Finite element model for masonry. *Journal of the Structural Division.* **104**(8), pp.1267-1285.

Pande, G.N., Liang, J.X., Middleton, J. 1989. Equivalent elastic moduli for brick masonry. *Computers and Geotechnics.* **8**(3), pp.243-265.

Papa, E.A. 1996. Unilateral damage model for masonry based on a homogenization procedure. *Mechanics of cohesive-frictional materials,* **1**, pp.349-66.

Papa, E., Taliercio, A., Mirabella, G. 2000. A damage model to predict the behaviour of masonry under sustained loading. *In: Proceedings of the 12th International Brick/Block Masonry Conference Proceedings*, pp.1777-1790.

Papa, E. and Taliercio, A. 2000. Prediction of the evolution of damage in ancient masonry towers. *In: Proceedings of the int. Symposium on 'bridging large spans from antiquity to the present'. Istanbul.* pp.135-144.

Papa, E. and Taliercio, A. 2005. A visco-damage model for brittle materials under monotonic and sustained stresses. *International journal for numerical and analytical methods in geomechanics.* **29**(3), pp.287-310.

Parnassus. 2013. *Protecting cultural heritage from flood and driven rain.* Available from: http://www.ucl.ac.uk/parnassus [Accessed 10/1/2013].

Pelà, L., Aprile, A., Benedetti, A. 2009. Seismic assessment of masonry arch bridges. *Engineering Structures.* **31**(8), pp.1777-1788.

Pela, L., Cervera, M., Roca, P. 2010. FEM analysis of orthotropic masonry walls via localized damage models. *In: 8th International Masonry Conference* Dresden: International Masonry Society, pp.217-226.

Pepper, D.W. and Heinrich, J. C. 1992. *The Finite Element method: Basic concepts and applications.* Taylor & Francis.

Pietruszczak, S. and Niu, X. 1992. A mathematical description of macroscopic behaviour of brick masonry. *International journal of solids and structures.* **29**(5), pp.531-546.

Pina-Henriques, J. and Lourenço, P.B. 2003. Testing and modelling of masonry creep and damage in uniaxial compression. *In: Proceedings of 8th STREMAH,* **8**(16), pp.151-160.

Pina-Henriques, J.L. 2005. *Masonry under compression: Failure analysis and long-term effects.* thesis, PhD Thesis. University of Minho.

Porto, F., Modena, C., Valluzzi, M.R., Binda, L., and Saisi, A. 2004. *Experimental tests on irregular masonry.* On-site investigaton techniques for the structural evaluation of historic masonry structures.

Rahman, A.H. and Suter, G.T. 1993. An analytical study of extreme temperatures in masonry building walls. *Masonry International.* **6**(3), pp.89-95.

Ramos, L.F. 2007. Damage identification on masonry structures based on vibration signatures.

Robinson, G.C. and Brown, R. H. 1988. Inadequacy of property specifications in ASTM C 270. *ASTM special technical publication,* pp.7-17.

Roca, P., Cervera, M., Pelą, L., Clemente, R., and Chiumenti, M. 2013. Continuum FE models for the analysis of Mallorca Cathedral. *Engineering Structures,* **46**. pp.653-670.

Roca, P. 2001. Studies on the structure of Gothic Cathedrals. *Historical constructions. University of Guimaraesr, Guimaraes*.

Roca, P., Cervera, M., Gariup, G. 2010. Structural analysis of masonry historical constructions. Classical and advanced approaches. *Archives of Computational Methods in Engineering.* **17**(3), pp.299-325.

Roca, P., Lourenço, P.B., González, J.L. and Oñate, E. 1998. Experimental and numerical issues in the modelling of the mechanical behaviour of masonry. *Structural analysis of historical constructions II,* Barcelona, pp. 57-91.

Rots, J.G. 1988. *Computational modeling of concrete fracture*. PhD thesis, Technische Hogeschool Delft.

Rots, J.G. 1997. *Structural masonry: An experimental/numerical basis for practical design rules (Cur Report 171).* Taylor & Francis.

Sabbioni, C., Cassar, M., Brimblecombe, P., Tidblad, J., Kozlowski, R., Drdácky, M. 2006. Global climate change impact on built heritage and cultural landscapes. *In*: *Heritage, weathering and conservation,* Taylor & Francis Group, pp.395-401.

Salami, A.W. and Adedeji, A.A. 2011. Environmental hazard: Flooding and its effects on residential buildings in Ilorin, Nigeria [online]. [Accessed 25/04/2012]

Sarhosis, V. 2011. *Computational modelling of low bond strength masonry*. PhD thesis, Department of Civil Engineering, University of Leeds.

Sarhosis, V., Sheng, Y., Garrity, S.W. 2010. Computational modelling of clay brickwork walls containing openings. *International Masonry Society Proceedings 11.* **3**, pp.1743-1752.

Sayed-Ahmed, E.Y., Shrive, N.G., Tilleman, D. 1998. Creep deformation of clay masonry structures: a parametric study. *Canadian Journal of Civil Engineering.* **25**(1), pp.67-80.

Sc Alf, M. and Waldum, M. 2009. *Historic materials and their diagnostic state of the art for masonry monuments in Norway*. Norwegian Building Research Institute.

Schlegel, R. and Rautenstrauch, K. 2004. Failure analysis of masonry shear walls. *In: Numerical modelling of discrete materials,* Edited by: Konietzky, London, Taylor & Francis, pp.15-18.

Schloeglmann, K. H. 2008. Long-term behavior of PUR-glued clay block masonry. *In: Proceedings of the 14th International Brick and Block Masonry Conference,* Sydney, *17–20 February 2008.*

Schubert, P. 1994. Tensile and flexural strenght of masonry- influences, test methods, test results. *Procedeeings of the 10th International Brick and Block Masonry Conference,* Calgary, Canada, pp. 895-08.

Shrive, N.G. and England, G.L. 1981. Elastic, creep and shrinkage behaviour of masonry. *Int. J. Masonry Constr.,* **1**(3), p103.

Shrive, N.G., Sayed, A., Ezzeldin, Y., Tilleman, D. 1997. Creep analysis of clay masonry assemblages. *Canadian Journal of Civil Engineering.* **24**(3), pp.367-379.

Simulia, D. 2013. *ABAQUS 6.13 Manual.* Available from: http://50.16.176.52/v6.13/.

Sinha, B.P. and Hendry, A.W. 1966. Further investigations of bond tension, bond shear and the effect of precompression on shear strength of model brick masonry couplets. *The British Ceramic Reasearch Association, note* 40.

Smith, B.S. and Carter, C. 1971. Hypothesis for shear failure of brickwork. *Journal of the Structural Division.* **97**(4), pp.1055-1062.

Smoohs. 2011. *Smart Monitoring of Historic Structures.* European Commission (EU).

Spalding, F.P. 2008. *Masonry structures.* BiblioBazaar, LLC.

Taha, M.M. and Shrive, N.G. 2006. A model of damage and creep interaction in a quasi-brittle composite material under axial loading. *Journal of Mechanics.* **22**(04), pp.339-347.

Theodossopoulos, D. 1995. *Structural analysis of Burgos cathedral and restoration proposals.* PhD thesis, University of Rome.

Throop, D. and Klingner, R.E. 2002. *Masonry: opportunities for the 21st century.* ASTM International.

Tilly, G. 2002. *Conservation of bridges.* London: Spon Press.

Tomor, A. and Verstrynge, E. 2013. A joint fatigue–creep deterioration model for masonry with acoustic emission based damage assessment. *Construction and Building Materials.* **43**, pp.575-588.

Twelmeier, H., Sperbeck, S.T., Budelmann, H. 2008. Restoration mortar for historical masonry- durability prediction by means of numerical and engineering models. *In: Proceedings of the 14th International Brick and Block Masonry Conference.* Sydney.

Tzamtzis, A.D. 1994. *Dynamic finite element analysis of complex discontinuous and jointed structural systems using interface elements*. PhD Thesis, Department of Civil Engineering, QMWC, University of London.

Usmani, A. 2010 *Numerical studies of the dynamic response of masonry structures subjected to blast and impact loads*. MSc Thesis, Department of Civil Engineering, University of Leeds.

Usmani, D. 2003. Case study of the failure of a Cross Vault: Church of Holyrood abbey. *Journal of Architectural Engineering.* **9**(3), pp. 109-117.

Valluzzi, M.R., Casarin, F., Garbin, E., Da Porto, F., and Modena, C. 2005. Long-term damage on masonry towers: case studies and intervention strategies. *In: Proc. of 11th international conference on fracture. Turin, Italy (on CD-ROM).*

Van Der Pluijm, R. 1999. *Out-of-plane bending of masonry: behaviour and strength*, PhD Thesis, Eindhoven University of Technology: Eindhoven.

Van Zijl, G.P.A.G. 2000. *Computational modelling of masonry creep and shrinkage*, PhD Thesis, Delft University of Technology, Netherlands.

Van Zijl, G.P.A.G., De Borst, R., Rots, J.G. 2001. The role of crack rate dependence in the long-term behaviour of cementitious materials. *International Journal of Solids and Structures.* **38**(30), pp.5063-5079.

Verstrynge, E., Ignoul, S., Schueremans, L., Van Gemert, D., Wevers, W. 2008. Long term behaviour of historical masonry-a quantitative acquisition of the damage evolution. *In: SAHC08- 6ᵗʰ International Conference on Structural Analysis of Historical Constructions*, Bath.

Verstrynge, E., Ignoul, S., Schueremans, L., and Van Gemert, D. 2008. Modelling of damage accumulation in masonry subjected to a long-term compressive load. *In: Proceedings of the 6ᵗʰ International Seminar on Structural Analysis of Historical Constructions*, Bath pp.525-532.

Verstrynge, E., Schueremans, L., Hendriks, M. 2009. Modeling of long-term deformations and damage accumulation in masonry. *In: Computational Modeling on Concrete, Masonry and Fiber-reinforced Composites*, Delft, Netherlands, pp.57-60.

Verstrynge, E. 2010a. *Long-term behaviour of monumetal masonry constructions: modelling and probabilistic evaluation*. PhD thesis, Leuven University, Belgium.
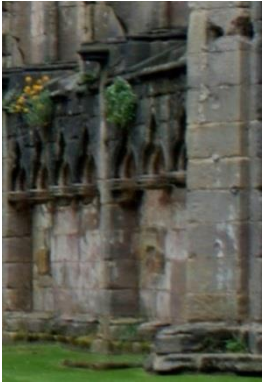
Verstrynge, E., Schueremans, L., Van Gemert, D., Hendriks, M.A.N. 2010b. A 3D damage model to describe creep deterioration in historical masonry. *In: Proceedings of the 8th International Masonry Conference,* Dresden, pp.267-276.

Verstrynge, E., Schueremans, L. Van Gemert, D., Hendriks, M. 2011. Modelling and analysis of time-dependent behaviour of historical masonry under high stress levels. *Engineering Structures.* **33**(1), pp.210-217.

Vlasov, V. P. 2009. Causes of deformations and crack formation in an administrative building in Magadan. *Soil Mechanics and Foundation Engineering.* **46**(4), pp.158-162.

Weaver, M.E. and Matero, F.G. 1997. *Conserving buildings: guide to techniques and materials.* Wiley.

Web, O.H. 2000. *General masonry inspection.* Available from: http://www.oldhouseweb.com/how-to-advice/general-masonry inspection.shtml [Accessed 05/08/13]

J. G. Webster, J. G. 2000, *Mechanical Variables Measurement. Solid, Fluid and Thermal,* 1st edition, CRC Press, Boca Raton, pp. 9-1.

Weeks, K.D. and Grimmer, A.E. 1995. *The secretary of the interior's standards for the treatment of historic properties: with guidelines for preserving, rehabilitation, restoring & reconstructing historic buildings.* DIANE Publishing.

Weitzman, M.L. 1998. The Noah's ark problem. *Econometrica*, pp.1279-1298.

Wescott, R.J., Watters, K.C., Heller, M. 1999. Implementation of a unified constitutive model into the ABAQUS finite element package, *DSTO Aeronutical and Maritime Research Laboratory,* Melbourne, Australisa.

Zucchini, A. and Lourenço, P.B. 2002. A micro-mechanical model for the homogenisation of masonry. *International Journal of Solids and Structures.* **39**(12), pp.3233-3255.

Zucchini, A. and Lourenço, P.B. 2004. A coupled homogenisation–damage model for masonry cracking. *Computers & structures.* **82**(11), pp.917-929.

Zucchini, A. and Lourenço, P.B. 2007. Mechanics of masonry in compression: Results from a homogenisation approach. *Computers & structures.* **85**(3), pp.193-204.

Appendices

Appendix A : Different types of biological growth appearing on historic structures

Biological growth	Colour	Appearance	Habitat	Effect on masonry	Examples
Algae	Usually green, occasionally black, red, orange or yellow	Mats, films, patches or streaks lacking defined borders	• Seen on wood, stone, soil, glass, plastic, etc. • Favours areas which are often moist. Requires relatively high light levels.	Unless growth is heavy, algae are normally benign, but may be slippery on paving stones.	 Fountains Abbey, Ripon
Lichens	White, grey, orange, red, black, yellow, or green	Variable surface crusts or leaf-like structures growing away from the surface with well-defined borders. Slow growing to several cm in diameter.	Stone, wood and soil. Often found in conditions that are too hostile for other organisms. Most species have a low tolerance to air pollution and are most common in rural sites.	Normally benign, although rare instances of blistering and pitting are known.	 Liverpool Anglican Cathedral

Biological growth	Colour	Appearance	Habitat	Effect on masonry	Examples
Mosses	Green or reddish	Leafy with a primitive root, often growing as a small clump loosely attached to the surface.	Found on wood, stone and soil. Requires a very damp environment, sunlight and some soil.	Can cause pitting and retains moisture on affected surfaces.	Fountains Abbey, Ripon
Cyanobacteria (previously known as bluegreen algae)	Blue-green, grey or green	Similar to the above	As above, but in areas away from direct sunlight, or in enclosed spaces adjacent to artificial lights.	Unless growth is heavy, algae are normally benign, but may be slippery on paving stones.	Kirkstall Abbey, Leeds

Biological growth	Colour	Appearance	Habitat	Effect on masonry	Examples
Higher plants		Leafy and some have woody roots.	Often found on chimneys, guttering and joints in upper levels of buildings.	Woody root growth can penetrate walls and dislodge stonework leading to structural damage.	Fountains Abbey, Ripon
Fungi	Yellow, orange, rust red, brown or black.	May appear as a film or spots that resemble general soiling. Large specimens may exhibit long strands (hyphae) or large, fruiting bodies.	Most common on organic substrates, also colonises masonry. Requires moisture, but no sunlight. Often associated with algae.	Normally benign, although some species cause pitting of marble and limestone surfaces.	Fountains Abbey, Ripon

Appendix B

The LSF method used in MATLAB code, in Section 4.4.2.1, to obtain the creep parameters is provided below. Note that the coordinates used as ET1, ET2, etc. are obtained from long-term creep experimental tests for each type of masonry.

```matlab
clear
clc
clear q
clear ET
%specify the number of m and n
numberofms=10;
numberofns=6;



dm=(-0.9-0)/(numberofms-1);
dn=(8-3)/(numberofns-1);
%in the following line, the q values should be entered
q=[1.6,2,2.3,2.6,2.8,3];
ET1=[0.5931 0.001026
............    ............
............    ............
............    ............];
ET2=[56.35   0.001128
............    ............
............    ............
............    ............];
ET3=[118     0.001564
............    ............
............    ............
............    ............];
ET4=[240.2   0.002282
............    ............
............    ............
............    ............];
ET5=[310.7   0.002409
............    ............
............    ............
............    ............];
ET6=[380.8   0.002667
............    ............
............    ............
............    ............];

% ETs=struct('et1',ET1,'et2',ET2,'et3',ET3,'et4',ET4,'et5',ET5,'et6');

y1=ET1(:,2)-ET1(1,2);
y2=ET2(:,2)-ET2(1,2);
y3=ET3(:,2)-ET3(1,2);
y4=ET4(:,2)-ET4(1,2);
y5=ET5(:,2)-ET5(1,2);
y6=ET6(:,2)-ET6(1,2);
y=[y1;y2;y3;y4;y5;y6];

t=[ET1(:,1);ET2(:,1);ET3(:,1);ET4(:,1);ET5(:,1);ET6(:,1)];
ep=[ET1(:,2);ET2(:,2);ET3(:,2);ET4(:,2);ET5(:,2);ET6(:,2)];
```

```matlab
mm=0;
for m=0:dm:-0.9
    mm=mm+1;
        nn=0;
    for n=6:dn:8
        nn=nn+1;
        nnn(mm,nn)=n;
        mmm(mm,nn)=m;
        x1=(q(1).^n)./(m+1).*((ET1(:,1)).^(m+1))-((ET1(1,1)).^(m+1));
        x2=(q(2).^n)./(m+1).*((ET2(:,1)).^(m+1))-((ET2(1,1)).^(m+1));
        x3=(q(3).^n)./(m+1).*((ET3(:,1)).^(m+1))-((ET3(1,1)).^(m+1));
        x4=(q(4).^n)./(m+1).*((ET4(:,1)).^(m+1))-((ET4(1,1)).^(m+1));
        x5=(q(5).^n)./(m+1).*((ET5(:,1)).^(m+1))-((ET5(1,1)).^(m+1));
        x6=(q(6).^n)./(m+1).*((ET6(:,1)).^(m+1))-((ET6(1,1)).^(m+1));
        x=[x1;x2;x3;x4;x5;x6];
        A=regress(y,x);
        Amatrix(mm,nn)=A;
        yprim=A*x;
        se(mm,nn)=sum((yprim-y).^2);
        %se is the estimation error
        yprim1=A*x1;
        yprim2=A*x2;
        yprim3=A*x3;
        yprim4=A*x4;
        yprim5=A*x5;
        yprim6=A*x6;
        yprim=[yprim1;yprim2;yprim3;yprim4;yprim5;yprim6];

        %estep1 is the estimated value of epsilon in the q1 region
        estep1=ET1(1,2)+yprim1;
        estep2=ET2(1,2)+yprim2;
        estep3=ET3(1,2)+yprim3;
        estep4=ET4(1,2)+yprim4;
        estep5=ET5(1,2)+yprim5;
        estep6=ET6(1,2)+yprim6;
        estep=[estep1;estep2;estep3;estep4;estep5;estep6];
    end
end
[II,JJ]=find(se==min(min(se)));
finalm=mmm(II,JJ)
finaln=nnn(II,JJ)
finalA=Amatrix(II,JJ)
sum_of_e2=min(min(se))
plot(t,ep,'r*',t,estep)
xlabel('time, sec');
ylabel('epsilon')
grid
```
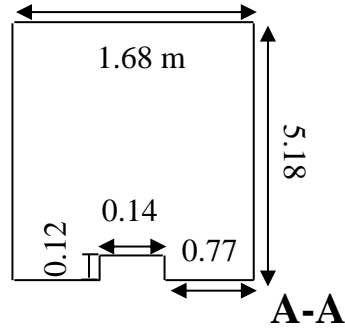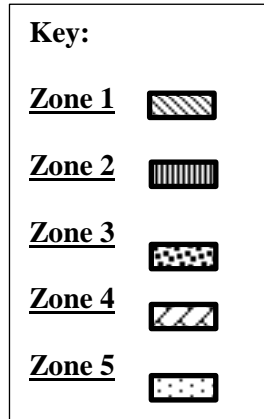
282

Appendix C: Drawings of pier 4 of Larpool viaduct
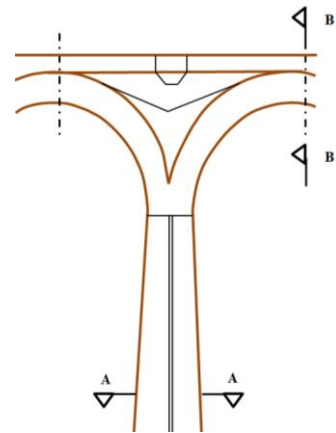
(a)Section along centre line of the pier

(b)Horizontal section through pier

A-A

1.68 m

5.18

0.14

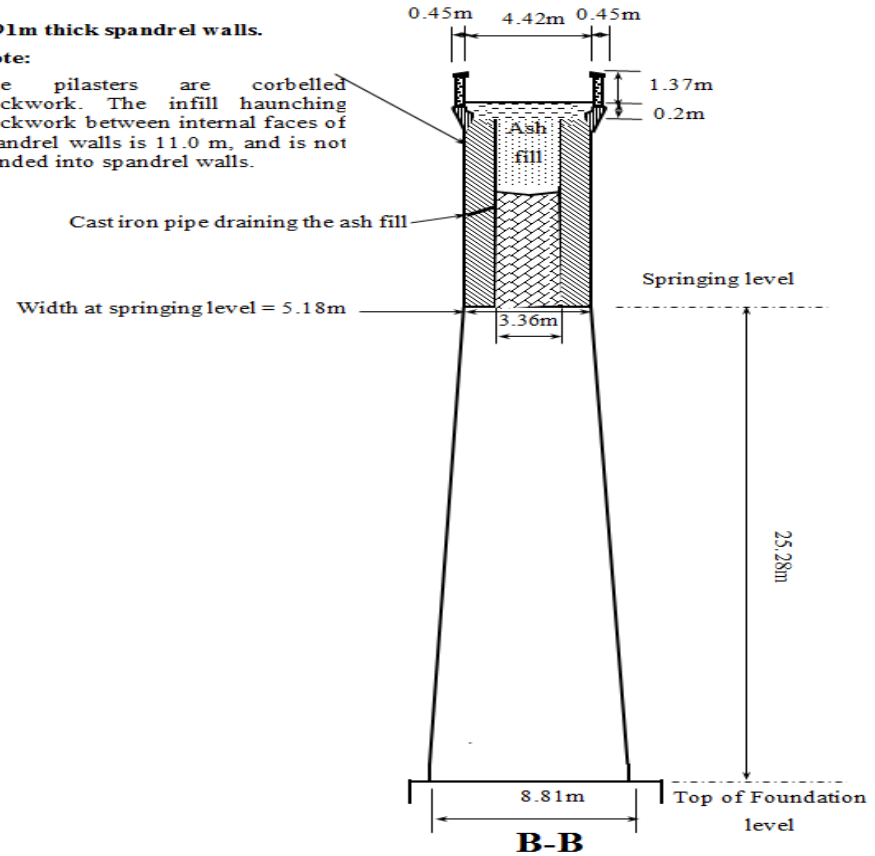0.12

0.77

Key:

Zone 1

Zone 2

Zone 3

Zone 4

Zone 5

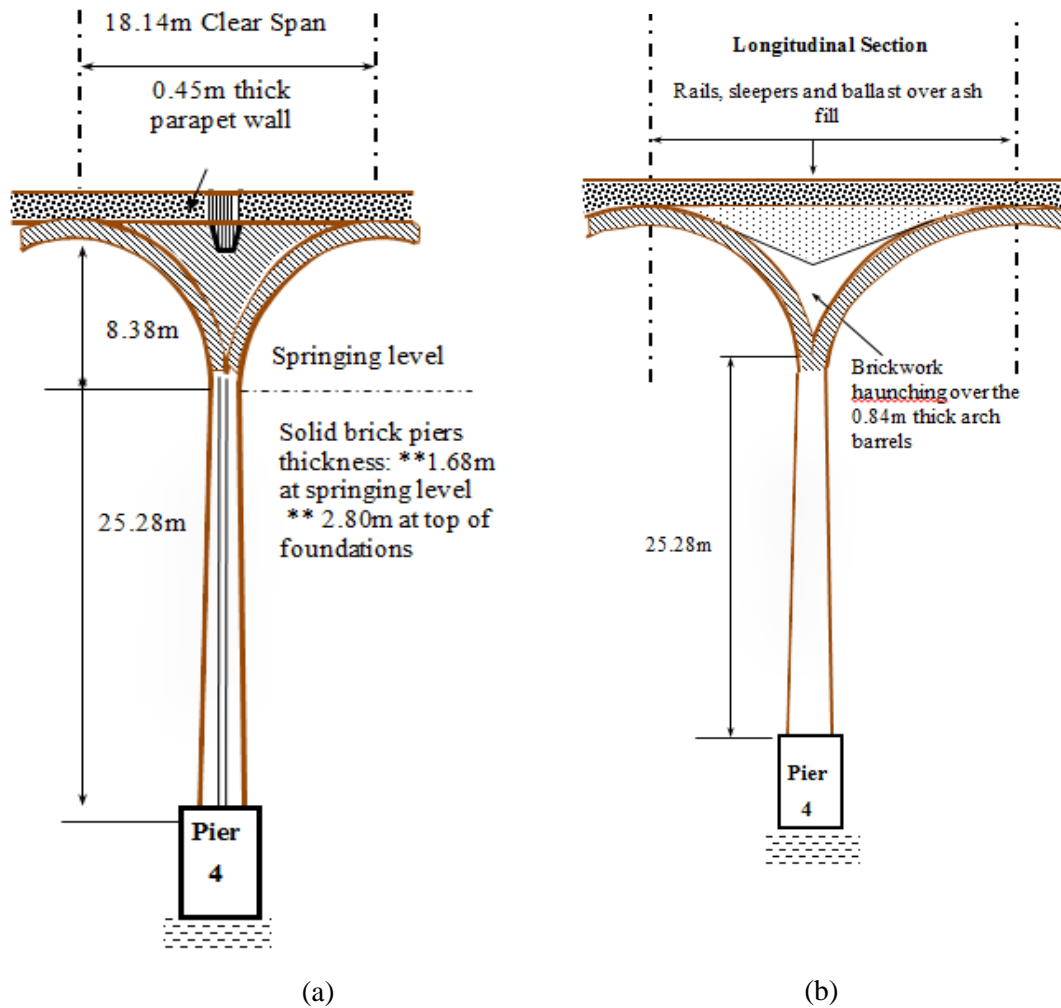(c)Legend for different material zones

0.91m thick spandrel walls.

Note:
The pilasters are corbelled brickwork. The infill haunching brickwork between internal faces of spandrel walls is 11.0 m, and is not bonded into spandrel walls.

Cast iron pipe draining the ash fill

Width at springing level = 5.18m

0.45m 4.42m 0.45m

1.37m

0.2m

Ash fill

Springing level

3.36m

25.28m

8.81m

Top of Foundation level

B-B

(d) Vertical section through the pier

Figure C.1: Sections of the pier 4

283

18.14m Clear Span

0.45m thick
parapet wall

8.38m

Springing level

Solid brick piers
thickness: **1.68m
at springing level
** 2.80m at top of
foundations

25.28m

Pier
4

(a)

Longitudinal Section

Rails, sleepers and ballast over ash
fill

Brickwork
haunching over the
0.84m thick arch
barrels

25.28m

Pier
4

(b)

Key:

Zone 1: **Brickwork in Spandrel wall**

Zone 2: **Brickwork in Pilasters**

Zone 3: **Brickwork in Parapet walls**

Zone 4 : **Brickwork below fill**

Zone 5 : **Fill (mixture of ash, crushed**

rock fill and brickwork waste)

Figure C.2: Illustrating the different construction materials in (a) Elevation, and (b) Longitudinal section of the pier.

284

Appendix D: Load calculations

This section provides a detailed load calculation of the initial weight of masonry above the pier. This is followed by load calculation for the pressure used in models of different section of the pier.
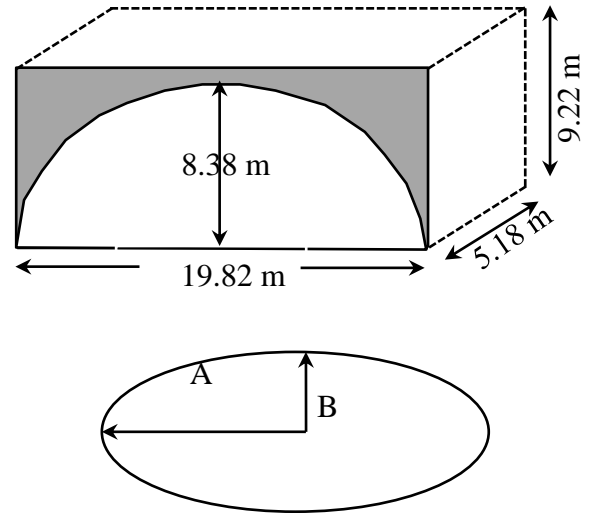
D.1: dead load calculation on pier

Area of rectangle = 9.22×19.82= 182.7m²

Area of ellipse = Π.A.B

= Π×9.7×8.38 = 238.78m²

Area of semi-ellipse = 238.78/2 = 119.4m²

Area of rectangle = 9.22×19.82 = 182.7m²

The outer layer of the pier is constructed of one layer of class B clay brick. Inside of the arch is filled with concrete and ashes. Therefore, the area of the arch; greyed area (brickwork). �

= 182.7 – 119.4 = 63.3m²

❖ *Weight of Zone 1 – (Spandrel Walls – Brickwork)*

Volume = Grey area × Thickness × 2 = 63.3 × 0.91 × 2 = 115.206 m^3

Weight = (115.206 × 2000) × 9.81 = 2260341 N

❖ *Weight of Zone 2 – (Pilasters – Brickwork)*

Area = 2.21 × 1.68 = 3.71

Volume = (3.71 × 0.15) × 2 = 1.113

Note: Depth of pilaster on each side of viaduct is assumed as 0.15 m.
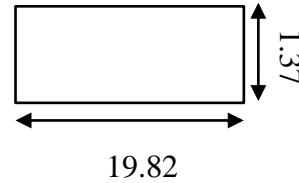
Weight = (1.113 × 2000) × 9.81 = 21837.06

$\cong$ 21837 N
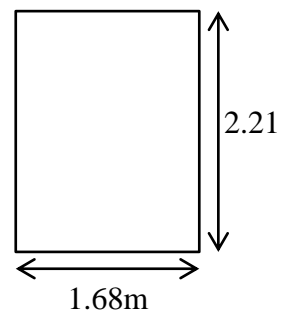
❖ **Weight of Zone 3 – (Parapet Walls – Brickwork)**

Area $= 19.82 \times 1.37 = 27.15$

Volume $= (27.15 \times 0.45) \times 2 = 24.44 \; m^3$

Weight $= (24.44 \times 2000) \times 9.81 = 479512.8$

$$\cong 479513 \; N$$

1.37

19.82

❖ **Weight of Zone 4 – (Brickwork below fill)**

Since don't know exact angle and dimension of this zone, a triangle is assumed.

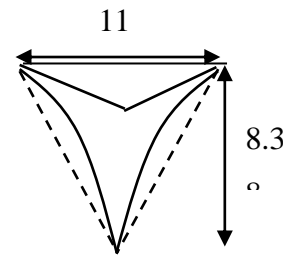Area of triangle $= \dfrac{b.h}{2} = \dfrac{11 \times 8.38}{2} = 46.09 \; m^2$

This area is an over-estimate of weight of brickwork, by approximately 20%.

$\therefore 46.09 \times 0.8 = 36.87 \; m^2 \rightarrow Area \; of \; Brickwork$

$Volume = 36.87 \times 3.36 = 123.88 \; m^3$

$Weight = (123.88 \times 2000) \times 9.81 = 2430588 \; N$

11

8.3

Note that the weight of drainage pipe separating brickwork and the fill is negligible, and thus is accounted as the boundary and brickwork.

❖ **Weight of Zone 5 – (fill)**

$Area \; of \; Zone \; 1 \; (Grey \; area) - Area \; of \; Zone \; 4 = 63.3 - 36.87 = 26.43 \; m^2$

$Volume = 26.43 \times 3.36 = 88.8 \; m^3$

Zones five and six are thought to be a mixture of ash and imported/crushed rock fill, combined with brickwork waste. There are uncertainties on fill load. However, the difference and its effect on result will be negligible. An average density of 1500 kg/m^2 is therefore assumed for both these zones.

$Weight = (88.8 \times 1500) \times 9.81 = 1306692 \; N$

❖ Weight of Zone 6 – (fill)

Since the author is unsure of depth of zone 6, where rails, sleepers and ballast are located, and hence a logical assumption of 0.2m is used in this calculation.
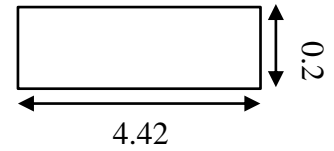
$Volume = (4.42 \times 0.2) \times 19.82 = 17.52 \ m^3$

$Weight = (17.52 \times 1500) \times 9.81 = 257807 \ N$

❖ Total weight of all zones (Total dead load applied to top surface of pier)

$= 2260341 + 21837 + 479513 + 2430588 + 1306692 + 257807 = 6756778 \ N$

$The \ area \ of \ drainage \ zone \ = \ 140 \times 120 = 16800 \ mm^2$

$Top \ surface \ area \ of \ pier \ (where \ load \ is \ applied \ to) = \ (5180 \times 1680) - 16800$

$= 8685600 \ mm^2$

$\therefore Pressure = \dfrac{6756778}{8685600} = 0.778 \ N/\ mm^2 = W1$
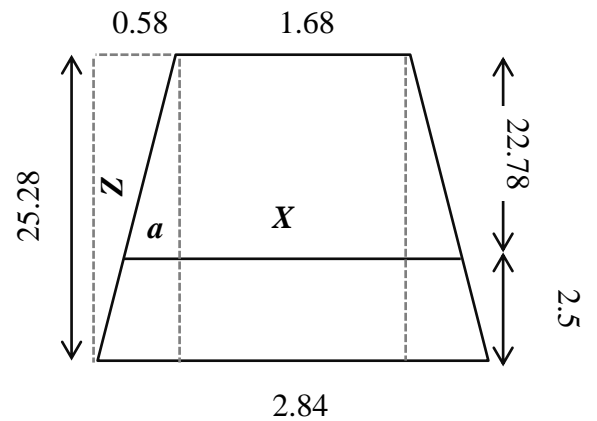
D.2: load calculations for the bottom

2.5 m model

$\dfrac{2.84 - 1.68}{2} = 0.58$

$\dfrac{2.5}{25.28} = \dfrac{Z}{0.58} \rightarrow z = 0.057$

$0.58 - 0.057 = 0.523 = a$

$x = (0.523 \times 2) + 1.68 = 2.726$

$$\frac{8.1 - 5.18}{2} = 1.46$$

$$\frac{2.5}{25.28} = \frac{Z}{1.46} \rightarrow Z = 0.144$$

$$a = 1.46 - 0.144 = 1.3156$$

$$Y = (1.3156 \times 2) + 5.18 = 7.811$$
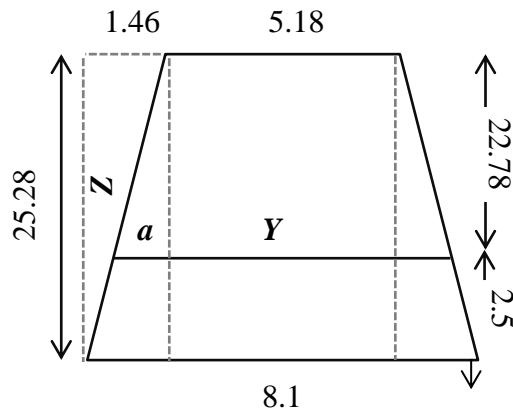
Volume of pier above 2.5 m

$$Volume = \frac{(A1 + A2 + \sqrt{A1.A2}).H}{3}$$

Where:

$A1 = $ Bottom area $= 2.726 \times 7.811 = 21.29$ m^2

$A2 = $ Top area $= 5.18 \times 1.68 = 8.70$ m^2

$$Volume = \frac{(21.29 + 8.70 + \sqrt{21.29 \times 8.70}) \times 22.78}{3}$$

$$Volume = 331.066 \, m^3$$

Volume of drainage $= (0.12 \times 0.14) \times 22.78 = 0.38$

Volume of brickwork $= 331.066 - 0.38 = 330.68 \, m^3$

Weight of brickwork $= mass \times gravity$

$$Mass = 330.68 \times 2000 = 661366.6$$

$$Weight = 661366.6 \times 9.81 = 6488006.3 \, N = W2$$

Total weight on bottom 2.5 m of pier = W1 (original weight) + W2 = 6756778 + 6488006.3 = 13244784 N

Area of drainage ➔ $0.12 \times 0.14 = 0.0168 \ m^2$

Surface where load is applied to:

$$= (2.726 \times 7.811) - 0.0168 = 21.275 = 21275986 \ mm^2$$

Pressures $= \frac{13244784}{21275986} = 0.623 \ N/mm^2$

❖ *After removing first layer:*

Reduction in weight and area with removal of each layer are 14440N and 31100mm[2] respectively

Layer 1 ➔ 13244784 – 14440 = 13230344

$$Pressure \ = \frac{13230344}{21261518} = 0.6222 \ N/mm^2$$

Layer 2 ➔ 13230344 – 14440 = 13215904

$$Pressure \ = 0.6224 \ N/mm^2$$

Layer 3 ➔ 13215904 – 14440 = 13201464

$$Pressure \ = 0.6227 \ N/mm^2$$

D.3: the load calculations for the top 3 metre

To calculate z:

$\dfrac{3}{25.28} = \dfrac{z}{0.58} \ \rightarrow z = 0.0688$

To calculate x:

$0.58 - 0.0688 = 0.511 = a$

$x = 1.68 + (0.511 \times 2)$

$x = \ 2.702$

To calculate y:
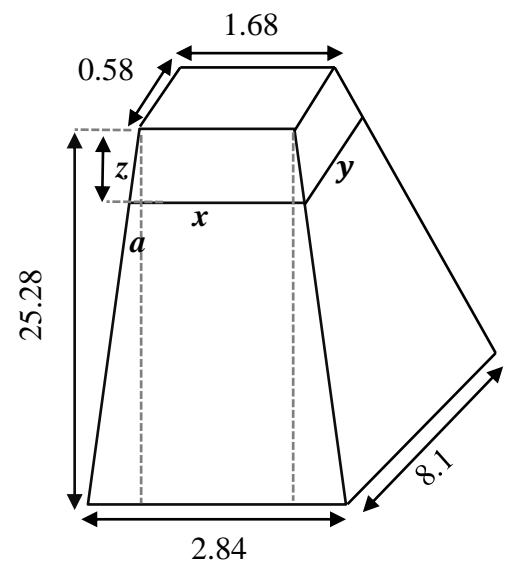
$$\frac{3}{25.28} = \frac{z}{1.46} \rightarrow z = 0.1732$$

$$1.46 - 0.1732 = 1.286$$

$$y = (1.286 \times 2) + 5.18 = 7.753 \rightarrow y$$

❖ *Volume of the total top 3 metre of the pier*

A_1 = Bottom Area = $2.70 \times 7.75 = 20.925 \ m^2$

A_2 = Top Area = $5.18 \times 1.68 = 8.70 \ m^2$

Volume of each exfoliation layer

$$= \frac{A_1 + A_2 + \left(\sqrt{A_1 A_2}\right) \cdot H}{3} = \frac{20.925 + 8.70 + \left(\sqrt{20.925 \times 8.70}\right) \times 3}{3} =$$

$$= 43.117 \ m^3$$
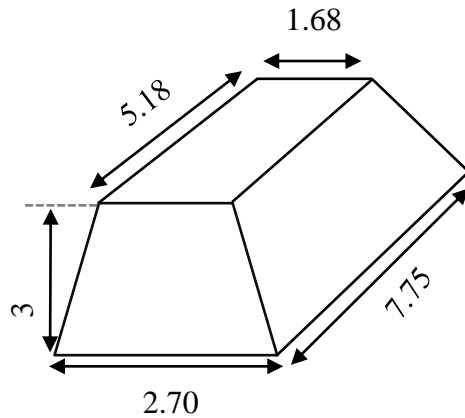
❖ *Volume of the each exfoliated layer, for the top 3m of the pier:*

Face 1

$$(0.115 \times 0.2) + (2.8 \times 0.920)$$
$$= 2.599 \ m^2$$

$$(2 \times 0.23) + (1 \times 0.46) = 0.92 \ mm^2$$
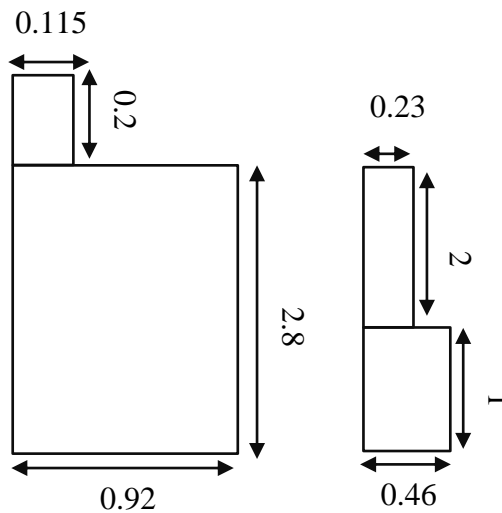
Face 2

$$3 \times 1.68 = 5.04 \ m^2$$
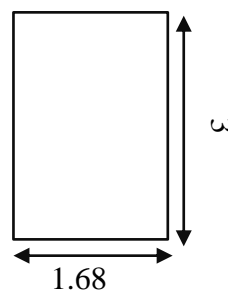
Face 3

$(0.115 \times 0.4) + (2.6 \times 1)$

$\qquad = 2.646 \, m^2$

$(0.69 \times 0.2) + (2.8 \times 0.58)$

$\qquad = 1.762 \, m^2$
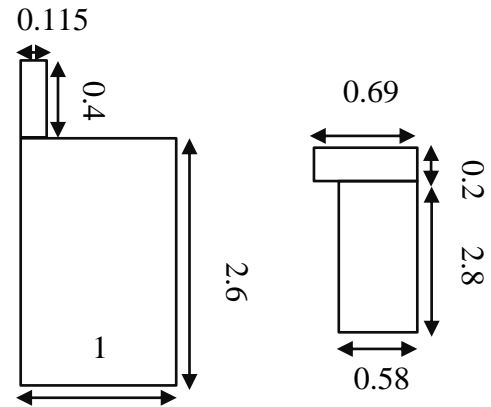
Face 4

$(3 \times 1.68) - 0.0168 = 5.02 \, m^2$

Drainage
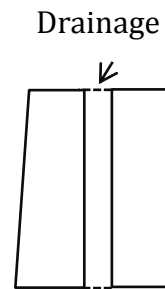
D.4: Load calculation for the top 3m repair model , where no exfoliation is taking place:

❖ The weight removed with each layer:
  Total area removed by 1 layer ➔ 17990200mm^2

  Total volume removed by 1 layer ➔ $17990200 \times 10 = 179902000mm^3 =$ 0.179m^3

  Weight $= (0.179 \times 2000) \times 9.81 = 3511.98 \cong 3512N$

❖ The area reduced of original area by removal of each layer:
  $(0.115 + 0.23 + 1.68 + 0.115 + 0.69 + (0.14 \times 2)) \times 0.01 = 0.031 \, m^2$

  $\qquad = 31100 \, mm^2$

❖ Original Load $= 6756778$ N
  Weight after 1st layer ➔ $6756778 - 3512 = 6753266 \, N$

❖ Original area:
  Area after 1st layer ➔ $8685600 - 31100 = 8654500 \, mm^2$

  New pressure after removal of 1st layer $= \dfrac{6753266}{8654500} = 0.78$ N/mm^2

  Pressure after removal of 2nd layer $= \dfrac{6749754}{8623400} = 0.783$ N/mm^2

  Pressure after removal of 3rd layer $= \dfrac{6746242}{8592300} = 0.785$ N/mm^2

Appendix E

A summary of different material properties used in the previous research are summarised in the tables below.

Table E.1: Different sources of elastic modulus values for brick masonry in the literature

Description	Elastic modulus (N/mm^2)			Reference
	Brickwork	**Brick**	**Mortar**	
Brick masonry	---	2400±200	335	(Brencich *et al*. 2002)
Clay brick	---	15700	---	(Abdulla 1989)
Clay brick wall	13900±1300	---	---	(Abdulla 1989)
Engineering clay brickwork (solid pier)	14500		---	(Abdulla 1989)
Generally bricks used in western countries	---	3500 to 34000	---	(Narayanan *et al* 2013)
Pressed red clay bricks	---	14000	---	(Narayanan *et al* 2013)
Fletton brickwork	4960	---	---	(Hendry 1990)
Clay brick walls	13500	---	---	(Budiwati 2009)
Brick masonry prisms	12300 5600	---	---	(Brencich *et al*. 2002)
Clay bricks	2220	---	---	(Knutsson and Nielsen, 1995)

Table E.2: Sources for maximum principal strain value in the literature

Description	MAXPE (Maximum principal strain)			Reference
	Brickwork	**Brick**	**Mortar**	
Axial strain for load perpendicular to bed-joints	$6.1 \times 10^{-3} \pm 3.4 \times 10^{-4}$	---	---	(Brencich *et al.*, 2002)
Concentrically loaded clay brick prisms	$\varepsilon_{el} = 0.0074$ $\varepsilon_{ult} = 0.0088$			(Brencich *et al.*, 2002)
Brick masonry	$\varepsilon_{ult} = 0.0087$			(Verstrynge, 2009)
Fletton brickwork	$\varepsilon_{ult} = 0.0045$			(Hendry, 1990)
Brickwork from ruins of Pavia tower	0.0008			
Soft mud clay brick	0.0066			
Long-term creep tests on columns of brickwork	**0.0005**			(Verstrynge, 2009)
Clay brick masonry	**0.00031**	0.00005	0.002	(Hughes and Harvey, 1995)

Appendix F: pictures of pier 4 of Larpool viaduct

Pictures exfoliation, repair, crack and spalling defects present on pier 4 of Larpool Viaduct are presented in this section.
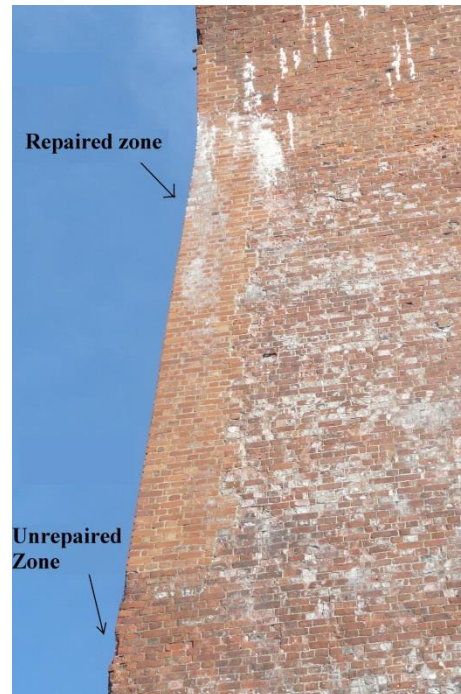
Figure F.1: The repaired and unrepaired zone on face 1 of the pier.

Figure F.2: Salt-damp defect on the top 9m of the pier, present on both repair and un-repaired parts.

Figure F.3: Weathering defects causing exfoliation of stone on face 4 of the pier.

Figure F.4: Face 4 of the pier, different between the repaired and unrepaired section of the face.

Figure F.5: The eroded zone around the drainage section on face 4 of the pier, showing plant growth close to the drainage pipes.

Figure F.6: Cracks on the outer faces of bricks, indicating spalling of face 1 surface.

Figure F.7: Vertical cracks seen on the bottom 2.5 meters of the pier

Figure F.8: Spalling of the outer layers of brick

Appendix G: Deterioration and repair of each exfoliation layer with time

The table presented below gives material properties of the three different materials used in the exfoliated layers, indicating deterioration (reduction in the elastic modulus value) and repair properties used in of modelling the zone one.

	Time (Year)	E for Layer 1 (N/mm²)	E for Layer 2 (N/mm²)	E for Layer 3 (N/mm²)
	1	5600	5600	5600
	2	5462.5	5531.25	5554.918
	3	5325	5462.5	5509.836
	4	5187.5	5394.599	5464.754
	5	5050	5326.698	5419.672
	6	4912.5	5258.796	5374.59
	7	4775	5190.895	5329.508
	8	4637.5	5122.994	5284.426
	9	4500	5055.093	5239.344
	10	4362.5	4987.191	5194.262
	11	4225	4919.29	5149.18
	12	4087.5	4851.389	5104.098
	13	3950	4783.488	5059.016
	14	3812.5	4715.586	5013.934
	15	3675	4647.685	4968.852
	16	3537.5	4579.784	4923.77
	17	3400	4511.883	4878.689
	18	3262.5	4443.981	4833.607
	19	3125	4376.08	4788.525
	20	2987.5	4308.179	4743.443
	21	2850	4240.278	4698.361
	22	2712.5	4172.377	4653.279
	23	2575	4104.475	4608.197
	24	2437.5	4036.574	4563.115
	25	2300	3968.673	4518.033
	26	2162.5	3900.772	4472.951
	27	2025	3832.87	4427.869
	28	1887.5	3764.969	4382.787
	29	1750	3697.068	4337.705
	30	1612.5	3629.167	4292.623
	31	1475	3561.265	4247.541
	32	1337.5	3493.364	4202.459
	33	1200	3425.463	4157.377
	34	1062.5	3357.562	4112.295
	35	925	3289.66	4067.213
	36	787.5	3221.759	4022.131
	37	650	3153.858	3977.049
	38	512.5	3085.957	3931.967
	39	375	3018.056	3886.885
	40	237.5	2950.154	3841.803
First layer is removed	41	100	2882.253	3796.721

298

42	100	2814.352	3751.639
43	100	2746.451	3706.557
44	100	2678.549	3661.475
45	100	2610.648	3616.393
46	100	2542.747	3571.311
47	100	2474.846	3526.23
48	100	2406.944	3481.148
49	100	2339.043	3436.066
50	100	2271.142	3390.984
51	100	2203.241	3345.902
52	100	2135.34	3300.82
53	100	2067.438	3255.738
54	100	1999.537	3210.656
55	100	1931.636	3165.574
56	100	1863.735	3120.492
57	100	1795.833	3075.41
58	100	1727.932	3030.328
59	100	1660.031	2985.246
60	100	1592.13	2940.164
61	100	1524.228	2895.082
62	100	1456.327	2850
63	100	1388.426	2804.918
64	100	1320.525	2759.836
65	100	1252.623	2714.754
66	100	1184.722	2669.672
67	100	1116.821	2624.59
68	100	1048.92	2579.508
69	100	981.0185	2534.426
70	100	913.1173	2489.344
71	100	845.216	2444.262
72	100	777.3148	2399.18
73	100	709.4136	2354.098
74	100	641.5123	2309.016
75	100	573.6111	2263.934
76	100	505.7099	2218.852
77	100	437.8086	2173.77
78	100	369.9074	2128.689
79	100	302.0062	2083.607
80	100	234.1049	2038.525

Second layer is removed

81	100	100	1993.443
82	100	100	1948.361
83	100	100	1903.279
84	100	100	1858.197
85	100	100	1813.115
86	100	100	1768.033
87	100	100	1722.951
88	100	100	1677.869
89	100	100	1632.787
90	100	100	1587.705
91	100	100	1542.623
92	100	100	1497.541
93	100	100	1452.459

299

94	100	100	1407.377
95	100	100	1362.295
96	100	100	1317.213
97	100	100	1272.131
98	100	100	1227.049
99	100	100	1181.967
100	100	100	1136.885
101	100	100	1091.803
102	100	100	1046.721
103	100	100	1001.639
104	100	100	956.5574
105	100	100	911.4754
106	100	100	866.3934
107	100	100	821.3115
108	100	100	776.2295
109	100	100	731.1475
110	100	100	686.0656
111	100	100	640.9836
112	100	100	595.9016
113	100	100	550.8197
114	100	100	505.7377
115	100	100	460.6557
116	100	100	415.5738
117	100	100	370.4918
118	100	100	325.4098
119	100	100	280.3279
120	100	100	235.2459
121	100	100	190.1639
122	100	100	145.082
123	100	100	100
124	5600	5600	5600
125	5600	5600	5600
126	5600	5600	5600
127	5600	5600	5600
128	5600	5600	5600
129	5600	5600	5600
130	5600	5600	5600

Third layer is removed
Repair is applied